# February bottom trawl survey biomasses of fishery species in Falkland Islands waters, 2010–2026

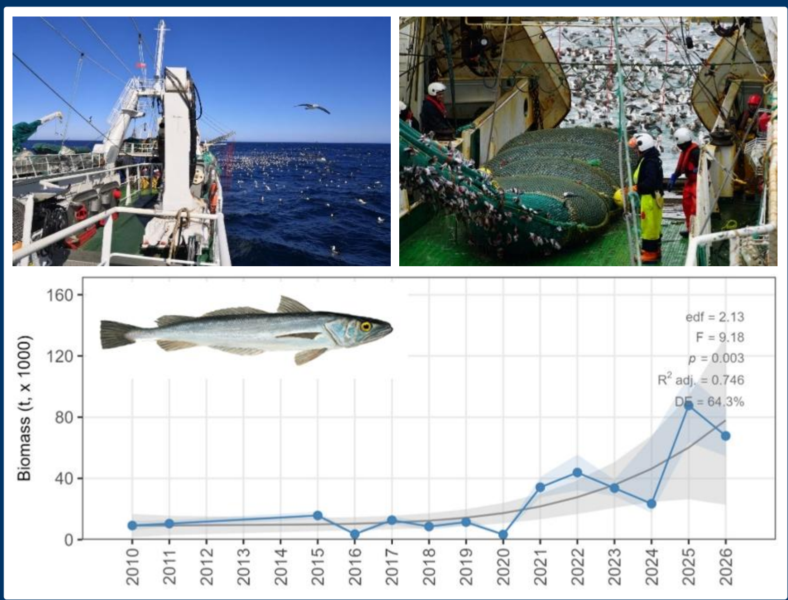


**Jorge E. Ramos**

**Fisheries Department**
**Directorate of Natural Resources**
**Falkland Islands Government**
**Stanley, Falkland Islands**

**SA-2026-02**

**For citation purposes this publication should be referenced as follows:**

Ramos JE (2026) February bottom trawl survey biomasses of fishery species in Falkland Islands waters, 2010–2026. SA-2026-02. Fisheries Department, Directorate of Natural Resources, Falkland Islands Government, Stanley, Falkland Islands. 157 p.



**Acknowledgements**

We thank the captains and crews of the commercial fishing vessels, and the scientific observers of the Falkland Islands Fisheries Department (FIFD), that facilitated and assisted in catch, oceanographic, and biological data collection. Toni Trevizan and scientific observers assisted with data checks. Comments provided by Andreas Winter. Cover photo credits: J.E. Ramos, FIFD (top left), Toni Trevizan, FIFD (top right).



Reviewed and approved on 12 August 2026 by:

James Wilson
Director of Natural Resources
Falkland Islands Government

## Table of Contents

# February bottom trawl survey biomasses of fishery species in Falkland Islands waters, 2010–2026


## 1. Summary

Biomass assessments were conducted for 11 commercially important fish stocks—Argentine shortfin squid, banded whiptail grenadier, common hake, hoki, kingclip, Patagonian squid, Patagonian toothfish, red cod, rock cod, southern blue whiting, and southern hake—across the northern and western areas of the Falkland Islands Interim Conservation and Management Zone (FICZ) and the Falkland Islands Outer Conservation Zone (FOCZ), including the 'Loligo Box'. These assessments were based on catch data from 1,974 bottom trawls conducted during the February parallel groundfish and calamari pre-season surveys in 2010, 2011, and 2015–2026. Changes in biomass were assessed by comparison of the biomass in 2026 to baseline years (2010, 2025, and 2023–2025 mean), and using Generalised Additive Models to model the temporal trends of the full time series (2010, 2011, and 2015–2026).

The February surveys reveal divergent biomass trajectories for Falkland Islands marine resources from 2010 to 2026. Common hake, Patagonian toothfish, and southern hake exhibited signs of increasing biomass. Hoki, kingclip, red cod, and rock cod exhibited signs of decreasing biomass. Argentine shortfin squid, banded whiptail grenadier, Patagonian squid, and southern blue whiting had no temporal trends in biomass. Rock cod and southern blue whiting biomass increased gradually in recent years but remains at low levels.

Common hake had a significant increasing trend in biomass from 2010 to 2026, but mainly from 2021 onwards, as revealed by the GAM. The 2026 biomass (67,767 t) was the second highest in the time series and represented a significant increase relative to 2010 (9,226 t) and 2023–2025 mean (48,264 t) levels. Densities increased predominantly along the south-west in the FICZ and in the 'Loligo Box'. Females contributed over 90% of the biomass across survey years, and maturity composition was dominated by post-spawning individuals. Body length had a significant decline throughout the time series.

Patagonian toothfish biomass had a significant increasing trend in biomass from 2010 to 2026. The 2026 biomass (15,847 t) was the highest in the time series and represented a significant increase relative to 2010 (9,345 t), 2025 (6,275 t) and 2023–2025 mean (4,541 t) levels, with densities increasing in discrete patches through the survey area, including the 'Loligo Box'. Nearly 63% of the biomass was comprised of immature females across survey years. It must be noted that bottom trawl demersal surveys are not representative of the adult component of the stock, which is caught by longlines.

Southern hake had a significant increase in biomass from 2010 to 2026. The 2026 biomass (8,228 t) was the highest in the time series and represented a significant increase relative to 2025 (2,156 t) and 2023–2025 mean (1,978 t) levels. Densities mainly increased in discrete patches of the survey area, including the 'Loligo Box'. Approximately 91% of the biomass was comprised of females across survey years, mostly in post-spawning maturity stages. These results should be interpreted with caution as estimates carry additional uncertainty arising from the difficulty of distinguishing this species from common hake (*M. hubbsi*) in bulk catches.

Hoki had a marginally non-significant declining trend in biomass from 2010 to 2026, as revealed by the GAM. The 2026 biomass (198,889 t) represented a significant decrease relative to 2010 (303,807 t), but an increase compared to 2025 (6,939 t) and 2023–2025 mean (62,827 t) levels. Moderate inter-annual variability in biomass may be caused in part by the patchy and aggregated distribution of this species, with large aggregations that may form in some years but not in others. Whether these aggregations are captured depends on their spatial overlap with the survey's fixed station array and timing. Densities mainly decreased through the survey area, except for discrete patches including the south and centre of the 'Loligo Box'. Females contributed approximately 64% of the biomass across survey years. Maturity composition was dominated by post-spawning individuals in both sexes. Body length had a significant increase since 2021.

Kingclip had a significant non-linear biomass trend from 2010 to 2026, with biomass remaining at low levels in recent years. Biomass in 2026 (12,275 t) was the second lowest in the time series and represented a significant decrease relative to the 2023–2025 mean (22,271 t). Densities decreased through the survey area, except for discrete patches including the south and centre of the 'Loligo Box'. Females contributed 67% of the biomass across survey years. Maturity composition was dominated by post-spawning individuals in both sexes. Body length had a significant increase since 2021.

Red cod had a significant decline in biomass from 2010 to 2026, and the biomass in 2026 (31,413 t) was the third lowest in the time series. Densities decreased through the survey area, except for discrete patches along the 'Loligo Box'. Approximately 70% of the biomass was comprised of females across survey years, and mostly by post-spawning individuals. No significant change in length was detected.

Rock cod had a significant decline in biomass from 2010 to 2026, although with stabilisation at low levels in recent years. The 2026 biomass (284,050 t) represented a significant decrease relative to 2010 (834,775 t), but an increase compared to 2025 (122,121 t) and 2023–2025 mean (104,412 t) levels. Minor increases in density were observed in discrete patches through the survey area, including the 'Loligo Box'. Approximately 53% of the biomass was comprised of males across survey years. Maturity composition was dominated by post-spawning individuals in both sexes. Body length had a significant declining trend.

Some of these species are not at their peak of abundance in Falkland Islands waters during February (e.g., common hake, kingclip) or they may be under-represented due to the fishing gear used for the surveys (i.e., bottom trawl, whereas the Argentine shortfin squid is mainly caught by jiggers, and the adult portion of the Patagonian toothfish stock is caught by longlines).

Many of the stocks assessed are targeted across multiple nations' Exclusive Economic Zones (EEZs), with the Falkland Islands contributing a relatively small proportion to the total shared catch for some species in the Southwest Atlantic and Southeast Pacific. Declines in biomass for some of these stocks may be partially attributed to fishing pressure outside Falklands waters. However, the Falkland Islands fisheries contribute a significant proportion to the total catch for certain stocks, such as rock cod and red cod, and several species' spawning grounds lie within the Falkland Islands shelf, including hoki, red cod, rock cod, and southern blue whiting. As such, management decisions made by the Falkland Islands Fisheries Department (FIFD) are critical for the sustainability of these stocks.

## 2. Introduction

The Falkland Islands shelf is located within the Patagonian Large Marine Ecosystem, one of the world's most productive fishing areas (Arkhipkin et al. 2012). The Patagonian Large Marine Ecosystem comprises two distinct sub-regions: a southern temperate ecosystem in the north and a sub-Antarctic ecosystem in the south (Boltovskoy 1999). The temperate ecosystem lies within waters of subtropical origin, transported onto the shelf by the Brazil Current and mixed with temperate shelf waters. The region's productivity is largely driven by tidal mixing oceanographic fronts and seasonal fronts formed by cold freshwater inflows from the Strait of Magellan. The sub-Antarctic ecosystem is influenced by waters of sub-Antarctic origin carried by the Falkland Current (Peterson & Whitworth 1989). The Falkland Current, which diverges from the Antarctic Circumpolar Current in the Drake Passage, splits into two branches at the continental slope south of the Falkland Islands—one weaker and one stronger—flowing around the west and east of the islands, respectively (Bianchi et al. 1982). These oceanographic features play a crucial role in the distribution and abundance of marine species, such as Argentine shortfin squid (*Illex argentinus*) and hoki (*Macruronus magellanicus*), which migrate to frontal zones for feeding and return to non-frontal zones for spawning (Agnew 2002). In contrast, deep-water species like Patagonian toothfish (*Dissostichus eleginoides*) are influenced by sub-Antarctic water intrusions into the shelf (Laptikhovsky et al. 2008; Arkhipkin & Laptikhovsky 2010).

Commercial squid and fish stocks around the Falkland Islands have been targeted by international fishing fleets for decades, with systematic catch data starting in 1987 (Falkland Islands Government 1989). Total catches reached a peak of 462,487 tonnes in 2015, largely due to an unusually large influx of *I. argentinus* into Falkland waters from April to May 2015, resulting in record catches of 332,862 t for the species (Winter 2015; Falkland Islands Government 1989, 2025). Finfish licence allocations in the Falkland Islands are determined using Total Allowable Effort (TAE), based on the catchability of an index species representing the main target of the fishery. This approach works under the assumption of consistent relationships among catch, effort, and biomass. The first index species for finfish TAE was southern blue whiting (*Micromesistius australis*). However, catches of southern blue whiting declined in the 1990s and the stock collapsed by 2009. Rock cod (*Patagonotothen ramsayi*) was first targeted in 2007 due to the lack of marketability in previous years (Winter et al. 2010), and its catches peaked in 2010 (Laptikhovsky et al. 2013; Ramos & Winter 2023a). The index species was re-examined (Payá et al. 2010) and switched in 2011 from southern blue whiting to rock cod to set effort allocation. However, catches of rock cod decreased considerably after 2010 (Ramos & Winter 2023a; Falkland Islands Government 2026). In parallel, catches of common hake (*Merluccius hubbsi*) increased, with a peak of 63,365 t in 2025 (Falkland Islands Government 2026). The use of an index species to manage all Falkland Islands commercial finfish species was thus considered unreliable, and the Falkland Islands Government, on advice from MacAlister Elliott & Partners Ltd, UK (MEP 2020), switched to assessing each individual commercial stock to better inform fisheries management.

Scientific surveys are a key source of fisheries-independent data, offering standardised sampling plan and constant catchability that are not influenced by commercial fishing activities (Hilborn & Walters 1992; Alglave et al. 2022; Gallo et al. 2022). The Falkland Islands Fisheries Department (FIFD) has conducted parallel groundfish and calamari (*Doryteuthis gahi*) pre-season surveys every February since 2010, except for 2012, 2013, and 2014. The groundfish surveys are conducted along the north, west and south-west in Falkland Islands waters. The calamari pre-season surveys are conducted along the 'Loligo Box' to the east of the Falkland Islands.

Initially, these surveys aimed to provide biomass estimates for rock cod on the entire Falklands fishing grounds during the austral summer (Winter et al. 2010), which has since been expanded to provide information on other commercial stocks. It is noted, however, that Falkland Islands waters represent only part of the range for most stocks examined. For certain migratory species, such as common hake (Arkhipkin et al. 2015) and kingclip (*Genypterus blacodes*) (Arkhipkin et al. 2012), the February surveys may not coincide with peak abundance periods. Therefore, July surveys that follow the same methodology as the February surveys have also been conducted since 2017 to estimate biomass during the austral winter. Increasing abundance of common hake in the Falkland Shelf in recent years (Ramos & Winter 2022a) triggered a demography survey conducted exclusively for this species during July 2020 (Randhawa et al. 2020).

This report summarises biomass estimates for key commercial species in Falkland Islands waters based on catch data from both the groundfish and calamari pre-season surveys conducted in February 2010, 2011, and 2015–2026.

## 3. Methods

### 3.1. Bottom trawl stations

Concurrent groundfish and calamari pre-season research surveys were carried out during February 2010–2011 and 2015–2026 onboard chartered fishing trawlers to cover the Falkland Islands fishing zone (Fig. 1). All trawls were bottom trawls; GPS latitude and longitude, net vertical opening, net horizontal opening, trawl door spread, and trawl speed were recorded on the ship's bridge when the net achieved the required configuration at the seafloor (based on net sensor readings, confirmed by the bridge officer), every 15 minutes during the progress of each trawl (in calamari pre-season surveys), and at the end of the trawl at the seafloor.

The duration of each trawl was approximately 60 min on the bottom during groundfish surveys, and 120 min on the bottom during calamari pre-season surveys. Characteristics of the trawl nets, trawl performance, and biological sampling during groundfish (Brickle & Laptikhovsky 2010; Arkhipkin et al. 2011, 2019; Gras et al. 2015, 2016, 2017, 2018; Randhawa et al. 2020; Trevizan et al. 2021, 2022, 2023; Ramos et al. 2024a, 2025; Soeth et al. 2026) and calamari pre-season (Arkhipkin et al. 2010; Winter et al. 2011, 2015, 2016, 2017, 2018, 2019, 2020, 2021, 2022, 2023; Chemshirova et al. 2024, 2025, 2026) surveys can be consulted in detail in their respective survey reports. These surveys were designed to be consistent in the number and position of stations across years. However, there were variations in the number of stations due to mechanical issues, unfavourable weather conditions, logistic setbacks (e.g., pandemic COVID-19), or objectives of each survey. For instance, a total of 42 stations were conducted in February 2022 instead of the usual number of stations (n ≈ 84) due to the survey being shortened because of COVID-19 quarantine requirements of the vessel's crew (Trevizan et al. 2022).

### 3.2. Catch recording

All species from the catch of each trawl station were sorted by FIFD scientific staff and the vessel's factory crew. FIFD scientific staff recorded the total catch of each species assessed by a combination of weighing on an electronic balance to the nearest 0.01 kg and factory production records when weighing of large catches was not logistically feasible.

Eleven commercial species were assessed; these species have been typically assessed in February parallel demersal surveys conducted in Falkland Islands waters and represent important commercial targets in the Falkland Islands and other neighbour nations' fishing zones (Table I).

Table I. Main commercial species assessed in groundfish and calamari pre-season surveys in Falkland Islands waters during February 2010–2011 and 2015–2026. Geographic distributions taken from http://www.fao.org/fishery/species/search/en

| Common name | Scientific name | Distribution |
|---|---|---|
| Argentine shortfin squid | *Illex argentinus* | Southwest Atlantic: Brazil, Uruguay, Argentina, Falkland Islands. |
| Banded whiptail grenadier | *Coelorinchus fasciatus* | Southwest Atlantic: Brazil, Uruguay, Argentina, Falkland Islands.<br>Southern Pacific: Chile, Australia, New Zealand.<br>Southern Indian: Africa, Australia. |
| Common hake | *Merluccius hubbsi* | Southwest Atlantic: Brazil, Uruguay, Argentina, Falkland Islands. |
| Hoki | *Macruronus magellanicus* | Southwest Atlantic: Argentina, Falkland Islands.<br>Southeast Pacific: Chile. |
| Kingclip | *Genypterus blacodes* | Southwest Atlantic: Brazil, Uruguay, Argentina, Falkland Islands.<br>Southern Pacific: Chile, Australia, New Zealand. |
| Patagonian squid | *Doryteuthis gahi* | Southwest Atlantic: Argentina, Falkland Islands.<br>Southern Pacific: Peru, Chile. |
| Patagonian toothfish | *Dissostichus eleginoides* | Southwest Atlantic: Argentina, Falkland Islands. Southeast Pacific: Chile.<br>Southwest Pacific: Macquarie Island.<br>Southern Ocean: South Georgia. |
| Red cod | *Salilota australis* | Southwest Atlantic: Argentina, Falkland Islands.<br>Southeast Pacific: Chile. |
| Rock cod | *Patagonotothen ramsayi* | Southwest Atlantic: Argentina, Falkland Islands. |
| Southern blue whiting | *Micromesistius australis* | Southwest Atlantic: Argentina, Falkland Islands.<br>Southeast Pacific: Chile.<br>Southern Ocean: South Georgia, South Shetland, South Orkney Islands. |
| Southern hake | *Merluccius australis* | Southwest Atlantic: Argentina, Falkland Islands.<br>Southern Pacific: Chile, New Zealand. |

Station and catch data recorded during the surveys were checked and corrected following each survey's standard data management procedures, with groundfish survey data verified record by record. Analyses were conducted once both surveys' data were available in the Falkland Islands Fisheries Department (FIFD) database in late March 2026.

### 3.3. Abundance calculations

Trawls were excluded from abundance calculations if not quantifiable for the following reasons: 1) the trawl doors did not open properly, 2) the net broke during the trawl, or 3) if the net was quickly filled with medusae, which resulted in the trawl being stopped prematurely.

Density (kg/km$^2$) was calculated as the species catch weight divided by the trawl area (Winter 2019). Trawl area was calculated as the trawl distance covered × net horizontal opening. Trawl distance covered was calculated using the *geodist* package (Padgham & Sumner 2025) in R (version 4.5.1; R Core Team 2025). For calamari pre-season surveys, net horizontal opening was derived from the distance between trawl doors (Seafish 2010). For groundfish surveys, the triangulation method that derives net horizontal opening from the distance between trawl doors is unsuitable because the geometry of the net is different (Ramos et al. 2024b). Since 2016, groundfish survey net horizontal opening has instead been measured directly from Marport sensors fitted to the extremities of the survey vessel's trawl net wings. Generalised Additive Models (GAMs; Wood 2017) were fitted using the *mgcv* package (Wood 2011) in R (version 4.5.1; R Core Team 2025) to calculate net horizontal opening when this was not recorded due to failure of the Marport sensors. Smooths were estimated by restricted maximum likelihood (REML; Wood 2011). The model assumed Gaussian distribution of the residuals and used an identity link. Smooth terms were used for door spread, net vertical opening, trawl speed, and depth, which were treated as random effects.

Yearly trawl biomass densities were extrapolated to the survey area combining the finfish zone (122,493.7 km$^2$) and 'Loligo Box' (31,296.9 km$^2$), partitioned into grids of 5×5 km$^2$. Position coordinates of trawls were converted to WGS 84 projection in UTM sector 21, and extrapolation was calculated using an inverse distance weighting algorithm (Winter 2019). The basic inverse distance weighting algorithm assigns a value *u* to any grid location *x* that is the weighted mean of a known scattered set of points $x_i$ according to the inverse of the *i* points' distances from the grid location *x*:

$$u(\mathrm{x}) = \begin{cases} \dfrac{\sum_{i=1}^{N} w_i(\mathrm{x}) u_i}{\sum_{i=1}^{N} w_i(\mathrm{x})}, & \text{if } d(\mathrm{x}, \mathrm{x_i}) \neq 0 \\ u_i, & \text{if } d(\mathrm{x}, \mathrm{x_i}) = 0 \end{cases}$$

where

$$w_i(\mathrm{x}) = \frac{1}{d(\mathrm{x}, \mathrm{x_i})^p}$$

The power parameter *p* (a positive real number) adjusts the weight of points $x_i$ as a function of distance ($x$, $x_i$); higher values of *p* put higher influence on the points $x_i$ closest to a given interpolated point *x*. For this survey analysis, an empirical approach to selecting *p* was used running the inverse distance weighting algorithm with *p* values from 1 to 25 by 0.25, and for each *p* calculating the aggregate of log proportional differences between the empirical values of density at every trawl and the interpolation at every trawl from all other trawls. The lowest aggregate of log proportional differences corresponded to the best *p* value. Because some points may be more clustered than others, an isolation parameter was assigned attributing more weight to points $x_i$ in proportion to being further away from any other point $x_i$. Isolation parameters (*s*) per yearly survey were calculated as the standardised mean of distances between each point $x_i$ and all other points $x_j$:

$$s(\mathrm{x_i}) = \overline{d(\mathrm{x_i}, \mathrm{x_j})}$$

An additional weighting factor was included to adjust for trawl differences in area coverage. Survey trawls are generally standardised (60 min duration in groundfish surveys and 120 min in calamari pre-season surveys) but may be shortened on immediate notice for reasons that include unmanageably large concentrations of fish accumulating in the net. Such instances will result in the trawl being stopped just when its biomass density is maximised, rather than being stopped independently of the biomass density, and thereby create a potential bias of the density estimate at that location. For shoaling fish in sparse, highly aggregated distributions, the effect can be substantial (i.e., hoki; Ramos & Winter 2022b). However, the trawl itself is not an error record that should be invalidated and removed from the data set. To mitigate the potential bias effect, the swept area of each trawl was taken as a proportional weighting parameter so that a shortened trawl covering, for example, only half as much ground would have only half as much weight. Like the isolation parameters $s(\mathrm{x_i})$, the area parameters $a(\mathrm{x_i})$ were standardised (divided by their mean among all trawls), then $s(\mathrm{x_i})$ and $a(\mathrm{x_i})$ were added together and divided again by their sum to give a factor centred on 1. The revised inverse distance weighting factor is:

$$w_i(\mathrm{x}) = \left( \frac{\left( \frac{s(\mathrm{x_i}) + a(\mathrm{x_i})}{\overline{\left(s(\mathrm{x_i}) + a(\mathrm{x_i})\right)}} \right)}{d(\mathrm{x}, \mathrm{x_i})} \right)^p$$

Distance $d(x, x_i)$ is inherently calculated as Euclidean (straight-line) distance. However, the survey area surrounds the Falkland Islands and between two remote points a fish or ship would have to travel a real distance longer than straight-line; circumnavigating the landmass. Therefore, an axial loop was drawn through the survey area (Fig. 1), and $d(x, x_i)$ was defined as the longer of either the Euclidean distance between $x$ and $x_i$, or the distance on the axial loop between its two points respectively closest to $x$ and $x_i$ (Winter 2019).

As an extrapolation algorithm, calculated biomass over a given area will depend on the spatial distribution of surveyed densities, not just their total or mean value. Accordingly, the total biomass (deterministic biomass) is considered an estimate. Densities were interpolated over the same area for all species.

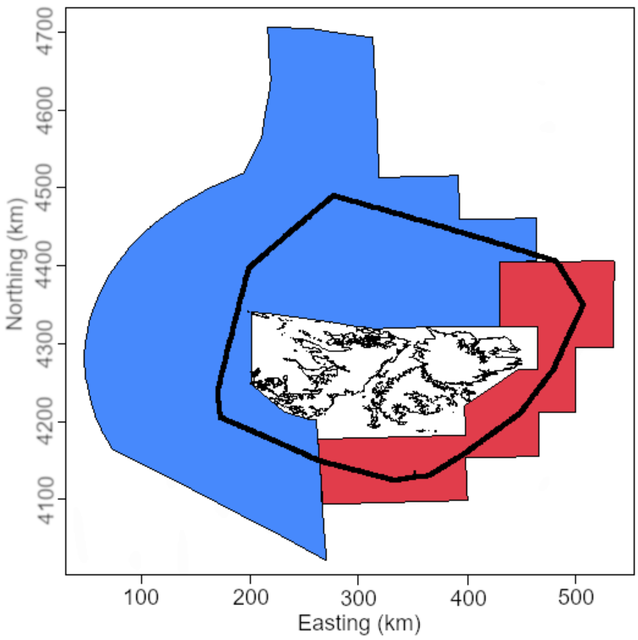


Fig. 1. Groundfish (blue) and calamari pre-season (red) survey areas, with axial loop (black line) used to define relative distances for the inverse distance weighting algorithm.

Uncertainty of the biomass estimate was calculated by a hierarchical bootstrap algorithm. First, survey trawls and their catches were randomly re-sampled with replacement for 10,000 iterations; each year's groundfish survey and parallel calamari pre-season survey were re-sampled separately so that both 'halves' of the survey area retained about the same relative coverage. Second, each re-sampled trawl was given a random uniform re-assignment of its coordinate position between start latitude and longitude and end latitude and longitude. Third, the isolation parameters were re-calculated for the randomised set of trawl data, and the inverse distance weighted algorithm re-applied. One iteration might thus re-sample any trawl twice or more, but each would have a slightly different position. The 95% confidence intervals (CI) of the 10,000 bootstrap iterations were used to infer uncertainty.

### 3.4. Temporal changes in biomass

3.4.1. Current year to baseline biomass comparisons

The difference in biomass across the 10,000 bootstrap samples was computed to assess the change in biomass of each species in the most recent year (2026) relative to a baseline year:

1) the most recent year (2026) relative to the first year (2010) in the time series. For February, the groundfish and calamari pre-season surveys were conducted in parallel for the first time in 2010. Therefore, 2010 was taken as the year one for comparative purposes. However, it must be noted that commercial fisheries have been conducted in the Southwest Atlantic for several decades already (Falkland Islands Government 1989), and that the state of the stocks in 2010 does not represent virgin stocks.

2) the most recent year (2026) relative to the previous year (2025) in the time series, and

3) the most recent year (2026) relative to the 2023–2025 mean. The three-year mean (2023–2025) minimise the influence of interannual variability in recent years, providing a more stable reference against which to assess the 2026 estimate. A total of 10,000 mean values were calculated from the respective 10,000 biomass samples from 2023, 2024, and 2025. These 10,000 mean values were then compared with the 10,000 biomass samples derived from 2026.

The change in biomass was calculated using the equation:

$$\Delta biomass = \frac{b.current}{b.baseline}$$

where *Δbiomass* is the ratio between *b.current* and *b.baseline*; *b.current* is the biomass calculated for the most recent year, i.e., 2026; *b.baseline* is the biomass calculated for the baseline year, i.e., 2010, 2025, 2023–2025 mean. *Δbiomass* > 1.0 indicates that *b.current* is higher than *b.baseline*, and therefore there was an increase in biomass in the current year compared to the baseline year, i.e., *Δbiomass* = 2.0 indicates a two-fold increase in biomass in the current year compared to the baseline year. *Δbiomass* = 1.0 indicates that *b.current* and *b.baseline* are equal, and therefore there was no change in biomass in the current year compared to the baseline year. *Δbiomass* < 1.0 indicates that *b.current* is lower than *b.baseline*, and therefore there was a decrease in biomass in the current year compared to the baseline year, i.e., *Δbiomass* = 0.5 indicates that the biomass in the current year corresponds to 50% of the biomass of the baseline year.

This method circumvented assumptions of normality and homogeneity of variance, which were violated by the distribution of biomass for certain species in some years. A difference was considered statistically significant if the 95% CI of the bootstrap distribution of differences excluded zero, indicating a deviation from equality. The Holm's method was used to control for the family-wise error rate when conducting multiple tests, to prevent the risk of Type I error (false positives) by adjusting the p-value threshold (Holm 1979):

$$p_{adjusted} = \frac{\alpha}{m} = \frac{0.05}{3} = 0.017$$

where $\alpha$ is the significance level, and $m$ is the number of tests (three comparisons: 2026 vs 2010, 2026 vs 2025, and 2026 vs 2023–2025 mean).

### 3.4.2. Temporal biomass trends

Temporal trends in annual biomass were modelled using Generalised Additive Models (GAMs; Wood 2017) fitted with the *mgcv* package (Wood 2011) in R (version 4.5.1; R Core Team 2025).

The error family was selected based on skewness of the full bootstrap biomass distribution (n = 140,000 replicates; 10,000 replicates × 14 years). Skewness quantifies the asymmetry of a distribution around its mean, with positive values indicating a longer right tail and negative values a longer left tail; a skewness of zero denotes a perfectly symmetric distribution. Skewness of the biomass distributions was calculated across all 10,000 bootstrap replicates pooled over years for each species using the skewness function from the *moments* package (Komsta & Novomestky 2022) in R (version 4.5.1; R Core Team 2025). Most species exhibited right-skewed biomass distributions: i.e., Argentine shortfin squid (skewness = 5.68), southern blue whiting (5.73), kingclip (2.25), rock cod (1.84), southern hake (1.49), red cod (1.41), common hake (1.37), Patagonian toothfish (0.984), banded whiptail grenadier (0.842), and hoki (0.737), with the exception of Patagonian squid (−0.030). A Gamma error distribution with a log link was used for species with right-skewed (skewness > 1) or moderately right-skewed (0.5–1.0) distributions, and a Gaussian error distribution with an identity link was tested for species with approximately symmetric distributions (skewness < 0.5).

For each species, the annual biomass was modelled as a smooth function of year using a penalised cubic regression spline (bs = "cr"), fitted by REML (Wood 2011). The basis dimension was set to k = min(10, $n$ − 1), where $n$ is the number of survey years available (2010, 2011, and 2015–2026), to prevent over-fitting given the relatively short time series (14 years).

To account for inter-annual differences in estimation uncertainty, observation weights were applied during model fitting, as initial unweighted fits indicated that some years dominated the smoother excessively. Weights were normalised within each species so that the maximum weight equalled one, ensuring numerical stability (Wood 2017). The weighting scheme was matched to the error family to maintain consistency between the assumed variance structure and the down-weighting of high-uncertainty years. For Gamma-family models, the normalised inverse coefficient of variation (CV) was used as the observation weight, as the CV measures relative variability and is therefore consistent with the Gamma variance structure, in which variance is proportional to the square of the mean (Ver Hoef & Boveng 2007). For Gaussian-family models, a square-root-normalised inverse variance was used. The square-root transformation was necessary because the untransformed inverse variance produced excessively large weight ratios, causing a small number of years to dominate the fit; taking the square root compresses the weight range while preserving the rank ordering of precision across years.

Four candidate model configurations were evaluated for each species, representing the two appropriate family–weight combinations (Table II). Models were compared using the Akaike Information Criterion (AIC; Akaike 1974) and ΔAIC relative to the best model for each species. The preferred model was the one with the lowest AIC among the family–weight combinations appropriate for the species' skewness. Model fit was further evaluated using the adjusted $R^2$ ($R^2_{adj}$), percentage deviance explained (DE%), and the F-statistic and associated p-value for the year smooth term. The adequacy of the basis dimension $k$ was verified using the $k$-index diagnostic (Wood 2017); a $k$-index substantially below 1.0 with a significant p-value (< 0.05) would indicate that the smoother was overly constrained and that $k$ should be increased. The selected model for each species was used to generate fitted biomass trends and 95% CI via back-transformation of the linear predictor ± 1.96 × SE on the link scale (type = response), yielding year-specific trend estimates on the original biomass scale.

Table II. Candidate generalised additive model configurations evaluated to assess the biomass trend for each species. All models included a penalised cubic regression spline smoother of year (bs = “cr”, *k* = 10) fitted by restricted maximum likelihood (REML).

| Model | Family | Link | Smoother | Weighing |
|---|---|---|---|---|
| M1 | Gamma | Log | s(Year) | Unweighted |
| M2 | Gamma | Log | s(Year) | Normalised inverse coefficient of variation |
| M3 | Gaussian | Identity | s(Year) | Unweighted |
| M4 | Gaussian | Identity | s(Year) | Square-root normalised inverse variance |

### 3.5. Spatial changes in biomass

The difference in density was computed for each grid (5×5 km$^2$) of the survey area to assess the change in biomass density of each species in the most recent year (2026) relative to a baseline year:

1) the most recent year (2026) relative to the first year (2010) in the time series. For February, the groundfish and calamari pre-season surveys were conducted in parallel for the first time in 2010. Therefore, 2010 was taken as the year one for comparative purposes. However, it must be noted that commercial fisheries have been conducted in the Southwest Atlantic for several decades already (Falkland Islands Government 1989), and that the state of the stocks in 2010 does not represent virgin stocks.

2) the most recent year (2026) relative to the previous year (2025) in the time series, and

3) the most recent year (2026) relative to the 2023–2025 mean. The three-year mean (2023–2025) minimise the influence of interannual variability in recent years, providing a more stable reference against which to assess the 2026 estimate. A mean density value was calculated for each grid from the 2023, 2024, and 2025 grid density values. The mean grid density values were then compared with the grid density from 2026.

The change in biomass density was calculated using the equation:

$$\Delta density = \frac{b.current}{b.baseline}$$

where *Δdensity* is the ratio between *b.current* and *b.baseline* at a grid square*; b.current* is the biomass calculated at grid square for the most recent year, i.e., 2026; *b.baseline* is the biomass calculated at grid square for the baseline year, i.e., 2010, 2025, 2023–2025 mean. The 2023–2025 mean at grid square was calculated as the mean of the density at grid square in 2023, 2024, and 2025. *Δdensity* > 1.0 indicates that *b.current* is higher than *b.baseline*, and therefore there was an increase in biomass at grid square in the current year compared to the baseline year. *Δdensity* = 1.0 indicates that *b.current* and *b.baseline* are equal, and therefore there was no change in biomass at grid square in the current year compared to the baseline year. *Δdensity* < 1.0 indicates that *b.current* is lower than *b.baseline*, and therefore there was a decrease in biomass at grid square in the current year compared to the baseline year.

### 3.6. Biological sampling

Random samples of up to 100 individuals of each species were collected in each station, and measured to the lowest 1 cm for finfish and to the lowest 0.5 cm for squid species. Dorsal mantle length was measured for Argentine shortfin squid and Patagonian squid (Calamari *D. gahi*). Total length was measured for common hake, kingclip, red cod (*Salilota australis*), rock cod, southern blue whiting, southern hake (*Merluccius australis*), and Patagonian toothfish. Pre-anal length was measured for banded whiptail grenadier (*Coelorinchus fasciatus*) and hoki. For finfish, macroscopic assessment of sex and maturity were conducted following an eight-stage maturity scale (Brickle et al. 2005, modified from Nikolsky 1963): 1, immature; 3, early developing; 4, late developing; 5, ripe; 6, running; 7, spent; 8, recovering spent; 2, resting. Except for Patagonian toothfish and rock cod, the finfish species assessed in this study are multiple batch spawners (Macchi et al. 2021; Brickle et al. 2006). Stage 2 (resting) denotes a post-spawning condition and is therefore presented last in developmental sequence. For squid, macroscopic assessment of sex and maturity were conducted following a six-stage maturity scale (Lipinski 1979): 1, young; 2, immature; 3, preparatory; 4, maturing; 5, mature; 6, spent.

The sampling of fish and squid was prioritised (sharks and skates included, although data on these taxa are not presented in the current report). Benthos sorting was conducted either concurrently with or following the sampling of the primary commercial species. Occasionally, small juvenile fish were encountered within the benthos samples after completing the processing of the 100 random samples, and therefore these were not included within the random samples.

### 3.7. Length composition

3.7.1. Length-weight relationship.

Length and weight data were retrieved from the FIFD database, records with missing length or weight values, or with length or weight values ≤ 0 were removed. Individuals recorded as hermaphrodites (database code H) or with unidentified sex were also removed. Length measurements were rounded to the lower 0.5 cm for squids, and to the lower 1.0 cm for finfish. To capture the smaller range of sizes, individuals recorded as juveniles were randomly assigned to either female or male with equal probability (50:50) using a fixed random seed to ensure reproducibility.

Length-weight relationships were fitted separately for each species and sex combination using the standard power function (Le Cren 1951):

$$W = a \cdot L^b$$

this was estimated via log-linearisation, fitting ordinary least squares regression of the form:

$$ln(W) = ln(a) + b \cdot ln(L)$$

where $W$ is total weight (g), $L$ is length (cm), $a$ is the condition factor, and $b$ is the allometric growth coefficient (Froese 2006).

An initial model was fitted per species-sex to identify and remove outliers. Observations with absolute standardised residuals exceeding 2.5 standard deviations were excluded (Froese 2006). Additional outliers considered biologically implausible or likely data entry errors were removed based on visual inspection of the data. Final length-weight parameters were estimated by refitting the model on the cleaned dataset. Length-weight relationships were visualised for each species and sex by overlaying fitted power curves on scatter plots of the observed data. To improve plot clarity where sample sizes were large, a random subsample of points was displayed, with a fixed random seed applied for reproducibility. However, the model and model parameters were drawn from the full cleaned data set (Appendix I). All plots were produced using the *ggplot2* (Wickham 2016) and the *patchwork* packages (Pedersen 2024) in R (version 4.5.1; R Core Team 2025). Final length-weight parameters were used to calculate weight (g) from length (cm) for each species random samples collected during the surveys.

### 3.7.2. Overall length composition

Biomass-at-length distributions were constructed at the species, survey, and sex levels (all years pooled), and for each species × year × sex combination. Extrapolation of sample weight-at-length class to total biomass estimate was done by summing the weight of individuals in each length class and calculating the proportion of the weight in each length class to the total sample weight. This proportion was then applied to the biomass estimate to obtain an extrapolated biomass per length class, and per sex in length class.

### 3.7.3. Comparative length composition at the survey and sex levels

The proportional biomass-at-length distribution was computed to assess differences in the size composition between groundfish and calamari pre-season surveys, and between sexes. Overlap between pairs of biomass-at-length distributions (groundfish vs. calamari pre-season surveys; females vs. males) was calculated following Swanson et al. (1974):

$$O = \left(1 - \frac{1}{2}\sum_{i=1}^{n}|p_{1i} - p_{2i}|\right) \times 100$$

where $O$ is the overlap index (%), $p_{1i}$ is the proportional biomass in length class $i$ for group 1, $p_{2i}$ is the proportional biomass in length class $i$ for group 2, $n$ is the total number of length classes, $\sum_{i=1}^{n} | p_{1i} - p_{2i} |$ is the sum of absolute differences across all length classes. The overlap index ranges from 0% (no overlap between distributions) to 100% (complete overlap).

Differences in the biomass-weighted mean length between groups were assessed using a weighted permutation test (10,000 permutations), in which the observed difference in biomass-weighted mean lengths between the two groups was compared against a null distribution generated by randomly permuting group labels while retaining the original biomass weights (Manly 2007). A fixed random seed was used to ensure reproducibility. The p-value was calculated as the proportion of permuted differences equal to or exceeding the absolute observed difference in weighted means, providing a two-tailed test of significance that requires no distributional assumptions.

For each species, survey, and sex biomass-at-length distribution, the biomass-weighted mean length was computed using the proportional biomass of each length class as weights, with its uncertainty expressed as the standard error of the weighted mean. The effective sample size ($n_{eff}$) was calculated as the inverse of the sum of squared biomass proportions ($n_{eff} = 1/\sum p_i^2$), which accounts for the unequal weighting of length classes and provides a more appropriate denominator for the standard error of the weighted mean than the raw count of length classes (Kish 1965). The standard error of the weighted mean was then computed as $SE = SD/\sqrt{n_{eff}}$. Biomass-weighted quantiles were calculated at the 0th, 2.5th, 50th, 97.5th, and 100th percentiles of the length distribution using proportional biomass as weights. Standard errors for all percentile estimates were derived by bootstrap resampling with replacement (10,000 resamples; Efron & Tibshirani 1993), with weights renormalised after each resample and the standard deviation of the bootstrap distribution taken as the standard error. All length metrics were rounded down to the nearest 0.5 cm for squids, and to the nearest 1.0 cm for finfish. Weighted quantiles and mean were calculated using the *Hmisc* package (Harrell 2024) in R (version 4.5.1; R Core Team 2025).

### 3.7.4. Yearly length composition

The yearly composition of biomass at length-class was analysed for each species. The biomass-weighted mean length, quantiles at the 0th, 2.5th, 50th, 97.5th, and 100th percentiles of the length distribution, and standard errors were calculated as per the previous section. To calculate modal length, GAM (Wood 2017) was fitted to the binned biomass-at-length class data (biomass per 0.5 cm length class for squids, and per 1.0 cm length class for finfish) using a Gaussian error distribution, with length class as the smooth predictor term:

$$B \sim s(length,\ k)$$

where *B* is the biomass per length class, *s* denotes a thin-plate regression spline (Wood 2003), and *k* is the maximum number of knots, set adaptively between 3 and 15 based on the number of unique length classes available per group. The modal length was extracted as the length class corresponding to the peak of the fitted GAM smooth. All GAMs were fitted by REML using the *mgcv* package (Wood 2011) in R (version 4.5.1; R Core Team 2025).

## 3.8. Sex and maturity composition

Biomass was extrapolated for each sex category (juvenile, female, male, and undetermined) for each species in every year, and expressed as a percentage of the total annual biomass for the species. Overall sex composition for each species was summarised as the mean annual proportion ± SE across the time series.

Sexual maturity composition was determined for each species, year and sex, with only females and males included. Individual weights were summed by maturity stage for each sex within each year, and expressed as a percentage of the total sampled weight for that sex. Maturity stage proportions were additionally applied to the annual biomass estimate for each species to extrapolate biomass by maturity stage.

# 4. Results and Discussion

## 4.1. Bottom trawl stations

A total of 1,974 bottom trawls were conducted during the February groundfish and calamari pre-season surveys in 2010–2011, and 2015–2026. In groundfish surveys, a range of 42 to 97 trawls were conducted, with catches between 45 and 196 t considering only the species assessed in this report. In calamari pre-season surveys, a range of 55 to 64 trawls were conducted, with catches between 169 and 967 t considering only the species assessed in this report.

In 2026, a total of 82 trawls (105 t) were conducted in the groundfish survey aboard the *F.V.* Argos Vigo (ZDLU1), and 64 trawls (597 t) were conducted in the calamari pre-season survey aboard the *F.V.* Monteferro (ZDLM3) (Table III).

## 4.2. Biomass estimates

For most species in February 2026, the 10,000 biomass sample iterations showed a Gaussian distribution. For these species, the deterministic, mean, and median biomass estimates were in close agreement, indicating that the biomass distributions were approximately symmetrical and that any of the three biomass estimates can be considered reliable (Fig. 2). For hoki, southern blue whiting and southern hake, the 10,000 biomass samples had multimodal distributions, and the mean diverged from the deterministic and the median biomass estimates. For hoki, the mean (157,724 t) was considerably below the deterministic (189,741 t) and the median (198,889 t) estimates, suggesting that the mean may underestimate biomass due to left-skewed biomass distribution. For southern blue whiting and for southern hake, the mean (47,634 t and 7,390 t, respectively) diverged from the deterministic (55,309 t and 8,233 t, respectively) and the median (56,941 t and 8,228 t, respectively) estimates (Fig. 2). In these cases, where the biomass distribution was skewed, the median was considered the most appropriate estimate as it is robust to extreme values and represents more appropriately the central tendency. Therefore, the median was selected to describe patterns of biomass through time and biomass-related calculations.

Biomass estimates from the February parallel demersal surveys conducted in 2010–2011, and 2015–2026 were as low as 205.68 t (146.47 – 263.11 t) for the Argentine shortfin squid in 2016 and as high as 877,550.22 t (716,079.56 – 1,064,218.58 t) for rock cod in 2011. In 2026, the lowest estimate of biomass was for the Argentine shortfin squid with 715.87 t (479.82 – 1,021.76 t), and the highest estimate of biomass was for rock cod with 284,049.54 t (171,313.65–397,708.75 t) (Table IV).

Of the 11 species assessed, three species exhibited signs of increasing biomass (common hake, Patagonian toothfish, and southern hake), four species exhibited signs of decreasing biomass (hoki, kingclip, red cod, and rock cod), and four species did not exhibit temporal biomass trends (Argentine shortfin squid, banded whiptail grenadier, Patagonian squid, and southern blue whiting) (Table V).

Table III. February groundfish and calamari pre-season surveys information. Catches per survey and combined total include Argentine shortfin squid, banded whiptail grenadier, common hake, hoki, kingclip, Patagonian squid, Patagonian toothfish, red cod, rock cod, southern blue whiting, and southern hake.

| Year | Groundfish survey | | | | Calamari pre-season survey | | | | Total | |
|---|---|---|---|---|---|---|---|---|---|---|
| | Vessel (Callsign) | No. of trawls | Trawls excluded | Catch (t) | Vessel (Callsign) | No. of trawls | Trawls excluded | Catch (t) | No. of trawls | Catch (t) |
| 2010 | Castelo (ZDLT1) | 87 | 478, 501 | 194.24 | Beagle F.I. (ZDLZ) | 55 | NA | 457.99 | 142 | 652.23 |
| 2011 | Castelo (ZDLT1) | 88 | NA | 196.05 | Venturer (ZDLP1) | 58 | NA | 257.28 | 146 | 453.33 |
| 2015 | Castelo (ZDLT1) | 89 | NA | 121.35 | Baffin Bay (MSPL9) | 57 | NA | 392.82 | 146 | 514.17 |
| 2016 | Castelo (ZDLT1) | 90 | NA | 87.32 | Sil (ZDLR1) | 56 | 638 | 206.62 | 146 | 293.94 |
| 2017 | Castelo (ZDLT1) | 90 | 2328 | 47.35 | Argos Vigo (ZDLU1) | 58 | 1002 | 254.29 | 148 | 301.64 |
| 2018 | Monteferro (ZDLM3) | 97 | 143,144,156,164,183 | 80.91 | Castelo (ZDLT1) | 59 | NA | 169.47 | 156 | 250.38 |
| 2019 | Monteferro (ZDLM3) | 79 | 240,242,244,246 | 45.09 | Argos Cíes (ZDLS3) | 52 | 25,29,37 | 418.44 | 131 | 463.53 |
| 2020 | Castelo (ZDLT1) | 80 | NA | 47.89 | Argos Cíes (ZDLS3) | 59 | NA | 283.83 | 139 | 331.72 |
| 2021 | Castelo (ZDLT1) | 80 | 3388,3391,3392,3393 | 74.67 | Capricorn (ZDLY) | 55 | NA | 347.85 | 135 | 422.52 |
| 2022 | Castelo (ZDLT1) | 42 | NA | 45.61 | Argos Cíes (ZDLS3) | 60 | NA | 445.51 | 102 | 491.12 |
| 2023 | Castelo (ZDLT1) | 84 | NA | 67.63 | Igueldo (ZDLE1) | 61 | 1174 | 610.63 | 145 | 678.26 |
| 2024 | Castelo (ZDLT1) | 84 | NA | 66.26 | New Polar (ZDLF2) | 64 | NA | 966.75 | 148 | 1,033.41 |
| 2025 | Argos Vigo (ZDLU1) | 84 | NA | 75.31 | Golden Chicha (ZDLC1) | 60 | NA | 420.98 | 144 | 496.29 |
| 2026 | Argos Vigo (ZDLU1) | 82 | NA | 105.34 | Monteferro (ZDLM3) | 64 | NA | 596.50 | 146 | 701.84 |

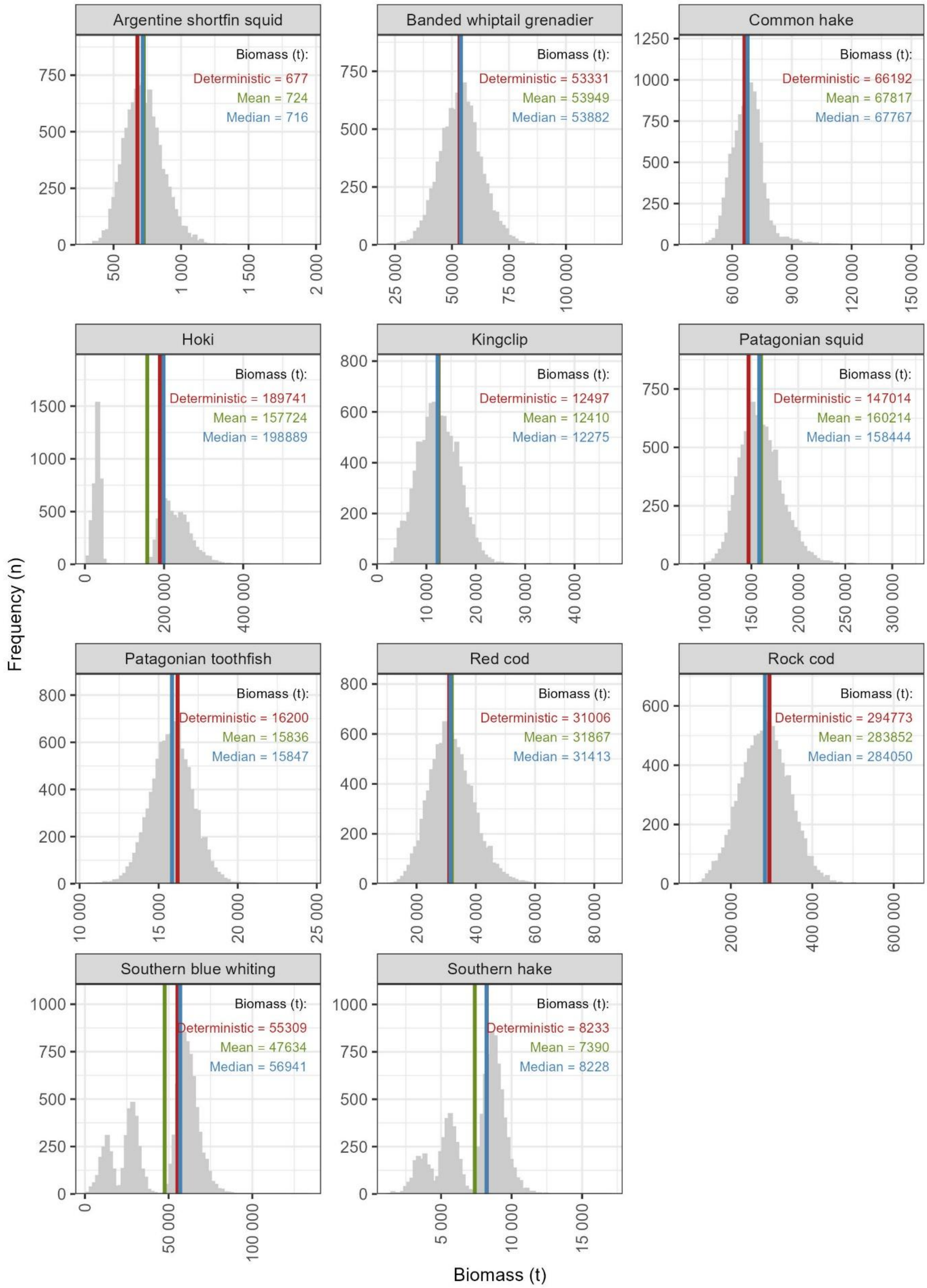


Fig. 2. Biomass (t) distribution of the 10,000 bootstrap samples estimated from February 2026 groundfish and calamari pre-season surveys conducted in Falkland Islands waters. Deterministic, mean, and median biomasses are indicated by the red, green, and blue vertical lines, respectively.

Table IV. Biomass estimates (t; median) of main commercial species during the February 2010–2011 and 2015–2026 groundfish and calamari pre-season surveys in Falkland Islands waters. The 95% confidence intervals are indicated in parentheses.

| Year | Argentine shortfin squid | Banded whiptail grenadier | Common hake | Hoki |
|---|---|---|---|---|
| 2010 | 8561.62 | 70414.52 | 9226.39 | 303807.12 |
| | (3510.35–13384.35) | (40514.45–98311.11) | (6280.46–12219.25) | (188264.88–457666.96) |
| 2011 | 9668.54 | 44097.54 | 10454.74 | 222428.08 |
| | (6777.82–12564.25) | (20547.39–73607.37) | (8330.32–12809.67) | (172507.38–281186.26) |
| 2015 | 214367.18 | 60136.64 | 15777.99 | 127304.43 |
| | (129839.58–365643.99) | (35864.88–77202.47) | (13700.90–18213.42) | (44674.67–179592.78) |
| 2016 | 205.68 | 35321.85 | 3618.28 | 162159.16 |
| | (146.47–263.11) | (8500.93–55042.45) | (2974.25–4175.68) | (79371.74–222823.65) |
| 2017 | 12385.14 | 33965.70 | 12708.88 | 28115.60 |
| | (7412.76–18225.10) | (19596.89–43533.35) | (10191.95–15538.58) | (16801.50–38817.08) |
| 2018 | 46782.80 | 35595.25 | 8576.35 | 148685.33 |
| | (30158.94–64394.07) | (27633.27–43657.43) | (6048.05–10877.41) | (92768.34–204228.49) |
| 2019 | 61285.80 | 22994.41 | 11460.22 | 42606.32 |
| | (40113.04–93531.22) | (9186.12–36085.96) | (9483.58–14419.93) | (5779.47–166317.90) |
| 2020 | 144318.47 | 24864.42 | 3354.24 | 77664.95 |
| | (89302.24–196203.10) | (8358.90–43250.89) | (2846.51–3971.84) | (20203.23–143531.23) |
| 2021 | 43038.39 | 69256.60 | 34184.59 | 232140.93 |
| | (20466.20–68912.67) | (32834.53–85342.42) | (27502.33–40938.52) | (92470.50–431476.19) |
| 2022 | 5802.28 | 51225.65 | 43833.05 | 147807.66 |
| | (2397.40–30856.33) | (25192.54–102067.28) | (32223.84–55471.45) | (12362.55–248962.54) |
| 2023 | 11361.95 | 35225.06 | 33684.98 | 133362.05 |
| | (7614.37–15619.55) | (22666.50–46028.90) | (28532.20–39221.03) | (37696.82– 212465.82) |
| 2024 | 66111.82 | 36649.36 | 23470.57 | 48180.8 |
| | (52241.58–81690.59) | (20129.73–49562.23) | (17585.78–66611.91) | (22017.84–77799.87) |
| 2025 | 53575.99 | 28151.94 | 87636.50 | 6939.02 |
| | (32561.35–74764.10) | (19309.04–36038.47) | (63653.77–107187.97) | (1973.31–12060.90) |
| 2026 | 715.87 | 53881.73 | 67767.40 | 198888.83 |
| | (479.82–1021.76) | (36978.66–72186.80) | (54460.41–85695.81) | (15796.05–302912.17) |

Table IV. *continued*

| Year | Kingclip | Patagonian squid | Patagonian toothfish | Red cod |
|---|---|---|---|---|
| 2010 | 21384.02 | 195368.45 | 9345.13 | 97398.08 |
| | (13705.30–28607.34) | (160421.18–239516.37) | (7096.05–11727.84) | (18335.99–158897.80) |
| 2011 | 43782.78 | 50035.50 | 10497.74 | 161971.29 |
| | (28424.85–63121.38) | (39537.83–62533.45) | (7859.83–13377.29) | (39230.31–258711.16) |
| 2015 | 77455.04 | 117822.69 | 3542.00 | 105434.82 |
| | (30150.81–124958.88) | (82994.09–164421.27) | (1359.57–4477.02) | (45278.81–160780.36) |
| 2016 | 25751.40 | 43724.10 | 7530.96 | 100370.44 |
| | (13955.05–39613.42) | (34357.75–53300.16) | (5373.64–10194.34) | (28384.22–149860.74) |
| 2017 | 19261.68 | 186794.16 | 8894.12 | 58643.11 |
| | (11873.32–28544.00) | (145101.61–234454.73) | (5662.92–11183.99) | (22863.35–86532.41) |
| 2018 | 15748.08 | 66682.27 | 8473.22 | 63750.35 |
| | (11069.78–21527.00) | (44073.52–96689.36) | (6276.48–10886.50) | (19277.51–117355.42) |
| 2019 | 20939.10 | 220848.11 | 6054.04 | 76432.13 |
| | (14764.62–28127.04) | (188175.67–259467.94) | (3162.82–7794.58) | (35235.62–119480.37) |
| 2020 | 16038.56 | 98557.06 | 2455.74 | 21650.86 |
| | (10052.06–26304.43) | (80832.08–126778.53) | (1621.34–3392.18) | (10993.21–32014.04) |
| 2021 | 23043.42 | 126960.64 | 4067.52 | 35970.33 |
| | (12901.88–35823.59) | (98119.16–165138.90) | (2825.50–4845.25) | (22852.74–51663.11) |
| 2022 | 41845.11 | 173244.49 | 3474.29 | 78514.56 |
| | (14738.11–80447.75) | (131702.50–235968.93) | (2080.95–5151.07) | (34162.13–129660.26) |
| 2023 | 36732.33 | 205025.57 | 3261.76 | 37650.32 |
| | (18884.19–58232.85) | (156060.20–262829.20) | (1991.62–4590.57) | (20178.92–56206.64) |
| 2024 | 18659.38 | 225026.78 | 4086.59 | 46725.28 |
| | (11950.68–27609.68) | (181079.58–288983.91) | (3078.91–5092.08) | (20903.51–70057.72) |
| 2025 | 11421.45 | 114447.18 | 6274.84 | 16605.17 |
| | (4415.44–21118.61) | (93488.70–141403.72) | (4806.11–7627.01) | (6578.36–30412.18) |
| 2026 | 12274.62 | 158443.57 | 15847.05 | 31413.00 |
| | (4991.59–20246.84) | (123029.34–207371.92) | (13311.85–18335.51) | (18894.33–47443.24) |

Table IV. *continued*

| Year | Rock cod | Southern blue whiting | Southern hake |
|---|---|---|---|
| 2010 | 834775.00 (519306.26–1306091.27) | 60270.74 (25380.63–91314.04) | 5220.65 (3910.63–6443.37) |
| 2011 | 877550.22 (716079.56–1064218.58) | 148296.01 (42459.43–357267.81) | 5424.16 (3445.99–8095.63) |
| 2015 | 349259.00 (269667.68–432687.92) | 38948.64 (12197.06–80184.05) | 2845.29 (1750.69–4350.03) |
| 2016 | 233997.91 (177911.14–306135.45) | 85373.60 (25096.46–204263.77) | 1987.98 (1204.90–2963.73) |
| 2017 | 143654.90 (113896.56–176351.05) | 51677.08 (1375.47–65699.77) | 1894.58 (1021.33–2478.36) |
| 2018 | 91185.20 (63308.48–122537.23) | 50583.68 (17839.34–69597.20) | 1494.74 (978.54–1947.08) |
| 2019 | 44076.33 (29040.32–66668.90) | 5704.46 (205.30–34084.93) | 433.29 (88.45–577.12) |
| 2020 | 18727.72 (11656.70–27065.20) | 4548.88 (26.73–15435.54) | 611.87 (230.37–868.25) |
| 2021 | 56340.15 (45689.57–66885.68) | 13397.02 (3616.43–25713.15) | 1978.28 (919.34–2941.07) |
| 2022 | 92278.64 (58753.11–131454.56) | 15795.10 (877.49–48977.89) | 991.01 (574.62–1471.85) |
| 2023 | 64885.28 (51235.90–78204.69) | 36517.64 (9904.22–67656.97) | 1373.10 (629.48–2028.57) |
| 2024 | 126229.23 (87911.52–164719.01) | 64561.70 (21635.73–134012.68) | 2405.36 (1734.88–5932.60) |
| 2025 | 122121.43 (68446.37–173470.28) | 67087.67 (33451.15–112700.16) | 2156.42 (1259.63–2924.16) |
| 2026 | 284049.54 (171313.65–397708.75) | 56940.91 (9327.11–74100.25) | 8228.23 (3134.54–10285.31) |

Table V. Indicators of change in biomass in 2026 relative to the 2010, 2025, and the 2023–2025 mean biomasses, and over the period 2010 to 2026, derived from February groundfish and calamari pre-season surveys in Falkland Islands waters. Indicators 2026 vs 2010, 2026 vs 2025, and 2026 vs 2023–2025 mean represent the magnitude of change in biomass. The increase or the decrease in biomass is indicated by the symbols + and -, respectively*. Significance ($p < 0.05$) is indicated with bold font (*p* adjusted threshold = 0.017 for year-to-baseline comparisons).

| Species | Biomass 2010 (t) | Biomass 2025 (t) | Biomass 2023–2025 mean (t) | Biomass 2026 (t) | 2026 vs 2010 | 2026 vs 2025 | 2026 vs 2023–2025 mean | GAM 2010–2026 (*p* value) |
|---|---|---|---|---|---|---|---|---|
| Argentine shortfin squid | 8561.62 | 53575.99 | 43683.25 | 715.87 | **-0.084** | **-0.013** | **-0.016** | 0.758 |
| Banded whiptail grenadier | 70414.52 | 28151.94 | 33342.12 | 53881.73 | -0.765 | **+1.91** | **+1.62** | 0.388 |
| Common hake | 9226.39 | 87636.50 | 48264.02 | 67767.40 | **+7.34** | -0.773 | **+1.40** | **0.003; +** |
| Hoki | 303807.12 | 6939.02 | 62827.30 | 198888.83 | -0.654 | **+28.66** | +3.17 | 0.057 |
| Kingclip | 21384.02 | 11421.45 | 22271.05 | 12274.62 | -0.574 | +1.07 | **-0.55** | **0.012; -** |
| Patagonian squid | 195368.45 | 114447.18 | 181499.84 | 158443.57 | -0.811 | **+1.38** | -0.873 | 0.407 |
| Patagonian toothfish | 9345.13 | 6274.84 | 4541.07 | 15847.05 | **+1.70** | **+2.53** | **+3.49** | **0.003; +** |
| Red cod | 97398.08 | 16605.17 | 33660.25 | 31413.00 | -0.323 | +1.89 | -0.933 | **< 0.001; -** |
| Rock cod | 834775.00 | 122121.43 | 104411.98 | 284049.54 | **-0.340** | **+2.32** | **+2.72** | **< 0.001; -** |
| Southern blue whiting | 60270.74 | 67087.67 | 56055.67 | 56940.91 | -0.945 | -0.849 | +1.02 | 0.154 |
| Southern hake | 5220.65 | 2156.42 | 1978.29 | 8228.23 | +1.58 | **+3.82** | **+4.16** | **0.003; +** |

* For interpretation, the negative value -0.084 for the Argentine shortfin squid biomass comparison of 2026 vs 2010 indicates that the biomass in 2026 decreased and corresponded to 8.4% of the biomass in 2010. In contrast, the positive value +1.91 for the banded whiptail grenadier biomass comparison of 2026 vs 2025 indicates that the biomass in 2026 represented an approximately two-fold increase relative to the 2025 biomass

### 4.3. Species summaries

#### 4.3.1. Argentine shortfin squid (*Illex argentinus*)

4.3.1.1. Temporal patterns of abundance

On average, 88% of the total Argentine shortfin squid catches in the time series were from groundfish surveys and 12% were from calamari pre-season surveys. The highest catch in the time series was reported in 2015 (31.87 t); the second lowest catch was reported in 2026 (0.29 t), corresponding to 33.2% of the 2010 catch (0.88 t), 2.3% of the 2025 catch (13.01 t), and 2.7% of the 2023–2025 mean (10.91 t; Fig. 3a; Appendix II).

The highest densities occurred in 2015 (1,458.44 ± 540.06 kg/km²; mean ± SE). The second lowest densities were reported in 2026 (4.99 ± 0.97 kg/km²), representing 16.8% of the 2010 densities (29.65 ± 9.91 kg/km²), 1.2% of the 2025 densities (430.07 ± 127.28 kg/km²), and 1.5% of the 2023–2025 mean (331.70 ± 53.68 kg/km²; Fig. 3b).

The highest biomass in the time series was recorded in 2015 (214,367.18 t). Biomass in 2026 (715.87 t) was the second lowest on record, representing 8.4% of 2010 levels (8,561.62 t), 1.3% of 2025 biomass (53,575.99 t), and 1.6% of the 2023–2025 mean (43,683.25 t), with all comparisons showing statistically significant declines ($p < 0.001$; Fig. 3c; Table IV–V; Appendix III–IV). Analysis of the full time series revealed no significant temporal trend in biomass (GAM: edf = 1.34, $F = 0.36$, $p = 0.758$). The fitted model explained only 4.5% of the deviance ($R^2$ adj. = −0.053), reflecting high interannual variability with no consistent directional change in biomass in the time series (Fig. 3c; Appendix V).

4.3.1.2. Spatial patterns of abundance

In 2026, *I. argentinus* was distributed in small densities mainly through the west, and the highest density (78 kg/km²) was observed to the north-west at approximately 50°S and 62°W, near the limit of the FICZ. Similar patterns of distribution were observed in 2010, and from 2023 to 2025, with comparatively higher densities in those years (Fig. 4). However, the highest density in the full time series was reported to the north of East Falkland during 2015 (74,434 kg/km²).

Analysis of the spatial change in density revealed an overall density decrease through the survey area. Comparison of densities in 2026 relative to 2010 showed that substantial decreases in density occurred to the north-west in the FICZ/FOCZ, while densities increased predominantly to the south in the FICZ, along the ‘Loligo Box’, and to the north-west of the northern limit of the ‘Loligo Box’. Comparisons of 2026 with 2025, as well as with the 2023–2025 mean, showed patchy increases in density to the south in the FICZ and in the south of the ‘Loligo Box’ (Fig. 5).

4.3.1.3. Length composition

Across all survey years combined, dorsal mantle length of the Argentine shortfin squid was in the range of 5.0 to 36.5 cm; however, 95% of the estimated biomass was comprised of individuals between 15.0 and 28.0 cm, with a median length of 24.0 ± 0.65 cm (median ± SE) and a mean length of 23.0 ± 0.79 cm (mean ± SE; Fig. 6a).

The distribution of biomass proportions by size class exhibited a 14% overlap between the groundfish and calamari pre-season surveys. Accordingly, the biomass-weighted mean length was significantly different ($p < 0.001$) between the groundfish (23.5 ± 0.75 cm; mean ± SE) and the calamari pre-season (15.0 ± 0.70 cm) surveys, i.e., individuals collected in the groundfish survey were generally larger than individuals collected in the calamari pre-season survey. In the groundfish survey, 95% of the biomass of Argentine shortfin squid was comprised of individuals between 16.5 and 28.0 cm dorsal mantle length, with a median length of 24.0 ± 0.64 cm. In the calamari pre-season survey, 95% of the biomass of Argentine shortfin squid was comprised of individuals between 10.5 and 22.0 cm, with a median length of 15.5 ± 0.76 cm (Fig. 6b).

The distribution of biomass proportions by size class exhibited an 80% overlap between females and males. However, the permutation analysis revealed that the biomass-weighted mean length was significantly different ($p = 0.003$) between females (24.0 ± 0.77 cm) and males (22.0 ± 0.83 cm). For females, 95% of the biomass was comprised of individuals between 16.5 and 28.5 cm, with a median length of 24.5 ± 0.63 cm. For males, 95% of the biomass was comprised of individuals between 13.5 and 25.5 cm, with a median length of 23.0 ± 0.62 cm (Fig. 6c).

The distribution of the biomass-at-length class was multimodal, with the smallest length-group exhibiting a modal length at 10.0–12.0 cm. At larger sizes, at least two length-groups were identified, with the modal lengths at 15.0–17.0 cm and 22.0–23.0 cm. Additional length-groups may have been present; however, they were not clearly distinguished because of overlap in size distributions (Fig. 7). In 2026, the size structure remained broad and multimodal. Dorsal mantle length was in the range of 6.0 to 28.0 cm; however, 95% of the biomass was comprised of individuals between 11.5 and 25.5 cm, with a median length of 19.0 ± 0.78 cm and a mean length of 18.5 ± 0.78 cm. For females, 95% of the biomass was comprised of individuals between 11.5 and 26.0 cm, with a median length of 19.5 ± 0.82 cm and a mean length of 19.0 ± 0.79 cm. For males, 95% of the biomass was comprised of individuals between 11.5 and 24.5 cm, with a median length of 18.5 ± 0.81 cm and a mean length of 18.0 ± 0.79 cm (Fig. 7).

Analysis of the full time series revealed no significant temporal trend in either mean (GAM: edf = 3.53, $F = 2.06$, $p = 0.169$, $R^2$ adj. = 0.389, DE = 55.5%) or median (GAM: edf = 3.12, $F = 1.56$, $p = 0.288$, $R^2$ adj. = 0.266, DE = 44.3%) dorsal mantle length. Despite the absence of a statistically significant trend, the fitted smooths captured moderate interannual variability, with both mean and median lengths declining from approximately 23–24 cm in 2010–2011 to a minimum of around 20 cm in 2015–2016, recovering to approximately 24–25 cm between 2017 and 2025, and declining again toward 2026 (Fig. 8). The low values observed in 2016 reflect an anomalous size composition associated to the collapse of this stock in that year.

#### 4.3.1.4. Sex and maturity composition

Across all survey years combined, the biomass composition of Argentine shortfin squid was dominated by females, comprising 65.2 ± 2.3% (mean ± SE) of total biomass, followed by males at 34.1 ± 2.2%, with juveniles and individuals of undetermined sex each accounting for 0.3 ± 0.3%, each. Interannual variability in sex composition was evident throughout the time series, with the female proportion ranging from 54% in 2015 to 83% in 2010, and the male proportion ranging from 17% in 2010 to 46% in 2015. Juveniles and individuals of undetermined sex were rare and recorded only in 2016 (4% of biomass, each). In 2026, the sex composition was characterised by a lower proportion of females (55%) and a correspondingly higher proportion of males (45%), with no juveniles or individuals of undetermined sex recorded (Fig. 9).

Maturity composition differed markedly between sexes throughout the time series (Fig. 10). Females were predominantly immature in most years (> 50%), with maturing and mature individuals rarely exceeding 10% combined. In contrast, males were predominantly mature in most years, except for 2015, 2016, and 2026, when the composition was dominated by less advanced maturity stages.

#### 4.3.1.5. Discussion

Analysis of the full time series revealed no significant temporal trend in biomass of Argentine shortfin squid in Falkland Islands waters, reflecting high interannual variability. This finding is supported by a flat, non-significant trend of commercial fishery CPUE data from 1984 to 2019 based on LOESS smoothing (Arkhipkin et al. 2022a). Females had a higher contribution to the biomass compared to males. Males reached advanced maturity within the survey area this time of the year while females remain largely pre-reproductive. In addition, mean and median dorsal mantle length had no significant temporal trends, suggesting that size composition has remained relatively stable over the time series despite the large fluctuations in abundance. A similar pattern was observed in commercial fishery data, where size at recruitment and size at maturity did not change significantly between 1984 and 2019 (Arkhipkin et al. 2022a). The low biomass and reduced mean and median lengths observed in 2016 are likely linked, reflecting the low availability and small size of squid in the survey area following the stock collapse after the peak in biomass in 2015. This pattern is consistent with commercial fishery data, with the highest catch on record in Falkland Islands waters reported in 2015 (357,724 t) followed by a collapse in 2016 (2,239 t; Falkland Islands Government 2025). Together, the biomass and length data suggest that the population of Argentine shortfin squid is characterised by high interannual variability in abundance but relative stability in size composition.

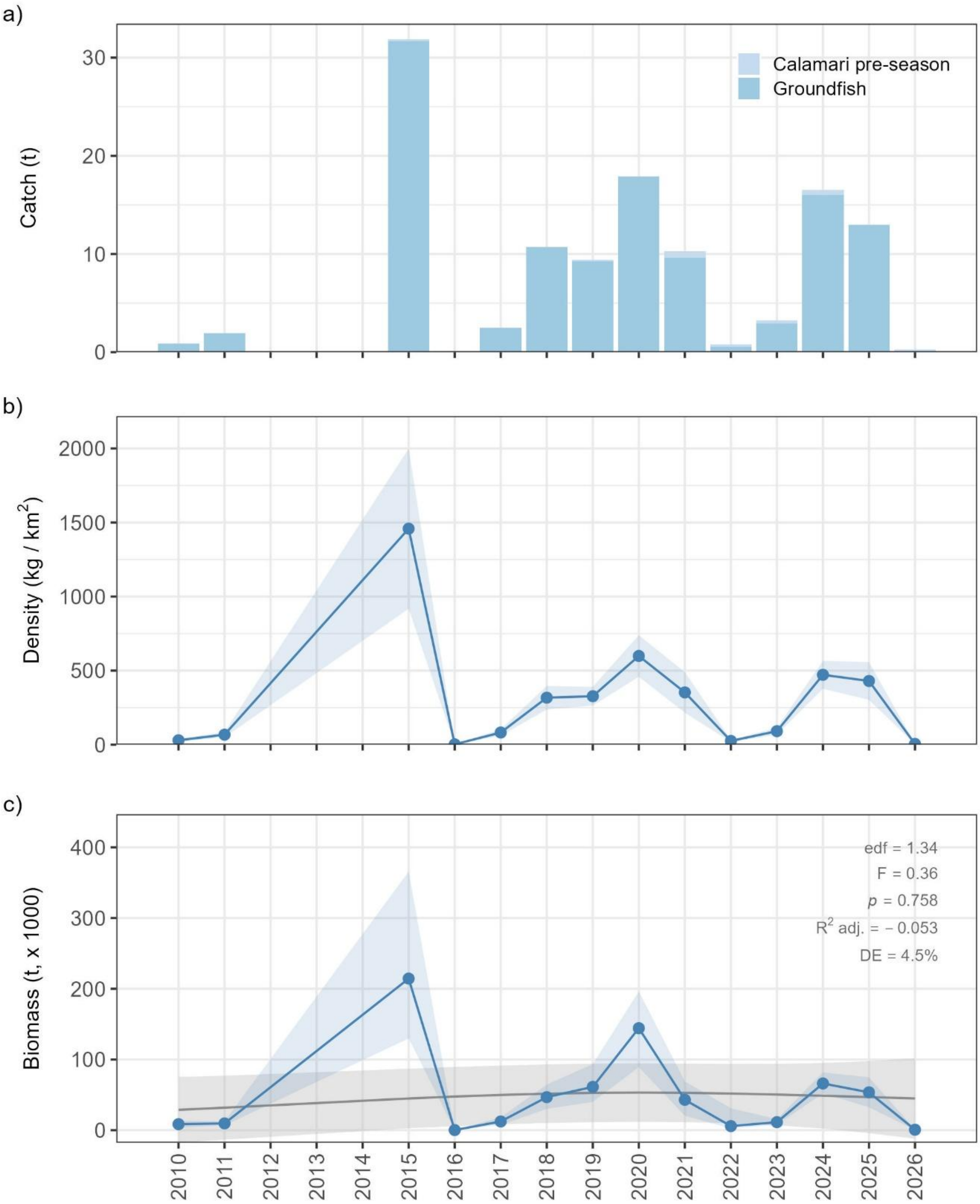


Fig. 3. Abundance of Argentine shortfin squid (*Illex argentinus*) during February groundfish and calamari pre-season surveys conducted in Falkland Islands waters in 2010–2011 and 2015–2026. (a) Catch per survey, (b) annual mean density ± SE represented by the blue line and shaded region, respectively, and (c) estimated biomass, where the blue line and shaded region represent the median and 95% pointwise confidence interval derived from 10,000 bootstrap biomass estimates, and the grey line and shaded region represent the fitted Generalised Additive Model (GAM) smooth and its 95% pointwise confidence interval.

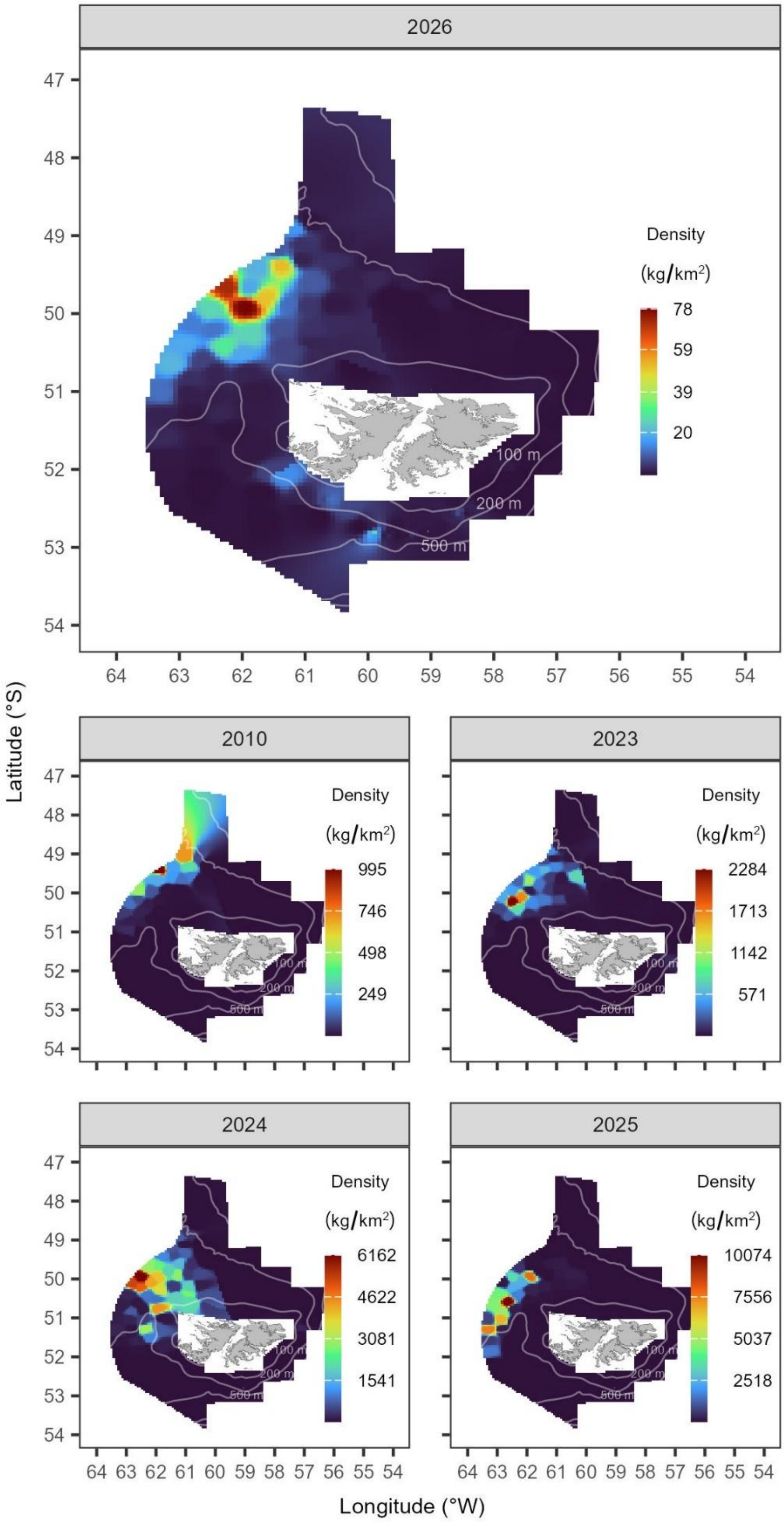


Fig. 4. Density distribution of the Argentine shortfin squid (*Illex argentinus*) derived from the February 2026 groundfish and calamari pre-season surveys in Falkland Islands waters, compared with the first year of the time series (2010) and the three preceding years (2023–2025). Colour scales are specific to each year. Isobaths at 100 m, 200 m, and 500 m are shown.

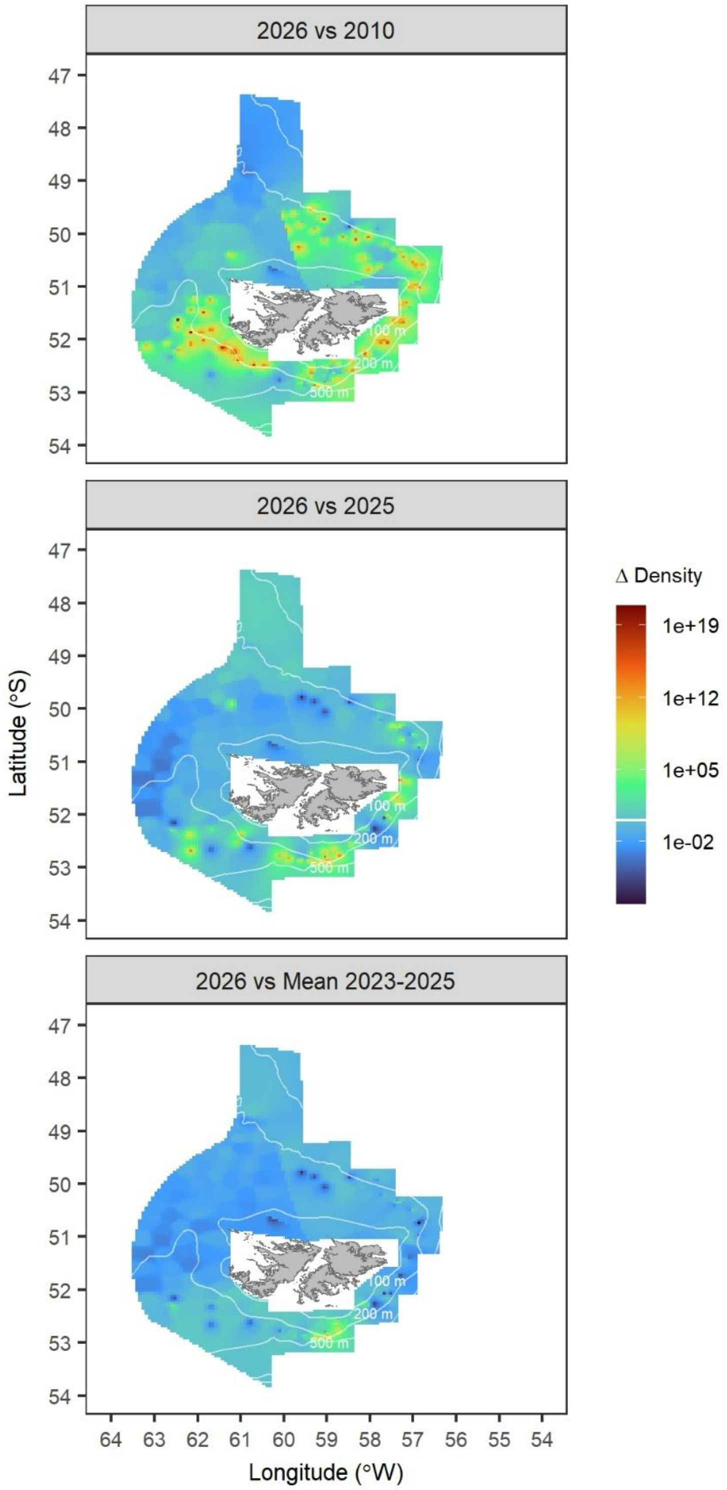


Fig. 5. Spatial change in density of the Argentine shortfin squid (*Illex argentinus*) derived from the February 2026 groundfish and calamari pre-season surveys in Falkland Islands waters, relative to the first year of the time series (2010), the previous year (2025), and the mean of the three preceding years (2023–2025). The spatial change in density is expressed as the ratio of density (kg/km$^2$) in 2026 relative to the density in the baseline year (2010, 2025, 2023–2025 mean). Isobaths at 100 m, 200 m, and 500 m are shown. The colour scale is $\log_{10}$-transformed to aid visualisation, with increases in density indicated above the horizontal white line towards dark red, and decreases in density indicated below the horizontal white line towards dark blue.

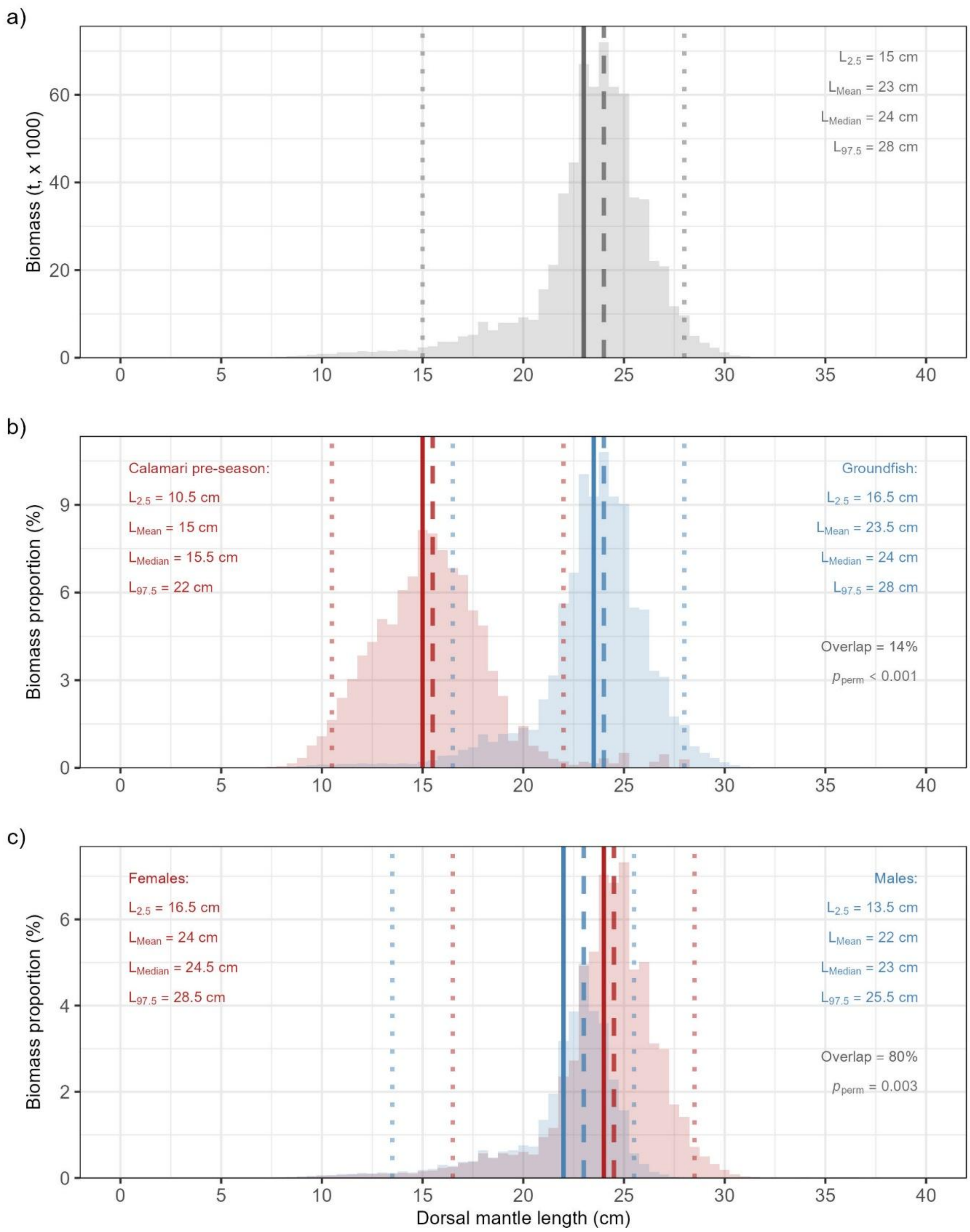


Fig. 6. Biomass-at-length class composition of Argentine shortfin squid (*Illex argentinus*) across all years combined, based on February groundfish and calamari pre-season surveys conducted in Falkland Islands waters in 2010–2011 and 2015–2026. a) Overall biomass-at-length frequency distribution. b) Overlap in biomass-at-length distributions between calamari pre-season (red) and groundfish (blue) surveys. c) Overlap in biomass-at-length distributions between females (red) and males (blue). Solid vertical lines indicate the mean length ($L_{Mean}$), dashed lines the median length ($L_{Median}$), and dotted lines the 2.5th and 97.5th length percentiles ($L_{2.5}$ and $L_{97.5}$, respectively). $p_{perm}$ is the significance of the weighted permutation test to assess differences between groups.

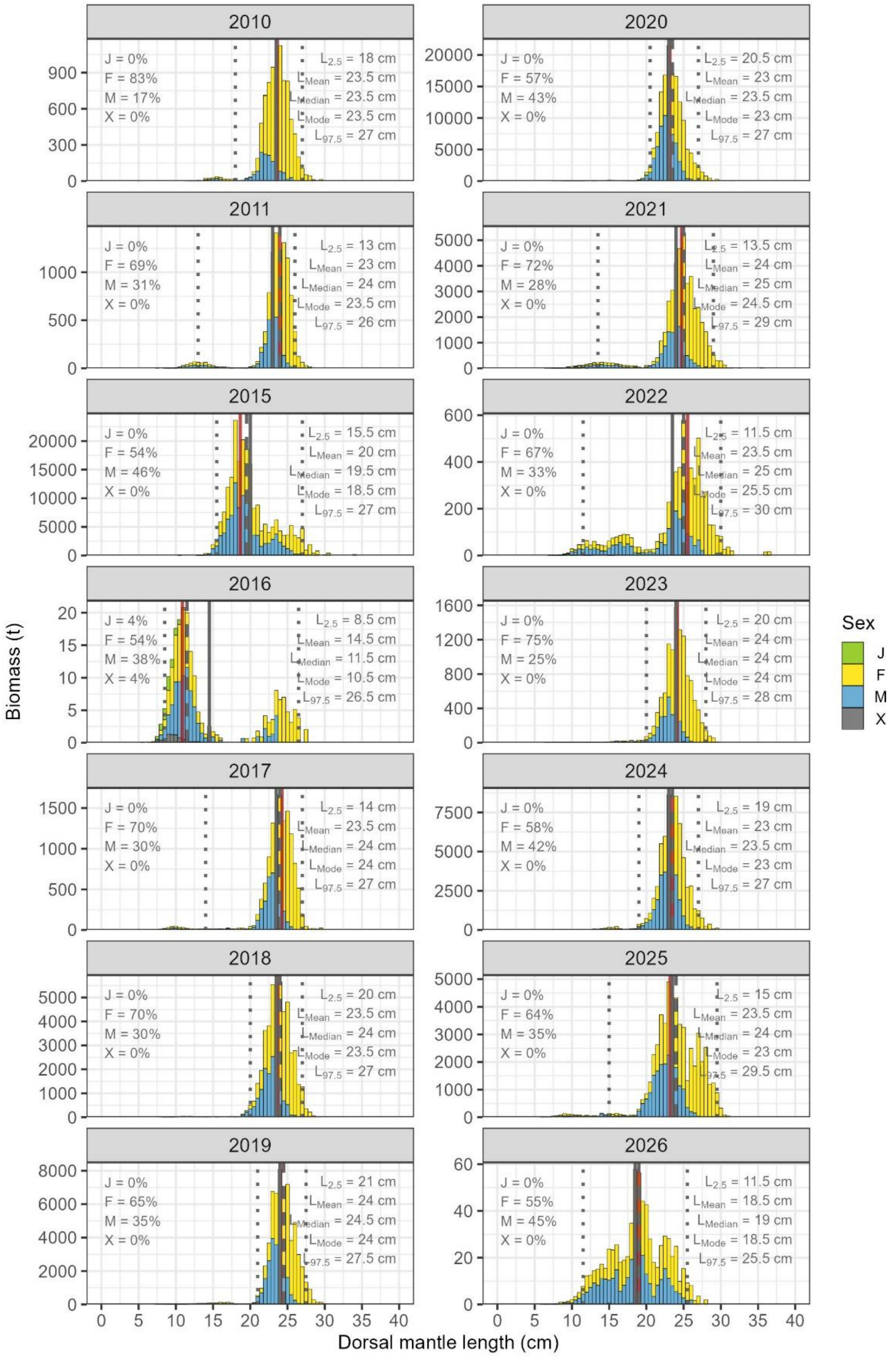


Fig. 7. Annual biomass-at-length class composition of Argentine shortfin squid (*Illex argentinus*) during February groundfish and calamari pre-season surveys conducted in Falkland Islands waters in 2010–2011 and 2015–2026. Stacked bars represent biomass (t) per 0.5 cm length class, partitioned by sex (J = juvenile; F = female; M = male; X = undetermined), with the proportion of total annual biomass for each sex indicated in the upper left of each panel. Vertical lines indicate the mean length ($L_{Mean}$, grey solid), median length ($L_{Median}$, grey dashed), modal length ($L_{Mode}$, red solid), and 2.5th and 97.5th percentiles ($L_{2.5}$ and $L_{97.5}$, grey dotted) of the biomass-weighted length distribution. Note the different y-axis scales among years.

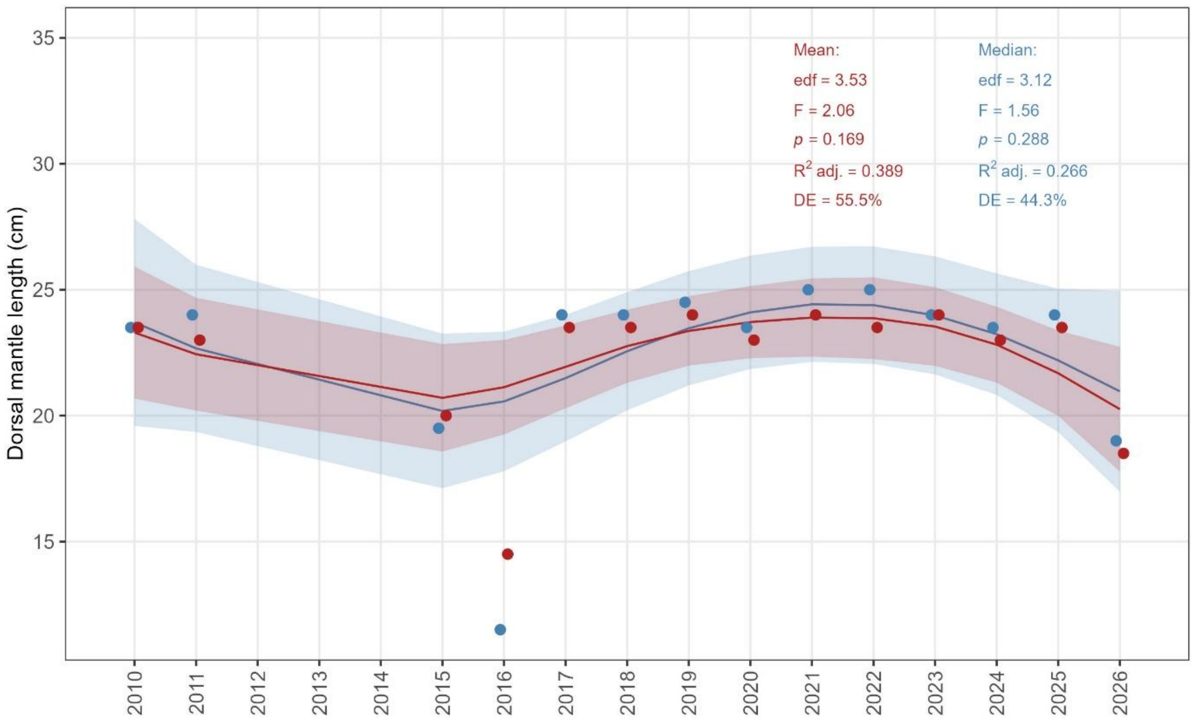


Fig. 8. Median (blue) and mean (red) dorsal mantle length of Argentine shortfin squid (*Illex argentinus*) during February groundfish and calamari pre-season surveys conducted in Falkland Islands waters in 2010–2011 and 2015–2026. The line and shaded region represent the fitted Generalised Additive Model (GAM) smooth and its 95% pointwise confidence interval.

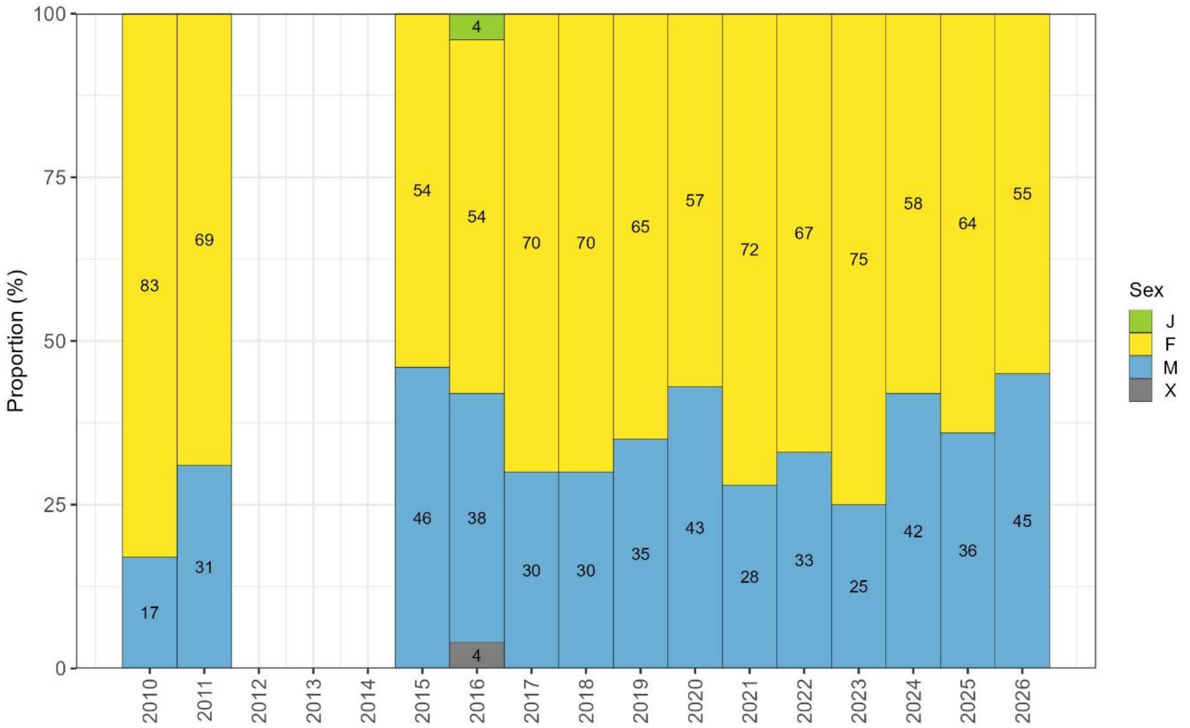


Fig. 9. Proportion by sex (J = juvenile; F = female; M = male; X = undetermined) of Argentine shortfin squid (*Illex argentinus*) during February groundfish and calamari pre-season surveys conducted in Falkland Islands waters in 2010–2011 and 2015–2026. Labels for proportions < 3% are omitted.

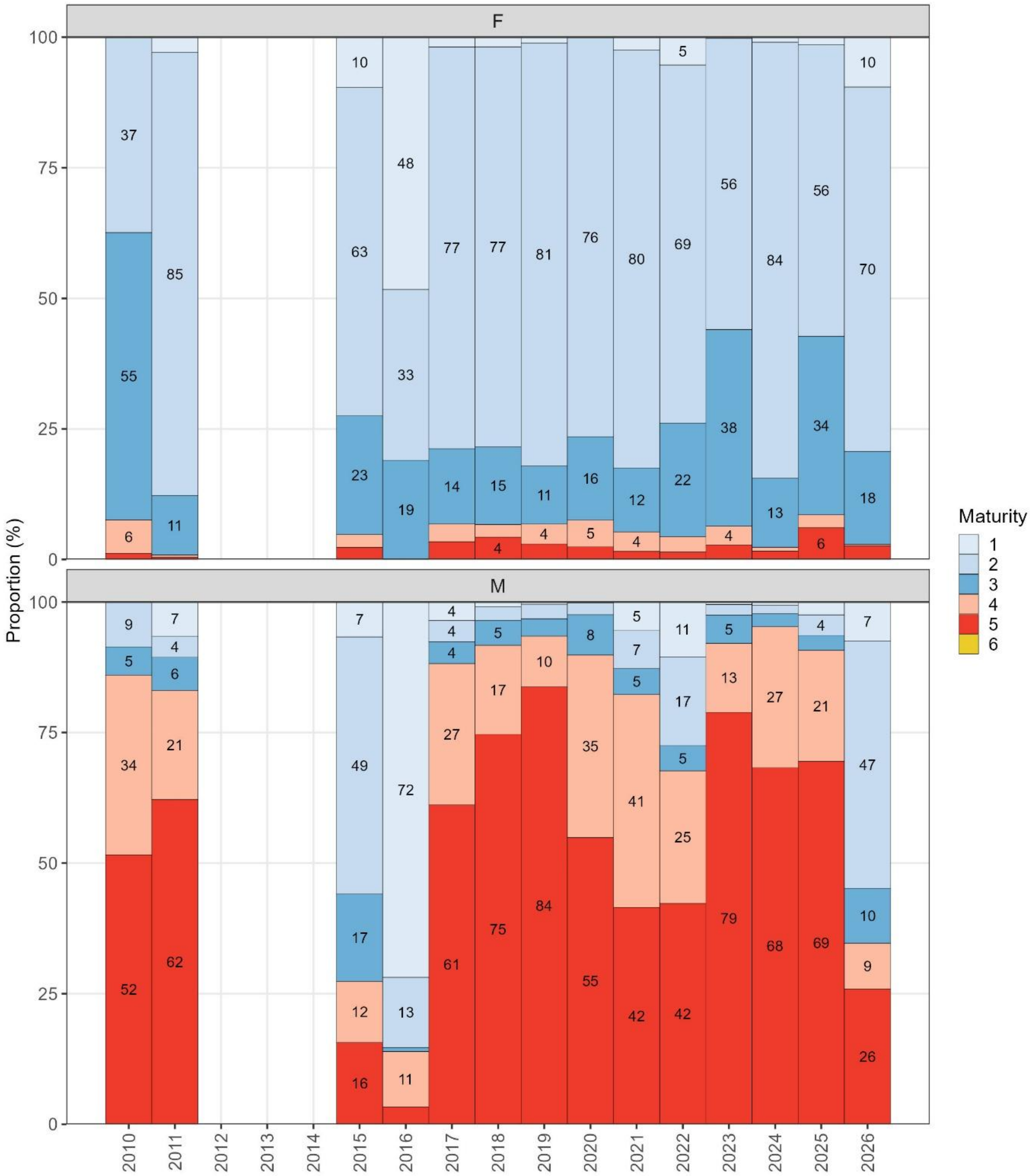


Fig. 10. Proportion by sexual maturity (1, young; 2, immature; 3, preparatory; 4, maturing; 5, mature; 6, spent) of Argentine shortfin squid (*Illex argentinus*) during February groundfish and calamari pre-season surveys conducted in Falkland Islands waters in 2010–2011 and 2015–2026. Labels for proportions < 3% are omitted.

### 4.3.2. Banded whiptail grenadier (*Coelorinchus fasciatus*)

4.3.2.1. Temporal patterns of abundance

Patterns of catch and biomass across years were variable, likely due to the typically small catches and patchy distribution of this species, which is reflected by wide biomass confidence intervals. On average, 90% of the total banded whiptail grenadier catches were from groundfish surveys, and 10% were from calamari pre-season surveys. The highest catch in the time series was reported in 2026 (8.96 t), representing an 11.3% increase relative to the 2010 catch (8.05 t), and nearly a two-fold increase relative to the 2025 catch (4.66 t) and the 2023–2025 mean catch (4.57 t; Fig. 11a; Appendix II).

The highest densities occurred in 2010 (327.47 ± 88.23 kg/km$^2$; mean ± SE). Densities in 2026 (263.27 ± 70.79 kg/km$^2$) were 80.4% of the 2010 levels. However, densities in 2026 showed a two-fold increase relative to the 2025 densities (130.86 ± 34.65 kg/km$^2$) and the 2023–2025 mean densities (132.04 ± 20.52 kg/km$^2$; Fig. 11b).

The highest biomass in the time series was recorded in 2021 (69,256.60 t), followed by a steep decline to 2025 (28,151.94 t). Biomass subsequently increased approximately two-fold in 2026 (53,881.73 t), corresponding to 76.5% of 2010 levels (70,414.52 t), a non-significant decrease relative to 2010 ($p > 0.05$). In contrast, the approximately two-fold increase in 2026 relative to 2025 was statistically significant ($p = 0.004$), as was the 62% increase compared to the 2023–2025 mean (33,342.12 t; $p = 0.012$; Fig. 11c; Table IV–V; Appendix III–IV). Analysis of the full time series revealed no significant temporal trend in biomass (GAM: edf = 1.52, $F$ = 1.32, $p = 0.388$), with the model explaining 20.7% of the deviance ($R^2$ adj. = 0.139), reflecting moderate interannual variability and no consistent directional change over the time series (Fig. 11c; Appendix V).

4.3.2.2. Spatial patterns of abundance

Banded whiptail grenadier was distributed to the south-west of West Falkland during 2026, with the maximum density (5,863 kg/km$^2$) at approximately 52.5°S and 62.2°W. The south-west in the FICZ was the main area of distribution in 2010, and from 2023 to 2025 (Fig. 12), as it was for the other years in the time series, and the highest density was calculated for 2011 (9,126 kg/km$^2$).

Analysis of the spatial change in density revealed that densities in 2026 relative to 2010 increased predominantly to the north-east in the FICZ, as well as in the 'Loligo Box' and in localised areas to the north-west in the FICZ, while substantial decreases were observed to the north of West Falkland. Comparison of 2026 with 2025, and with the 2023–2025 mean, revealed overall decreases in densities through the survey area, with densities decreasing mainly along the 'Loligo Box' and to the north-west in the FICZ. However, densities in 2026 had a substantial increase to the north-west in the FOCZ compared with 2025 (Fig. 13).

4.3.2.3. Length composition

Across all survey years combined, the size structure of banded whiptail grenadier exhibited a range of pre-anal lengths between 2 and 15 cm; however, 95% of the estimated biomass was comprised of individuals between 7 and 13 cm, with a median length of 10 ± 0.82 cm (median ± SE) and a mean length of 10 ± 0.71 cm (mean ± SE; Fig. 14a).

The distribution of biomass proportions by size class exhibited a 53% overlap between the groundfish and calamari pre-season surveys. The permutation analysis revealed that the biomass-weighted mean length was not significantly different ($p > 0.05$) between the groundfish (10 ± 0.71 cm; mean ± SE) and the calamari pre-season (10 ± 0.94 cm) surveys. In the groundfish survey, 95% of the biomass of banded whiptail grenadier was comprised of individuals between 7 and 13 cm, with a median length of 10 ± 0.82 cm. In the calamari pre-season survey, 95% of the biomass of banded whiptail grenadier was comprised of individuals between 6 and 14 cm, with a median length of 12 ± 1.24 cm (Fig. 14b).

The distribution of biomass proportions by size class exhibited a 67% overlap between females and males. The permutation analysis revealed that the biomass-weighted mean length was not significantly different ($p > 0.05$) between females (10.0 ± 0.70 cm) and males (8.0 ± 0.68 cm), indicating similar size structure between females and males. For females, 95% of the biomass was comprised of individuals between 8 and 13 cm, with a median length of 10 ± 0.79 cm. For males, 95% of the biomass was comprised of individuals between 6 and 11 cm, with a median length of 9 ± 0.76 cm (Fig. 14c).

The distribution of biomass-at-length was unimodal and generally consistent across years at approximately 10 cm, with the mean and median pre-anal lengths at 9–11 cm. In 2026, the size structure was similar to previous years. Lengths were in the range of 3 to 13 cm; however, 95% of the biomass was comprised of individuals between 7 and 12 cm, with a median length of 10 ± 0.73 cm and a mean length of 9 ± 0.62 cm. For females, 95% of the biomass was comprised of individuals between 7 and 12 cm, with a median length of 10 ± 0.78 cm and a mean length of 10 ± 0.69 cm. For males, 95% of the biomass was comprised of individuals between 7 and 10 cm, with a median length of 9 ± 0.74 cm and a mean length of 8 ± 0.64 cm (Fig. 15).

Analysis of the full time series revealed no significant temporal trend in either mean (GAM: edf = 1.0, $F = 3.55$, $p = 0.084$, $R^2$ adj. = 0.164, DE = 22.8%) or median (GAM: edf = 1.32, $F = 0.31$, $p = 0.597$, $R^2$ adj. = 0.003, DE = 10.3%) pre-anal length (Fig. 16).

#### 4.3.2.4. Sex and maturity composition

Across all survey years combined, the biomass composition of banded whiptail grenadier was strongly dominated by females, comprising 83.5 ± 2.4% (mean ± SE) of total biomass, followed by males at 16.0 ± 2.4%, with individuals of undetermined sex accounting for 0.5 ± 0.2% and no juveniles recorded in any survey year. Interannual variability in sex composition was evident throughout the time series, with the female proportion ranging from 67% in 2016 to 100% in 2011, and the male proportion ranging from 0% in 2011 to 33% in 2016. The 2026 sex composition was consistent with the time-series mean, with females comprising 86% of the biomass, males 12%, individuals of undetermined sex 2%, and no juveniles recorded (Fig. 17).

Maturity composition was dominated by post-spawning individuals (spent, recovering spent and resting) in both sexes in most years (Fig. 18). Females were characterised by a substantial post-spawning component throughout the time series (> 50% in most years since 2018). Males were predominantly in the resting stage, except in 2010, 2025 and 2026 when early developing individuals were dominant. Late developing, ripe and running individuals were scarce in both sexes, rarely exceeding 8% in any year.

#### 4.3.2.5. Discussion

Analysis of the full time series revealed no significant temporal trend in biomass of banded whiptail grenadier, reflecting moderate interannual variability and no consistent directional change over the time series. Females contributed to most of the biomass. The scarcity of ripe and running individuals, combined with the predominance of post-spawning stages, indicates that the spawning period occurs before February or that spawning does not take place within the survey area at this time of year. Both mean and median pre-anal length had no significant temporal trends. Comparison of biomass estimates with external data is limited given the scarcity of species-level information for grenadiers in Falkland Islands waters. The only stock assessment conducted for grenadiers in Falkland Islands waters (Winter & Lee 2018) produced contrasting results depending on the method applied; CMSY indicated higher biomass in 2017 relative to 1988, while OCOM indicated the opposite. In the commercial bottom trawl fisheries, banded whiptail grenadier accounts for approximately 68.3% of total grenadier catches in Falkland Islands waters, of which over 85% are discarded (Winter & Lee 2018), highlighting the potential for substantial unreported mortality and its implications for the long-term abundance of this species.

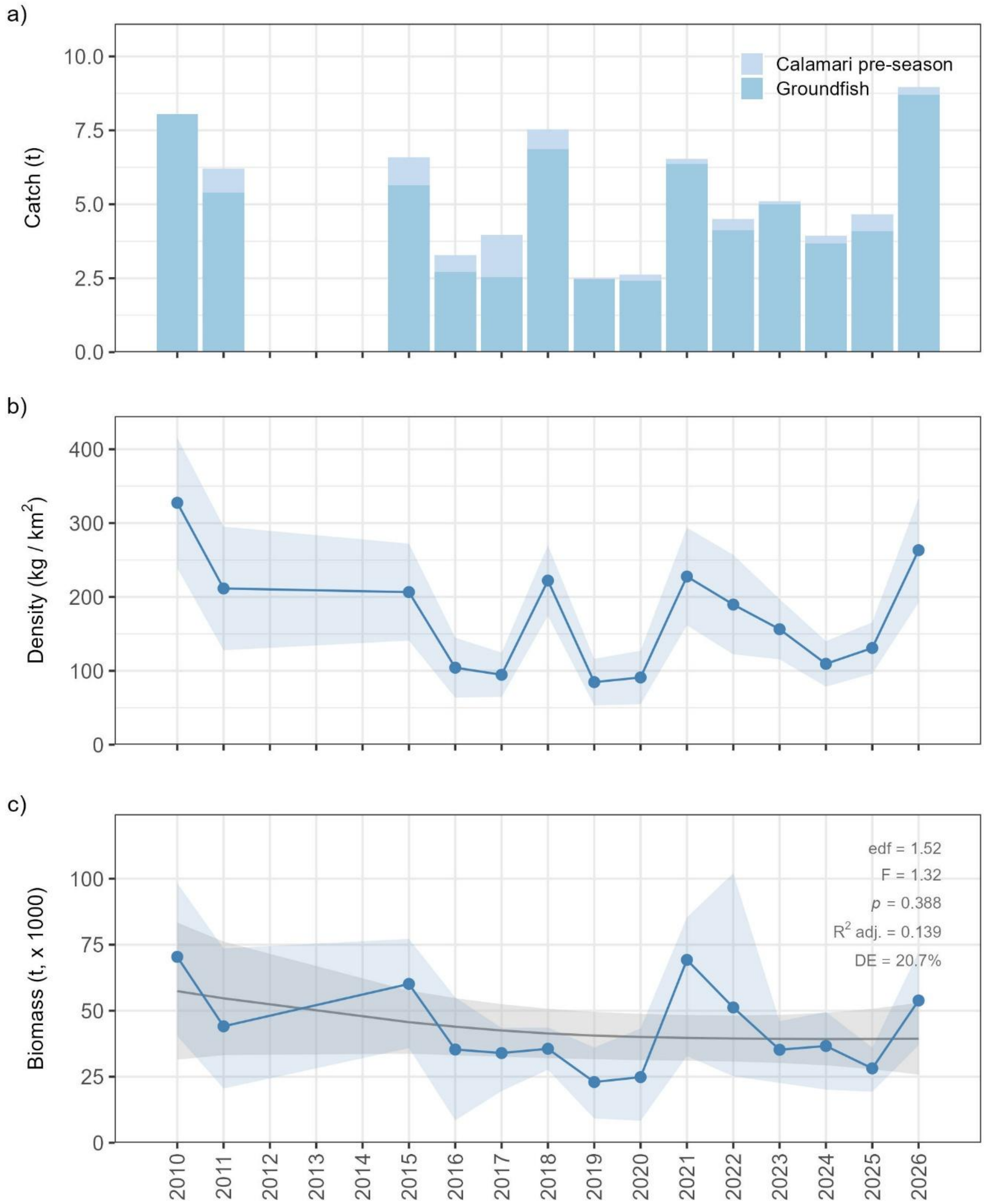


Fig. 11. Abundance of banded whiptail grenadier (*Coelorinchus fasciatus*) during February groundfish and calamari pre-season surveys conducted in Falkland Islands waters in 2010–2011 and 2015–2026. (a) Catch per survey, (b) annual mean density ± SE represented by the blue line and shaded region, respectively, and (c) estimated biomass, where the blue line and shaded region represent the median and 95% pointwise confidence interval derived from 10,000 bootstrap biomass estimates, and the grey line and shaded region represent the fitted Generalised Additive Model (GAM) smooth and its 95% pointwise confidence interval.

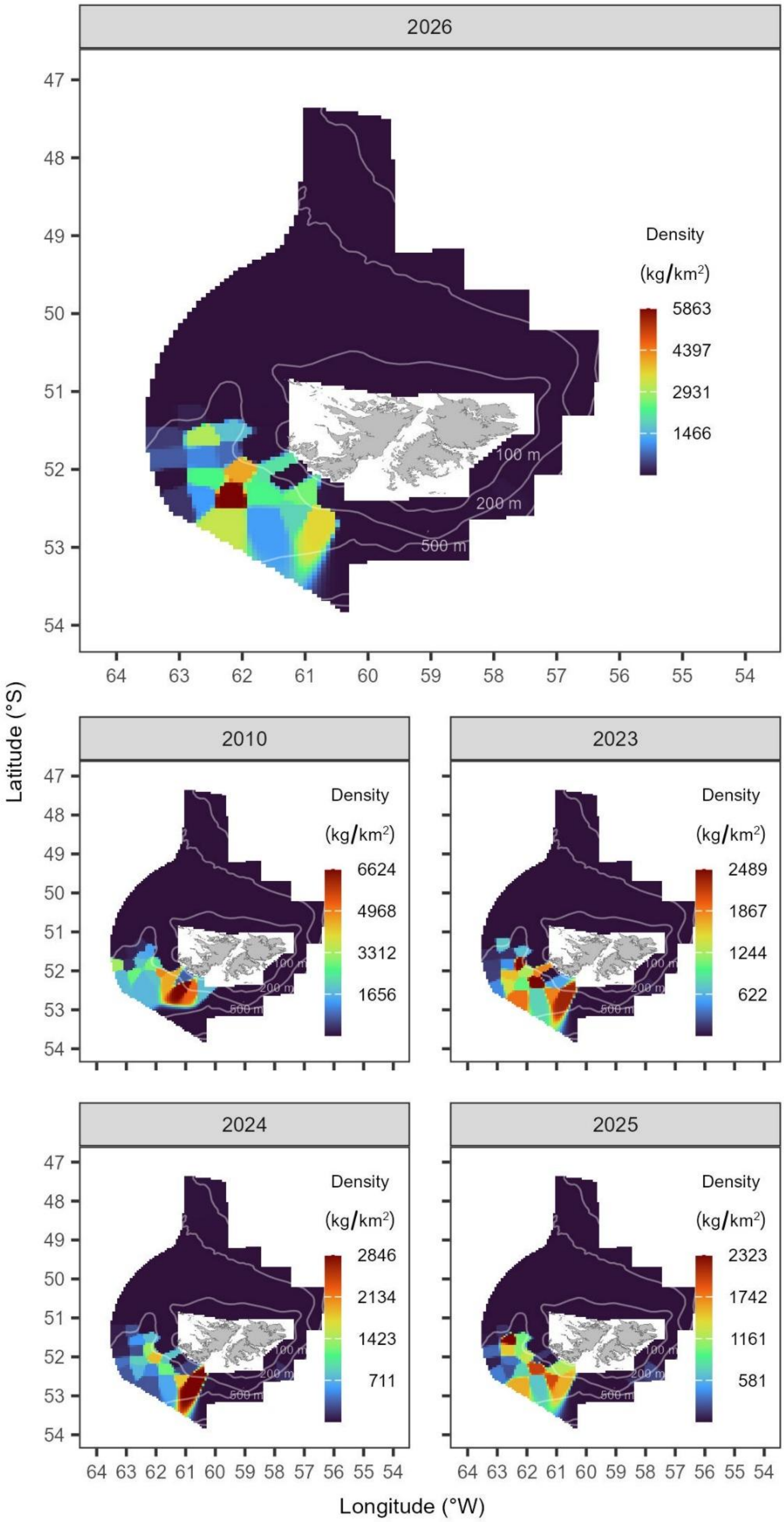


Fig. 12. Distribution and abundance of banded whiptail grenadier (*Coelorinchus fasciatus*) derived from the February 2026 groundfish and calamari pre-season surveys in Falkland Islands waters, compared with the first year of the time series (2010) and the three preceding years (2023–2025). Colour scales are specific to each year. Isobaths at 100 m, 200 m, and 500 m are shown.

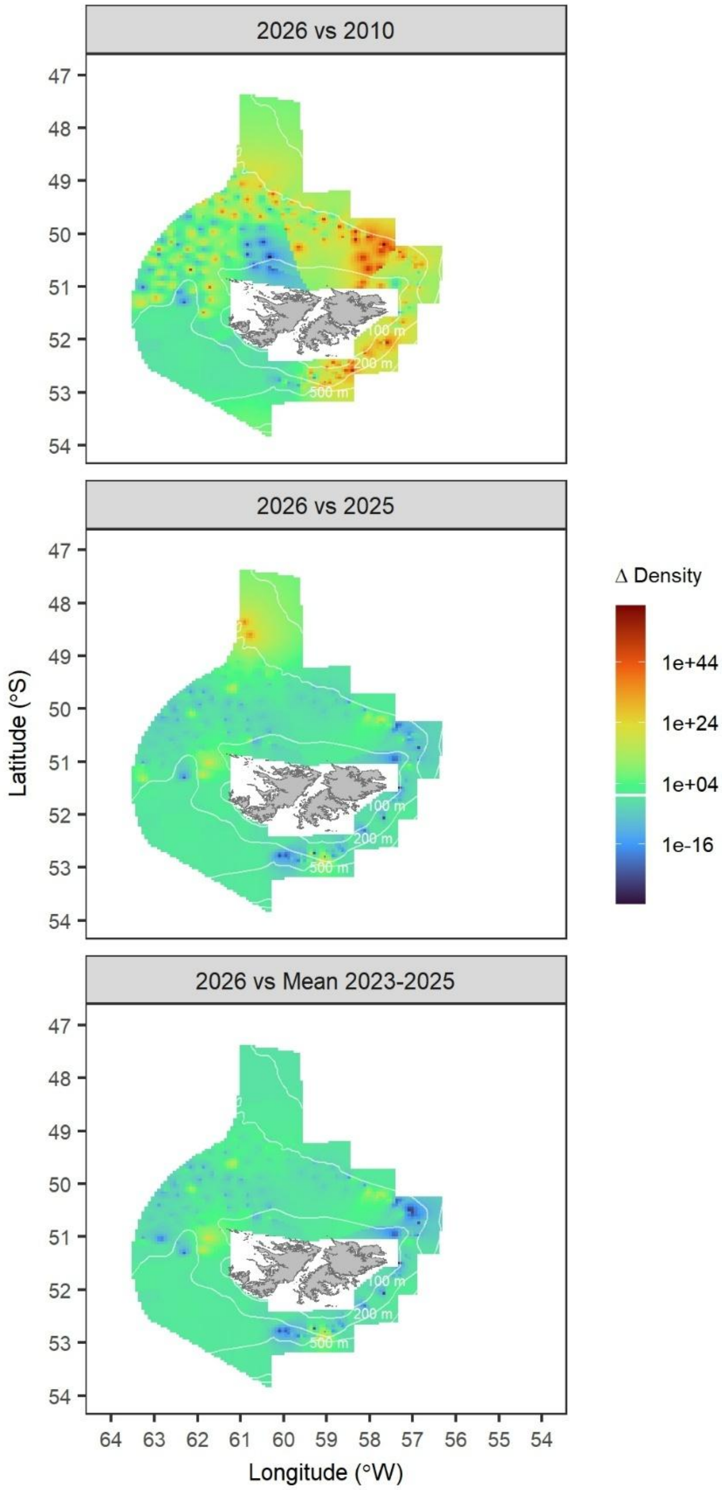


Fig. 13. Spatial change in density of banded whiptail grenadier (*Coelorinchus fasciatus*) derived from the February 2026 groundfish and calamari pre-season surveys in Falkland Islands waters, relative to the first year of the time series (2010), the previous year (2025), and the mean of the three preceding years (2023–2025). The spatial change in density is expressed as the ratio of density (kg/km$^2$) in 2026 relative to the density in the baseline year (2010, 2025, 2023–2025 mean). Isobaths at 100 m, 200 m, and 500 m are shown. The colour scale is $\log_{10}$-transformed to aid visualisation, with increases in density indicated above the horizontal white line towards dark red, and decreases in density indicated below the horizontal white line towards dark blue.

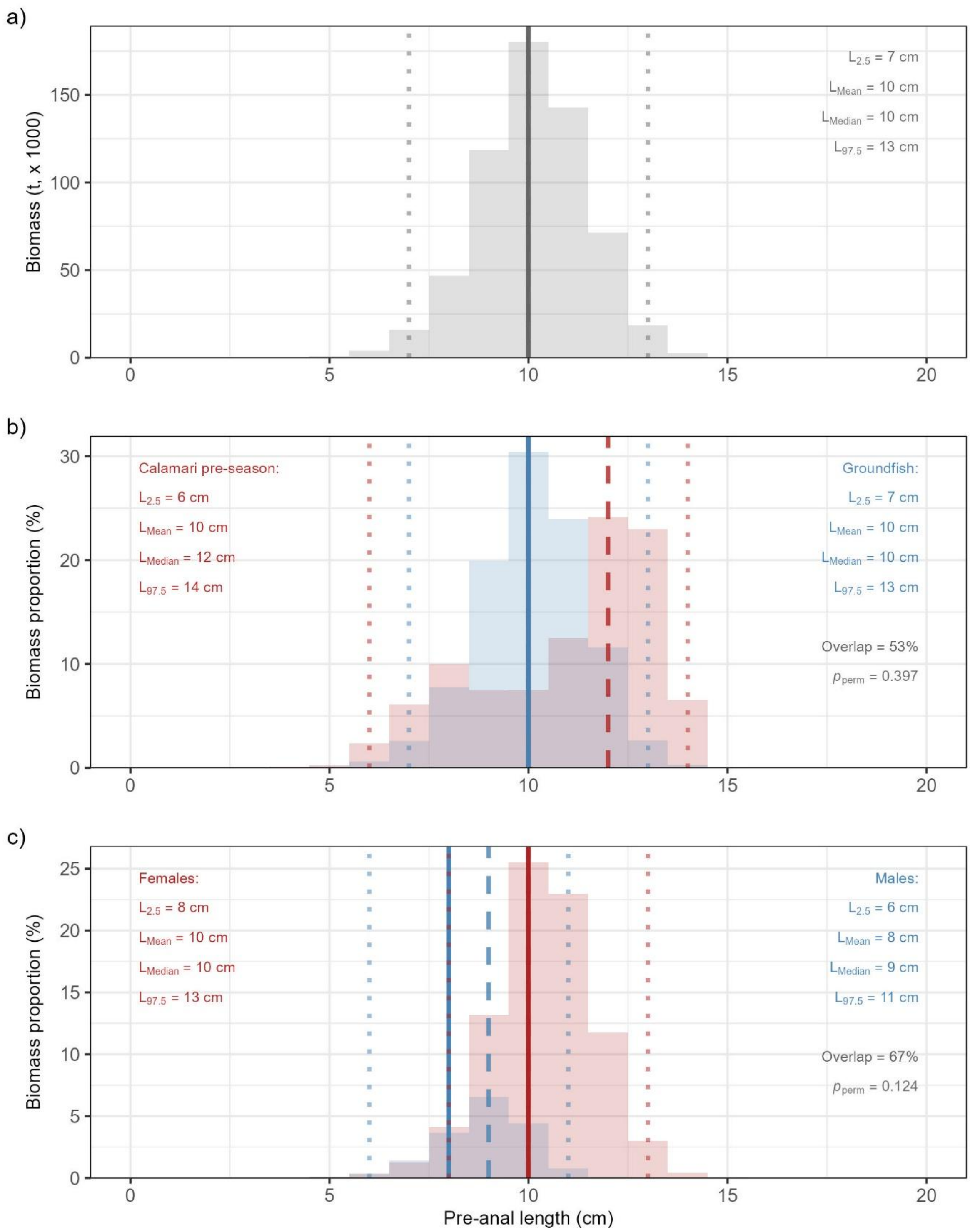


Fig. 14. Biomass-at-length class composition of banded whiptail grenadier (*Coelorinchus fasciatus*) across all years combined, based on February groundfish and calamari pre-season surveys conducted in Falkland Islands waters in 2010–2011 and 2015–2026. a) Overall biomass-at-length frequency distribution. b) Overlap in biomass-at-length distributions between calamari pre-season (red) and groundfish (blue) surveys. c) Overlap in biomass-at-length distributions between females (red) and males (blue). Solid vertical lines indicate the mean length ($L_{Mean}$), dashed lines the median length ($L_{Median}$), and dotted lines the 2.5th and 97.5th length percentiles ($L_{2.5}$ and $L_{97.5}$, respectively). $p_{perm}$ is the significance of the weighted permutation test to assess differences between groups.

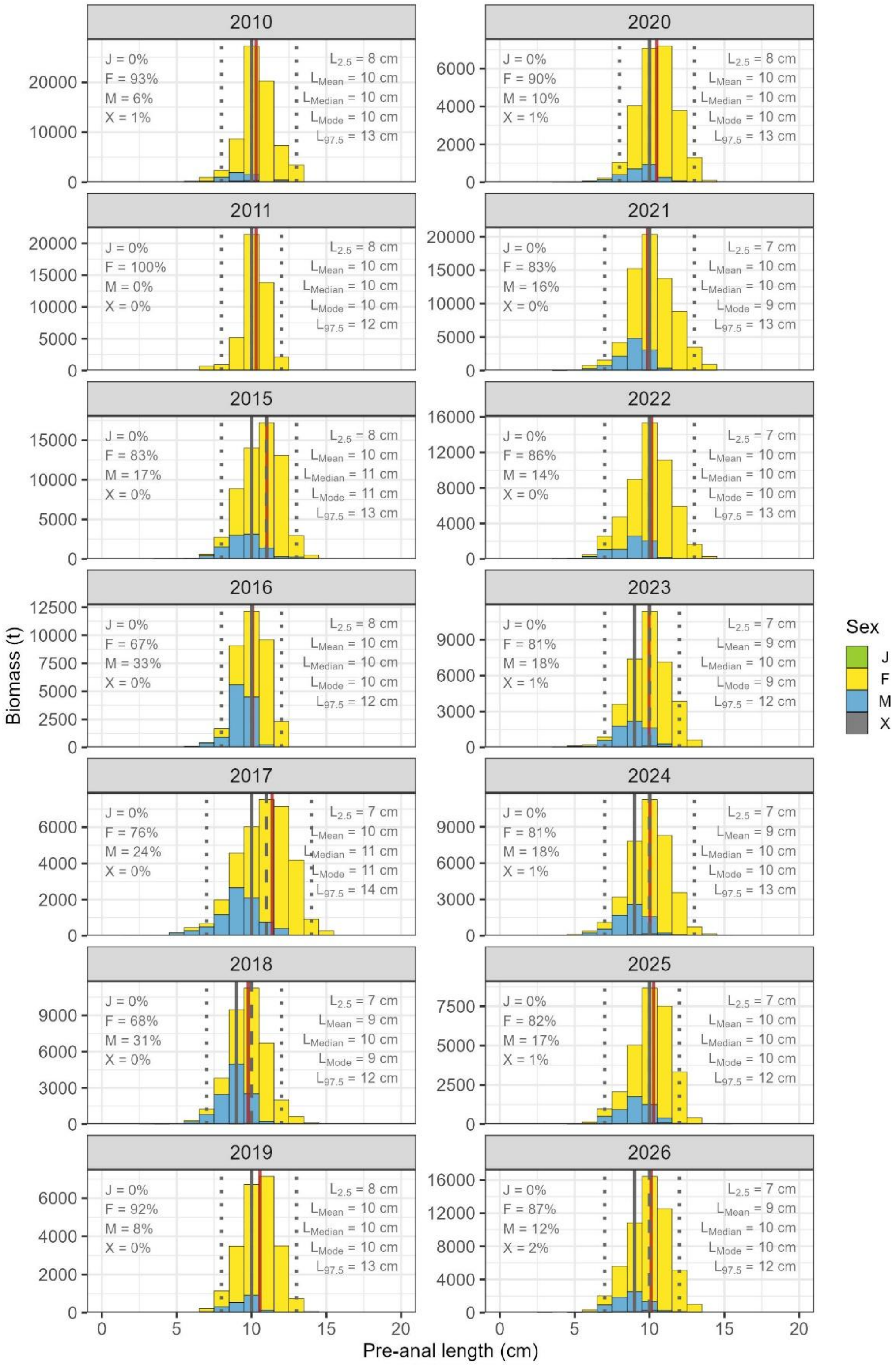


Fig. 15. Annual biomass-at-length class composition of banded whiptail grenadier (*Coelorinchus fasciatus*) during February groundfish and calamari pre-season surveys conducted in Falkland Islands waters in 2010–2011 and 2015–2026. Stacked bars represent biomass (t) per 1.0 cm length class, partitioned by sex (J = juvenile; F = female; M = male; X = undetermined), with the proportion of total annual biomass for each sex indicated in the upper left of each panel. Vertical lines indicate the mean length ($L_{Mean}$, grey solid), median length ($L_{Median}$, grey dashed), modal length ($L_{Mode}$, red solid), and 2.5th and 97.5th percentiles ($L_{2.5}$ and $L_{97.5}$, grey dotted) of the biomass-weighted length distribution. Note the different y-axis scales among years.

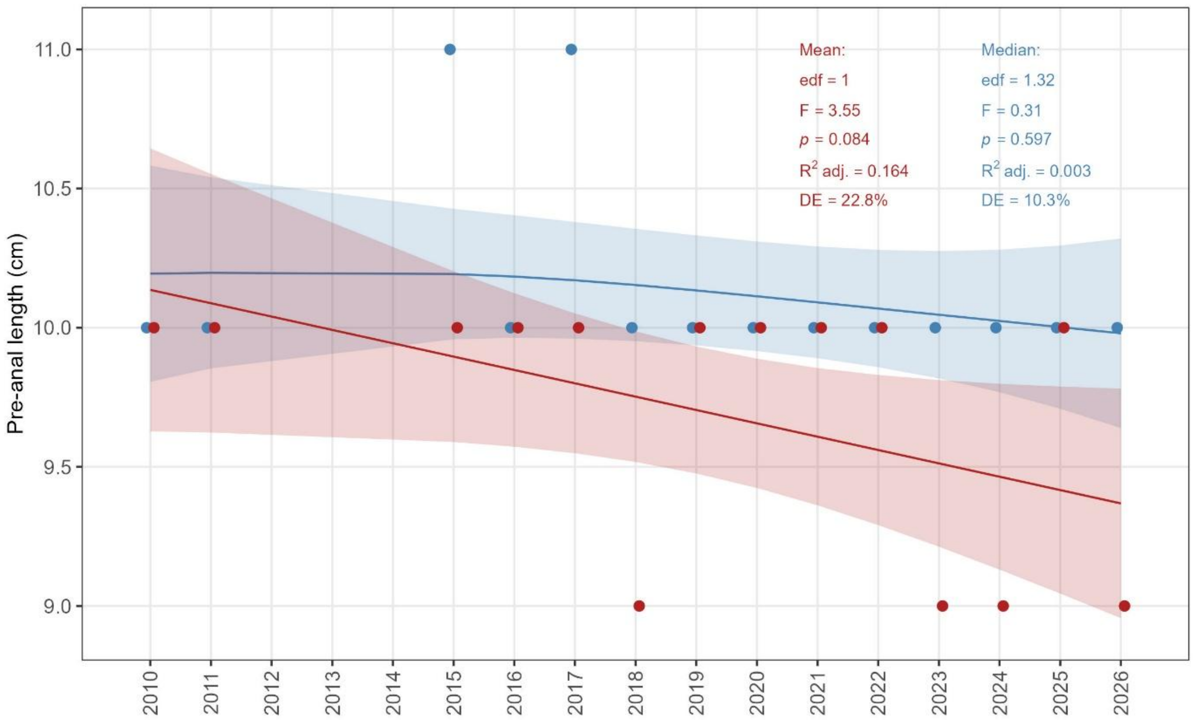


Fig. 16. Median (blue) and mean (red) dorsal mantle length of banded whiptail grenadier (*Coelorinchus fasciatus*) during February groundfish and calamari pre-season surveys conducted in Falkland Islands waters in 2010–2011 and 2015–2026. The line and shaded region represent the fitted Generalised Additive Model (GAM) smooth and its 95% pointwise confidence interval.

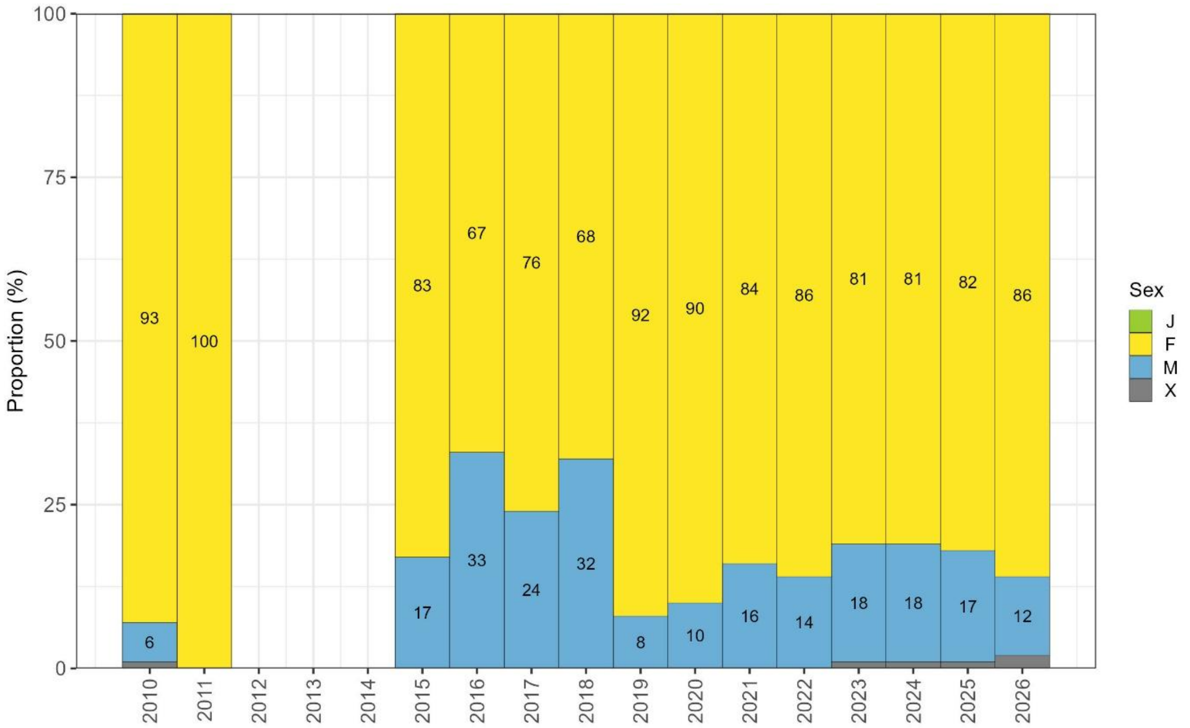


Fig. 17. Proportion by sex (J = juvenile; F = female; M = male; X = undetermined) of banded whiptail grenadier (*Coelorinchus fasciatus*) during February groundfish and calamari pre-season surveys conducted in Falkland Islands waters in 2010–2011 and 2015–2026. Labels for proportions < 3% are omitted.

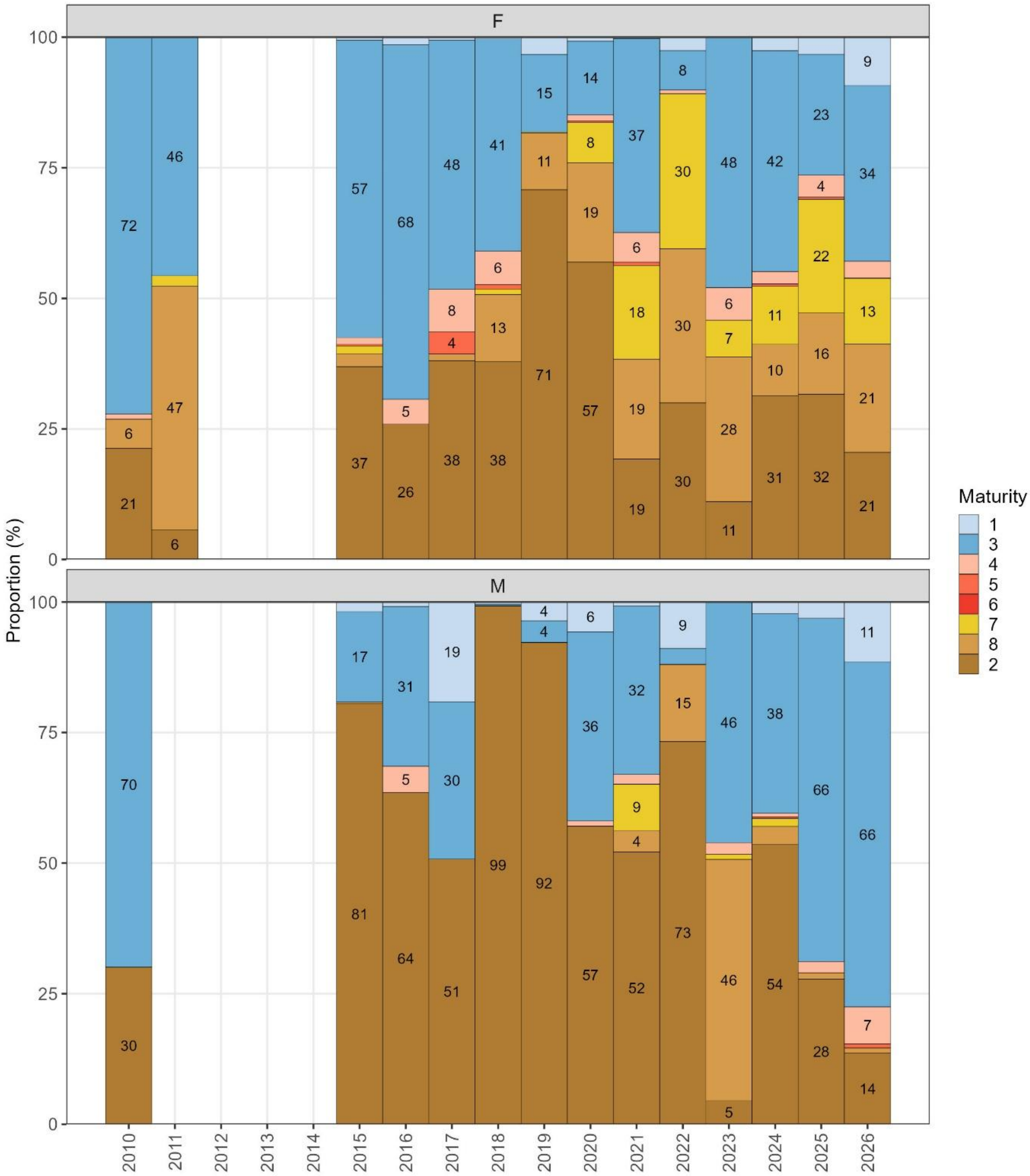


Fig. 18. Proportion by sexual maturity (1, immature; 3, early developing; 4, late developing; 5, ripe; 6, running; 7, spent; 8, recovering spent; 2, resting) of banded whiptail grenadier (*Coelorinchus fasciatus*) during February groundfish and calamari pre-season surveys conducted in Falkland Islands waters in 2010–2011 and 2015–2026. Maturity stages ordered by developmental sequence. Labels for proportions < 3% are omitted.

### 4.3.3. Common hake (*Merluccius hubbsi*)

4.3.3.1. Temporal patterns of abundance

On average, 99% of the total common hake catches in the time series were from groundfish surveys and 1% were from calamari pre-season surveys. The highest catch was reported in 2025 (16.99 t), and the second highest catch in 2026 (14.75 t). Catches in 2026 represented an eleven-fold increase relative to 2010 catches (1.31 t), corresponded to 86.8% of the 2025 catches, and were 39.7% higher relative to the 2023–2025 mean catch (10.56 t; Fig. 19a; Appendix II).

The highest densities in the time series occurred in 2025 (557.16 ± 100.37 kg/km²; mean ± SE), and the second highest densities in 2026 (456.91 ± 89.38 kg/km²). Densities in 2026 represented a ten-fold increase relative to the 2010 densities (45.62 ± 8.93 kg/km²), corresponded to 82% of the 2025 densities, and were 38.3% higher than the 2023–2025 mean (330.41 ± 40.08 kg/km²; Fig. 19b).

The biomass of common hake increased steeply from 2010 (9,226.39 t) to 2025 (87,636.50 t), the highest biomass recorded in the time series, before declining in 2026 (67,767.40 t), the second highest biomass on record. Biomass in 2026 represented a significant seven-fold increase relative to 2010 levels ($p < 0.001$). In contrast, it represented 77.3% of 2025 levels, a non-significant decrease relative to the previous year ($p > 0.05$). Biomass in 2026 was also 40.4% higher than the 2023–2025 mean (48,264.02 t), a significant increase in comparison ($p = 0.02$; Fig. 19c; Table IV–V; Appendix III–IV ). Analysis of the full time series revealed a significant increasing trend in biomass (GAM: edf = 2.13, $F = 9.18$, $p = 0.003$), with the model explaining 64.3% of the deviance ($R^2$ adj. = 0.746), indicating a strong and consistent increase in biomass over the time series (Fig. 19c; Appendix V).

4.3.3.2. Spatial patterns of abundance

In 2026, common hake was mainly distributed through the north-west in the FICZ, and its highest density (9,267 kg/km$^2$; the highest density in the time series) occurred to the north-west limit of the FICZ at approximately 50.5°S and 63°W. Similar patterns of distribution were observed in 2010, and from 2023 to 2025, although the highest densities were observed to the north-west near East Falkland during 2025 instead of near the north-west limit of the FICZ as it was observed in other years (Fig. 20). Migration of common hake into Falkland Islands waters is likely driven by specific oceanographic conditions and takes place in February when the surveys are being conducted. Hence, changes in oceanographic conditions may result in year-to-baseline abundance variability for this species during February in Falkland Islands waters that may not be proportional to overall population abundance.

Analysis of the spatial change in density revealed an overall increase in densities through the survey area in 2026 relative to 2010, with densities predominantly increasing along the south-west in the FICZ and in the 'Loligo Box', while densities decreased primarily to the north-west of the northern limit of the 'Loligo Box' and near the south-west limit of the FICZ. Comparison of densities in 2026 relative to 2025, and relative to the 2023–2025 mean showed increases to the south-west in the FICZ, and in the centre and the north of the 'Loligo Box'; densities decreased mainly in the south of the 'Loligo Box' and to the north-west of the northern limit of the 'Loligo Box' (Fig. 21).

#### 4.3.3.3. Length composition

Across all survey years combined, total length of common hake was in the range of 13 to 95 cm; however, 95% of the estimated biomass was comprised of individuals between 32 and 73 cm, with a median length of 43 ± 1.73 cm (median ± SE) and a mean length at 45 ± 2.02 cm (mean ± SE; Fig. 22a).

The distribution of biomass proportions by size class exhibited a 62% overlap between the groundfish and calamari pre-season surveys. Accordingly, the biomass-weighted mean length was significantly different ($p = 0.016$) between the groundfish (45 ± 2.02 cm; mean ± SE) and the calamari pre-season (51 ± 2.18 cm) surveys, indicating different size structure between surveys. In the groundfish survey, 95% of the biomass of common hake was comprised of individuals between 32 and 73 cm, with a median length of 43 ± 1.72 cm. In the calamari pre-season survey, 95% of the biomass of common hake was comprised of individuals between 38 and 72 cm, with a median length of 50 ± 3.63 cm (Fig. 22b).

The distribution of biomass proportions by size class exhibited a 57% overlap between females and males. Accordingly, the biomass-weighted mean length was significantly different ($p = 0.002$) between females and males, i.e., females (45 ± 2.03 cm) were larger than males (38 ± 1.50 cm). For females, 95% of the biomass was comprised of individuals between 33 and 74 cm, with a median length of 43 ± 1.78 cm. In contrast, 95% of the biomass of males was comprised of individuals between 29 and 50 cm, with a median length of 38 ± 1.38 cm (Fig. 22c).

Through the time series, the size structure of common hake was broad and with several length groups that are not clearly distinguished because of size overlap. Main modal length decreased from 47 cm in 2010–2011 to 40 cm in 2026 (Fig. 23). In 2026, the size structure remained broad and likely multimodal. Lengths were in the range of 29 to 82 cm; however, 95% of the biomass was comprised of individuals between 36 and 66 cm, with a median length of 42 ± 1.61 cm and a mean length of 44 ± 1.72 cm. For females, 95% of the biomass was comprised of individuals between 36 and 67 cm, with a median length of 43 ± 1.68 cm and a mean length of 44 ± 1.81 cm. For males, 95% of the biomass was comprised of individuals between 34 and 46 cm, with a median length of 38 ± 1.16 cm, and a mean length of 38 ± 0.99 cm (Fig. 23).

Analysis of the full time series revealed a significant decline in mean length (GAM: edf = 2.43, $F = 8.28$, $p = 0.004$, $R^2$ adj. = 0.648, DE = 71.6%), decreasing from approximately 56 cm in 2010 to around 41 cm in 2026, with the steepest decline occurring between 2010 and 2019 and a relative stabilisation thereafter (Fig. 24). The median length showed a similar downward pattern but was marginally not statistically significant (GAM: edf = 2.11, $F = 3.34$, $p = 0.060$, $R^2$ adj. = 0.379, DE = 48.8%), declining from approximately 51 cm in 2010 to around 41 cm in 2026. Mean lengths were consistently higher than median lengths throughout the time series, reflecting a right-skewed length distribution due to the presence of larger individuals, particularly in earlier years (Fig. 23).

#### 4.3.3.4. Sex and maturity composition

Across all survey years combined, the biomass composition of common hake was dominated by females, comprising 92.4 ± 1.3% (mean ± SE) of total biomass, followed by males at 7.5 ± 1.2%, with no juveniles or individuals of undetermined sex recorded in any survey year. There was moderate interannual variability in female proportion, ranging from 83% in 2015 to 98% in 2011 and 2024. The 2026 sex composition was consistent with the time-series mean, with females comprising 96% and males comprising 4% of the biomass (Fig. 25). The high contribution of females to the biomass is in agreement with the larger size of females compared to males (Fig. 25).

Maturity composition was dominated by post-spawning individuals (spent, recovering spent, and resting) in both sexes in most years (Fig. 26). Females showed a substantial post-spawning component throughout the time series, reaching > 90% of the female biomass between 2020 and 2023; early developing individuals were dominant in 2015, 2017, 2018 and 2024 (57–68%). Males were characterised by spent individuals in most years; however, male composition shifted towards late developing and ripe stages since 2024. Running individuals were scarce in both sexes, except for males in 2016 and 2019.

4.3.3.5. Discussion

Analysis of the full time series revealed a significant increasing trend in the biomass of common hake in Falkland Islands waters, driven primarily by a marked increase in abundance from 2021 onwards, and with females contributing over 90% of the biomass. The predominance of post-spawning individuals throughout most of the time series indicates that the spawning period occurs before the February survey. According to Macchi et al. (2010) and Arkhipkin et al. (2015), the spawning grounds are located beyond Falkland Islands waters, in the Argentine continental shelf. Marked shifts in maturity stages between years may reflect a response to environmental variability or may be due to inconsistencies in the maturity scale used at FIFD, which is currently under review. The February 2026 biomass estimate was the second highest recorded in February surveys from 2010 to 2026, consistent with the increasing trend observed in July surveys, where the July 2025 biomass was the second highest in the 2017–2025 period (Ramos 2025). These findings are consistent with CPUE data from commercial trawlers in the FICZ/FOCZ, which indicated a peak in abundance in 2021 (Ramos & Winter 2022a; although no post-2021 abundance indices are available for comparison), and with biomass trends of the southern stock (south of 41°S) in Argentine waters, where biomass increased from the late 2000s and reached a maximum in 2023 (Santos et al. 2024), suggesting that the increase observed in Falkland Islands waters may reflect a broader regional increase in common hake abundance.

In contrast to the increasing biomass trend, both mean and median total length declined significantly or near-significantly over the same period. This pattern is supported by the apparent decline in modal lengths observed in July groundfish and calamari pre-season surveys between 2017 and 2025 (females: 45 cm to 42 cm; males: 41 cm to 38 cm; Ramos 2025). However, declining trends in lengths found in these studies contrast with the median, upper quartile (75%), and 90th percentile (90%) lengths contributions to the total biomass that suggest the increase in lengths in 2025 compared with the 2022–2024 mean, and with 2024 based on July groundfish survey data alone (Soeth et al. 2025).

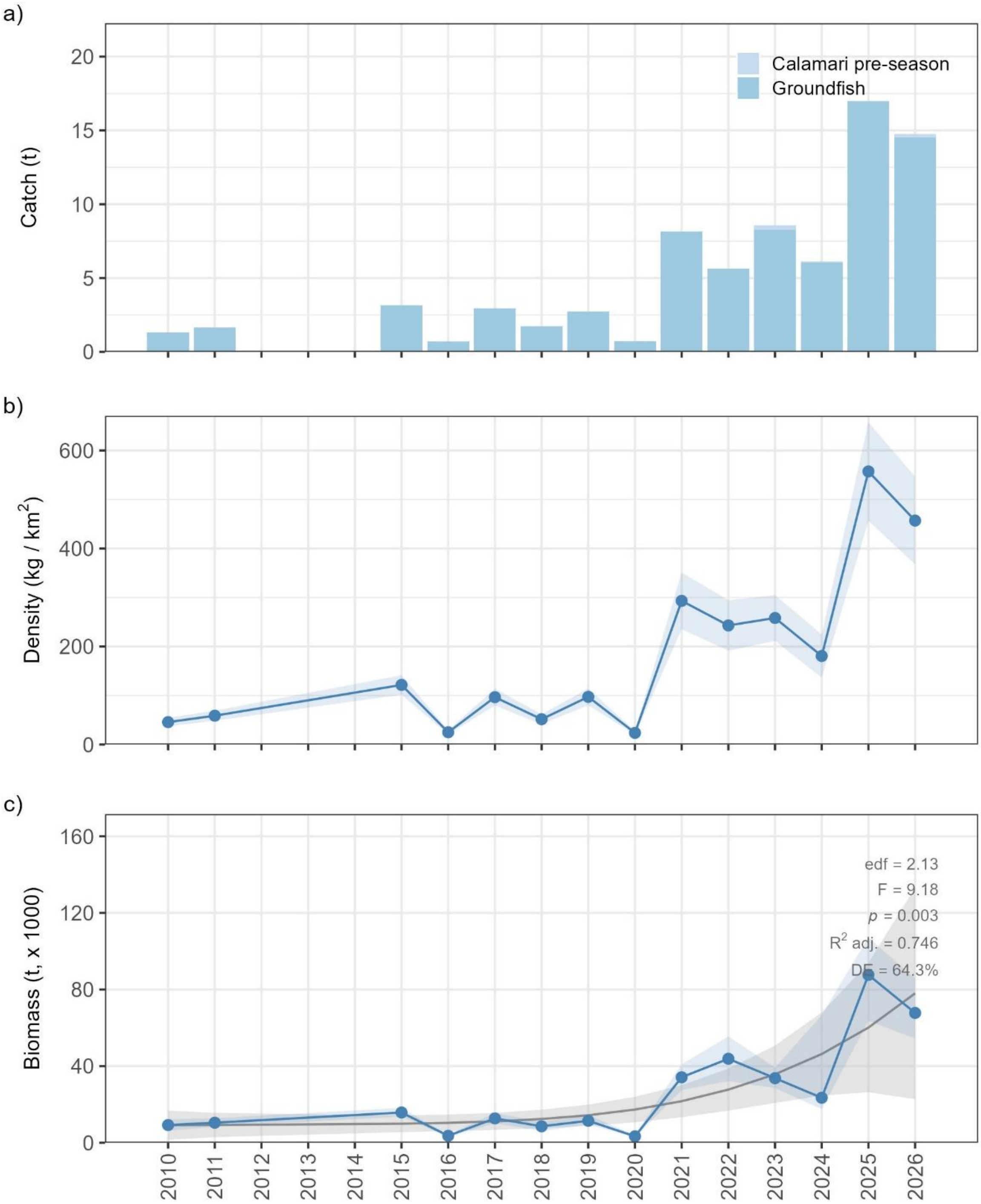


Fig. 19. Abundance of common hake (*Merluccius hubbsi*) during February groundfish and calamari pre-season surveys conducted in Falkland Islands waters in 2010–2011 and 2015–2026. (a) Catch per survey, (b) annual mean density ± SE represented by the blue line and shaded region, respectively, and (c) estimated biomass, where the blue line and shaded region represent the median and 95% pointwise confidence interval derived from 10,000 bootstrap biomass estimates, and the grey line and shaded region represent the fitted Generalised Additive Model (GAM) smooth and its 95% pointwise confidence interval.

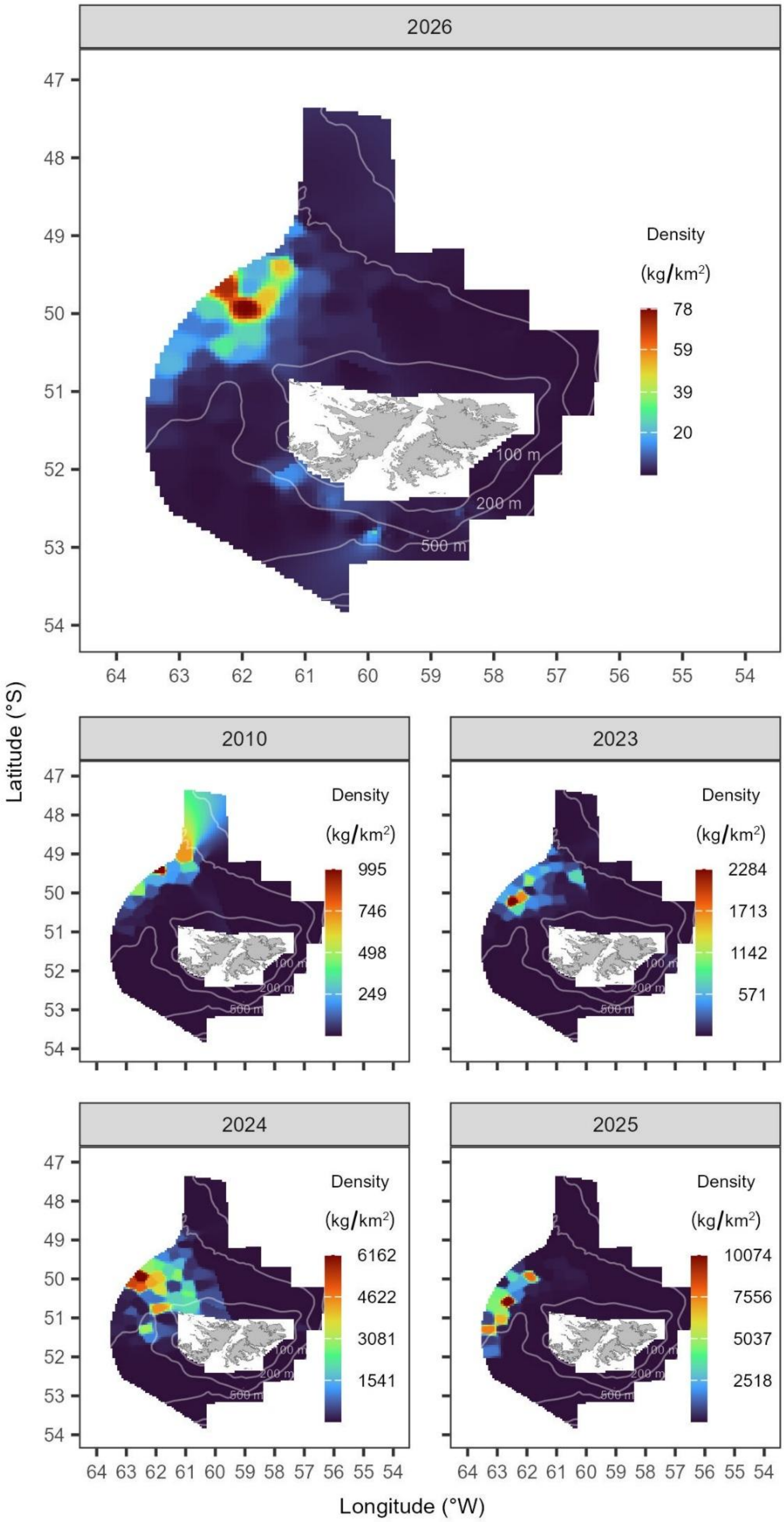


Fig. 20. Distribution and abundance of common hake (*Merluccius hubbsi*) derived from the February 2026 groundfish and calamari pre-season surveys in Falkland Islands waters, compared with the first year of the time series (2010) and the three preceding years (2023–2025). Colour scales are specific to each year. Isobaths at 100 m, 200 m, and 500 m are shown.

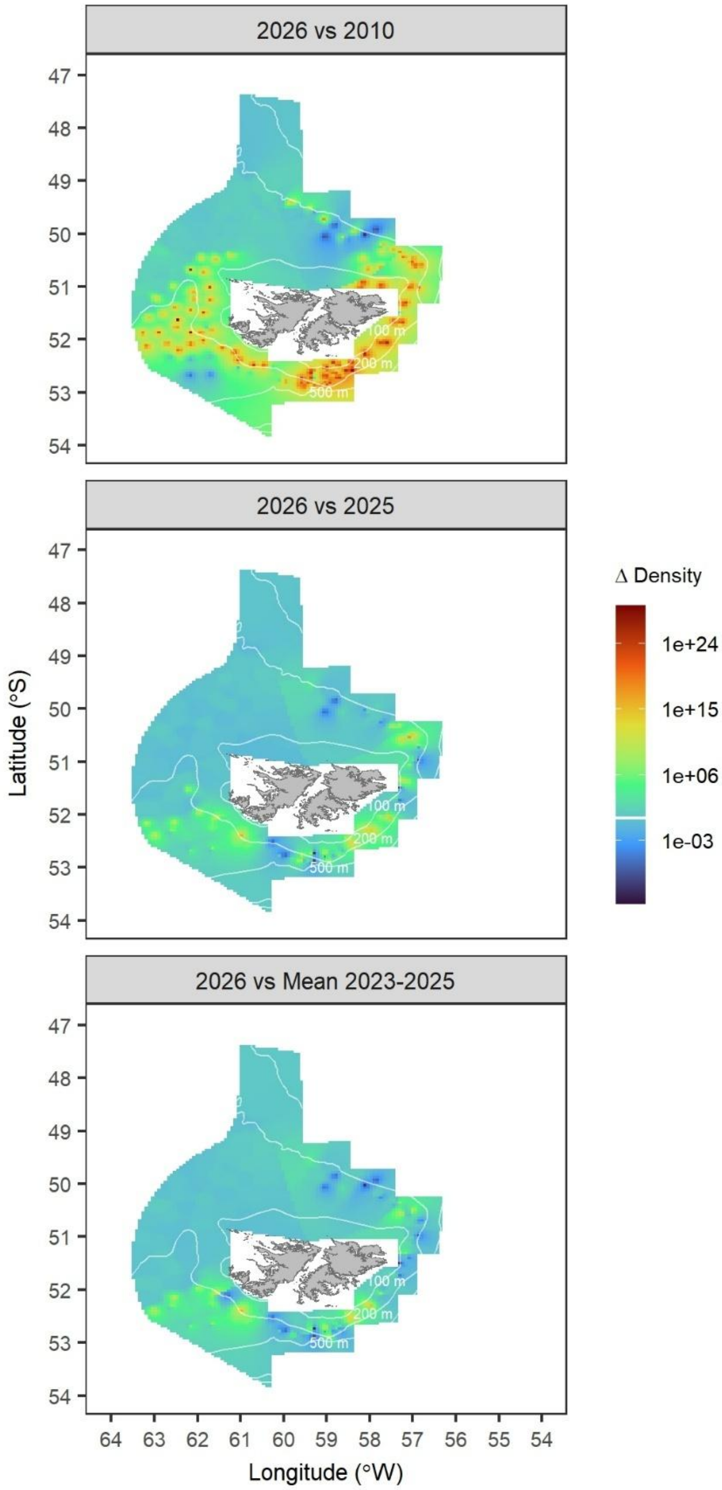


Fig. 21. Spatial change in density of common hake (*Merluccius hubbsi*) derived from the February 2026 groundfish and calamari pre-season surveys in Falkland Islands waters, relative to the first year of the time series (2010), the previous year (2025), and the mean of the three preceding years (2023–2025). The spatial change in density is expressed as the ratio of density (kg/km$^2$) in 2026 relative to the density in the baseline year (2010, 2025, 2023–2025 mean). Isobaths at 100 m, 200 m, and 500 m are shown. The colour scale is $log_{10}$-transformed to aid visualisation, with increases in density indicated above the horizontal white line towards dark red, and decreases in density indicated below the horizontal white line towards dark blue.

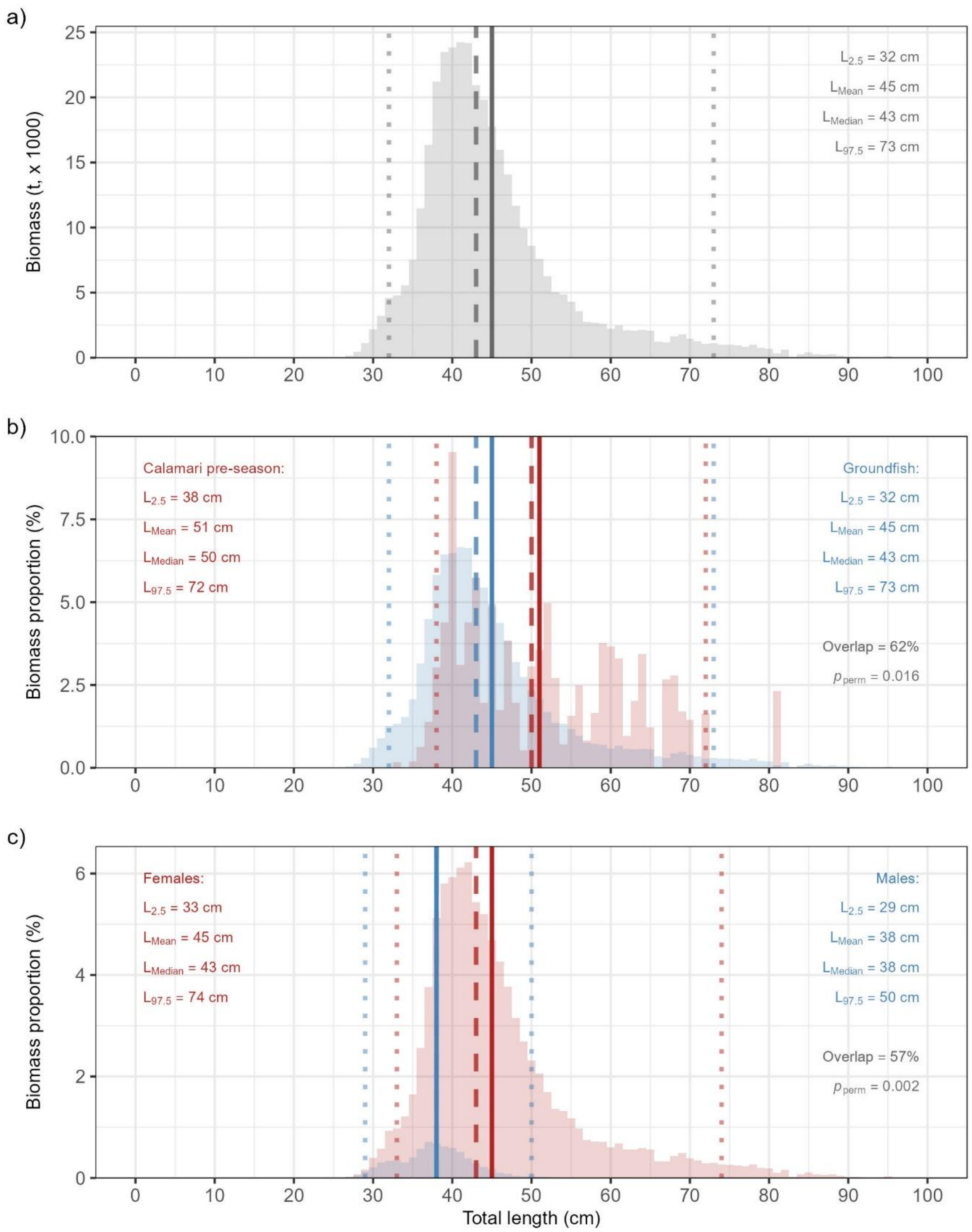


Fig. 22. Biomass-at-length class composition of common hake (*Merluccius hubbsi*) across all years combined, based on February groundfish and calamari pre-season surveys conducted in Falkland Islands waters in 2010–2011 and 2015–2026. a) Overall biomass-at-length frequency distribution. b) Overlap in biomass-at-length distributions between calamari pre-season (red) and groundfish (blue) surveys. c) Overlap in biomass-at-length distributions between females (red) and males (blue). Solid vertical lines indicate the mean length ($L_{Mean}$), dashed lines the median length ($L_{Median}$), and dotted lines the 2.5th and 97.5th length percentiles ($L_{2.5}$ and $L_{97.5}$, respectively). $p_{perm}$ is the significance of the weighted permutation test to assess differences between groups.

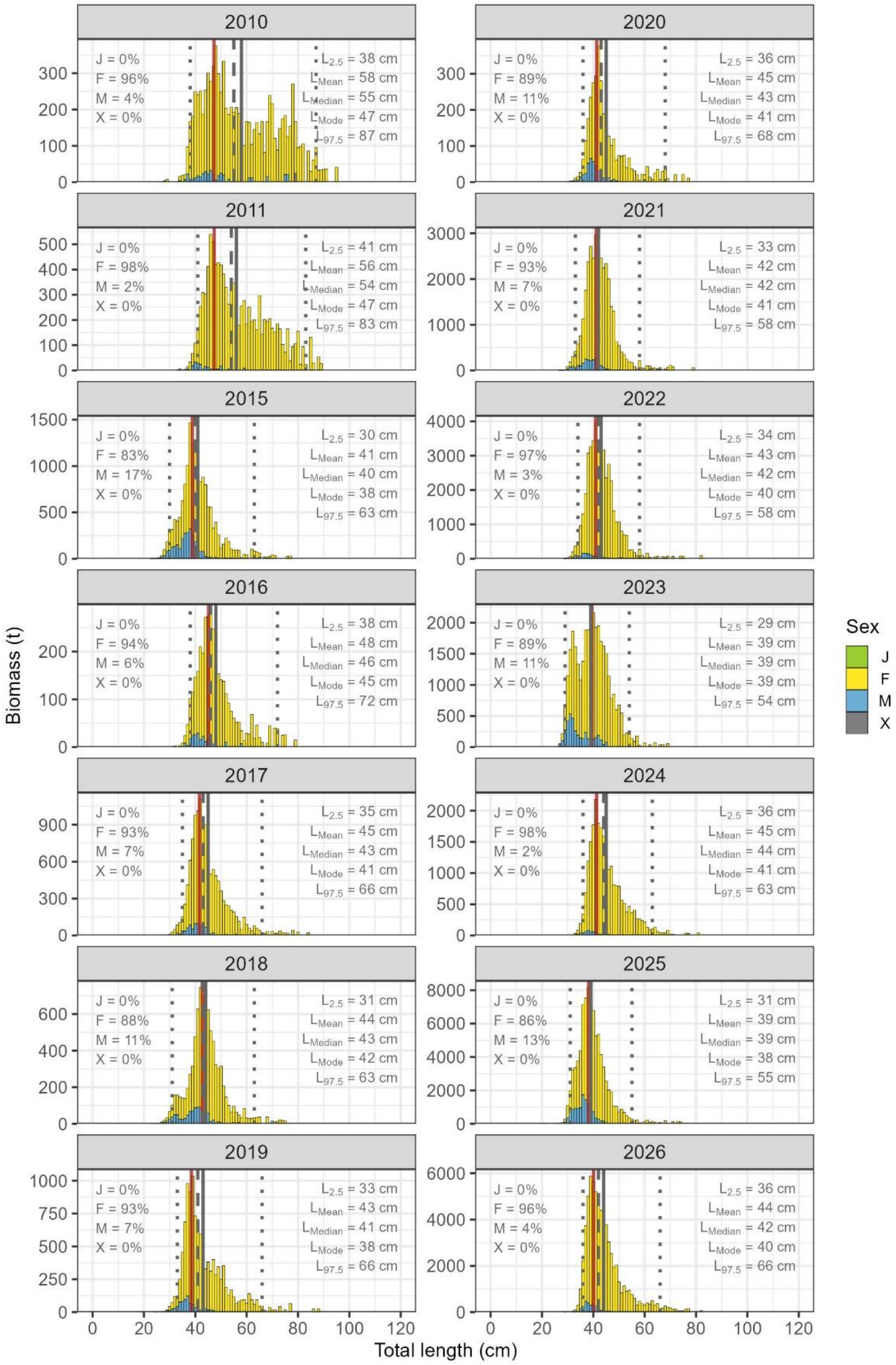


Fig. 23. Annual biomass-at-length class composition of common hake (*Merluccius hubbsi*) during February groundfish and calamari pre-season surveys conducted in Falkland Islands waters in 2010–2011 and 2015–2026. Stacked bars represent biomass (t) per 1.0 cm length class, partitioned by sex (J = juvenile; F = female; M = male; X = undetermined), with the proportion of total annual biomass for each sex indicated in the upper left of each panel. Vertical lines indicate the mean length ($L_{Mean}$, grey solid), median length ($L_{Median}$, grey dashed), modal length ($L_{Mode}$, red solid), and 2.5th and 97.5th percentiles ($L_{2.5}$ and $L_{97.5}$, grey dotted) of the biomass-weighted length distribution. Note the different y-axis scales among years.

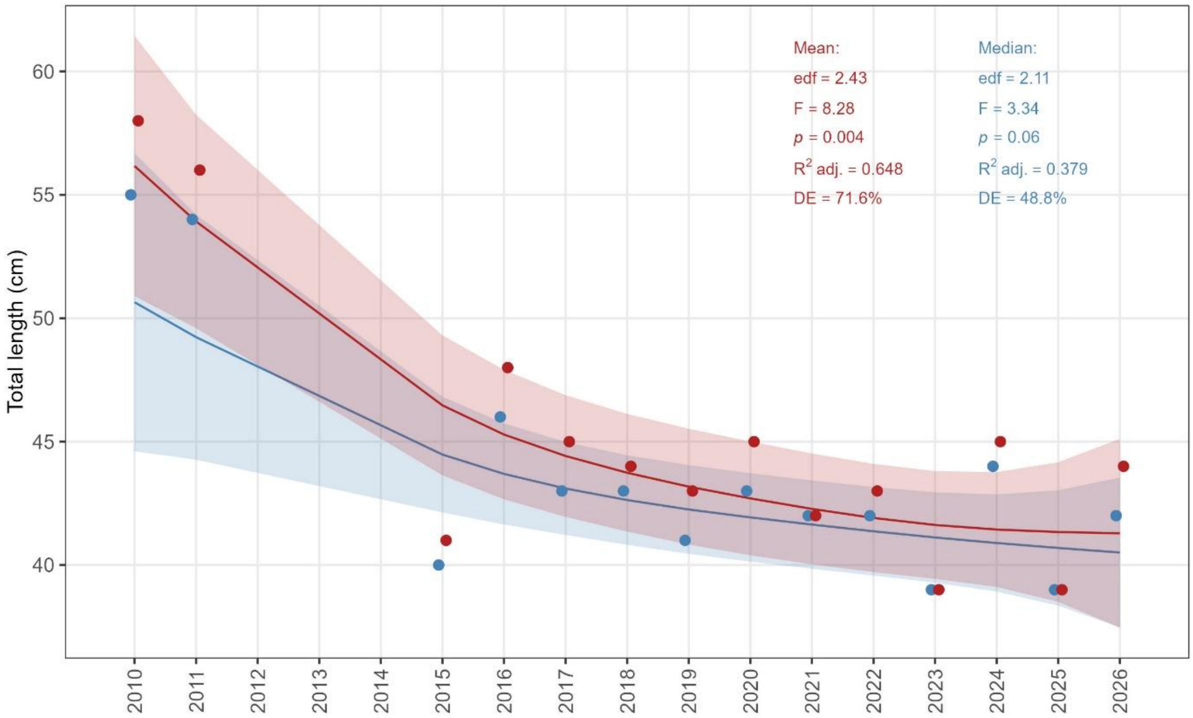


Fig. 24. Median (blue) and mean (red) total length of common hake (*Merluccius hubbsi*) during February groundfish and calamari pre-season surveys conducted in Falkland Islands waters in 2010–2011 and 2015–2026. The line and shaded region represent the fitted Generalised Additive Model (GAM) smooth and its 95% pointwise confidence interval.

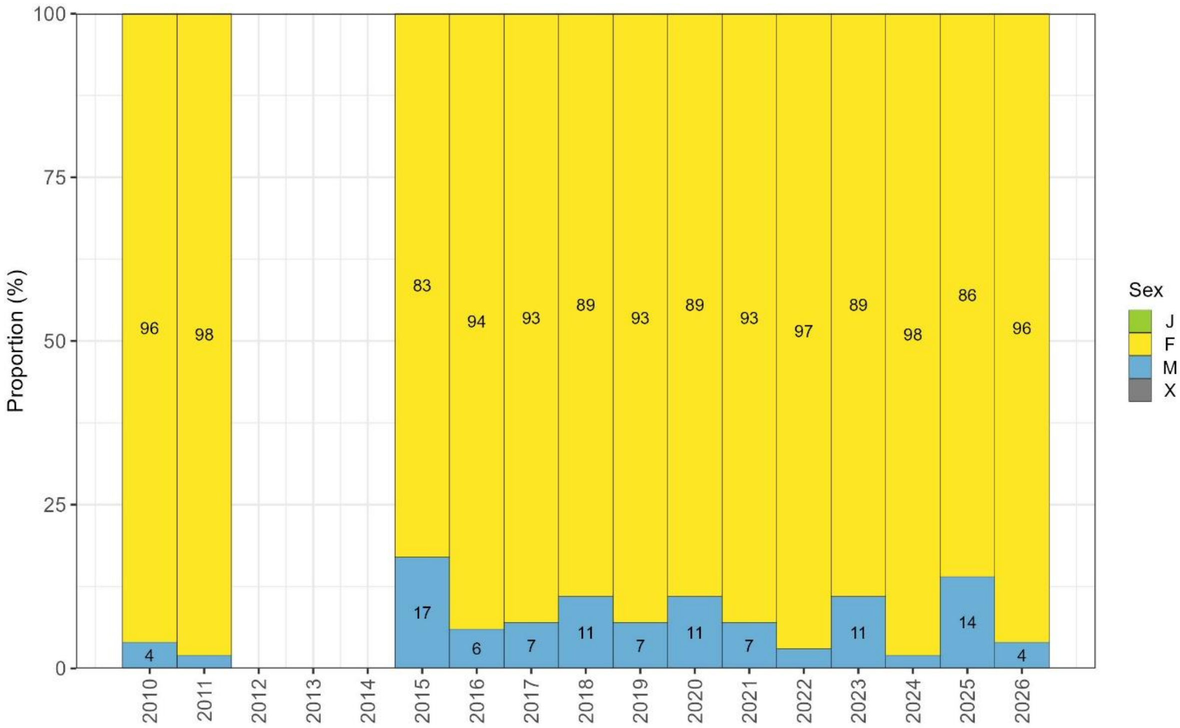


Fig. 25. Proportion by sex (J = juvenile; F = female; M = male; X = undetermined) of common hake (*Merluccius hubbsi*) during February groundfish and calamari pre-season surveys conducted in Falkland Islands waters in 2010–2011 and 2015–2026. Labels for proportions < 3% are omitted.

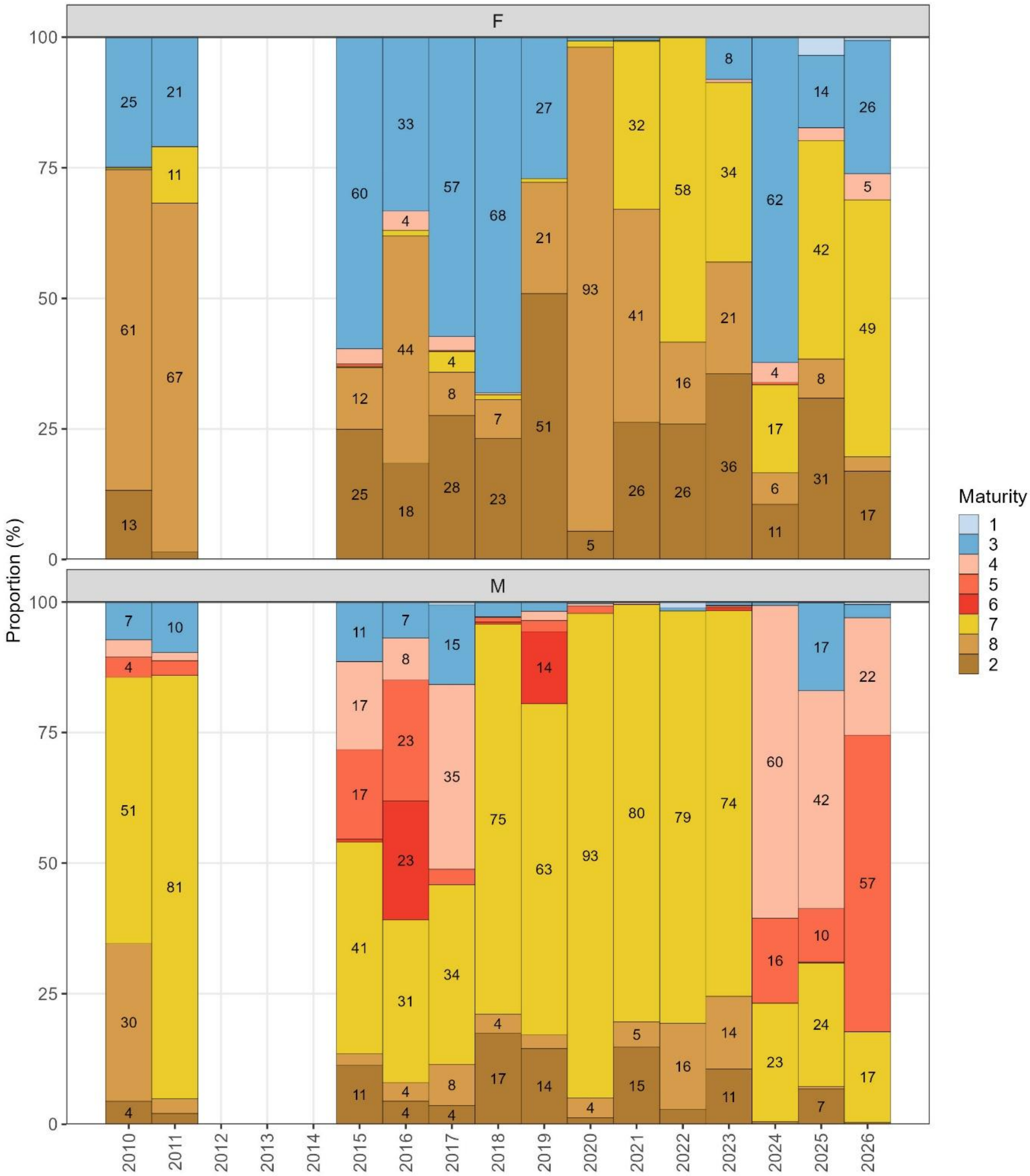


Fig. 26. Proportion by sexual maturity (1, immature; 3, early developing; 4, late developing; 5, ripe; 6, running; 7, spent; 8, recovering spent; 2, resting) of common hake (*Merluccius hubbsi*) during February groundfish and calamari pre-season surveys conducted in Falkland Islands waters in 2010–2011 and 2015–2026. Maturity stages ordered by developmental sequence. Labels for proportions < 3% are omitted.

### 4.3.4. Hoki (*Macruronus magellanicus*)

4.3.4.1. Temporal patterns of abundance

On average, 75% of the total hoki catches in the time series were obtained from groundfish surveys and 25% from calamari pre-season surveys. The highest catch was reported in 2010 (79.78 t). Hoki catch in 2026 (21.14 t) corresponded to 26.5% of the 2010 catch. In contrast, 2026 represented a nineteen-fold increase relative to the 2025 catch (1.09 t), and it was 74.6% higher than the 2023–2025 mean catch (12.11 t; Fig. 27a; Appendix II).

The highest densities occurred in 2010 (2,304 ± 660.67 kg/km²; mean ± SE). Densities in 2026 (429.04 ± 300.83 kg/km²) corresponded to 18.6% of the 2010 densities but represented a fifteen-fold increase relative to 2025 densities (27.81 ± 13.64 kg/km²) and an approximately two-fold increase relative to the 2023–2025 mean densities (235.63 ± 70.07 kg/km²; Fig. 27b).

The highest biomass in the time series was recorded in 2010 (303,807.12 t). Biomass declined over the following years, with marked interannual oscillations, reaching its lowest level in 2025 (6,939.02 t), before increasing substantially in 2026 (198,888.83 t). Hoki biomass in 2026 corresponded to 65% of 2010 levels, a non-significant decrease relative to 2010 ($p > 0.05$). However, biomass in 2026 showed a significant 29-fold increase relative to 2025 ($p = 0.001$), although the nearly three-fold increase relative to the 2023–2025 mean (62,827.30 t) was non-significant ($p > 0.05$; Fig. 27c; Table IV–V; Appendix III–IV). Analysis of the full time series revealed a marginally non-significant temporal trend in biomass (GAM: edf = 1.00, $F = 4.42$, $p = 0.057$), with the model explaining 20.2% of the deviance ($R^2$ adj. = 0.390), reflecting moderate interannual variability and no consistent directional change over the time series (Fig. 27c; Appendix V).

4.3.4.2. Spatial patterns of abundance

In 2026, hoki were found close to the south-west limit of the FICZ, with the highest density (43,458 kg/km$^2$) at around 52.5°S and 61.7°W (Fig. 28). The distribution of hoki has been patchy and variable from year to year. From 2010 to 2015, hoki occurred over the entire FICZ and FOCZ. However, its distribution was localised mainly to the south-west of West Falkland from 2016 to 2025; the highest density in the time series occurred close to the south-west limit of the FICZ in 2021 (146,194 kg/km$^2$).

Analysis of the spatial change in density revealed an overall decrease in densities through the survey area in 2026 relative to 2010; however, substantial increase in densities were observed in the south of the 'Loligo Box'. Comparisons of 2026 with 2025, and with the 2023–2025 mean, revealed that densities increased to the north-west in the FICZ and in two distinct areas in the south of the 'Loligo Box' (Fig. 29).

4.3.4.3. Length composition

Across all survey years combined, pre-anal length of hoki was in the range of 11 to 47 cm; however, 95% of the estimated biomass was comprised of individuals between 18 and 38 cm, with a median length of 28 ± 1.46 cm (median ± SE) and a mean length of 28 ± 1.23 cm (mean ± SE; Fig. 30a).

The distribution of biomass proportions by size class exhibited an 87% overlap between the groundfish and calamari pre-season surveys. Accordingly, the biomass-weighted mean length was not significantly different ($p > 0.05$) between the groundfish (28 ± 1.23 cm; mean ± SE) and the calamari pre-season (28 ± 1.11 cm) surveys, indicating similar size structure between surveys. In the groundfish survey, 95% of the biomass of hoki was comprised of individuals between 18 and 38 cm, with a median of 28 ± 1.43 cm. In the calamari pre-season survey, 95% of the biomass of hoki was comprised of individuals between 21 and 36 cm, with a median of 29 ± 1.43 cm (Fig. 30b).

The distribution of biomass proportions by size class exhibited an 86% overlap between females and males. Accordingly, the biomass-weighted mean length was not significantly different ($p > 0.05$) between females (28 ± 1.23 cm) and males (27 ± 1.19 cm), indicating similar size structure between females and males. For females, 95% of the biomass was comprised of individuals between 19 and 39 cm, with a median length of 29 ± 1.48 cm. For males, 95% of the biomass was comprised of individuals between 18 and 36 cm, with a median length of 27 ± 1.41 cm (Fig. 30c).

The size structure of hoki was broad and multimodal. Several length-groups were present and not clearly distinguished because of size overlap in most years. The main modal length decreased from 29 cm in 2010 to 21 cm in 2019, and increased over the following years (Fig. 31). In 2026, the size structure remained broad and likely multimodal. Pre-anal lengths were in the range of 13 to 43 cm; however, 95% of the biomass was comprised of individuals between 21 and 32 cm, with a median length of 27 ± 0.98 cm and a mean length of 26 ± 0.72 cm. For females, 95% of the individuals were between 21 and 33 cm, with a median length of 28 ± 1.37 cm and a mean length of 27 ± 1.01 cm. For males, 95% of the biomass was comprised of individuals between 22 and 31 cm, with a median length of 26 ± 1.15 cm and a mean length of 26 ± 1.03 cm (Fig. 31).

Analysis of the full time series revealed significant temporal trends in both mean and median pre-anal length. Mean length declined significantly over the time series (GAM: edf = 4.18, $F = 8.76$, $p = 0.003$, $R^2$ adj. = 0.771, DE = 84.5%), as did median length (GAM: edf = 3.69, $F = 7.27$, $p = 0.006$, $R^2$ adj. = 0.711, DE = 79.4%). Both metrics explained a high proportion of deviance and indicated non-linear trends. Both mean and median pre-anal lengths were approximately 29–30 cm in 2010, declined steadily and reached a minimum of approximately 24 cm in 2020–2021, and increased again to approximately 26–28 cm by 2026 (Fig. 32).

#### 4.3.4.4. Sex and maturity composition

Across all survey years combined, the biomass composition of hoki was dominated by females, comprising 63.9 ± 0.9% (mean ± SE) of total biomass, followed by males at 36.1 ± 0.9%, with no juveniles or individuals of undetermined sex recorded in any survey year. Interannual variability in sex composition was relatively low, with the female proportion ranging from 58% in 2019 to 70% in 2025, and the male proportion ranging from 30% in 2025 to 42% in 2019, reflecting a broadly stable sex ratio throughout the time series. The 2026 sex composition was thus consistent with the time-series mean, with females comprising 61% of biomass and males 39% (Fig. 33).

Maturity composition was dominated by post-spawning individuals (resting) in both sexes throughout the time series (Fig. 34). Females were characterised by a predominance of resting individuals (71–98%) in most years, except for 2015 (43%), and between 2023 and 2026 (47–55%), when early developing and recovering spent individuals had a relatively higher contribution compared with other years. Males also showed a considerable proportion of resting individuals (46–97%) in most years, although early developing individuals were abundant in 2010, 2024 and 2025 (≥ 46%). Late developing, ripe and running individuals were not observed throughout the series.

#### 4.3.4.5. Discussion

Analysis of the full time series revealed a (marginally) non-significant declining trend in hoki biomass in Falkland Islands waters, characterised by high interannual variability. Females contributed a higher proportion of the biomass (58–70%) compared to males, and individuals at resting maturity stage were dominant, indicating that hoki do not spawn within the survey area at this time of year. The biomass declining trend is consistent with patterns from July surveys, where hoki biomass declined between 2017 and 2025 (Ramos 2025), and with stock assessment applying data-poor methods to commercial data, which estimated that 2018 biomass was approximately 13% of the 1987 level (Ramos & Winter 2019). At a broader regional scale, Zavatteri & Giussi (2022) reported that hoki biomass in Argentine and adjacent waters peaked in 2000, declined sharply to a minimum in 2016, and showed a modest recovery in 2017–2019, a pattern consistent with the low biomass values observed in February surveys around 2016–2017. The absence of biomass estimates from Falkland Islands commercial data since 2019 (Ramos & Winter 2022c) limits more recent fishery-survey comparisons.

In contrast to the (marginally) non-significant biomass trend, both mean and median pre-anal length showed significant non-linear temporal trends, declining from 2010 to a minimum in 2020–2021, before partially recovering by 2026. The partial recovery in length from 2021 onwards, may indicate that while abundance remained low in recent years, the size composition is shifting back towards larger individuals. This may be linked to the establishment since December 2023 of a year-round closed area in the south-western FICZ (south of 52.5°S and west of 60.5°W) implemented to reduce bycatch of Patagonian toothfish (FIFD, *unpublished internal document*), which overlaps with areas of historically higher hoki occurrence, reducing fishing pressure and aiding the recovery of the stock.

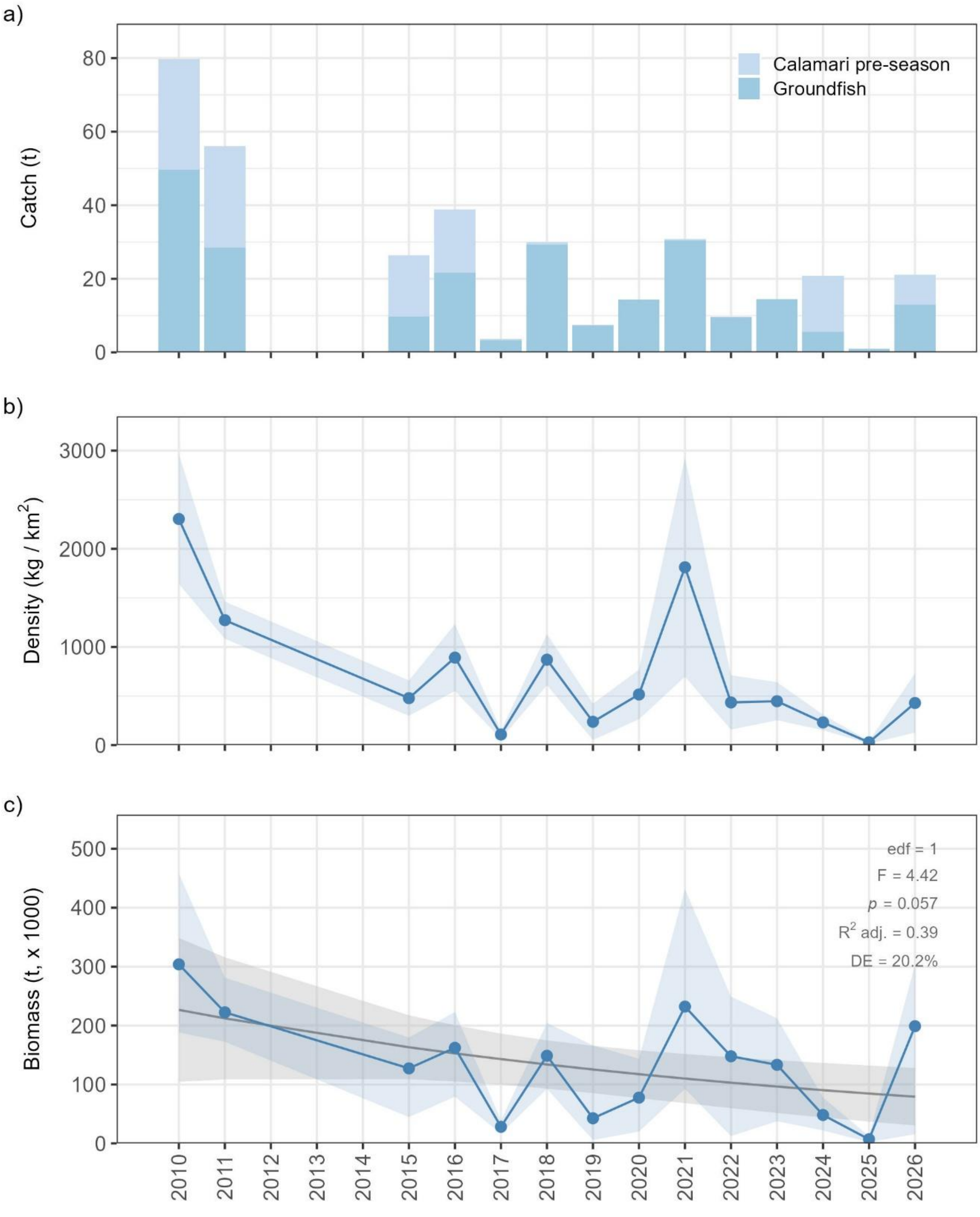


Fig. 27. Abundance of hoki (*Macruronus magellanicus*) during February groundfish and calamari pre-season surveys conducted in Falkland Islands waters in 2010–2011 and 2015–2026. (a) Catch per survey, (b) annual mean density ± SE represented by the blue line and shaded region, respectively, and (c) estimated biomass, where the blue line and shaded region represent the median and 95% pointwise confidence interval derived from 10,000 bootstrap biomass estimates, and the grey line and shaded region represent the fitted Generalised Additive Model (GAM) smooth and its 95% pointwise confidence interval.

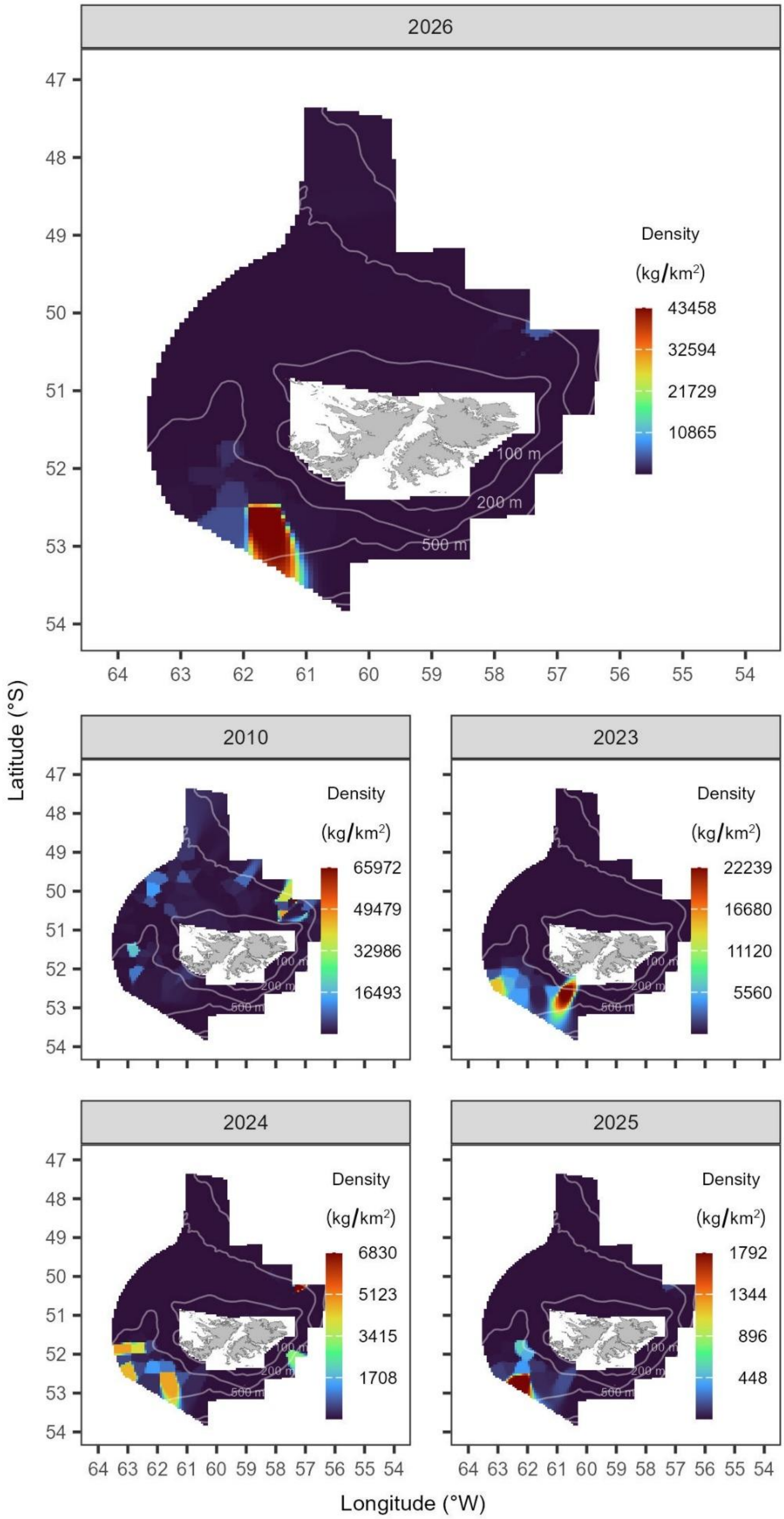


Fig. 28. Distribution and abundance of hoki (*Macruronus magellanicus*) derived from the February 2026 groundfish and calamari pre-season surveys in Falkland Islands waters, compared with the first year of the time series (2010) and the three preceding years (2023–2025). Colour scales are specific to each year. Isobaths at 100 m, 200 m, and 500 m are shown.

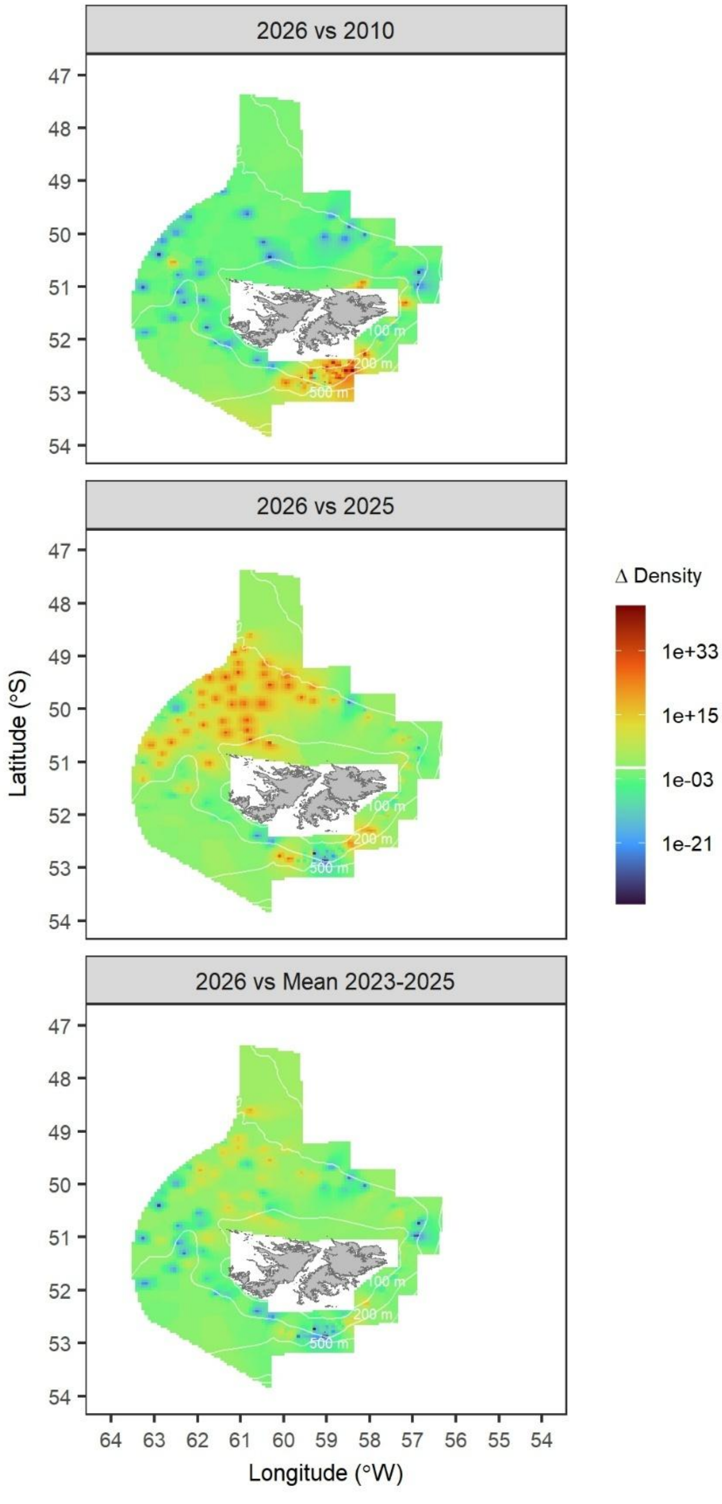


Fig. 29. Spatial change in density of hoki (*Macruronus magellanicus*) derived from the February 2026 groundfish and calamari pre-season surveys in Falkland Islands waters, relative to the first year of the time series (2010), the previous year (2025), and the mean of the three preceding years (2023–2025). The spatial change in density is expressed as the ratio of density (kg/km$^2$) in 2026 relative to the density in the baseline year (2010, 2025, 2023–2025 mean). Isobaths at 100 m, 200 m, and 500 m are shown. The colour scale is $log_{10}$-transformed to aid visualisation, with increases in density indicated above the horizontal white line towards dark red, and decreases in density indicated below the horizontal white line towards dark blue.

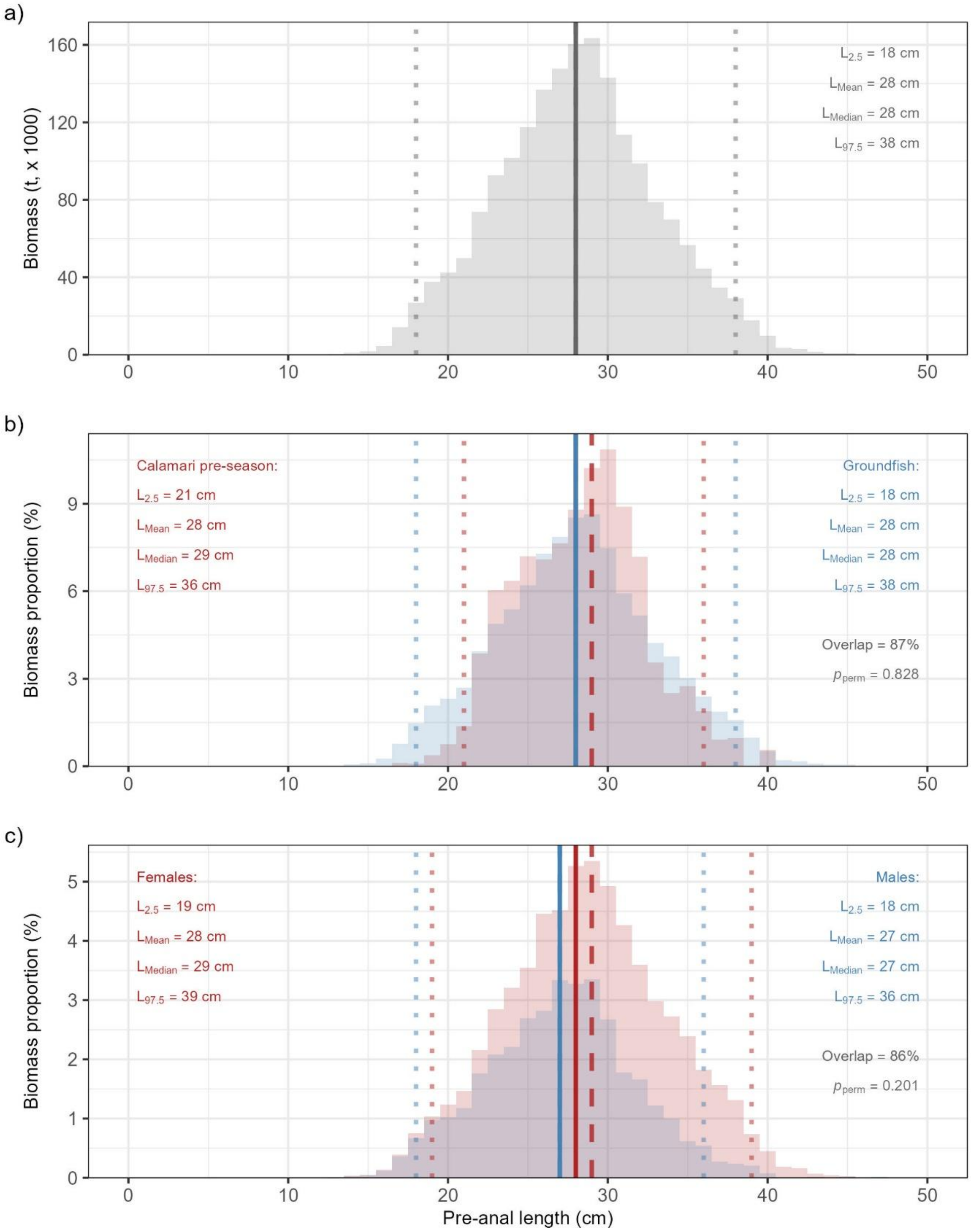


Fig. 30. Biomass-at-length class composition of hoki (*Macruronus magellanicus*) across all years combined, based on February groundfish and calamari pre-season surveys conducted in Falkland Islands waters in 2010–2011 and 2015–2026. a) Overall biomass-at-length frequency distribution. b) Overlap in biomass-at-length distributions between calamari pre-season (red) and groundfish (blue) surveys. c) Overlap in biomass-at-length distributions between females (red) and males (blue). Solid vertical lines indicate the mean length ($L_{Mean}$), dashed lines the median length ($L_{Median}$), and dotted lines the 2.5th and 97.5th length percentiles ($L_{2.5}$ and $L_{97.5}$, respectively). $p_{perm}$ is the significance of the weighted permutation test to assess differences between groups.

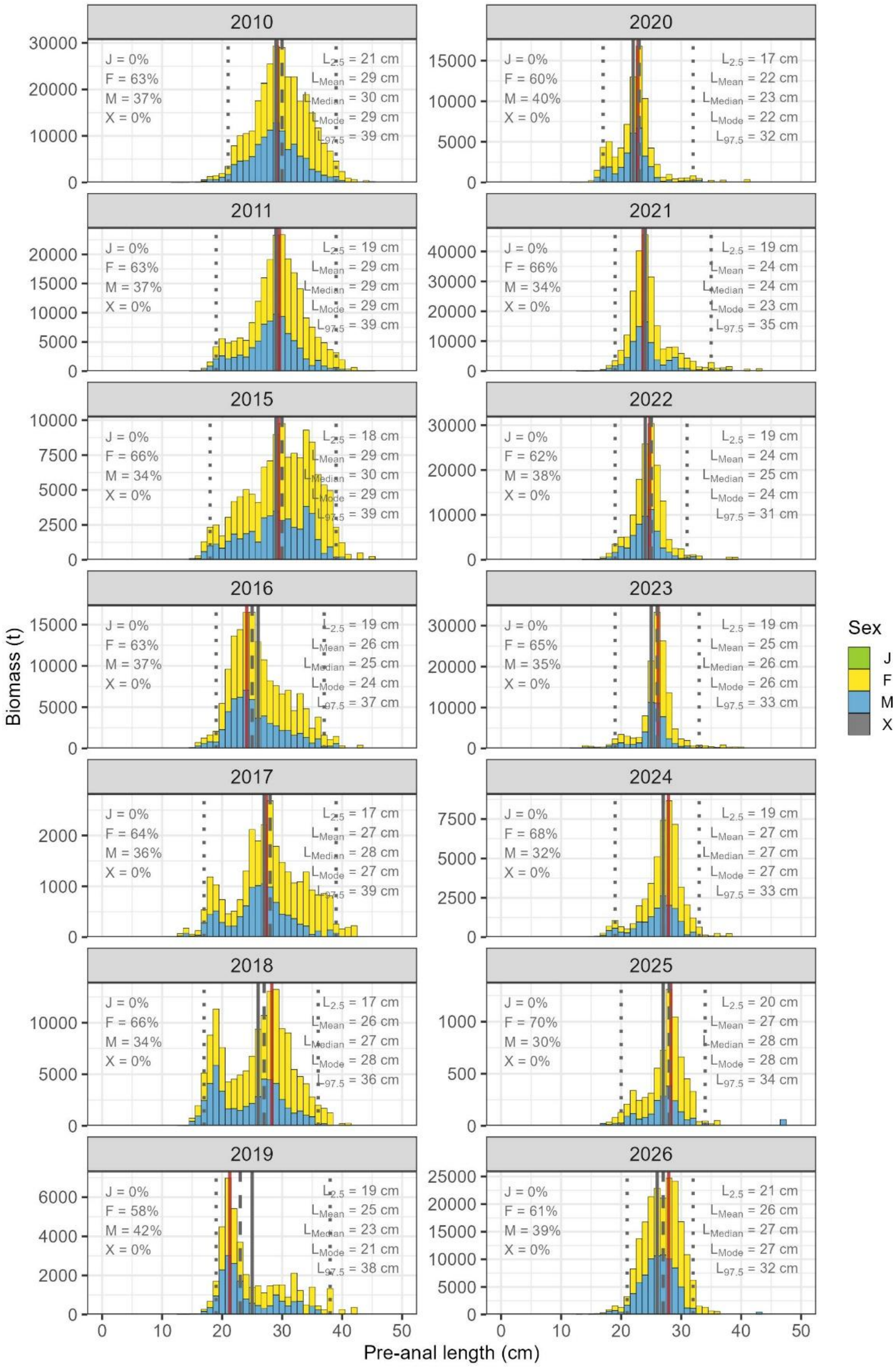


Fig. 31. Annual biomass-at-length class composition of hoki (*Macruronus magellanicus*) during February groundfish and calamari pre-season surveys conducted in Falkland Islands waters in 2010–2011 and 2015–2026. Stacked bars represent biomass (t) per 1.0 cm length class, partitioned by sex (J = juvenile; F = female; M = male; X = undetermined), with the proportion of total annual biomass for each sex indicated in the upper left of each panel. Vertical lines indicate the mean length ($L_{Mean}$, grey solid), median length ($L_{Median}$, grey dashed), modal length ($L_{Mode}$, red solid), and 2.5th and 97.5th percentiles ($L_{2.5}$ and $L_{97.5}$, grey dotted) of the biomass-weighted length distribution. Note the different y-axis scales among years.

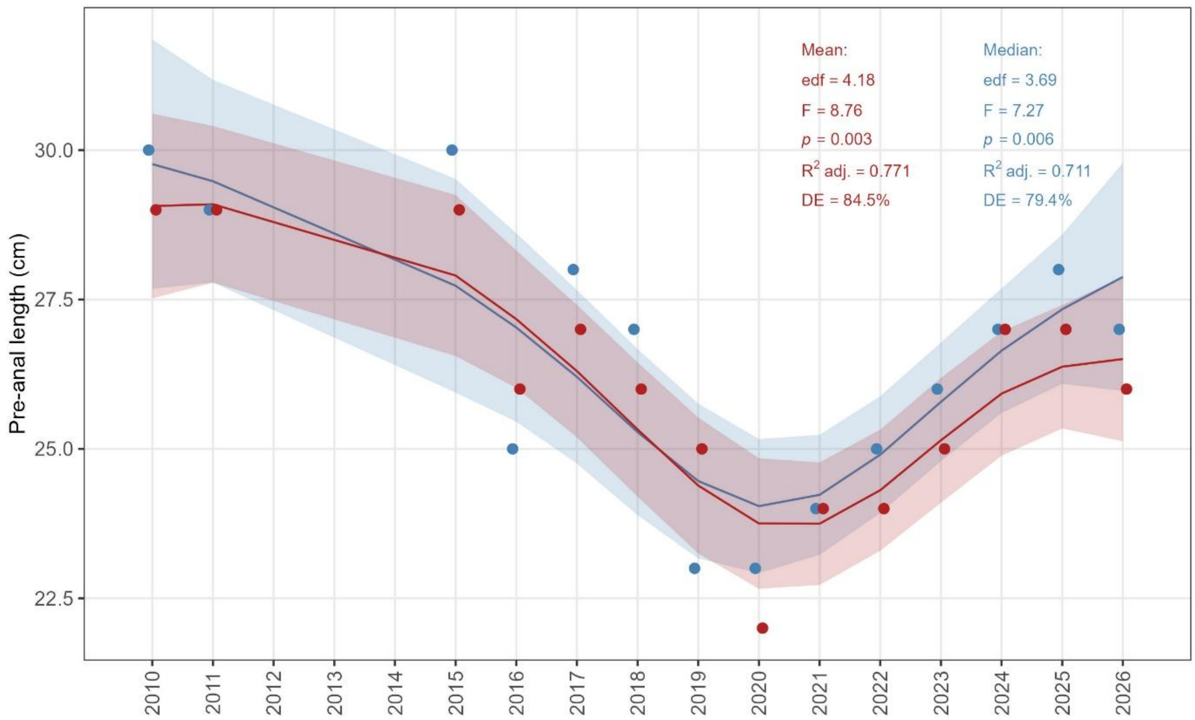


Fig. 32. Median (blue) and mean (red) pre-anal length of hoki (*Macruronus magellanicus*) during February groundfish and calamari pre-season surveys conducted in Falkland Islands waters in 2010–2011 and 2015–2026. The line and shaded region represent the fitted Generalised Additive Model (GAM) smooth and its 95% pointwise confidence interval.

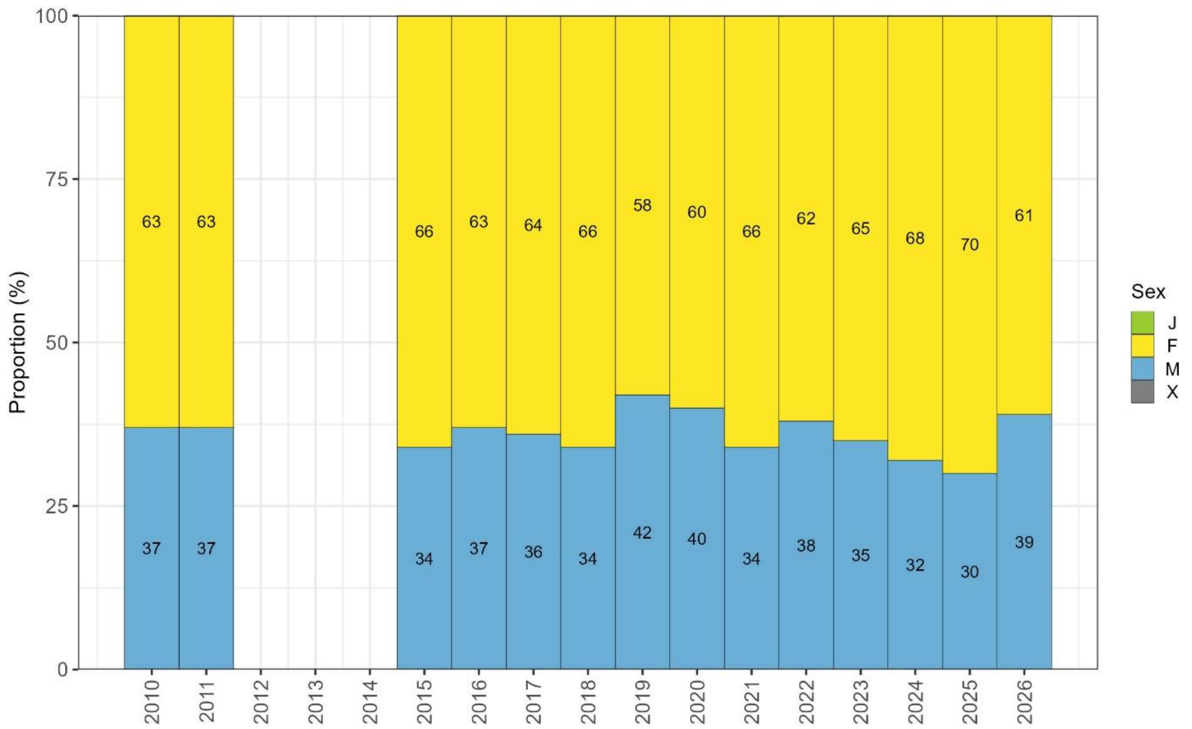


Fig. 33. Proportion by sex (J = juvenile; F = female; M = male; X = undetermined) of hoki (*Macruronus magellanicus*) during February groundfish and calamari pre-season surveys conducted in Falkland Islands waters in 2010–2011 and 2015–2026. Labels for proportions < 3% are omitted.

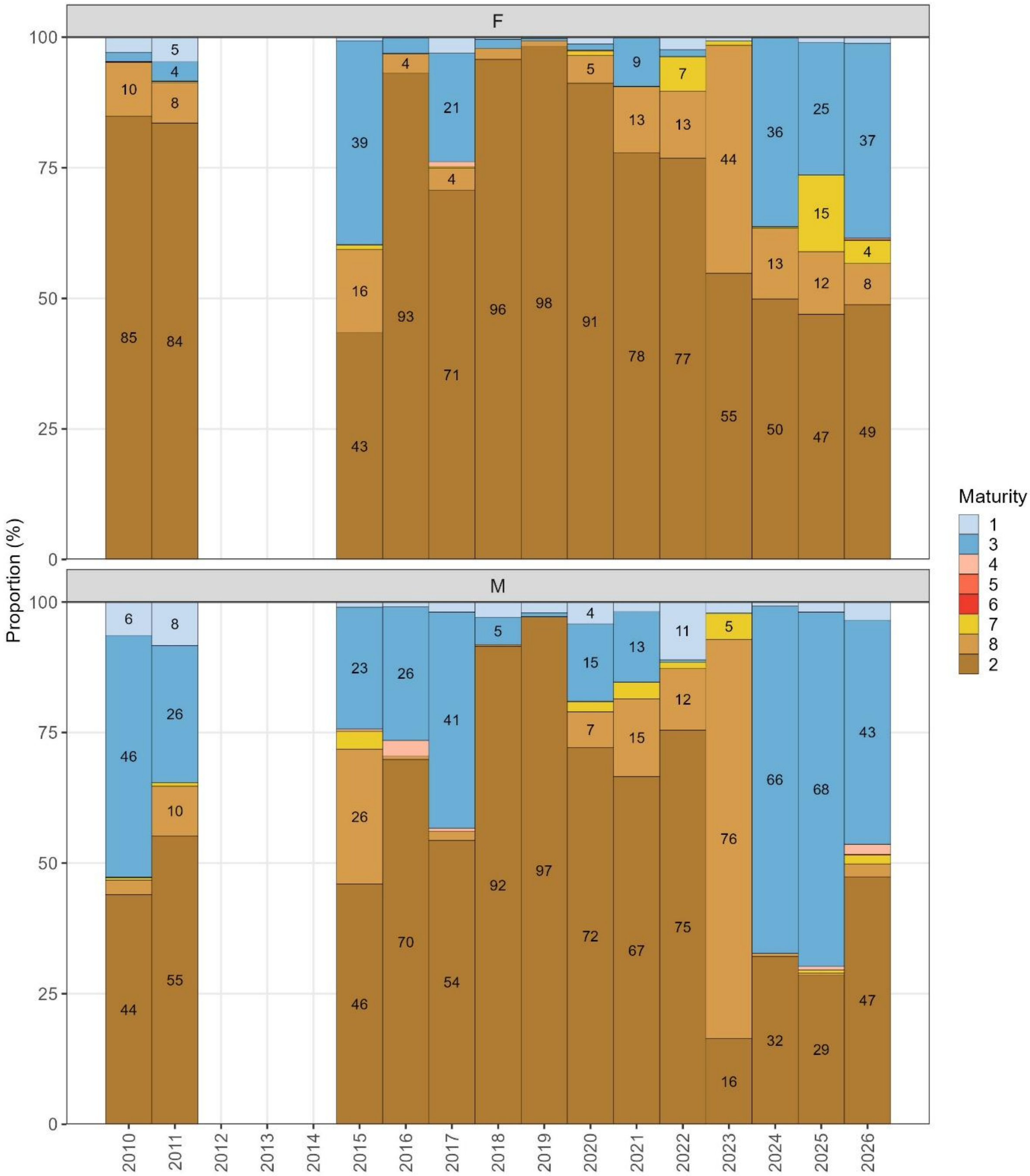


Fig. 34. Proportion by sexual maturity (1, immature; 3, early developing; 4, late developing; 5, ripe; 6, running; 7, spent; 8, recovering spent; 2, resting) of hoki (*Macruronus magellanicus*) during February groundfish and calamari pre-season surveys conducted in Falkland Islands waters in 2010–2011 and 2015–2026. Maturity stages ordered by developmental sequence. Labels for proportions < 3% are omitted.

### 4.3.5. Kingclip (*Genypterus blacodes*)

4.3.5.1. Temporal patterns of abundance

On average, 91% of the total kingclip catches in the time series were obtained from groundfish surveys and 9% from calamari pre-season surveys. The highest catch of kingclip occurred in 2015 (14.73 t). Catch in 2026 (3.96 t) represented a 22.2% increase relative to the 2010 catch (3.24 t), a 63.2% increase relative to the 2025 catch (2.42 t), and corresponded to 65.2% of the 2023–2025 mean (6.07 t; Fig. 35a; Appendix II).

The highest densities were recorded in 2015 (554.29 ± 246.06 kg/km²; mean ± SE). Densities in 2026 (73.99 ± 26.05 kg/km²) corresponded to 62.5% of the 2010 densities (118.46 ± 24.61 kg/km²), 95.8% of the 2025 densities (77.23 ± 35.29 kg/km²), and 42.1% of the 2023–2025 mean catch (175.75 ± 42.34 kg/km²; Fig. 35b).

Kingclip biomass was highest in 2015 (77,455.04 t), although confidence intervals for this estimate were wide. The lowest biomass was recorded in 2025 (11,421.45 t). Biomass in 2026 (12,274.62 t) was the second lowest in the time series, corresponding to 57.4% of 2010 levels (21,384.02 t), a non-significant decrease relative to 2010 ($p > 0.05$). Biomass in 2026 represented a 7.5% increase relative to 2025 that was non-significant ($p > 0.05$). In contrast, biomass in 2026 corresponded to 55.1% of the 2023–2025 mean (22,271.05 t), a significant decrease ($p = 0.036$; Fig. 35c; Table IV–V; Appendix III–IV). Analysis of the full time series revealed a significant non-linear trend in biomass (GAM: edf = 6.71, $F = 7.51$, $p = 0.012$), with the model explaining 92.3% of the deviance ($R^2$ adj. = 0.753), indicating a complex but consistent pattern of change over the time series (Fig. 35c; Appendix V).

4.3.5.2. Spatial patterns of abundance

In 2026, the highest density (2,915 kg/km$^2$) of kingclip occurred to the north, near the northern limit of the FICZ at approximately 49.5°S and 60.5°W. A secondary aggregation with moderate density was also detected to the north-west in the FICZ, at 50.5°S and 62.5°W. Kingclip spatial distribution was patchy in 2010, and from 2023 to 2025 (Fig. 36). For the full time series, the highest density (32,774 kg/km$^2$) was observed to the north-west in 2015.

Analysis of the spatial change in density revealed an overall decrease in densities through the survey area. Comparison of densities in 2026 relative to 2010 showed substantial decreases in densities through the survey area, and particularly in the north of the 'Loligo Box' and to the north of West Falkland, while densities increased in the south and centre of the 'Loligo Box'. Comparisons of 2026 with 2025 showed predominant decreases in density through the survey area, and patchy increases in densities along the 'Loligo Box', as well as through the north and west in the FICZ. Comparisons of 2026 with the 2023–2025 mean revealed that densities predominantly decreased through the survey area; in contrast, densities increased in distinct areas in the south and north of the 'Loligo Box', and to the north-west in the FICZ (Fig. 37).

4.3.5.3. Length composition

Across all survey years combined, total length of kingclip was in the range of 23 to 153 cm; however, 95% of the estimated biomass was comprised of individuals between 48 and

111 cm, with a median length of 76 ± 2.71 cm (median ± SE) and a mean length of 76 ± 2.17 cm (mean ± SE; Fig. 38a).

The distribution of biomass proportions by size class exhibited a 48% overlap between the groundfish and calamari pre-season surveys. Accordingly, the biomass-weighted mean length was significantly different ($p = 0.024$) between the groundfish (76 ± 2.17 cm; mean ± SE) and the calamari pre-season (85 ± 2.95 cm) surveys. Individuals collected in the groundfish survey were generally smaller than individuals collected in the calamari pre-season survey. In the groundfish survey, 95% of the biomass of kingclip was comprised of individuals between 48 and 111 cm, with a median length of 76 ± 2.74 cm. In the calamari pre-season survey, 95% of the biomass of kingclip was comprised of individuals between 58 and 108 cm, with a median length of 86 ± 4.20 cm (Fig. 38b).

The distribution of biomass proportions by size class exhibited an 82% overlap between females and males. Despite the high overlap, the permutation analysis revealed that the biomass-weighted mean length was significantly different ($p < 0.001$) between females (79 ± 2.13 cm) and males (70 ± 2.24 cm). This difference in size structure was in part due to the presence of females > 65 cm that were not as abundant for males. For females, 95% of the biomass was comprised of individuals between 50 and 112 cm, with a median length of 79 ± 2.57 cm. For males, 95% of the biomass was comprised of individuals between 47 and 109 cm, with a median length of 69 ± 2.27 cm (Fig. 38c).

Through the time series, the size structure of kingclip was broad and multimodal. Several length-groups were present and not clearly distinguished because of size overlap. The main modal length increased from 64 cm in 2010 to 85 cm in 2026 (Fig. 39). In 2026, the size structure remained broad and multimodal. Lengths were between 34 and 122 cm; however, 95% of the biomass was comprised of individuals between 56 and 107 cm, with a median length of 83 ± 2.22 cm and a mean length of 81 ± 1.60 cm. For females, 95% of the biomass was comprised of individuals between 56 and 107 cm, with a median length of 85 ± 2.50 cm and a mean length of 83 ± 2.10 cm. For males, 95% of the biomass was comprised of individuals between 54 and 98 cm, with a median length of 76 ± 2.66 cm and a mean length of 76 ± 1.98 cm (Fig. 39).

Strongly significant non-linear trends were observed for the mean (GAM: edf = 7.32, $F = 40.72$, $p < 0.001$, $R^2$ adj. = 0.963, DE = 98.4%) and the median (GAM: edf = 6.65, $F = 26.42$, $p < 0.001$, $R^2$ adj. = 0.940, DE = 97.1%) lengths. Both mean and median lengths were approximately 74–78 cm in 2010, remained relatively stable through to 2016, declined to a minimum of approximately 69–70 cm in 2020–2021, and recovered to approximately 81–83 cm by 2026 (Fig. 40).

#### 4.3.5.4. Sex and maturity composition

Across all survey years combined, the biomass composition of kingclip was consistently dominated by females, comprising 67.4 ± 1.3% (mean ± SE) of the total biomass, followed by males at 32.4 ± 1.3%, with individuals of undetermined sex accounting for a negligible 0.2 ± 0.1% and no juveniles recorded in any survey year. Interannual variability in sex composition was relatively low throughout the time series, with the female proportion ranging from 61% in 2021 to 78% in 2025, and the male proportion ranging from 21% in 2025 to 39% in 2021. The proportion of females increased since 2023. The 2026 sex composition was consistent with the time-series mean, with females comprising 70% and males 30% of the biomass (Fig. 41).

Maturity composition was dominated by post-spawning individuals (resting) in both sexes in most years (Fig. 42). Females were characterised by a predominance of resting individuals (51–92%) between 2010 and 2025. For males, resting individuals comprised > 50% of the male biomass in most years, except for 2015, and between 2023 and 2026. Late developing, ripe, and running individuals were reported in relatively small proportions (< 28% combined). Composition in 2026 departed markedly from this pattern, and was characterised by a shift towards immature and early developing individuals, with the lowest proportion of resting individuals in the time series.

#### 4.3.5.5. Discussion

The significant non-linear biomass trend of kingclip in Falkland Islands waters reflects a complex temporal pattern characterised by relatively low levels in recent years. Females contributed approximately 67% of the biomass, with predominance of post-spawning (resting) individuals through most of the time series, indicating that the spawning period precedes the February survey. The February surveys biomass pattern contrasts with July surveys, where the biomass in July 2025 was the highest since July 2017, although with wide confidence intervals (Ramos 2025), suggesting seasonal differences in kingclip availability within the survey area. However, low biomass levels in recent February surveys are consistent with declining CPUE in the Falkland Islands finfish fishery since 2013 (García 2024), and with analyses of Argentine survey and fishery data showing an overall biomass decline from 1987 to 2021, with a period of stability from 2014 to 2017, and a gradual increase thereafter (Di Marco 2022). The biomass trends observed in February surveys conducted in Falkland Islands waters thus may reflect broader regional dynamics.

The highly significant non-linear trends in both mean and median total length showed correspondence between the biomass and length patterns from 2010 to 2022, both peaked around 2015–2016, declined to minima around 2020–2021, and increased in 2022. After 2022, both mean and median length continued increasing despite low biomass levels. Because kingclip are caught at relatively small sizes in the Falkland Islands and stock status remains below the limit reference point, harvesting closer to 80 cm has been recommended to improve fishing mortality and yield per recruit, facilitating stock recovery (García 2025). The frequent presence of large individuals (70–95 cm) in recent February and July surveys suggests that such animals are available in the FICZ/FOCZ, and the recent recovery in mean and median length towards and beyond 80 cm may indicate an improving size structure that could support more selective harvesting strategies. Additional work is needed to evaluate whether restricting fishing in specific grid squares or adjusting fishing gear could reduce catches of small individuals and further facilitate stock recovery.

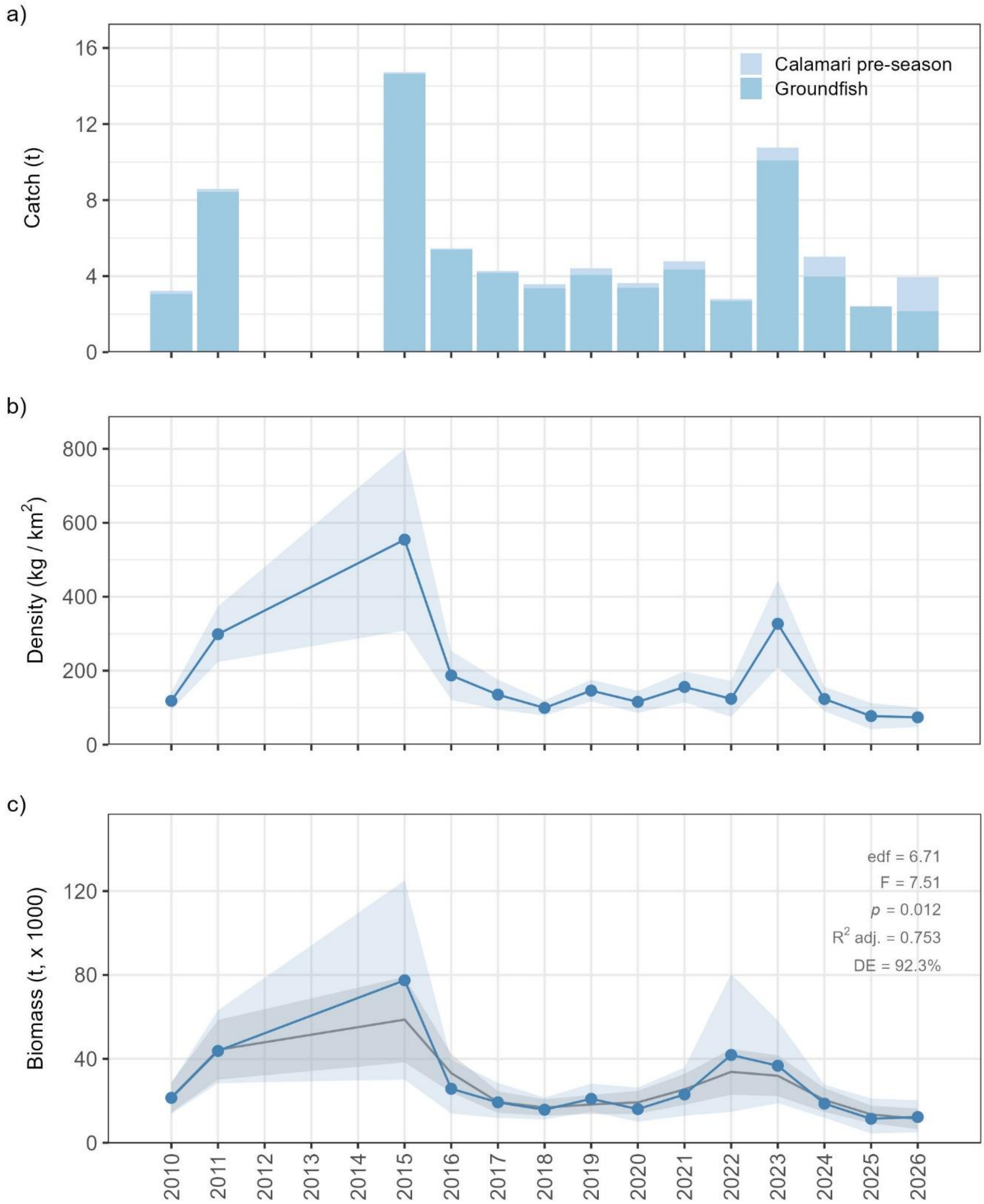


Fig. 35. Abundance of kingclip (*Genypterus blacodes*) during February groundfish and calamari pre-season surveys conducted in Falkland Islands waters in 2010–2011 and 2015–2026. (a) Catch per survey, (b) annual mean density ± SE represented by the blue line and shaded region, respectively, and (c) estimated biomass, where the blue line and shaded region represent the median and 95% pointwise confidence interval derived from 10,000 bootstrap biomass estimates, and the grey line and shaded region represent the fitted Generalised Additive Model (GAM) smooth and its 95% pointwise confidence interval.

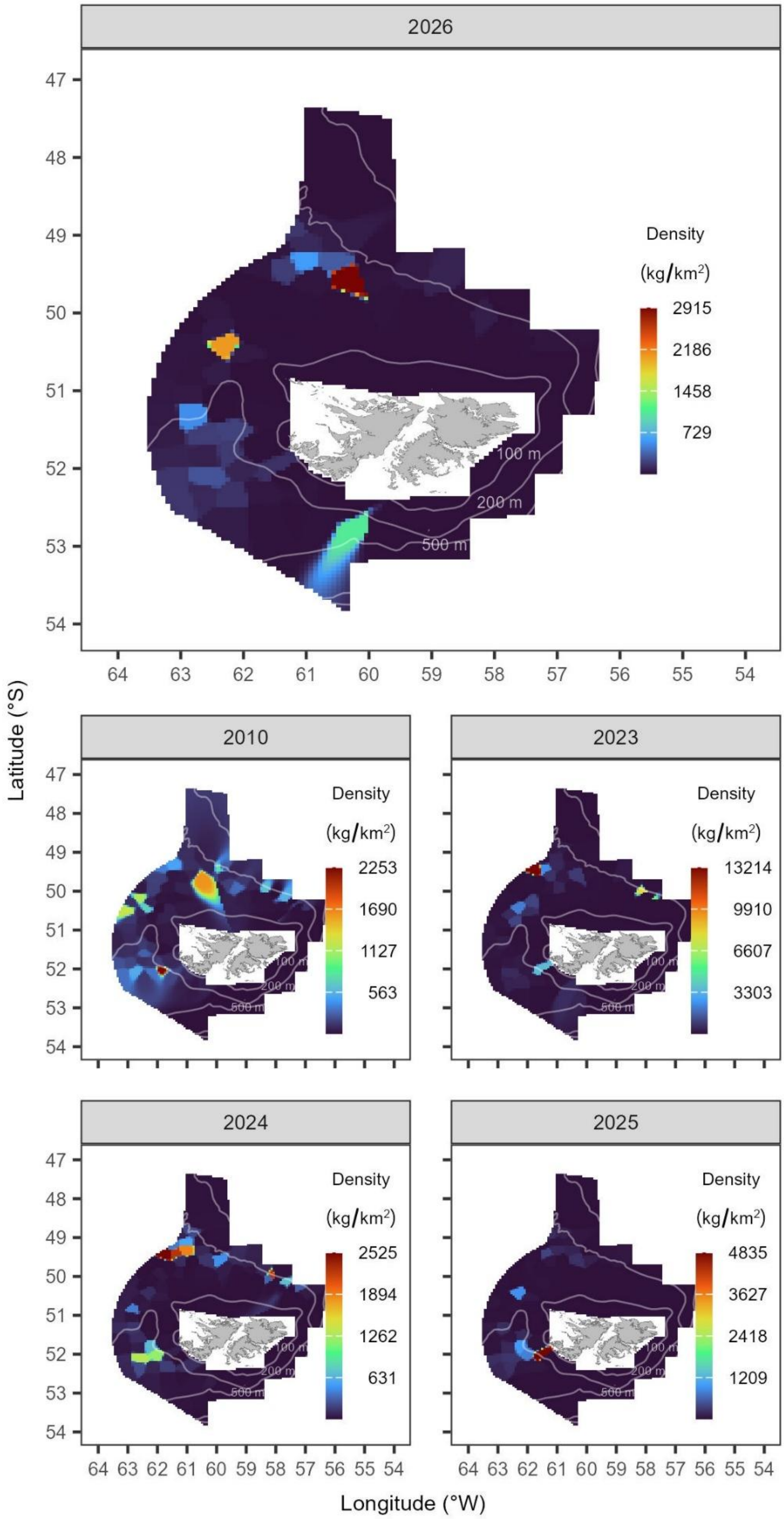


Fig. 36. Distribution and abundance of kingclip (*Genypterus blacodes*) derived from the February 2026 groundfish and calamari pre-season surveys in Falkland Islands waters, compared with the first year of the time series (2010) and the three preceding years (2023–2025). Colour scales are specific to each year. Isobaths at 100 m, 200 m, and 500 m are shown.

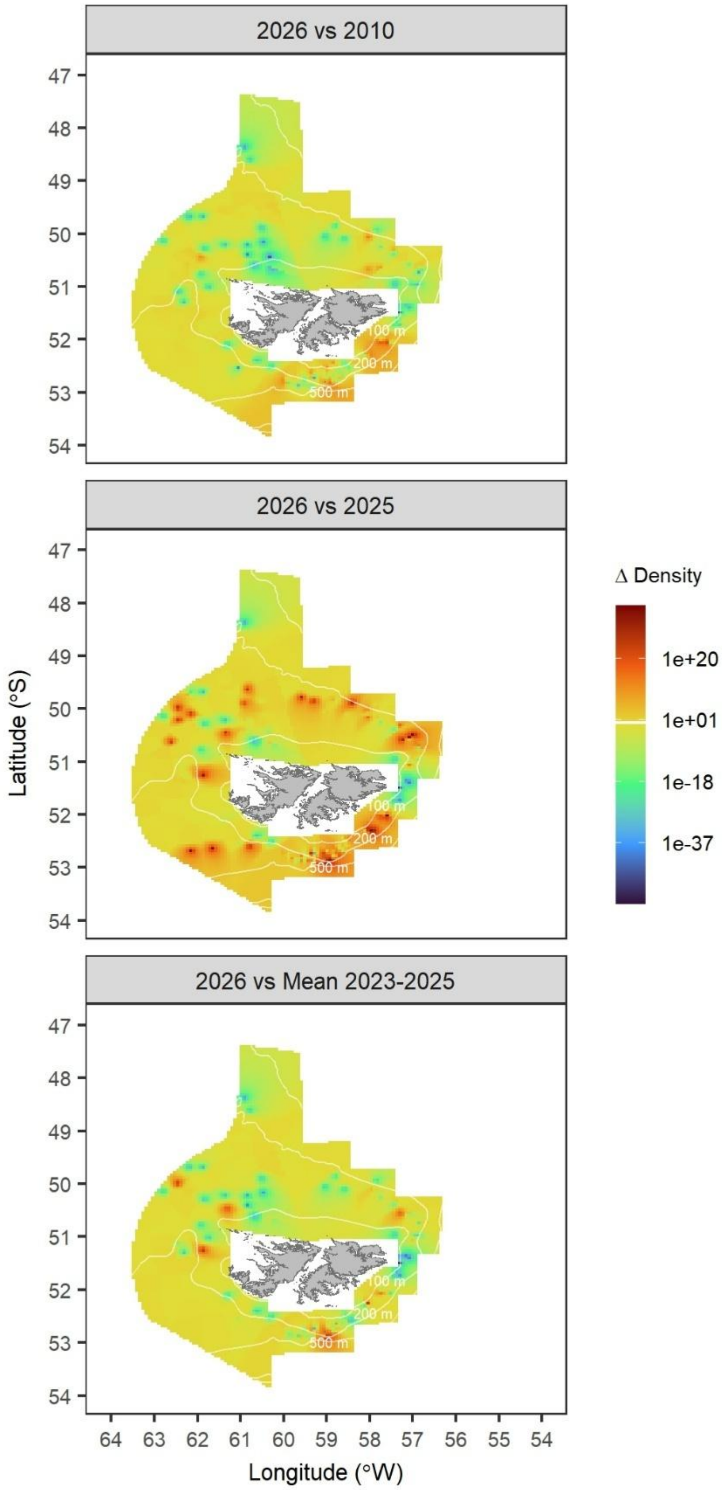


Fig. 37. Spatial change in density of kingclip (*Genypterus blacodes*) derived from the February 2026 groundfish and calamari pre-season surveys in Falkland Islands waters, relative to the first year of the time series (2010), the previous year (2025), and the mean of the three preceding years (2023–2025). The spatial change in density is expressed as the ratio of density (kg/km$^2$) in 2026 relative to the density in the baseline year (2010, 2025, 2023–2025 mean). Isobaths at 100 m, 200 m, and 500 m are shown. The colour scale is $\log_{10}$-transformed to aid visualisation, with increases in density indicated above the horizontal white line towards dark red, and decreases in density indicated below the horizontal white line towards dark blue.

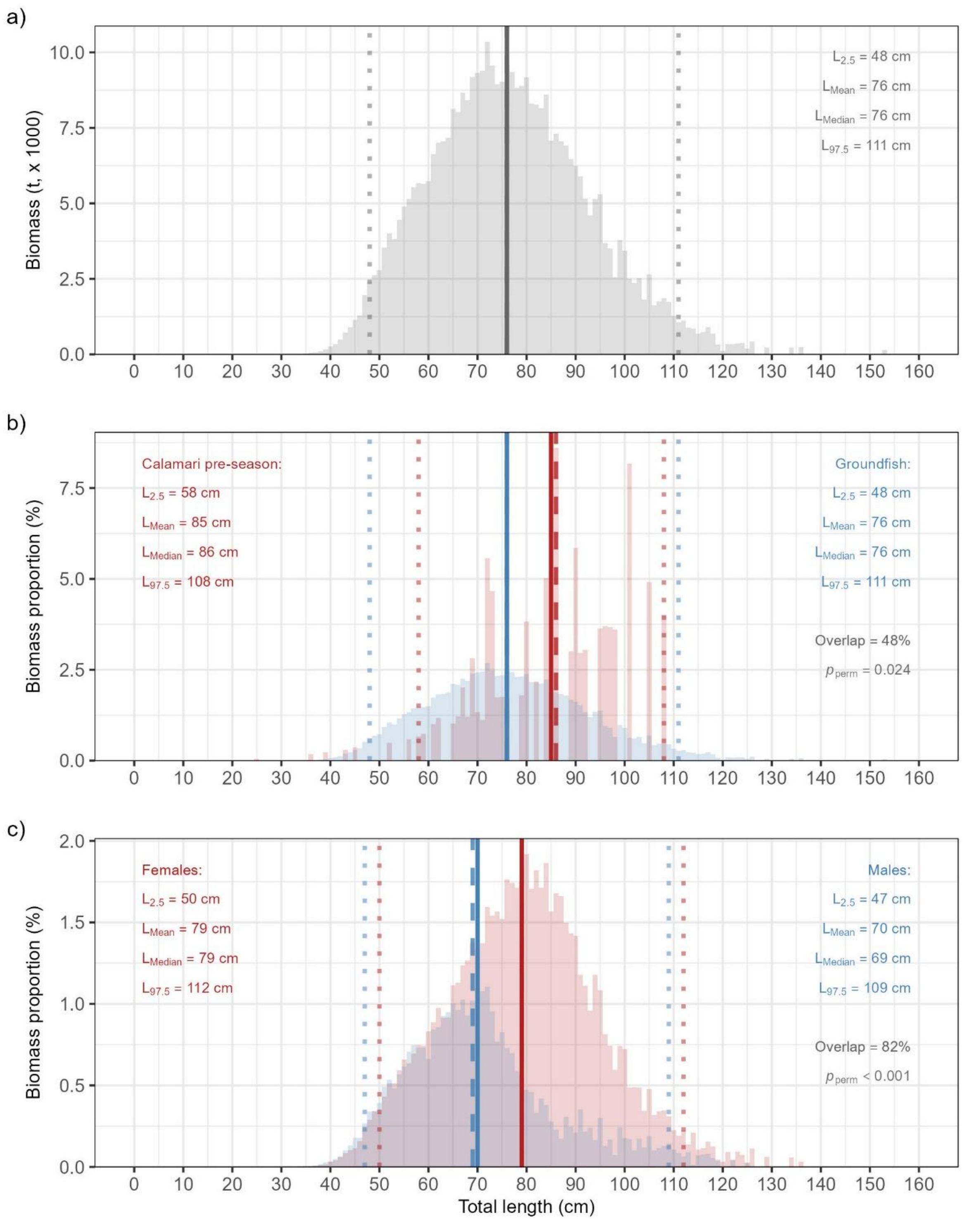


Fig. 38. Biomass-at-length class composition of kingclip (*Genypterus blacodes*) across all years combined, based on February groundfish and calamari pre-season surveys conducted in Falkland Islands waters in 2010–2011 and 2015–2026. a) Overall biomass-at-length frequency distribution. b) Overlap in biomass-at-length distributions between calamari pre-season (red) and groundfish (blue) surveys. c) Overlap in biomass-at-length distributions between females (red) and males (blue). Solid vertical lines indicate the mean length ($L_{Mean}$), dashed lines the median length ($L_{Median}$), and dotted lines the 2.5th and 97.5th length percentiles ($L_{2.5}$ and $L_{97.5}$, respectively). $p_{perm}$ is the significance of the weighted permutation test to assess differences between groups.

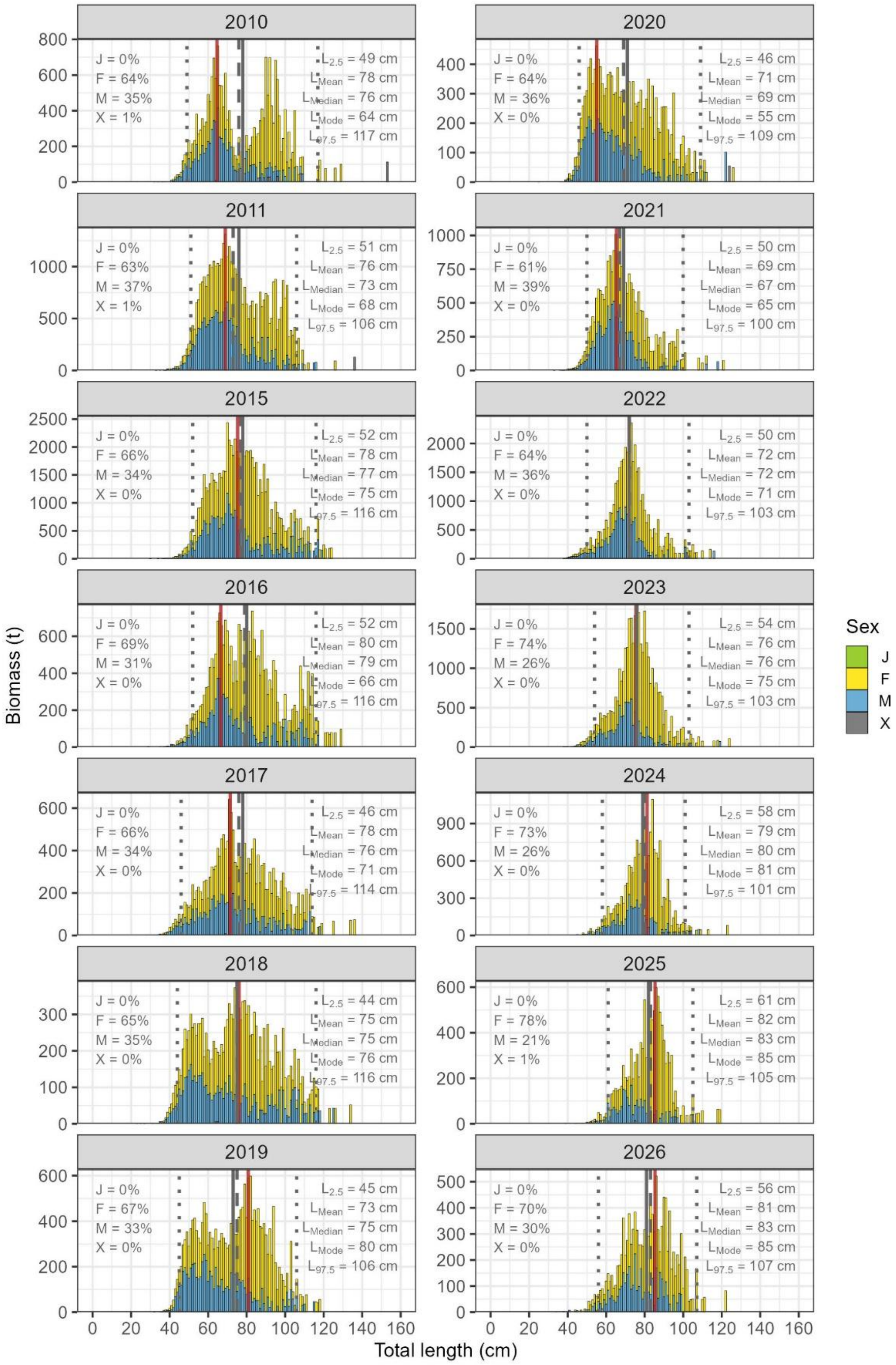


Fig. 39. Annual biomass-at-length class composition of kingclip (*Genypterus blacodes*) during February groundfish and calamari pre-season surveys conducted in Falkland Islands waters in 2010–2011 and 2015–2026. Stacked bars represent biomass (t) per 1.0 cm length class, partitioned by sex (J = juvenile; F = female; M = male; X = undetermined), with the proportion of total annual biomass for each sex indicated in the upper left of each panel. Vertical lines indicate the mean length ($L_{Mean}$, grey solid), median length ($L_{Median}$, grey dashed), modal length ($L_{Mode}$, red solid), and 2.5th and 97.5th percentiles ($L_{2.5}$ and $L_{97.5}$, grey dotted) of the biomass-weighted length distribution. Note the different y-axis scales among years.

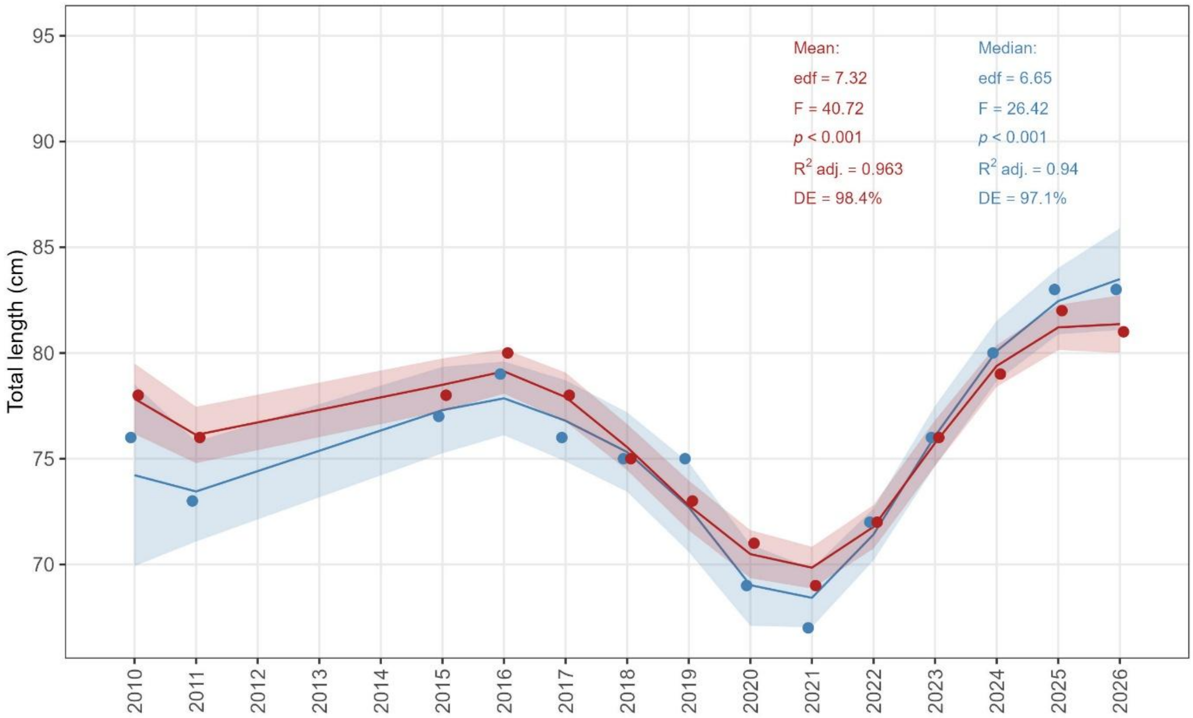


Fig. 40. Median (blue) and mean (red) total length of kingclip (*Genypterus blacodes*) during February groundfish and calamari pre-season surveys conducted in Falkland Islands waters in 2010–2011 and 2015–2026. The line and shaded region represent the fitted Generalised Additive Model (GAM) smooth and its 95% pointwise confidence interval.

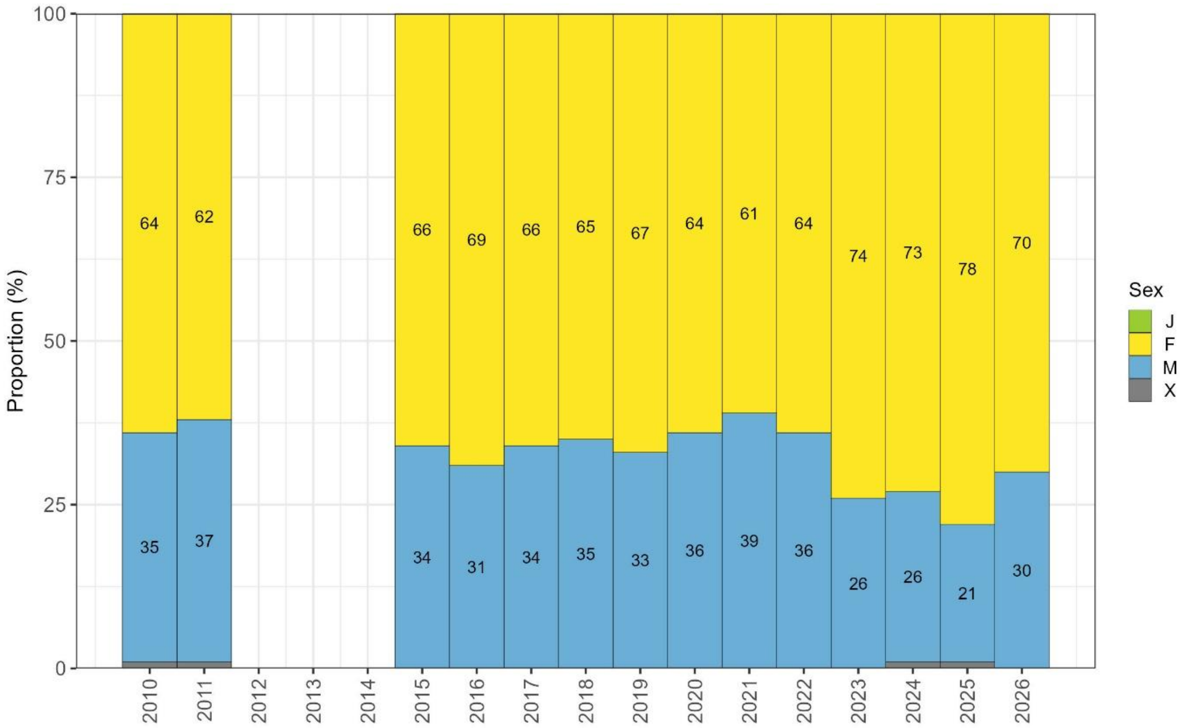


Fig. 41. Proportion by sex (J = juvenile; F = female; M = male; X = undetermined) of kingclip (*Genypterus blacodes*) during February groundfish and calamari pre-season surveys conducted in Falkland Islands waters in 2010–2011 and 2015–2026. Labels for proportions < 3% are omitted.

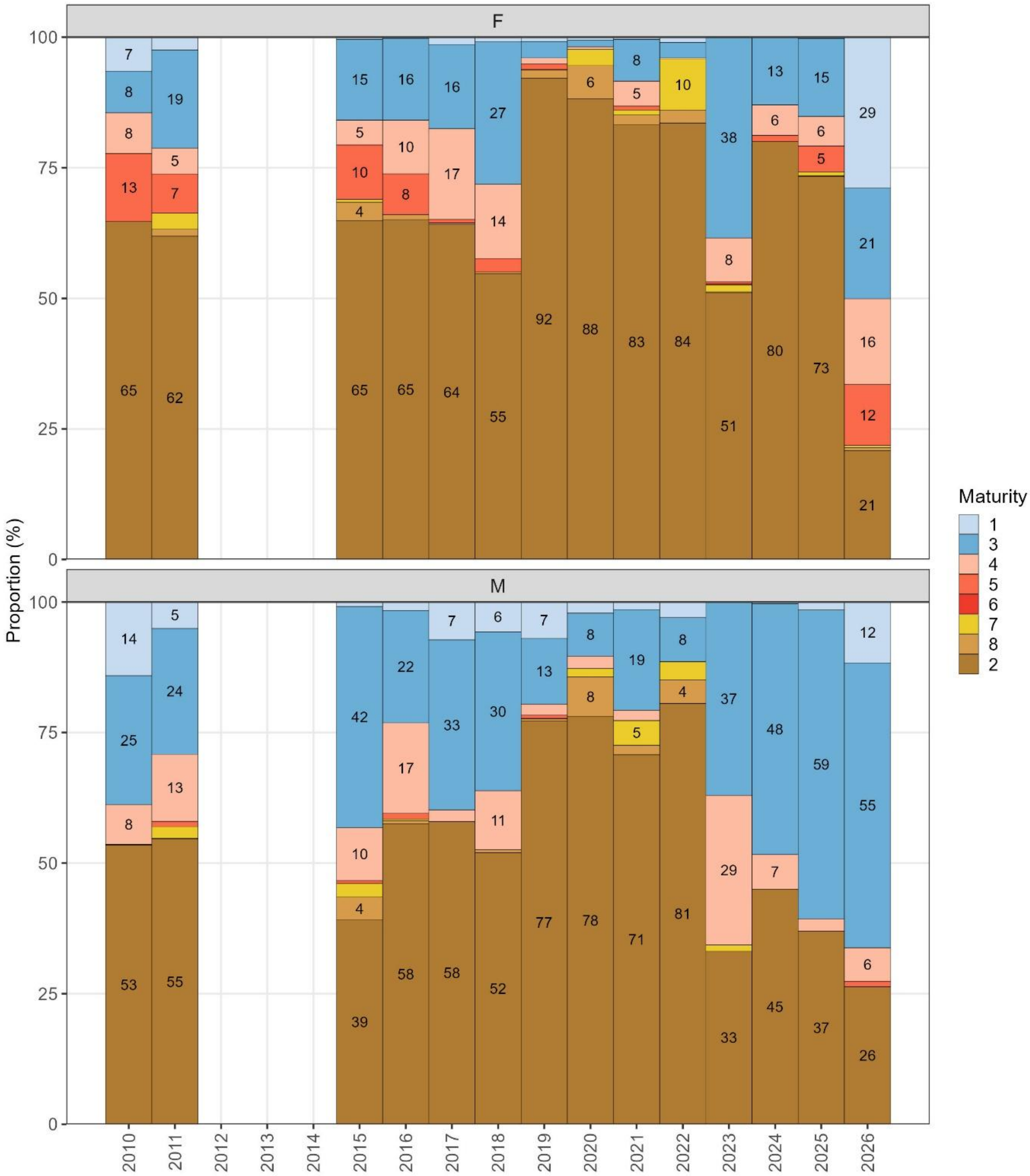


Fig. 42. Proportion by sexual maturity (1, immature; 3, early developing; 4, late developing; 5, ripe; 6, running; 7, spent; 8, recovering spent; 2, resting) of kingclip (*Genypterus blacodes*) during February groundfish and calamari pre-season surveys conducted in Falkland Islands waters in 2010–2011 and 2015–2026. Maturity stages ordered by developmental sequence. Labels for proportions < 3% are omitted.

### 4.3.6. Patagonian squid (*Doryteuthis gahi*)

4.3.6.1. Temporal patterns of abundance

On average, 2% of the Patagonian squid catches were obtained from groundfish surveys and 98% from calamari pre-season surveys. Catches decreased from 2010 (356.76 t) to 2011 (50.51 t) but increased over the following years and reached the highest catch in 2024 (683.31 t). The third highest catch in the time series was reported in 2026 (549.85 t). Catch in 2026 showed a 54.1% increase relative to the catch in 2010, a 58.9% increase relative to the catch in 2025 (346.15 t), and a 4.1% increase relative to the 2023–2025 mean catch (528.13 t; Fig. 43a; Appendix II).

The highest densities were recorded in 2010 (3,396.59 ± 591.47 kg/km²; mean ± SE). Densities in 2026 (2,620.18 ± 477.09 kg/km²) were the fifth highest in the time series, corresponding to 77.1% of the 2010 densities. However, densities in 2026 represented a 60.1% increase relative to the 2025 densities (1,636.45 ± 295.92 kg/km²), and were similar to the 2023–2025 mean densities (2,602.60 ± 278.51 kg/km²; Fig. 43b).

Patagonian squid biomass was highest in 2019 (220,848.11 t) and lowest in 2016 (43,724.10 t). Biomass in 2026 (158,443.57 t) represented 81.1% of 2010 levels (195,368.45 t), a non-significant change relative to 2010 ($p > 0.05$). Biomass in 2026 represented a statistically significant ($p = 0.027$) 38.4% increase relative to 2025 (114,447.18 t). In contrast, biomass in 2026 corresponded to 87.3% of the 2023–2025 mean (181,499.84 t), a non-significant decrease ($p > 0.05$; Fig. 43c; Table IV–V; Appendix III–IV). Analysis of the full time series revealed no significant temporal trend in biomass (GAM: edf = 1.00, $F = 0.74$, $p = 0.407$), with the model explaining only 5.2% of the deviance ($R^2$ adj. = −0.004), reflecting high interannual variability and no consistent directional change over the time series (Fig. 43c; Appendix V).

4.3.6.2. Spatial patterns of abundance

In 2026, the highest densities (28,408 kg/km²) were recorded to the south of East Falkland within the 'Loligo Box', at approximately 53°S and 59°W (Fig. 44). The highest densities consistently occurred to the south within the 'Loligo Box' through the time series, and the highest density in the full time series was calculated for 2023 (40,205 kg/km²).

Analysis of the spatial change in density revealed an overall decrease in densities through the survey area. Comparison of densities in 2026 relative to 2010 revealed that densities decreased through the survey area but with substantial decreases in the centre of the 'Loligo Box' and to the south-west in the FICZ; in contrast, densities increased in the north of the 'Loligo Box'. Comparisons of 2026 with 2025, and with the 2023–2025 mean also showed that densities decreased through the survey area, with substantial decreases from the north-east in the FICZ towards the north of West Falkland, as well as to the south-west in the FICZ; however, densities increased to the north and north-west in the FICZ (Fig. 45).

4.3.6.3. Length composition

Across all survey years combined, the size structure of Patagonian squid showed sizes in the range of 2.5 to 36.0 cm dorsal mantle length; however, 95% of the estimated biomass was comprised of individuals between 7.0 and 15.0 cm, with a median length of 10.5 ± 0.70 cm (median ± SE) and a mean length of 10.5 ± 0.60 cm (mean ± SE; Fig. 46a).

The distribution of biomass proportions by size class exhibited a 59% overlap between the groundfish and calamari pre-season surveys. Accordingly, the biomass-weighted mean length was significantly different ($p = 0.012$) between the groundfish (9.5 ± 0.61 cm; mean ± SE) and the calamari pre-season (11.0 ± 0.59 cm) surveys, indicating different size structure between surveys. Individuals collected in the groundfish survey were generally smaller than individuals collected in the calamari pre-season survey. In the groundfish survey, 95% of the biomass of Patagonian squid was comprised of individuals between 6.5 and 14.5 cm, with a median length of 9.5 ± 0.72 cm. In the calamari pre-season survey, 95% of the biomass of Patagonian squid was comprised of individuals between 8.0 and 15.5 cm, with a median length of 11.0 ± 0.63 cm (Fig. 46b).

The distribution of biomass proportions by size class exhibited a 92% overlap between females and males. Accordingly, the biomass-weighted mean length was not significantly different ($p > 0.05$) between females (10.5 ± 0.68 cm) and males (10.5 ± 0.72 cm), indicating similar size structure between females and males. For females, 95% of the biomass was comprised of individuals between 7.0 and 14.5 cm, with a median length of 10.5 ± 0.68 cm. For males, 95% of the biomass was comprised of individuals between 7.0 and 16.0 cm, with a median length of 10.5 ± 0.72 cm (Fig. 46c).

The size structure was mostly unimodal, with modal length in the range of 7.5 cm in 2016 to 12.0 cm in 2011 and no evident temporal pattern. In 2026, dorsal mantle lengths were in the range of 3.0 to 18.5 cm; however, 95% of the biomass was comprised of individuals between 7.0 and 14.0 cm, with a median length of 10.5 ± 0.49 cm and a mean length of 10.0 ± 0.37 cm. For females, 95% of the individuals were between 7.0 and 13.5 cm, with a median length of 10.5 ± 0.6 cm and a mean length of 10.0 ± 0.52 cm. For males, 95% of the biomass was comprised of individuals between 7.0 and 14.5 cm, with a median length of 10.5 ± 0.69 cm and a mean length of 10.0 ± 0.55 cm (Fig. 47).

Analysis of the full time series revealed no significant temporal trend in either mean (GAM: edf = 1, $F = 0.08$, $p = 0.785$, $R^2$ adj. = −0.077, DE = 0.6%) or median (GAM: edf = 1, $F = 0.95$, $p = 0.349$, $R^2$ adj. = −0.004, DE = 7.3%) dorsal mantle lengths. Both models converged to a linear smoother (edf = 1) and explained negligible deviance. The fitted smooths for mean and median dorsal mantle lengths remained consistently around 10–11 cm throughout the time series (Fig. 48).

#### 4.3.6.4. Sex and maturity composition

Across all survey years combined, the biomass composition of Patagonian squid was comprised of 55.9 ± 0.7% (mean ± SE) females, followed by 44.1 ± 0.7% males, with no juveniles or individuals of undetermined sex recorded in any survey year. Interannual variability was minimal, with the female proportion ranging only from 50% in 2022 to 60% in 2015, and the male proportion ranging from 40% in 2015 to 50% in 2022. The 2026 sex composition was similar to the time series mean, with females comprising 55% and males 45% of the biomass (Fig. 49).

Maturity composition was dominated by young and immature individuals throughout the time series (Fig. 50). For females, immature individuals were predominant throughout the time series (66–91%), young individuals contributed 5–31%, and preparatory, maturing and mature individuals combined contributed < 12% in each year. Males had a greater representation of preparatory, maturing and mature stages combined, accounting for < 27% in most years.

#### 4.3.6.5. Discussion

The absence of a significant temporal trend in Patagonian squid biomass in February surveys conducted in Falkland Islands waters reflects high inter-annual variability, although with an apparent increase in recent years. Given the spatial distribution of Patagonian squid within the FICZ/FOCZ, the biomass pattern observed in February surveys was primarily driven by the calamari pre-season survey component. Differences between the Patagonian squid biomass estimated here and that reported from the calamari pre-season survey alone (Chemshirova et al. 2026) must be noted, as the latter uses a smaller 'Loligo Box' area and accounts for habitat preference. While abundance during the first commercial fishing season has been generally consistent in recent years, the second commercial fishing season has experienced low abundances. July 2024 densities in the 'Loligo Box' produced the lowest second-season biomass estimate since 2006 (Falkland Islands Government 2025), prompting cancellation of the 2024 second fishing season. This low abundance was apparently associated with the northward displacement of *D. gahi* due to strong and colder oceanic currents, which resulted in the fleet fishing in international waters north of the FOCZ (Falkland Islands Government 2025). In 2025, the second season yielded the second lowest catch since 2016 (Skeljo & Winter 2025). These patterns suggest a divergence between first and second season availability that requires attention, as persistent declines in second season abundance could indicate environmental effects, earlier spawning migration, shifts in the distribution of recruits, or reduced survival between seasons, all of which have implications for the management of the commercial fishery.

The absence of a temporal trend in both mean and median dorsal mantle length combined with stable sex and maturity composition throughout the time series, suggests that despite large interannual fluctuations in abundance, the biological characteristics of the Patagonian squid population have not shown remarkable changes over the survey period. A similar pattern was observed in commercial fishery data, where size at recruitment and size at maturity did not change significantly between 1989 and 2019 (Arkhipkin et al. 2022a).

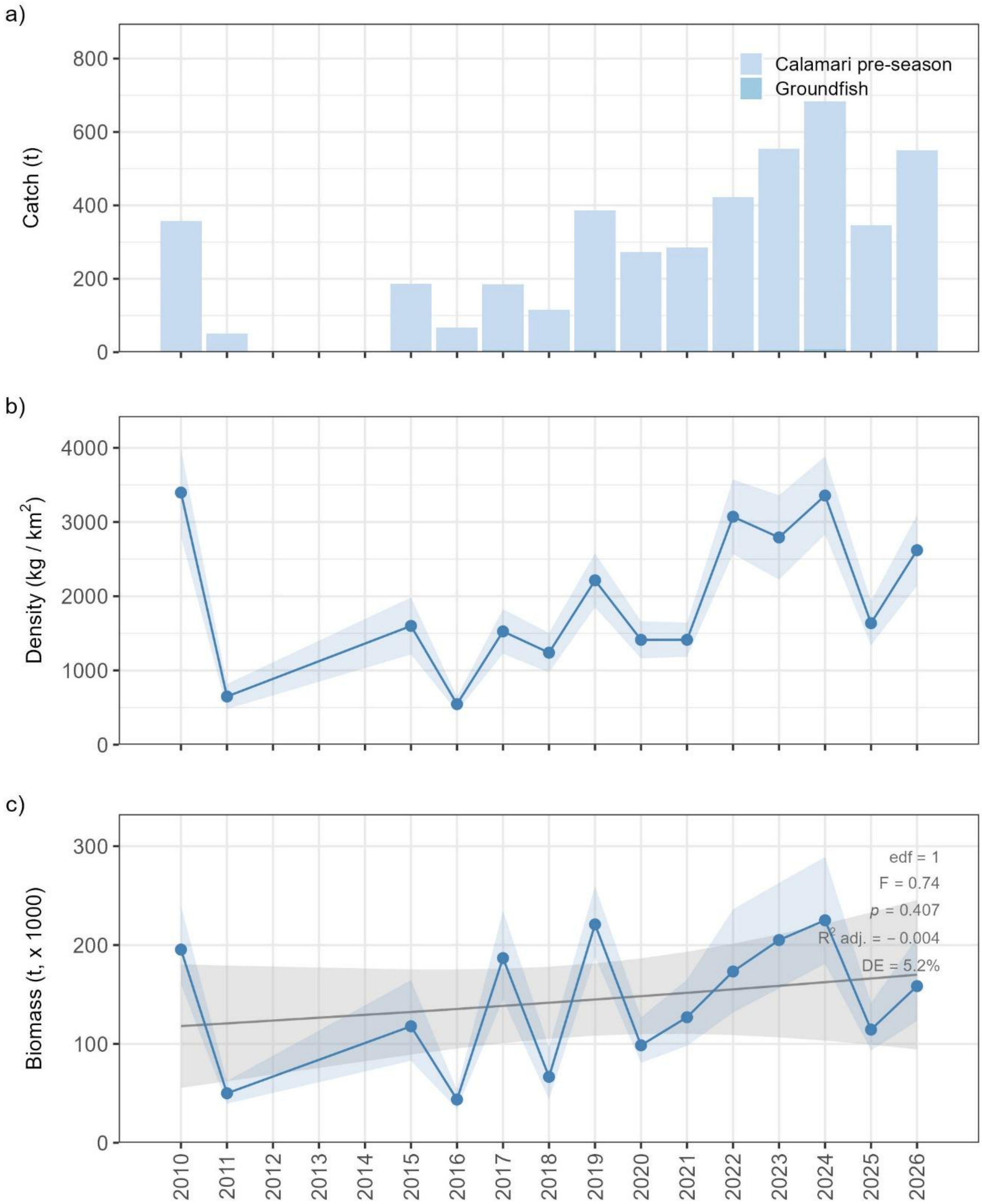


Fig. 43. Abundance of Patagonian squid (*Doryteuthis gahi*) during February groundfish and calamari pre-season surveys conducted in Falkland Islands waters in 2010–2011 and 2015–2026. (a) Catch per survey, (b) annual mean density ± SE represented by the blue line and shaded region, respectively, and (c) estimated biomass, where the blue line and shaded region represent the median and 95% pointwise confidence interval derived from 10,000 bootstrap biomass estimates, and the grey line and shaded region represent the fitted Generalised Additive Model (GAM) smooth and its 95% pointwise confidence interval.

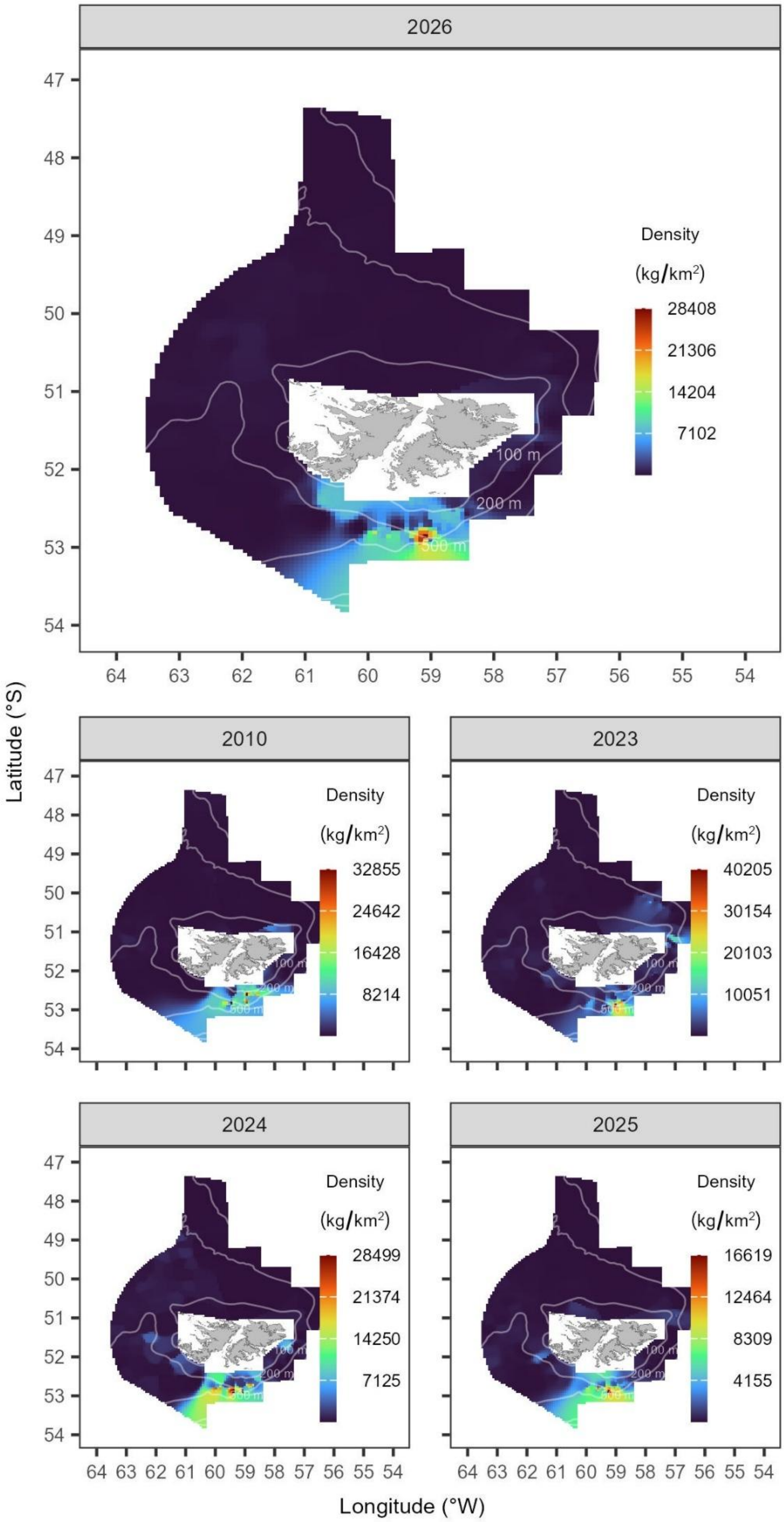


Fig. 44. Distribution and abundance of the Patagonian squid (*Doryteuthis gahi*) derived from the February 2026 groundfish and calamari pre-season surveys in Falkland Islands waters, compared with the first year of the time series (2010) and the three preceding years (2023–2025). Colour scales are specific to each year. Isobaths at 100 m, 200 m, and 500 m are shown.

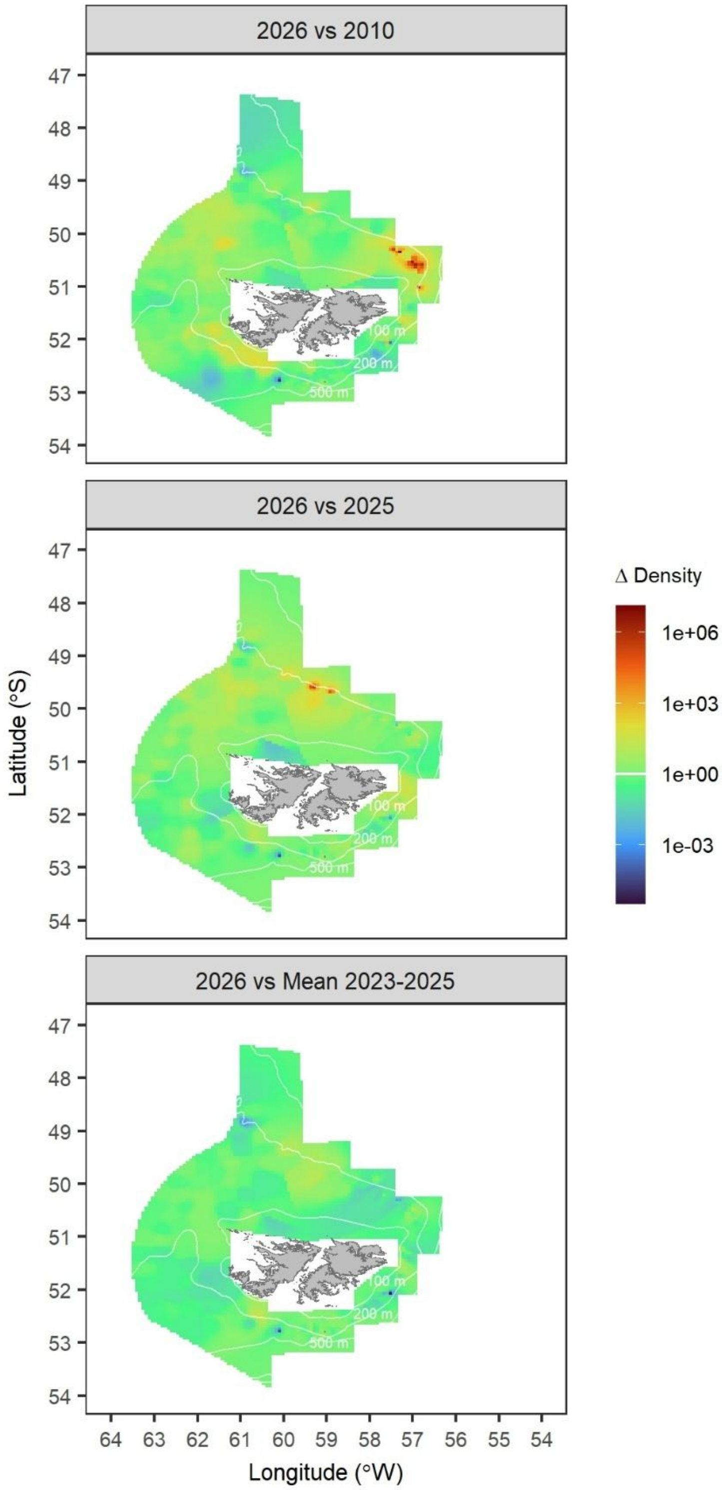


Fig. 45. Spatial change in density of the Patagonian squid (*Doryteuthis gahi*) derived from the February 2026 groundfish and calamari pre-season surveys in Falkland Islands waters, relative to the first year of the time series (2010), the previous year (2025), and the mean of the three preceding years (2023–2025). The spatial change in density is expressed as the ratio of density (kg/km$^2$) in 2026 relative to the density in the baseline year (2010, 2025, 2023–2025 mean). Isobaths at 100 m, 200 m, and 500 m are shown. The colour scale is $\log_{10}$-transformed to aid visualisation, with increases in density indicated above the horizontal white line towards dark red, and decreases in density indicated below the horizontal white line towards dark blue.

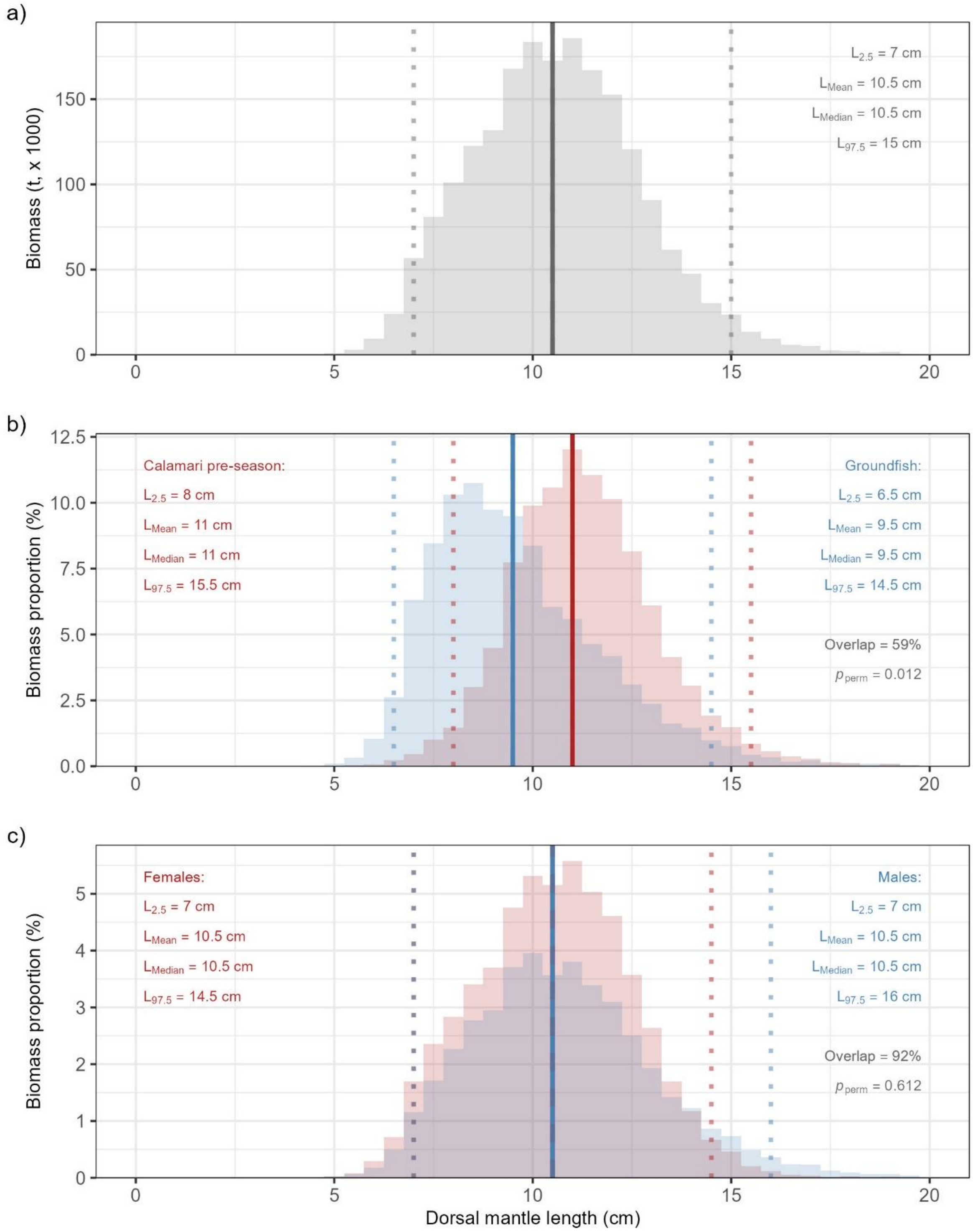


Fig. 46. Biomass-at-length class composition of the Patagonian squid (*Doryteuthis gahi*) across all years combined, based on February groundfish and calamari pre-season surveys conducted in Falkland Islands waters in 2010–2011 and 2015–2026. a) Overall biomass-at-length frequency distribution. b) Overlap in biomass-at-length distributions between calamari pre-season (red) and groundfish (blue) surveys. c) Overlap in biomass-at-length distributions between females (red) and males (blue). Solid vertical lines indicate the mean length ($L_{Mean}$), dashed lines the median length ($L_{Median}$), and dotted lines the 2.5th and 97.5th length percentiles ($L_{2.5}$ and $L_{97.5}$, respectively). $p_{perm}$ is the significance of the weighted permutation test to assess differences between groups.

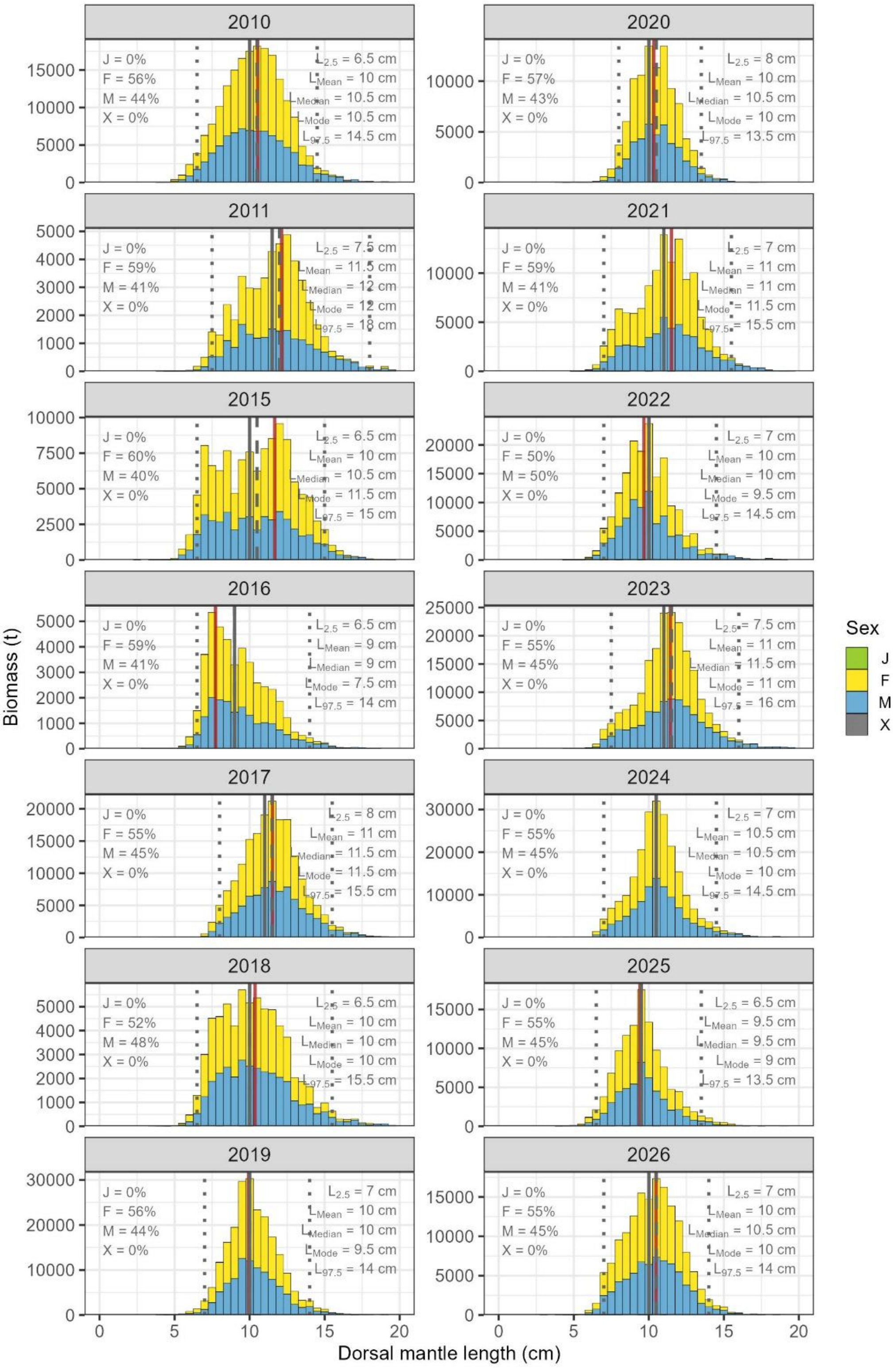


Fig. 47. Annual biomass-at-length class composition of the Patagonian squid (*Doryteuthis gahi*) during February groundfish and calamari pre-season surveys conducted in Falkland Islands waters in 2010–2011 and 2015–2026. Stacked bars represent biomass (t) per 0.5 cm length class, partitioned by sex (J = juvenile; F = female; M = male; X = undetermined), with the proportion of total annual biomass for each sex indicated in the upper left of each panel. Vertical lines indicate the mean length ($L_{Mean}$, grey solid), median length ($L_{Median}$, grey dashed), modal length ($L_{Mode}$, red solid), and 2.5th and 97.5th percentiles ($L_{2.5}$ and $L_{97.5}$, grey dotted) of the biomass-weighted length distribution. Note the different y-axis scales among years.

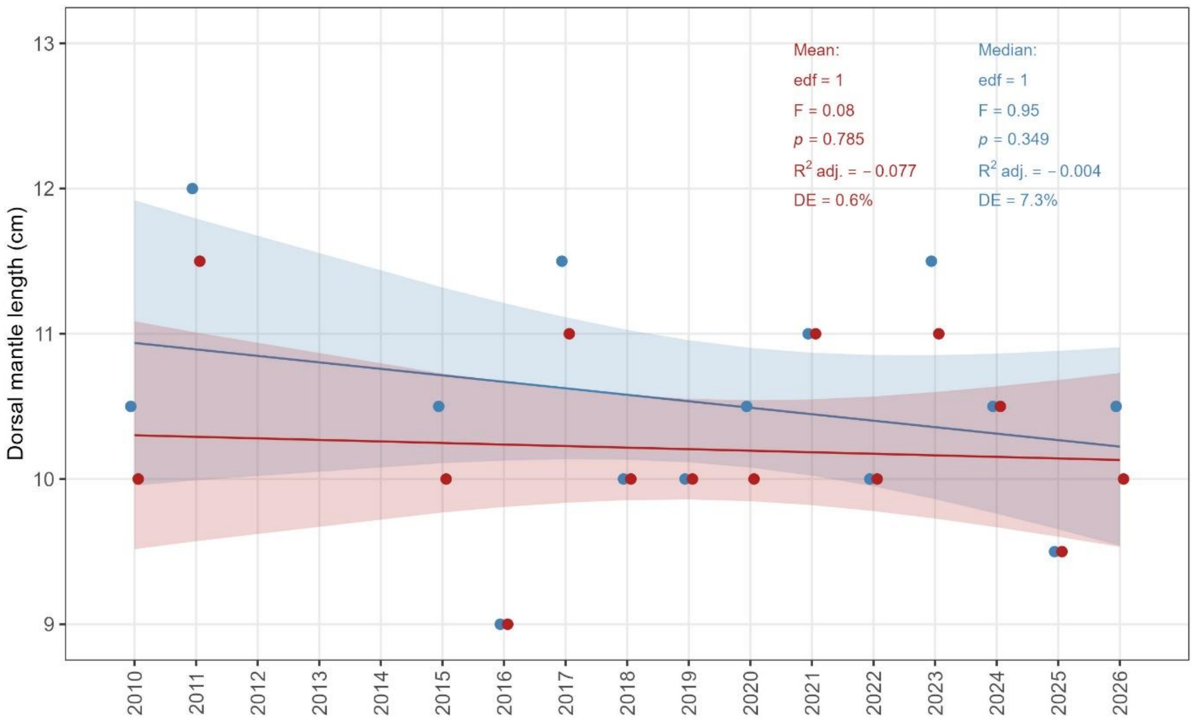


Fig. 48. Median (blue) and mean (red) dorsal mantle length of the Patagonian squid (*Doryteuthis gahi*) during February groundfish and calamari pre-season surveys conducted in Falkland Islands waters in 2010–2011 and 2015–2026. The line and shaded region represent the fitted Generalised Additive Model (GAM) smooth and its 95% pointwise confidence interval.

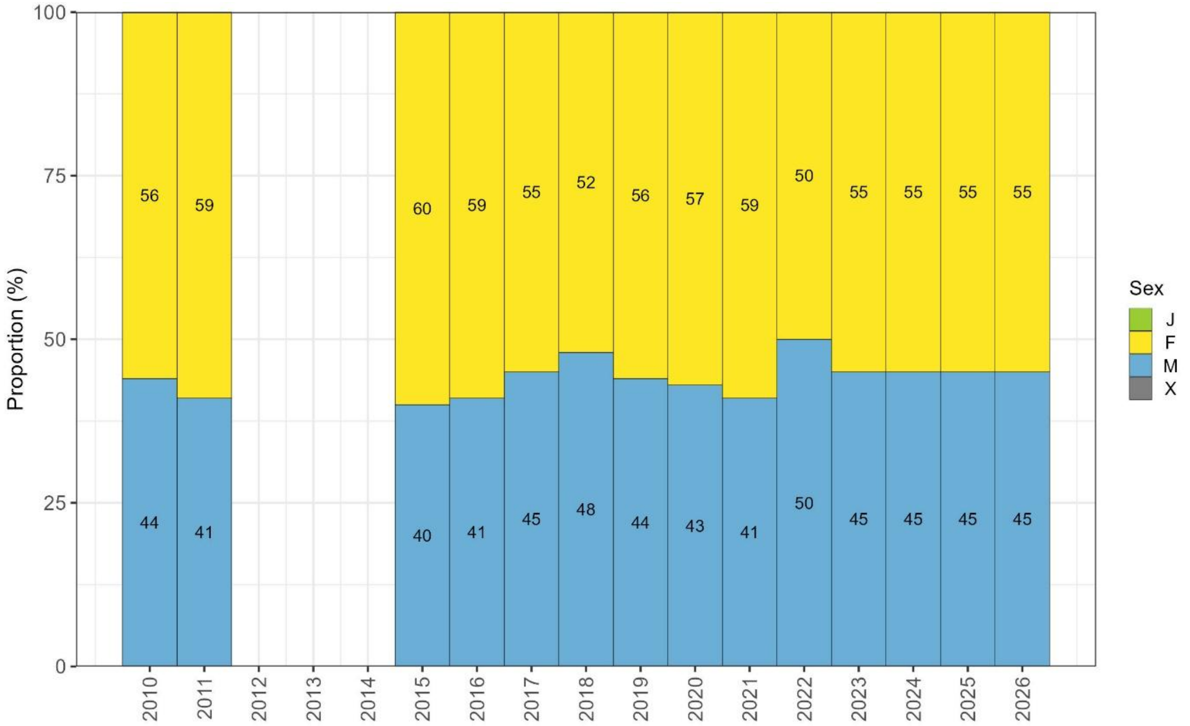


Fig. 49. Proportion by sex (J = juvenile; F = female; M = male; X = undetermined) of the Patagonian squid (*Doryteuthis gahi*) during February groundfish and calamari pre-season surveys conducted in Falkland Islands waters in 2010–2011 and 2015–2026. Labels for proportions < 3% are omitted.

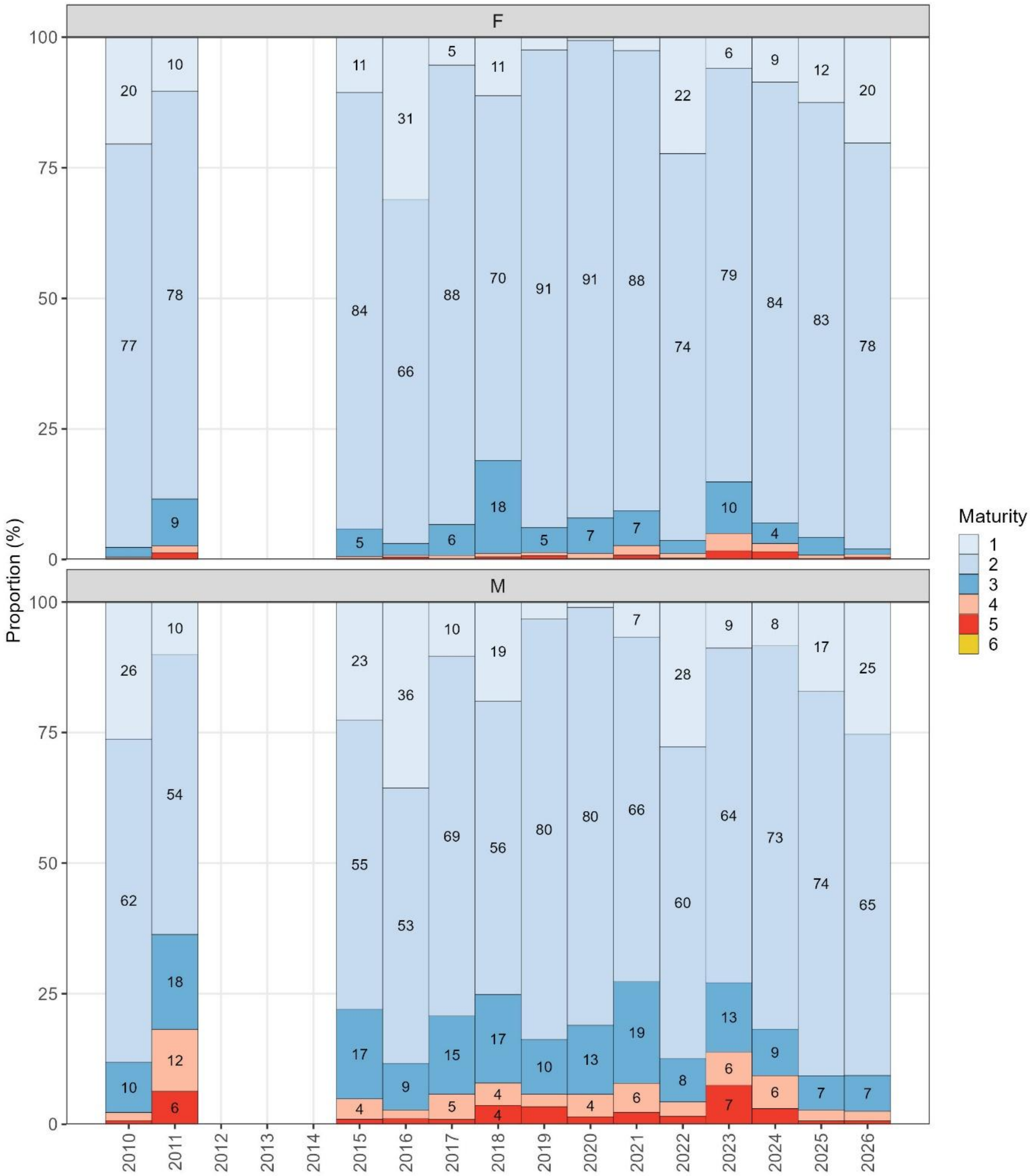


Fig. 50. Proportion by sexual maturity (1, young; 2, immature; 3, preparatory; 4, maturing; 5, mature; 6, spent) of the Patagonian squid (*Doryteuthis gahi*) during February groundfish and calamari pre-season surveys conducted in Falkland Islands waters in 2010–2011 and 2015–2026. Labels for proportions < 3% are omitted.

### 4.3.7. Patagonian toothfish (*Dissostichus eleginoides*)

4.3.7.1. Temporal patterns of abundance

On average, 46% of the total Patagonian toothfish catches in the time series were obtained from groundfish surveys and 54% from calamari pre-season surveys. The highest catch occurred in 2026 (4.95 t), representing approximately a four-fold increase relative to the 2010 catch (1.39 t), a two-fold increase relative to the 2025 catch (2.14 t), and a three-fold increase relative to the 2023–2025 mean catch (1.69 t; Fig. 51a; Appendix II).

The highest densities were recorded in 2026 (83.29 ± 10.14 kg/km²; mean ± SE), representing approximately a two-fold increase relative to the 2010 densities (47.86 ± 7.58 kg/km²), a three-fold increase relative to the 2025 densities (30.21 ± 4.41 kg/km²), and a four-fold increase relative to the 2023–2025 mean densities (19.92 ± 2.02 kg/km²; Fig. 51b).

The highest biomass of Patagonian toothfish in the time series was recorded in 2026 (15,847.05 t), representing a significant 69.6% increase relative to 2010 levels (9,345.13 t; $p < 0.001$), a significant 2.5-fold increase relative to 2025 (6,274.84 t; $p < 0.001$), and a significant 3.5-fold increase relative to the 2023–2025 mean (4,541.07 t; $p < 0.001$; Fig. 51c; Table IV–V; Appendix III–IV). Analysis of the full time series revealed a significant non-linear trend in biomass (GAM: edf = 4.93, F = 9.47, $p = 0.003$), with the model explaining 86.6% of the deviance ($R^2$ adj. = 0.855), indicating a strong and consistent pattern of increase in recent years (Fig. 51c; Appendix V).

4.3.7.2. Spatial patterns of abundance

In 2026, Patagonian toothfish were scattered across the FICZ, with the highest concentration (742 kg/km²) to the north-west at approximately 50.5°S and 62°W (Fig. 52). Patagonian toothfish have had a patchy distribution around the Falkland Islands through the time series, but with higher densities to the south-west in the FICZ. The highest density in the full time series was reported in 2018 to the west and south-west of West Falkland (902 kg/km²).

Analysis of the spatial change in density revealed that substantial increases in distinct areas buffered the overall decrease in densities through the survey area. Comparison of densities in 2026 relative to 2010 showed that densities increased substantially in the south and centre of the 'Loligo Box', and to the north-west in the FICZ. Comparisons of 2026 with 2025, and with the 2023–2025 mean showed the main increases in densities to the north-west in the FICZ, and in small and patchy areas of the 'Loligo Box' (Fig. 53).

4.3.7.3. Length composition

Across all survey years combined, total length of Patagonian toothfish was in the range of 5 to 115 cm; however, 95% of the estimated biomass was comprised of individuals between 31 and 81 cm, with a median length of 52 ± 2.26 cm (median ± SE) and a mean length of 53 ± 2.03 cm (mean ± SE; Fig. 54a).

The distribution of biomass proportions by size class exhibited a 76% overlap between the groundfish and calamari pre-season surveys. Moreover, the biomass-weighted mean length was not significantly different ($p > 0.05$) between the groundfish (54 ± 1.95 cm; mean

± SE) and the calamari pre-season (51 ± 2.24 cm) surveys, indicating similar size structure between surveys. In the groundfish survey, 95% of the biomass of Patagonian toothfish was comprised of individuals between 32 and 79 cm, with a median length of 54 ± 2.26 cm. In the calamari pre-season survey, 95% of the biomass of Patagonian toothfish was comprised of individuals between 30 and 83 cm, with a median length of 49 ± 1.92 cm (Fig. 54b).

The distribution of biomass proportions by size class exhibited an 87% overlap between females and males. Despite the high overlap, the permutation analysis revealed that the biomass-weighted mean length was significantly different ($p = 0.01$) between females (55 ± 2.06 cm) and males (50 ± 1.84 cm). This difference was in part due to individuals > 45 cm that were more abundant for females compared to males. For females, 95% of the biomass was comprised of individuals between 31 and 84 cm, with a median length of 54 ± 2.39 cm. For males, 95% of the biomass was comprised of individuals between 30 and 71 cm, with a median length of 49 ± 1.93 cm (Fig. 54c).

Through the time series, the size structure of Patagonian toothfish was broad and multimodal, with several length-groups not clearly distinguished because of size overlap. A small group with modal length at 30–36 cm was present in several years. However, this group was not evident since 2025, probably indicating low recruitment (Fig. 55). In 2026, the size structure remained broad and multimodal. Lengths were in the range of 10 to 100 cm; however, 95% of the biomass was comprised of individuals between 45 and 75 cm, with a median length of 53 ± 1.88 cm and a mean length of 55 ± 2.08 cm. For females, 95% of the biomass was comprised of individuals between 45 and 90 cm, with a median length of 55 ± 1.99 cm and a mean length of 58 ± 2.17 cm. For males, 95% of the biomass was comprised of individuals between 44 and 72 cm, with a median length of 51 ± 1.57 cm and a mean length of 52 ± 1.65 cm (Fig. 55).

Both mean (GAM: edf = 8.32, $F = 20.01$, $p = 0.002$, $R^2$ adj. = 0.931, DE = 97.5%) and median (GAM: edf = 7.53, $F = 8.01$, $p = 0.017$, $R^2$ adj. = 0.836, DE = 93.1%) total lengths had highly significant temporal trends; these trends were complex and with fluctuations. Both mean and median total length were approximately 53–54 cm in 2010, declined to a minimum of approximately 45–46 cm in 2016, increased steeply and remained at approximately 54–59 cm between 2019 and 2023, declined to around 48–50 cm in 2025, and increased again at approximately 53–55 cm in 2026 (Fig. 56). This oscillatory pattern likely reflects recurring recruitment pulses or shifts in the size composition of this portion of the population.

#### 4.3.7.4. Sex and maturity composition

Across all survey years combined, the biomass composition of Patagonian toothfish was consistently dominated by females, comprising 62.6 ± 0.9% (mean ± SE) of the total biomass, followed by males with 37.3 ± 0.9%; juveniles and individuals of undetermined sex accounted for a negligible 0.1 ± 0.1% each. Interannual variability in sex composition was low, with the female proportion ranging from 58% in 2010 to 69% in 2020, and the male proportion ranging from 30% in 2020 to 42% in 2010. Juveniles were recorded only in 2015 (approximately 1% of biomass), and individuals of undetermined sex appeared solely in 2020 at low levels. The 2026 sex composition was consistent with the time series mean, with females comprising 60% and males 40% of the biomass (Fig. 57).

Maturity composition was characterised by immature and “resting” individuals throughout the time series (Fig. 58). For Patagonian toothfish, “resting” individuals are effectively immature individuals, given that the groundfish and calamari pre-season surveys conducted with bottom trawl do not capture adult individuals, which instead are primarily caught with longlines at greater depths. Early developing individuals occurred sporadically and contributed < 4% in either sex.

4.3.7.5. Discussion

The significant non-linear biomass trend of Patagonian toothfish in Falkland Islands waters reflects a complex but increasing pattern in recent years. The relatively high biomass estimated in February 2026 is consistent with high biomass recorded in July 2025 (Ramos 2025). This increase may be attributable in part to the growth of recruits detected in 2022–2023, coupled with reduced fishing pressure following the all-year-round closure of fishing grid squares to the south-west of the FICZ (south of 52.5°S and west of 60.5°W) since December 2023 (FIFD, *unpublished internal document*). It is important to note that the groundfish and calamari pre-season surveys do not effectively sample adult Patagonian toothfish, which are primarily caught with longlines at greater depths; consequently, the biomass estimates presented here are not representative of the adult stock and should be interpreted as an index of juvenile and sub-adult abundance from bottom trawl surveys. The “resting” maturity stage should be revised and corrected accordingly to appropriately describe the juvenile and sub-adult components of this stock.

The highly significant oscillatory trends in both mean and median total length may indicate recruitment pulses at irregular intervals. The recent decline in mean and median length in 2024–2025, followed by a partial recovery in 2026, may reflect the presence of a cohort of larger individuals or continued growth of the 2022–2023 recruits.

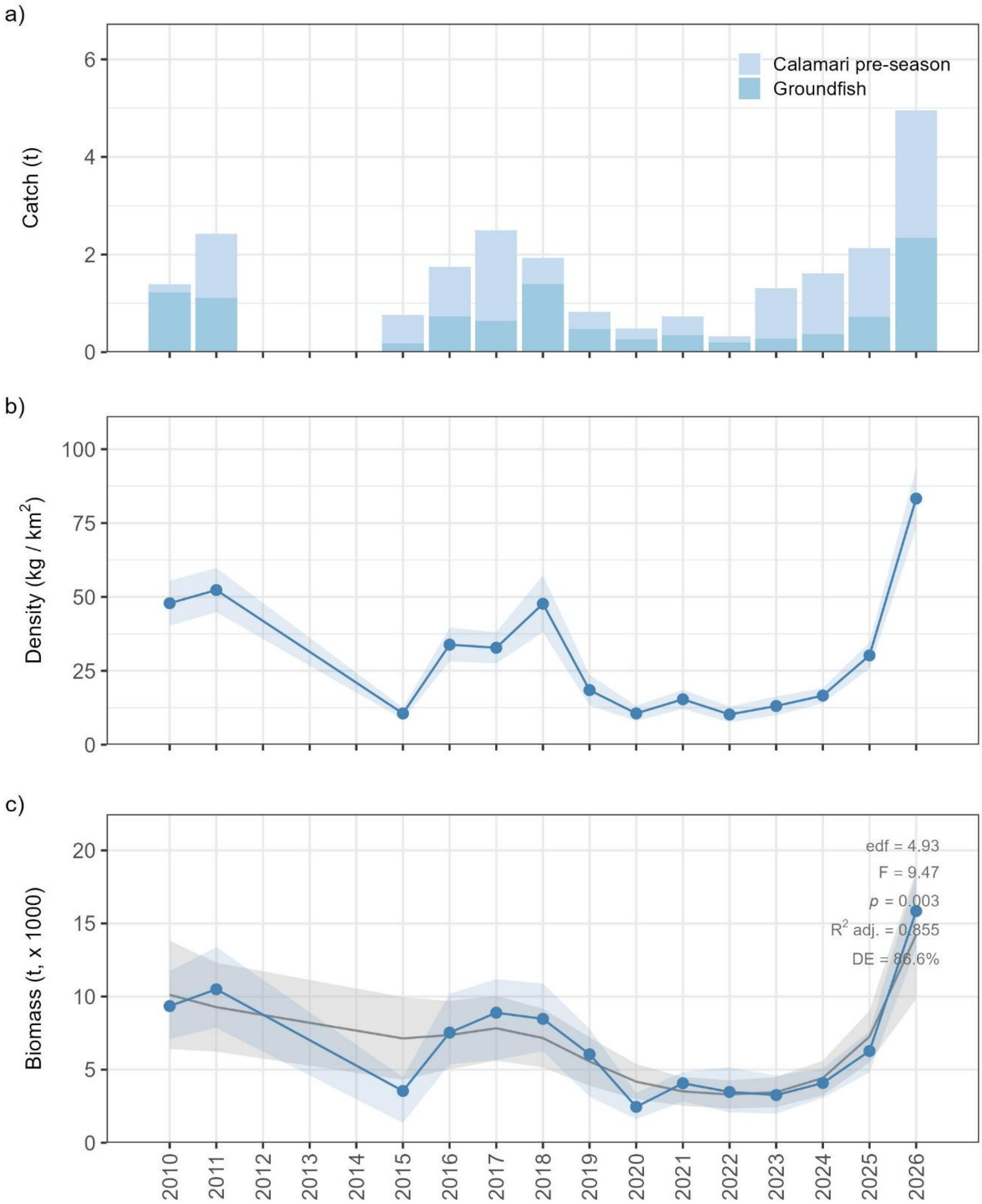


Fig. 51. Abundance of Patagonian toothfish (*Dissostichus eleginoides*) during February groundfish and calamari pre-season surveys conducted in Falkland Islands waters in 2010–2011 and 2015–2026. (a) Catch per survey, (b) annual mean density ± SE represented by the blue line and shaded region, respectively, and (c) estimated biomass, where the blue line and shaded region represent the median and 95% pointwise confidence interval derived from 10,000 bootstrap biomass estimates, and the grey line and shaded region represent the fitted Generalised Additive Model (GAM) smooth and its 95% pointwise confidence interval.

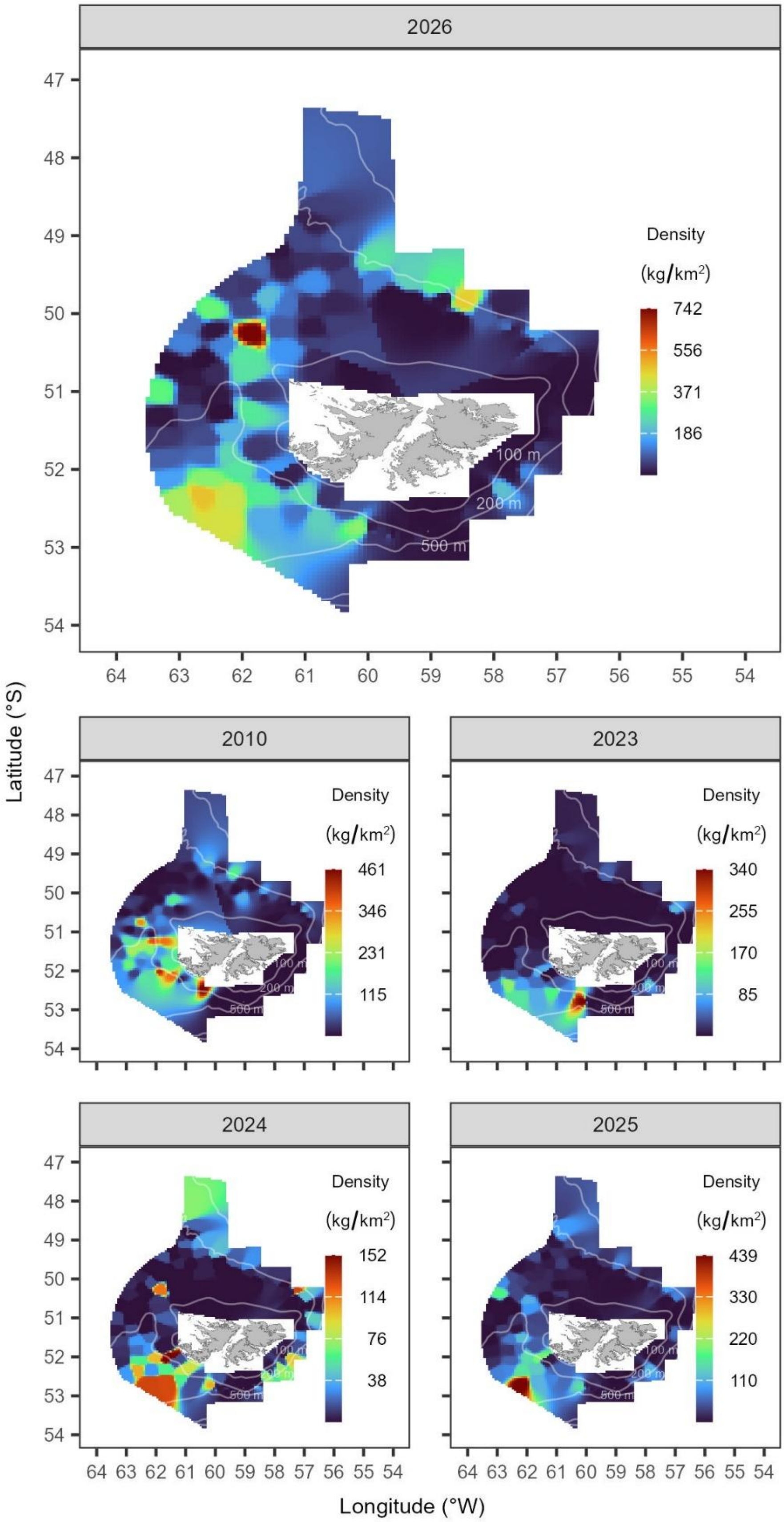


Fig. 52. Distribution and abundance of Patagonian toothfish (*Dissostichus eleginoides*) derived from the February 2026 groundfish and calamari pre-season surveys in Falkland Islands waters, compared with the first year of the time series (2010) and the three preceding years (2023–2025). Colour scales are specific to each year. Isobaths at 100 m, 200 m, and 500 m are shown.

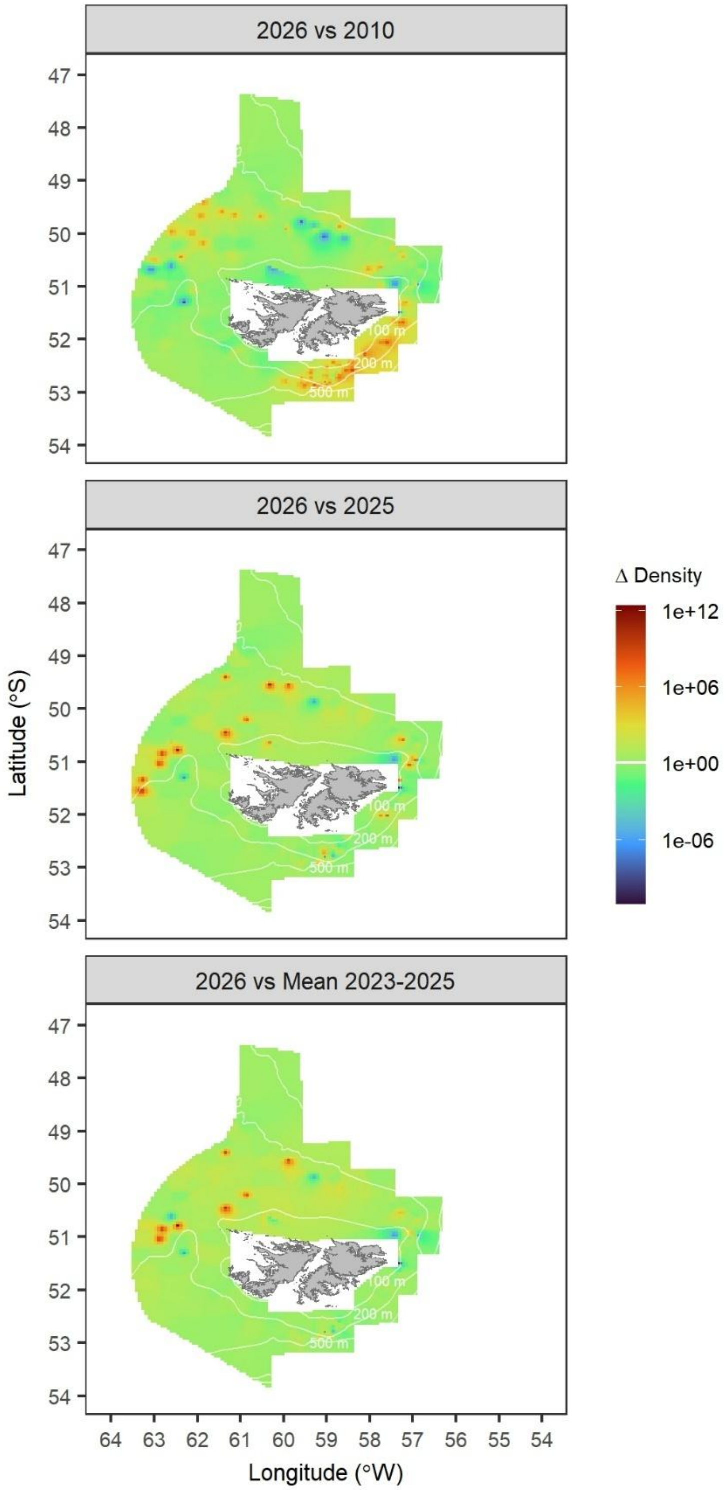


Fig. 53. Spatial change in density of Patagonian toothfish (*Dissostichus eleginoides*) derived from the February 2026 groundfish and calamari pre-season surveys in Falkland Islands waters, relative to the first year of the time series (2010), the previous year (2025), and the mean of the three preceding years (2023–2025). The spatial change in density is expressed as the ratio of density (kg/km$^2$) in 2026 relative to the density in the baseline year (2010, 2025, 2023–2025 mean). Isobaths at 100 m, 200 m, and 500 m are shown. The colour scale is $\log_{10}$-transformed to aid visualisation, with increases in density indicated above the horizontal white line towards dark red, and decreases in density indicated below the horizontal white line towards dark blue.

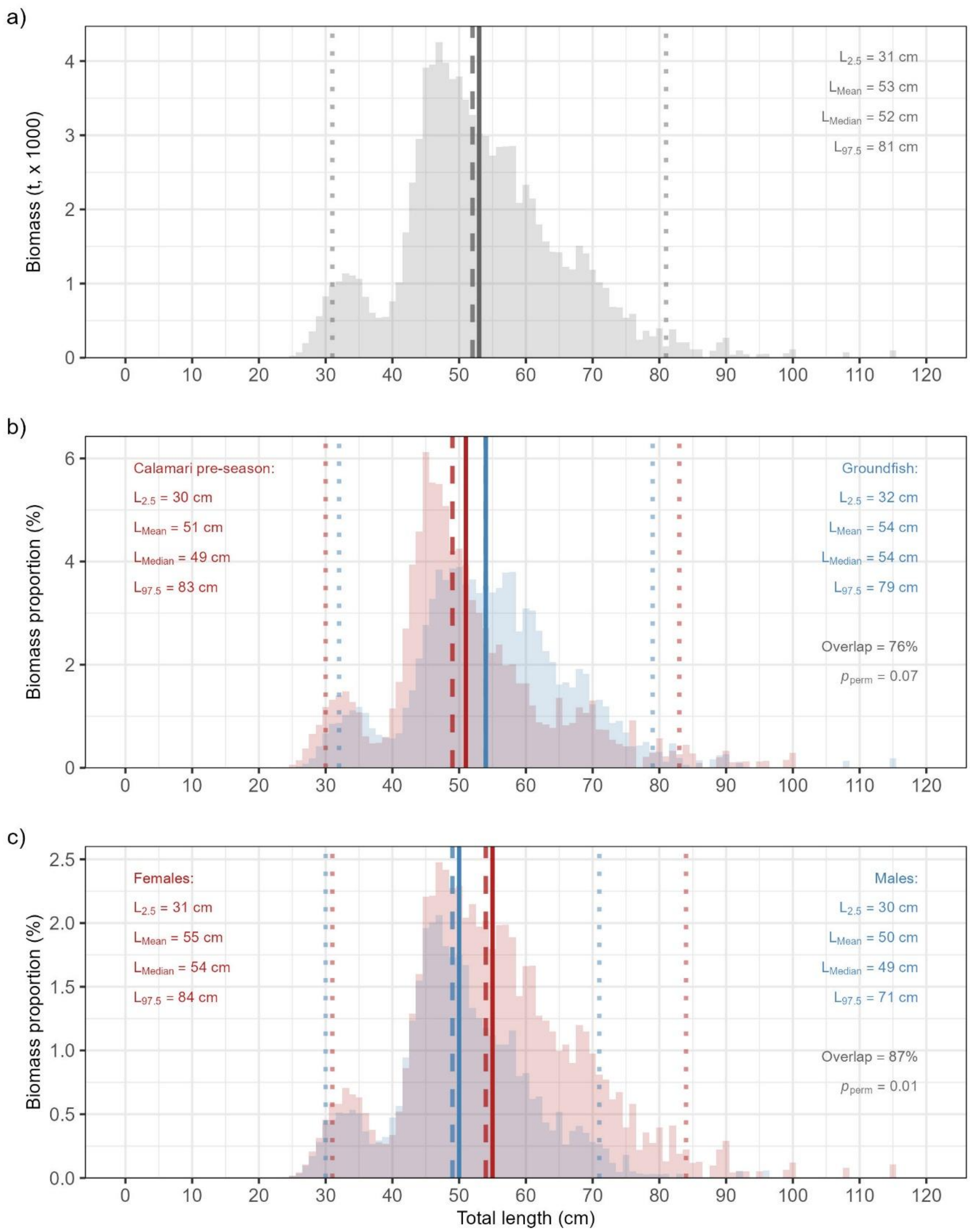


Fig. 54. Biomass-at-length class composition of Patagonian toothfish (*Dissostichus eleginoides*) across all years combined, based on February groundfish and calamari pre-season surveys conducted in Falkland Islands waters in 2010–2011 and 2015–2026. a) Overall biomass-at-length frequency distribution. b) Overlap in biomass-at-length distributions between calamari pre-season (red) and groundfish (blue) surveys. c) Overlap in biomass-at-length distributions between females (red) and males (blue). Solid vertical lines indicate the mean length ($L_{Mean}$), dashed lines the median length ($L_{Median}$), and dotted lines the 2.5th and 97.5th length percentiles ($L_{2.5}$ and $L_{97.5}$, respectively). $p_{perm}$ is the significance of the weighted permutation test to assess differences between groups.

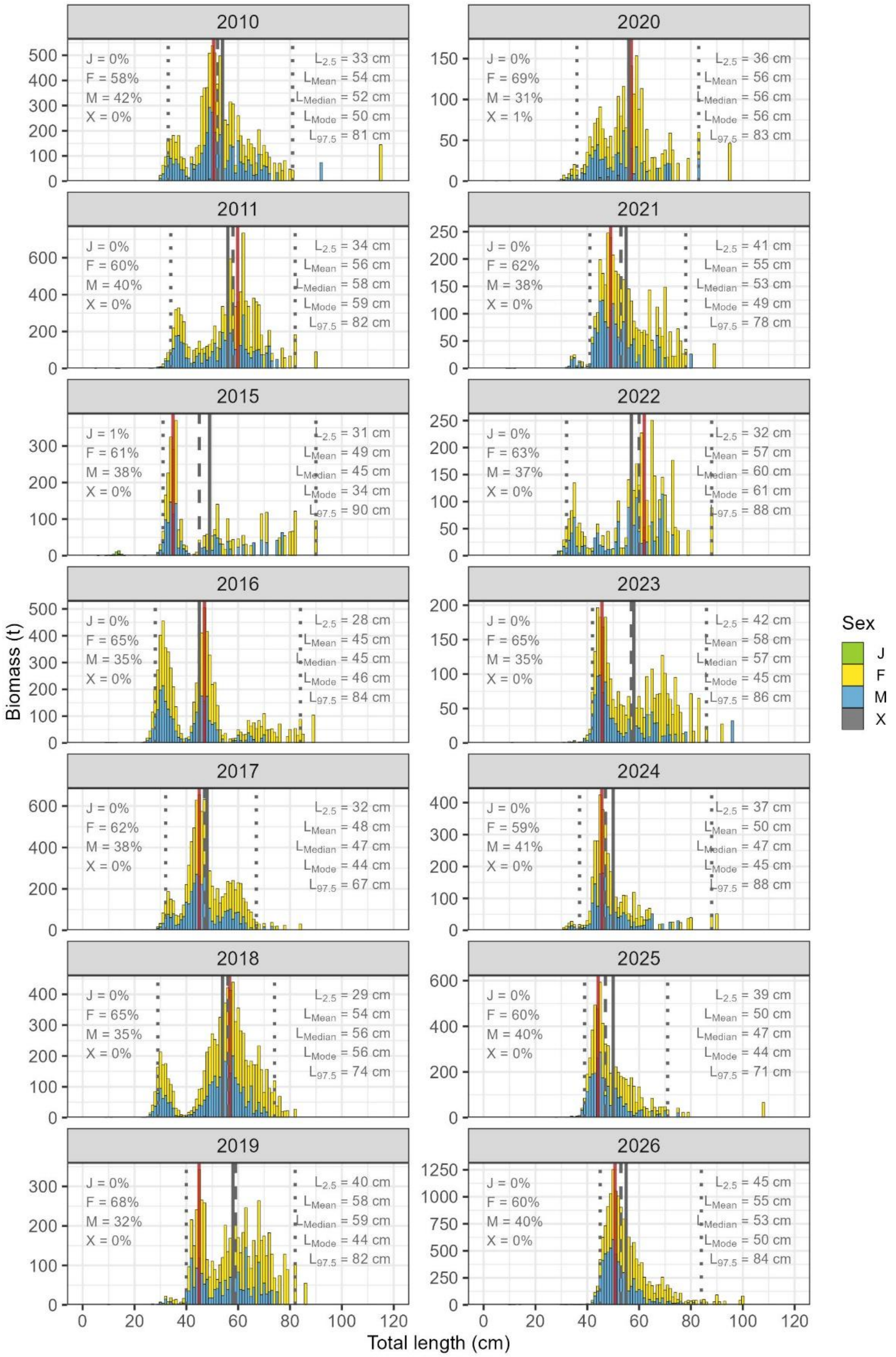


Fig. 55. Annual biomass-at-length class composition of Patagonian toothfish (*Dissostichus eleginoides*) during February groundfish and calamari pre-season surveys conducted in Falkland Islands waters in 2010–2011 and 2015–2026. Stacked bars represent biomass (t) per 1.0 cm length class, partitioned by sex (J = juvenile; F = female; M = male; X = undetermined), with the proportion of total annual biomass for each sex indicated in the upper left of each panel. Vertical lines indicate the mean length ($L_{Mean}$, grey solid), median length ($L_{Median}$, grey dashed), modal length ($L_{Mode}$, red solid), and 2.5th and 97.5th percentiles ($L_{2.5}$ and $L_{97.5}$, grey dotted) of the biomass-weighted length distribution. Note the different y-axis scales among years.

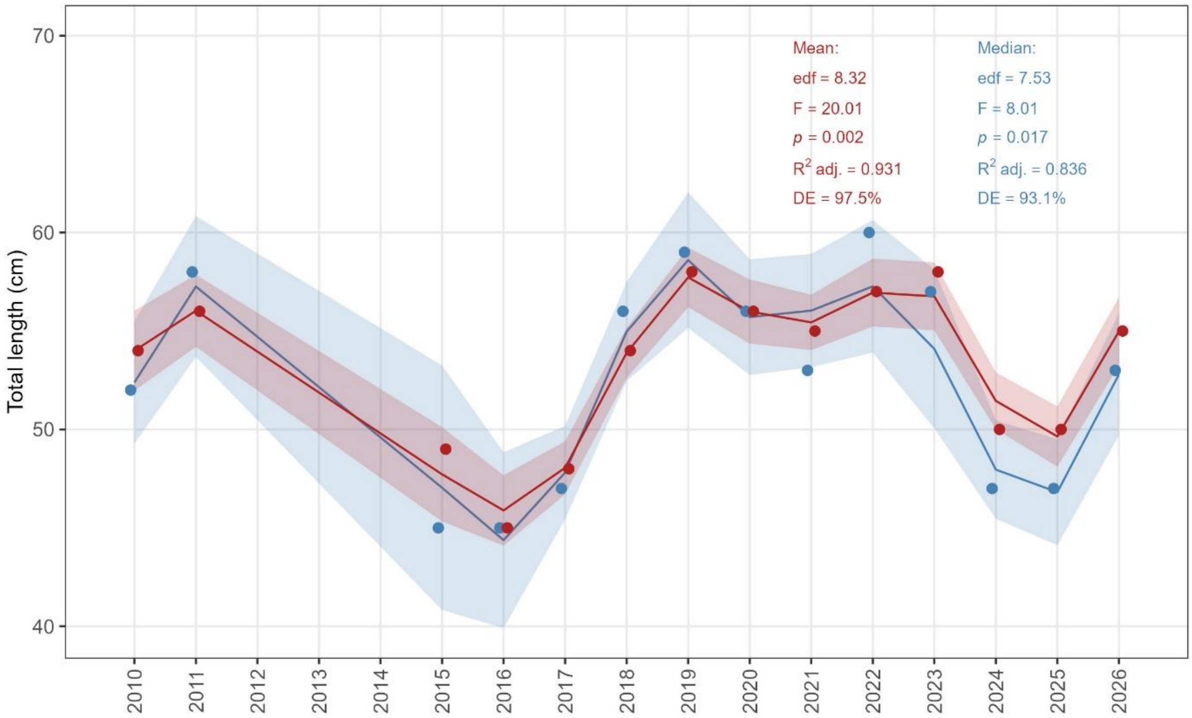


Fig. 56. Median (blue) and mean (red) total length of Patagonian toothfish (*Dissostichus eleginoides*) during February groundfish and calamari pre-season surveys conducted in Falkland Islands waters in 2010–2011 and 2015–2026. The line and shaded region represent the fitted Generalised Additive Model (GAM) smooth and its 95% pointwise confidence interval.

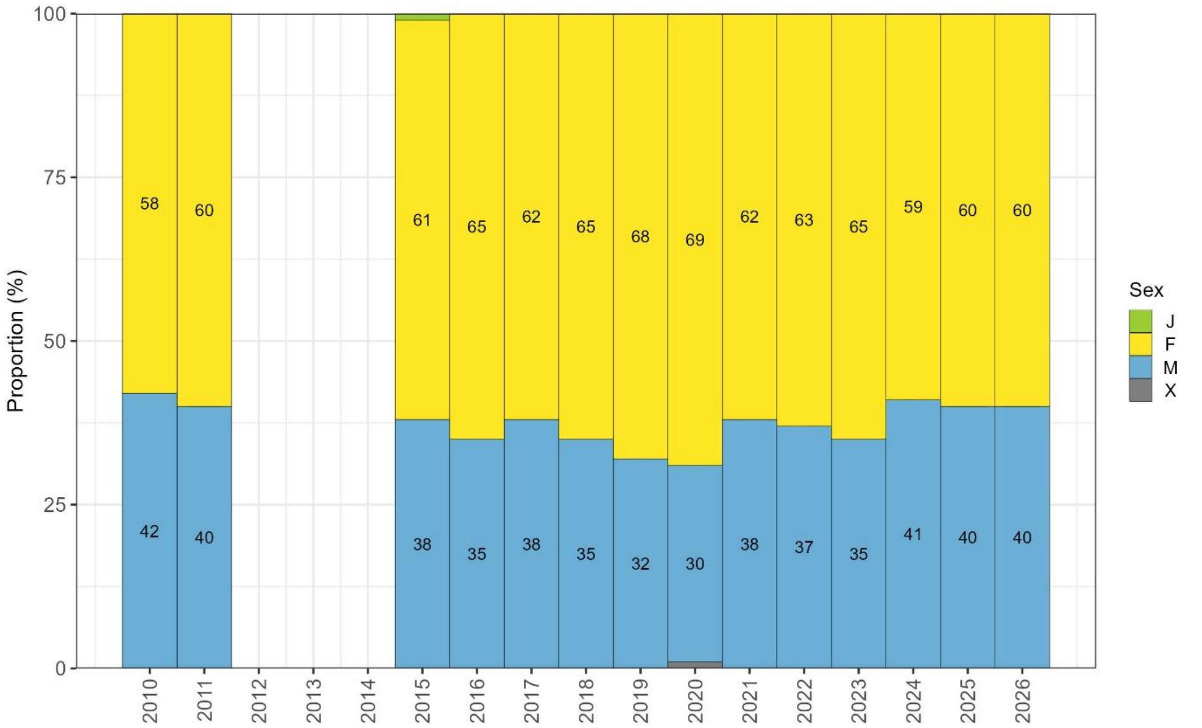


Fig. 57. Proportion by sex (J = juvenile; F = female; M = male; X = undetermined) of Patagonian toothfish (*Dissostichus eleginoides*) during February groundfish and calamari pre-season surveys conducted in Falkland Islands waters in 2010–2011 and 2015–2026. Labels for proportions < 3% are omitted.

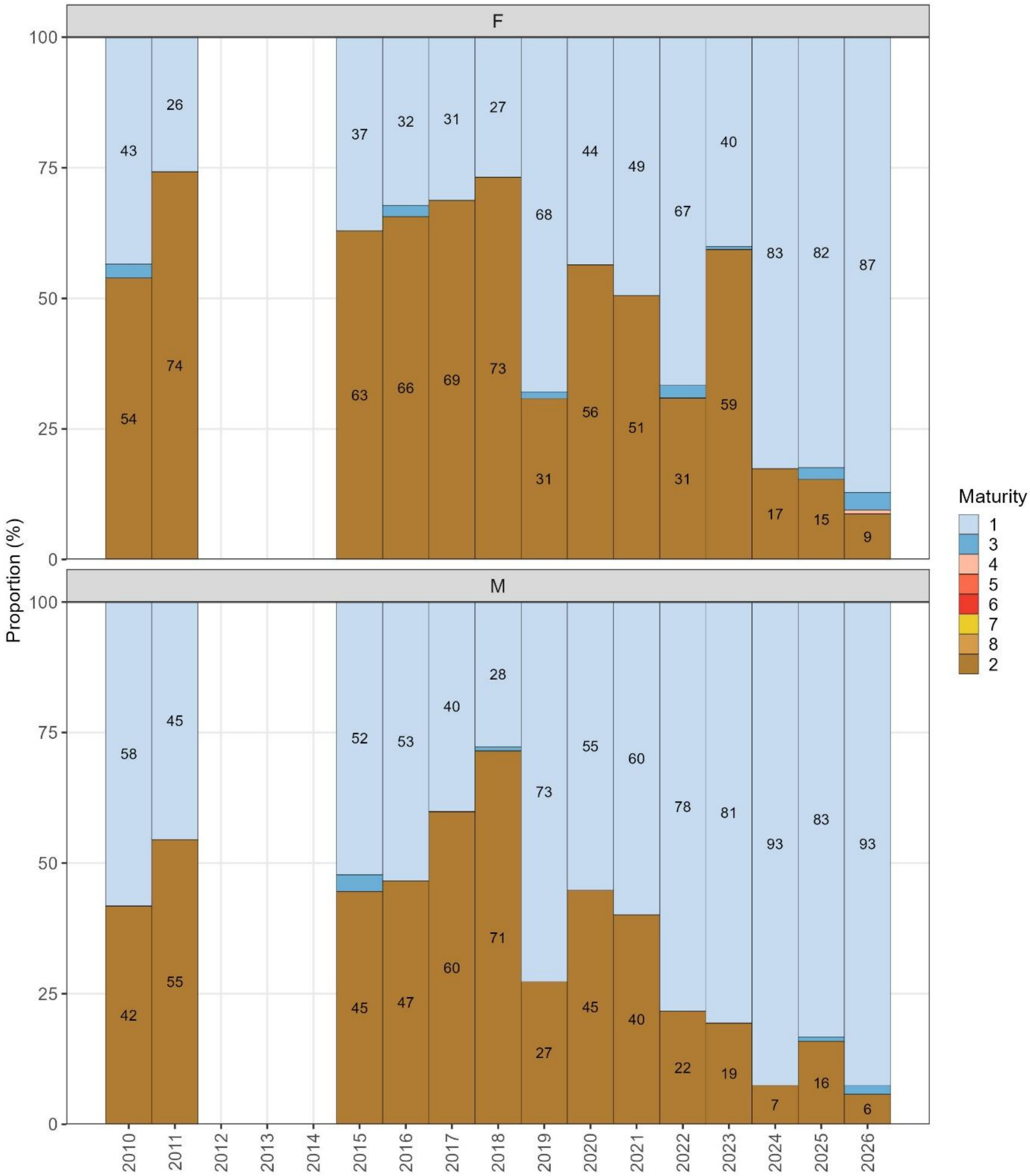


Fig. 58. Proportion by sexual maturity (1, immature; 3, early developing; 4, late developing; 5, ripe; 6, running; 7, spent; 8, recovering spent; 2, resting) of Patagonian toothfish (*Dissostichus eleginoides*) during February groundfish and calamari pre-season surveys conducted in Falkland Islands waters in 2010–2011 and 2015–2026. Maturity stages ordered by developmental sequence. Labels for proportions < 3% are omitted.

### 4.3.8. Red cod (*Salilota australis*)

4.3.8.1. Temporal patterns of abundance

On average, 90% of the total red cod catches in the time series were obtained from groundfish surveys and 10% from calamari pre-season surveys. The highest catch occurred in 2011 (23.54 t). The catch in 2026 (7.48 t; Fig. 59a; Appendix II) was the fifth lowest in the time series, and it corresponded to 55.3% of the 2010 catch (13.54 t). However, the catch in 2026 represented a two-fold increase relative to the 2025 catch (3.35 t), and a 7.8% increase relative to the 2023–2025 mean catch (6.94 t).

The highest densities were recorded in 2011 (765.03 ± 307.64 kg/km²; mean ± SE). Densities in 2026 (188.73 ± 51.21 kg/km²) corresponded to 38.5% of the 2010 densities (490.17 ± 268.96 kg/km²). However, these represented a two-fold increase relative to the 2025 densities (99.06 ± 37.55 kg/km²), and were only 2.3% higher relative to the 2023–2025 mean (184.73 ± 42.52 kg/km²; Fig. 59b).

Red cod biomass was highest in 2011 (161,971.29 t; although confidence intervals for this estimate were wide). Biomass in 2026 (31,413 t) was the third lowest in the time series, corresponding to 32.3% of 2010 levels (97,398.08 t). Biomass in 2026 represented a nearly two-fold increase relative to 2025 (16,605.17 t) and 93.3% of the 2023–2025 mean (33,660.25 t). These were non-significant changes in biomass ($p > 0.05$; Fig. 59c; Table IV–V; Appendix III–IV). However, analysis of the full time series revealed a significant linear declining trend in biomass (GAM: edf = 1.00, F = 19.82, $p < 0.001$), with the model explaining 60.2% of the deviance ($R^2$ adj. = 0.637), indicating a consistent decrease in biomass over the time series (Fig. 59c; Appendix V).

4.3.8.2. Spatial patterns of abundance

In 2026, the highest densities (4,214 kg/km$^2$) occurred to the west at approximately 51.5°S and 62.3°W, and to the north-west limit of the FICZ at approximately 50°S and 63°W (Fig. 60). Similar patterns were observed in 2010, and from 2023 to 2025, with variable location of the highest densities. Through the full time series, the highest density (38,175 kg/km$^2$) was recorded to the west limit of the FICZ in 2016.

Analysis of the spatial change in density revealed an overall decrease in densities through the survey area. Comparison of densities in 2026 relative to 2010 showed substantial decrease in densities in distinct areas to the north-east in the FICZ; however, densities increased along the 'Loligo Box'. Comparisons of 2026 with 2025 revealed substantial increases in distinct areas to the north-west in the FICZ, as well as to the north-east in the FICZ and in the south and north of the 'Loligo Box'. Comparisons of 2026 with the 2023–2025 mean showed that densities increased in the south and north of the 'Loligo Box', and to the north in the FICZ (Fig. 61).

4.3.8.3. Length composition

Across all survey years combined, total length of red cod was in the range of 6 to 87 cm; however, 95% of the estimated biomass was comprised of individuals between 24 and 76 cm, with a median length of 50 ± 2.57 cm (median ± SE) and a mean length of 49 ± 1.98 cm (mean ± SE; Fig. 62a).

The distribution of biomass proportions by size class exhibited a 54% overlap between the groundfish and calamari pre-season surveys. Accordingly, the biomass-weighted mean length was significantly different ($p = 0.02$) between the groundfish (49 ± 1.98 cm; mean ± SE) and the calamari pre-season (57 ± 2.95 cm) surveys, indicating different size structure between surveys. In the groundfish survey, 95% of the biomass of red cod was comprised of individuals between 24 and 76 cm, with a median length of 50 ± 2.55 cm. In the calamari pre-season survey, 95% of the biomass of red cod was comprised of individuals between 26 and 81 cm, with a median length of 61 ± 4.24 cm (Fig. 62b).

The distribution of biomass proportions by size class exhibited an 80% overlap between females and males. Despite the high overlap, the permutation analysis revealed that the biomass-weighted mean length was significantly different ($p = 0.009$) between females (51 ± 1.97 cm) and males (45 ± 1.95 cm). This difference was in part due to individuals > 25 cm that were more abundant for females compared to males. For females, 95% of the biomass was comprised of individuals between 25 and 77 cm, with a median length of 52 ± 2.57 cm. For males, 95% of the biomass was comprised of individuals between 20 and 72 cm, with a median length of 45 ± 2.29 cm (Fig. 62c).

Through the time series, the size structure of red cod was broad and multimodal, with several length-groups not clearly distinguished because of size overlap. The main modal length ranged between 39 and 68 cm, suggesting that more than one length-group was dominant in the time series. Recruits were in the range of 15 to 19 cm; poor recruitment seemed to occur in 2010, 2018, and from 2023 to 2025 (Fig. 63). In 2026, the size structure remained broad and multimodal. Lengths were in the range of 11 to 87 cm; however, 95% of the biomass was comprised of individuals between 19 and 75 cm, with a median length of 52 ± 1.53 cm and a mean length of 51 ± 1.59 cm. For females, 95% of the biomass was comprised of individuals between 24 and 76 cm, with a median length of 53 ± 1.88 cm and a mean length of 53 ± 2.02 cm. For males, 95% of the biomass was comprised of individuals between 17 and 72 cm, with a median length of 48 ± 1.83 cm and a mean length of 47 ± 2.12 cm (Fig. 63).

Considerable interannual variability in mean and median total lengths was observed, which resulted in non-statistically significant temporal trends in mean (GAM: edf = 2.58, $F = 3.08$, $p = 0.077$, $R^2$ adj. = 0.407, DE = 52.5%) and median (GAM: edf = 2.71, $F = 2.99$, $p = 0.082$, $R^2$ adj. = 0.417, DE = 53.7%) total lengths. Both models explained a moderate proportion of deviance and captured consistent non-linear patterns, with the mean and median total lengths declining from approximately 52–54 cm in 2010 to a minimum of approximately 46–47 cm in 2016, followed by a gradual recovery to approximately 52 cm in 2026 (Fig. 64).

#### 4.3.8.4. Sex and maturity composition

Across all survey years combined, the biomass composition of red cod was consistently dominated by females, comprising 69.8 ± 0.8% (mean ± SE) of the total biomass, followed by males with 30.1 ± 0.8%; no juveniles or individuals of undetermined sex were recorded in any survey year. Interannual variability in sex composition was low, with the female proportion ranging from 65% in 2016 to 75% in 2025, and the male proportion ranging from 25% in 2025 to 35% in 2016. The 2026 sex composition was consistent with the time series mean, with females comprising 72% and males 28% of the biomass (Fig. 65).

Maturity composition was dominated by post-spawning individuals (recovering spent and resting) in both sexes in most years (Fig. 66). Females were characterised by recovering spent and resting stages combined in every year (≥ 73%); immature, developing and ripe stages were scarce throughout the time series (< 13% combined in every year). For males, post-spawning stages (spent, recovering spent, and resting) were predominant in 2018 and 2021–2023, contributing up to 92% of the male biomass, whereas early developing individuals were predominant in 2017, and 2024–2026 (57–65%). Late developing and ripe males accounted for up to 18% in some years.

#### 4.3.8.5. Discussion

The significant declining trend in red cod biomass in Falkland Islands waters is consistent with the recent downward trend observed in July surveys (Ramos 2025), declining CPUE from finfish-licensed vessels in the FICZ (Ramos & Winter 2022d), and low biomass of spawning red cod reported from a survey that included the spawning ground to the south and south-west of West Falkland in September 2022 (Arkhipkin et al. 2022b). The commercial fishery has exhibited significant fluctuations in CPUE, with notable peaks in 1996 and 2011 followed by a sustained decline since 2013 (Ramos & Winter 2022d; FIFD, *unpublished data*). At a regional scale, red cod biomass in Argentine waters also declined from 1980 to 2015, with the 2023 biomass representing only 58% of the 1980 level despite a slow recovery since 2015 (Troccoli et al. 2024), indicating that the declining trend observed in Falkland Islands waters may reflect broader regional trends.

The (marginally) non-significant trends in both mean and median total length with a U-shaped pattern suggest that changes in size composition may be occurring as biomass declines, although high interannual variability in mean and median length limits the interpretation of these results. Given the sustained biomass decline and that approximately 70% of the biomass is comprised of females, most of which are in post-spawning maturity stages, the closure of red cod spawning grounds to the south and south-west of West Falkland since 2010 (Ramos & Winter 2022d) represents an important conservation measure that should be maintained, and additional management measures may be necessary.

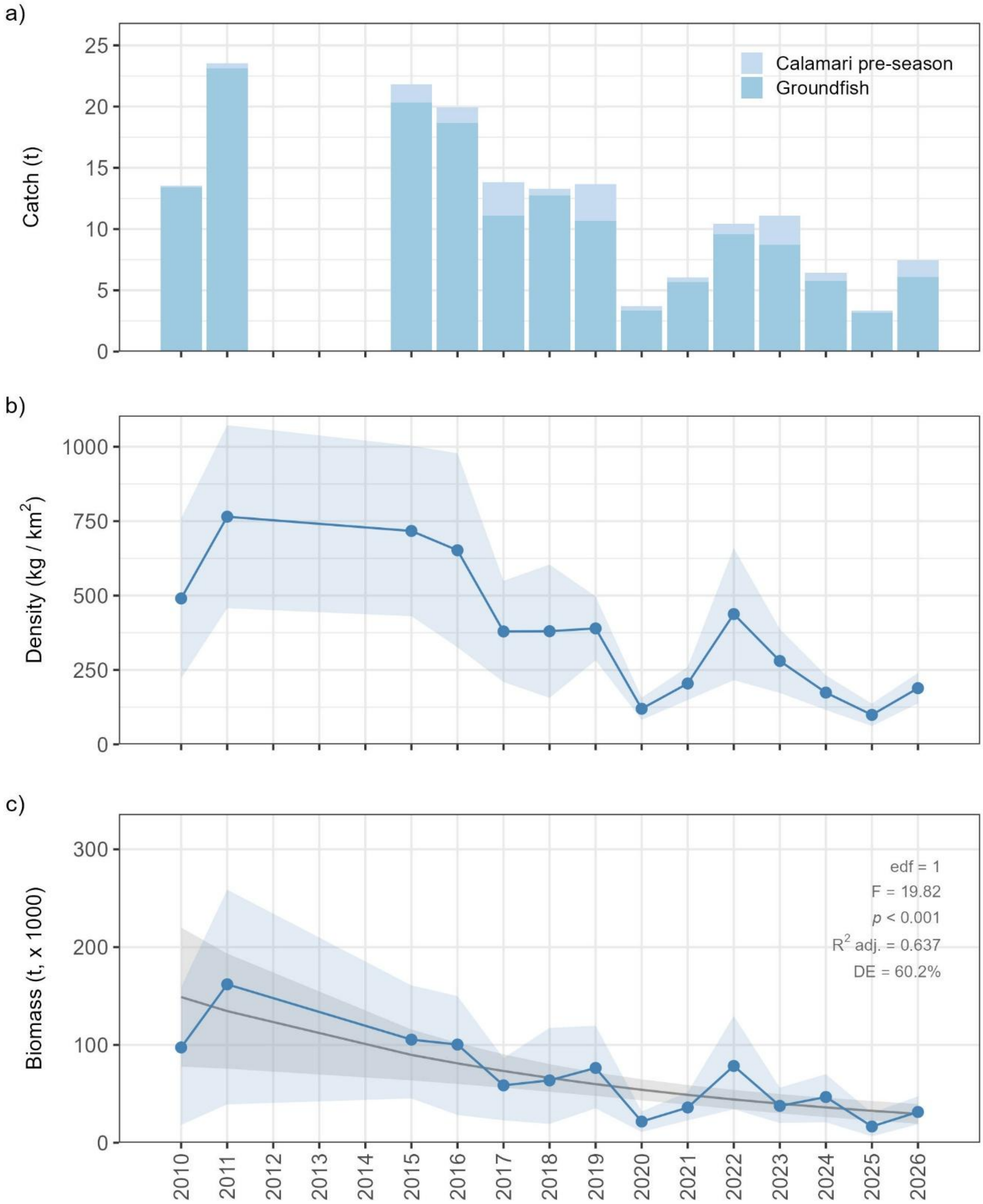


Fig. 59. Abundance of red cod (*Salilota australis*) during February groundfish and calamari pre-season surveys conducted in Falkland Islands waters in 2010–2011 and 2015–2026. (a) Catch per survey, (b) annual mean density ± SE represented by the blue line and shaded region, respectively, and (c) estimated biomass, where the blue line and shaded region represent the median and 95% pointwise confidence interval derived from 10,000 bootstrap biomass estimates, and the grey line and shaded region represent the fitted Generalised Additive Model (GAM) smooth and its 95% pointwise confidence interval.

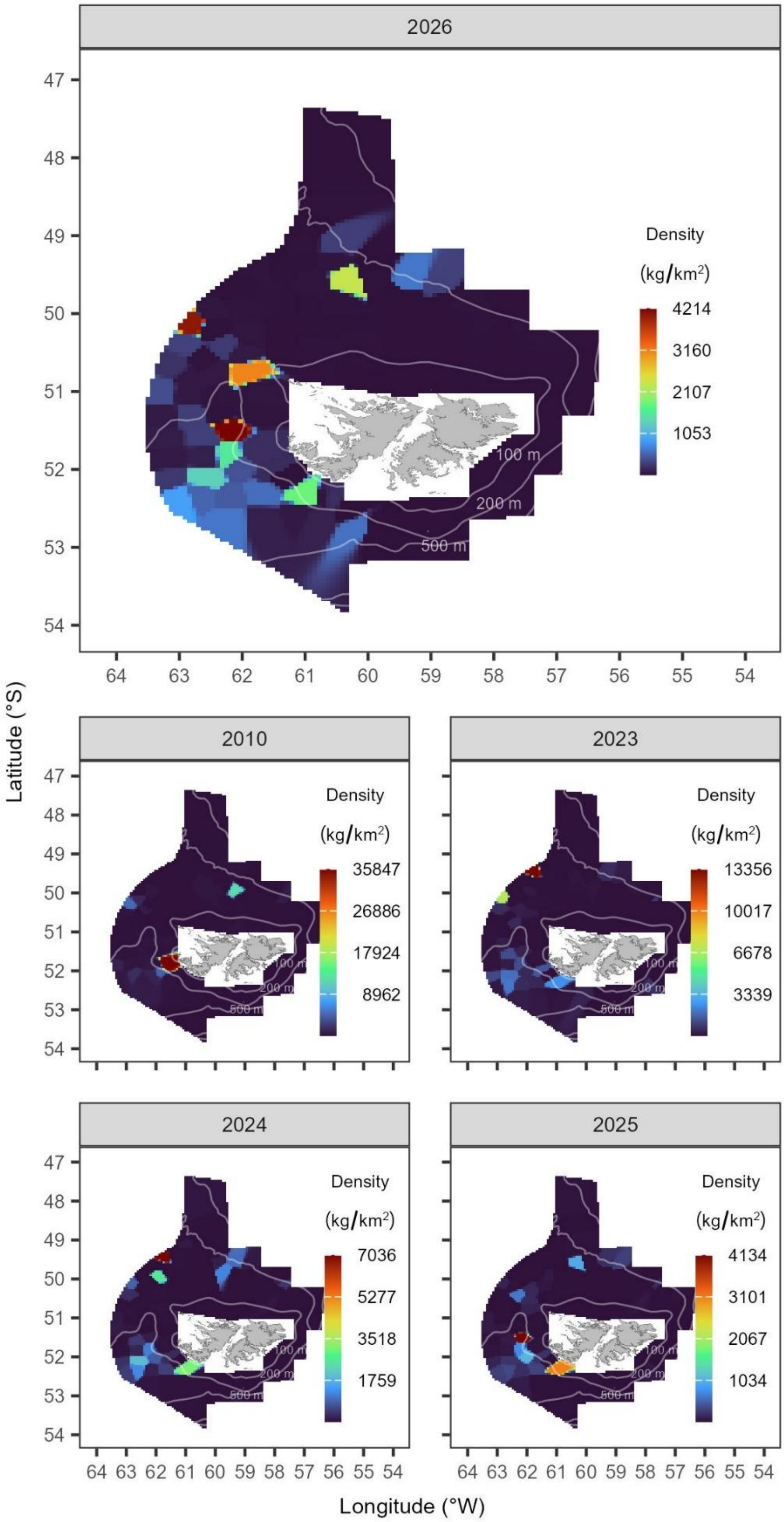


Fig. 60. Distribution and abundance of red cod (*Salilota australis*) derived from the February 2026 groundfish and calamari pre-season surveys in Falkland Islands waters, compared with the first year of the time series (2010) and the three preceding years (2023–2025). Colour scales are specific to each year. Isobaths at 100 m, 200 m, and 500 m are shown.

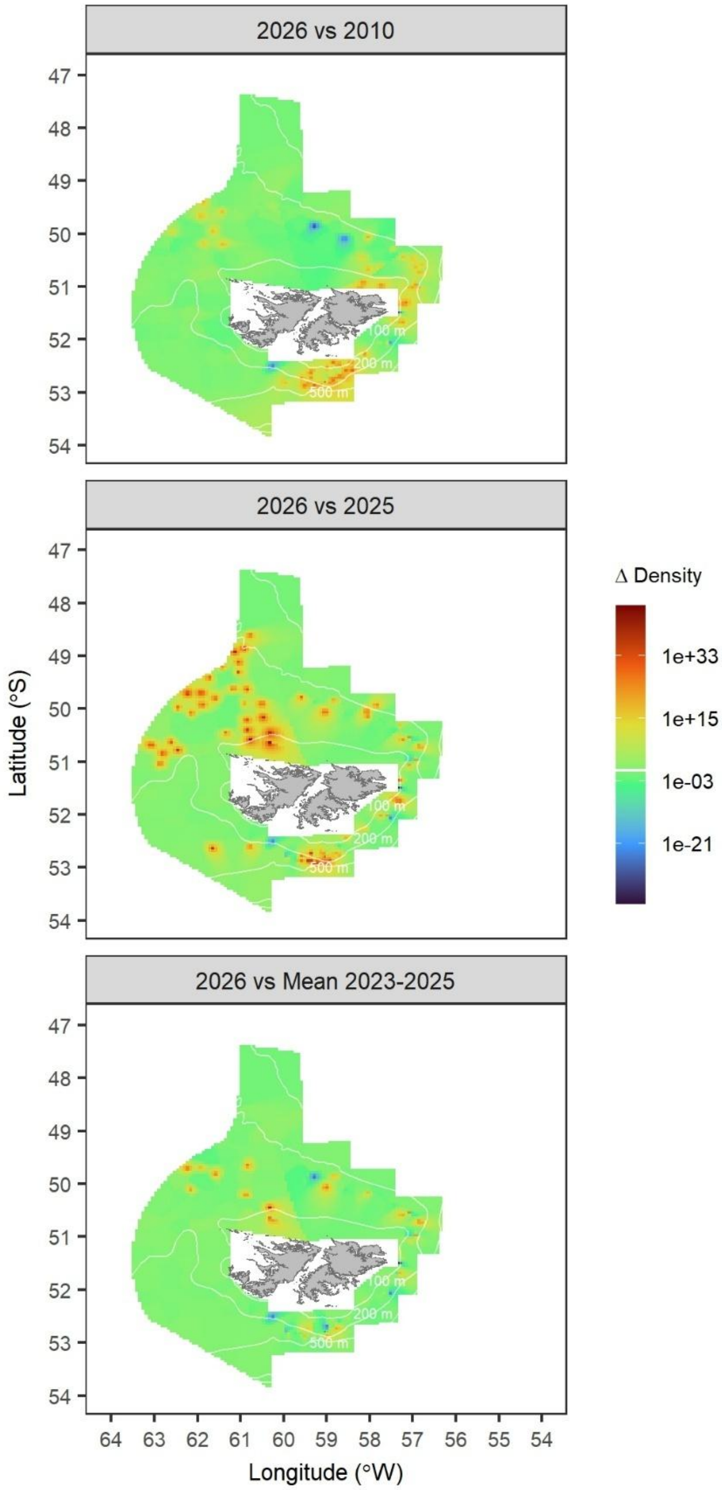


Fig. 61. Spatial change in density of red cod (*Salilota australis*) derived from the February 2026 groundfish and calamari pre-season surveys in Falkland Islands waters, relative to the first year of the time series (2010), the previous year (2025), and the mean of the three preceding years (2023–2025). The spatial change in density is expressed as the ratio of density (kg/km$^2$) in 2026 relative to the density in the baseline year (2010, 2025, 2023–2025 mean). Isobaths at 100 m, 200 m, and 500 m are shown. The colour scale is $log_{10}$-transformed to aid visualisation, with increases in density indicated above the horizontal white line towards dark red, and decreases in density indicated below the horizontal white line towards dark blue.

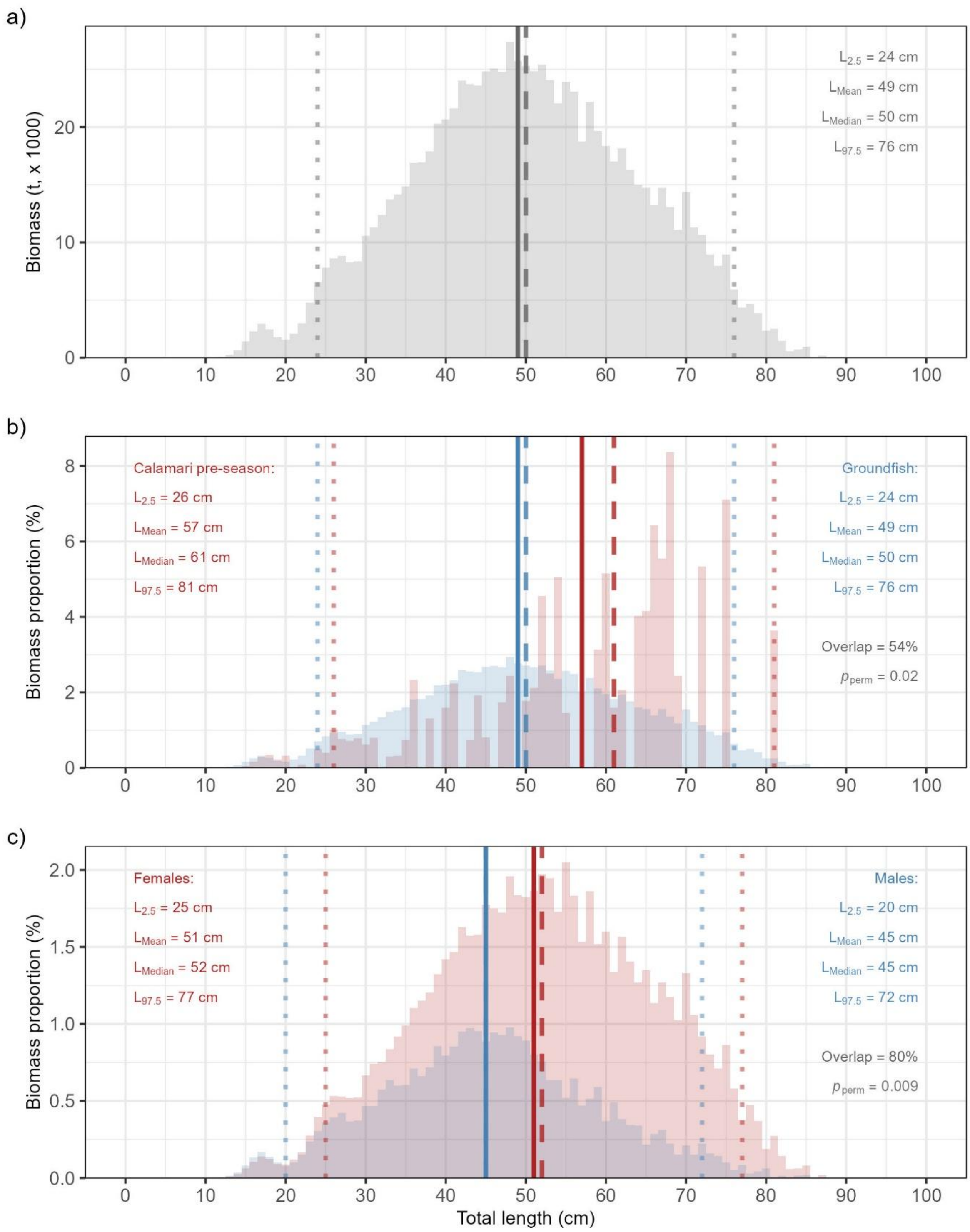


Fig. 62. Biomass-at-length class composition of red cod (*Salilota australis*) across all years combined, based on February groundfish and calamari pre-season surveys conducted in Falkland Islands waters in 2010–2011 and 2015–2026. a) Overall biomass-at-length frequency distribution. b) Overlap in biomass-at-length distributions between calamari pre-season (red) and groundfish (blue) surveys. c) Overlap in biomass-at-length distributions between females (red) and males (blue). Solid vertical lines indicate the mean length ($L_{Mean}$), dashed lines the median length ($L_{Median}$), and dotted lines the 2.5th and 97.5th length percentiles ($L_{2.5}$ and $L_{97.5}$, respectively). $p_{perm}$ is the significance of the weighted permutation test to assess differences between groups.

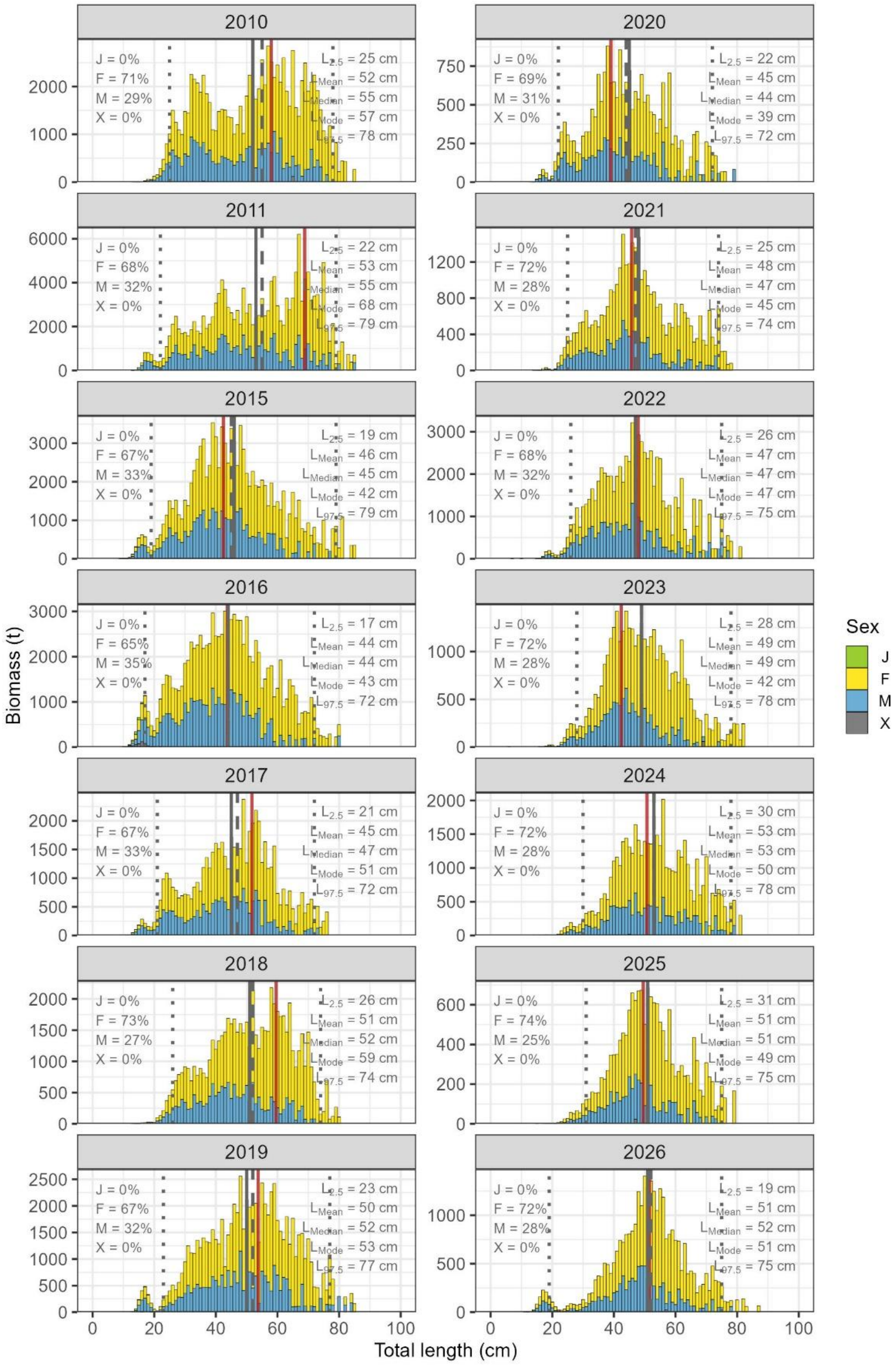


Fig. 63. Annual biomass-at-length class composition of red cod (*Salilota australis*) during February groundfish and calamari pre-season surveys conducted in Falkland Islands waters in 2010–2011 and 2015–2026. Stacked bars represent biomass (t) per 1.0 cm length class, partitioned by sex (J = juvenile; F = female; M = male; X = undetermined), with the proportion of total annual biomass for each sex indicated in the upper left of each panel. Vertical lines indicate the mean length ($L_{Mean}$, grey solid), median length ($L_{Median}$, grey dashed), modal length ($L_{Mode}$, red solid), and 2.5th and 97.5th percentiles ($L_{2.5}$ and $L_{97.5}$, grey dotted) of the biomass-weighted length distribution. Note the different y-axis scales among years.

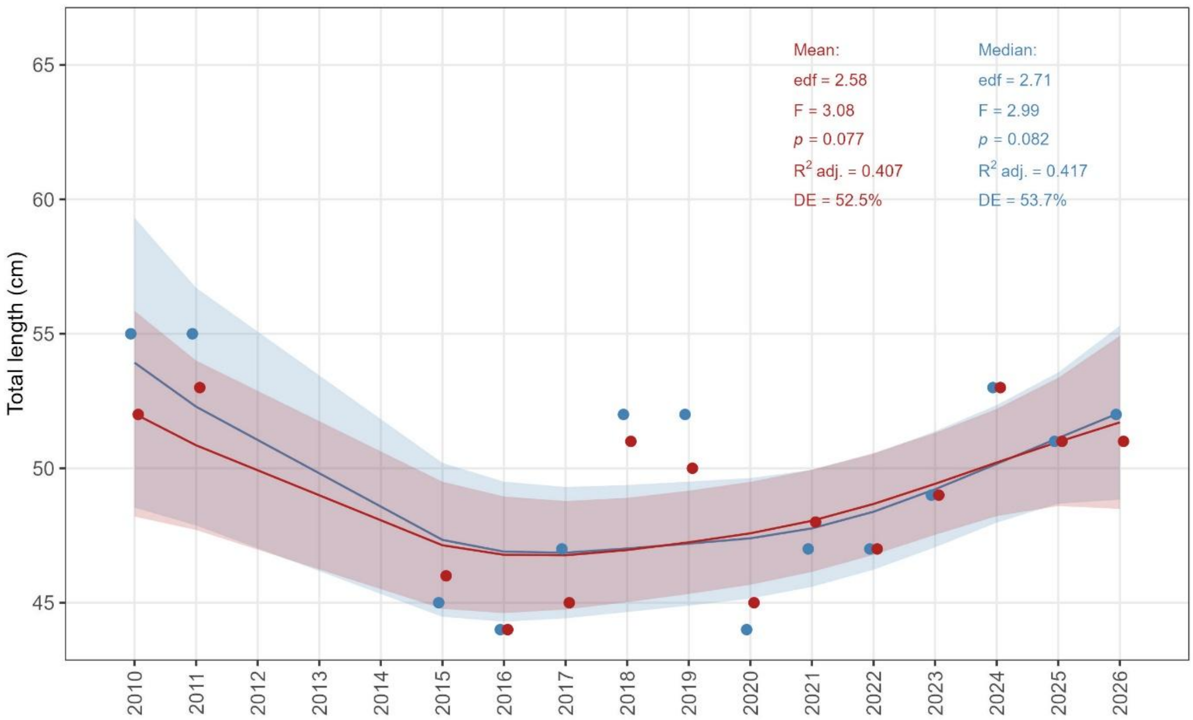


Fig. 64. Median (blue) and mean (red) total length of red cod (*Salilota australis*) during February groundfish and calamari pre-season surveys conducted in Falkland Islands waters in 2010–2011 and 2015–2026. The line and shaded region represent the fitted Generalised Additive Model (GAM) smooth and its 95% pointwise confidence interval.

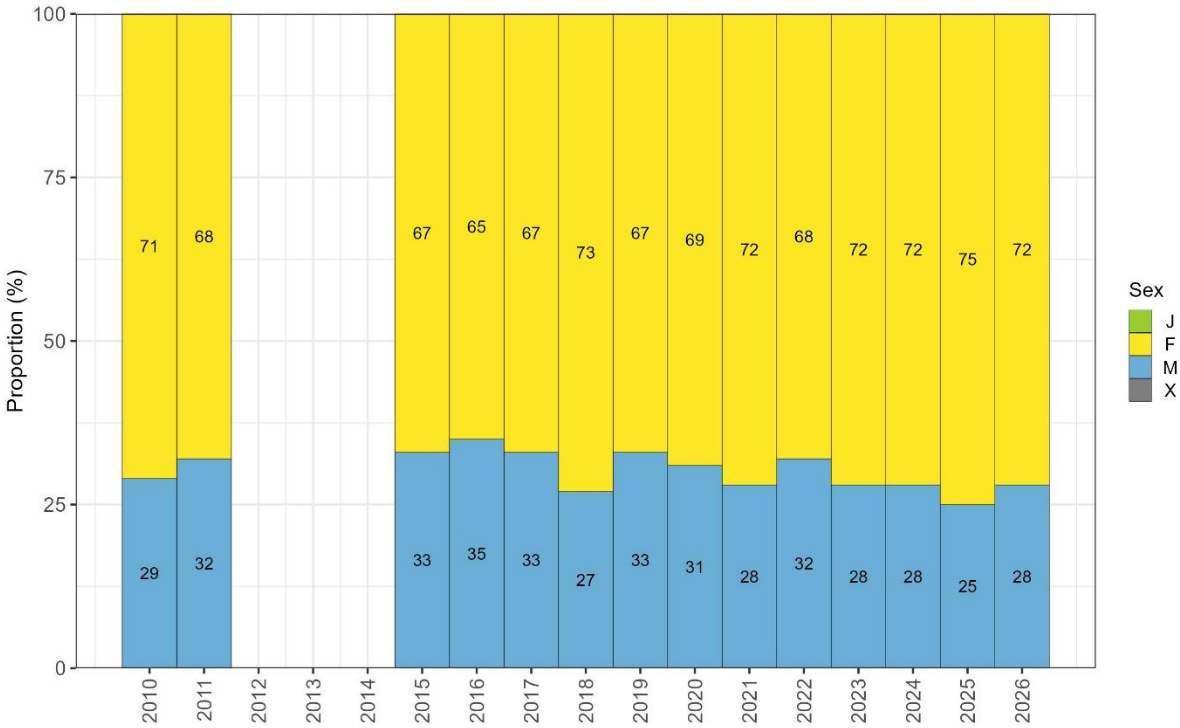


Fig. 65. Proportion by sex (J = juvenile; F = female; M = male; X = undetermined) of red cod (*Salilota australis*) during February groundfish and calamari pre-season surveys conducted in Falkland Islands waters in 2010–2011 and 2015–2026. Labels for proportions < 3% are omitted.

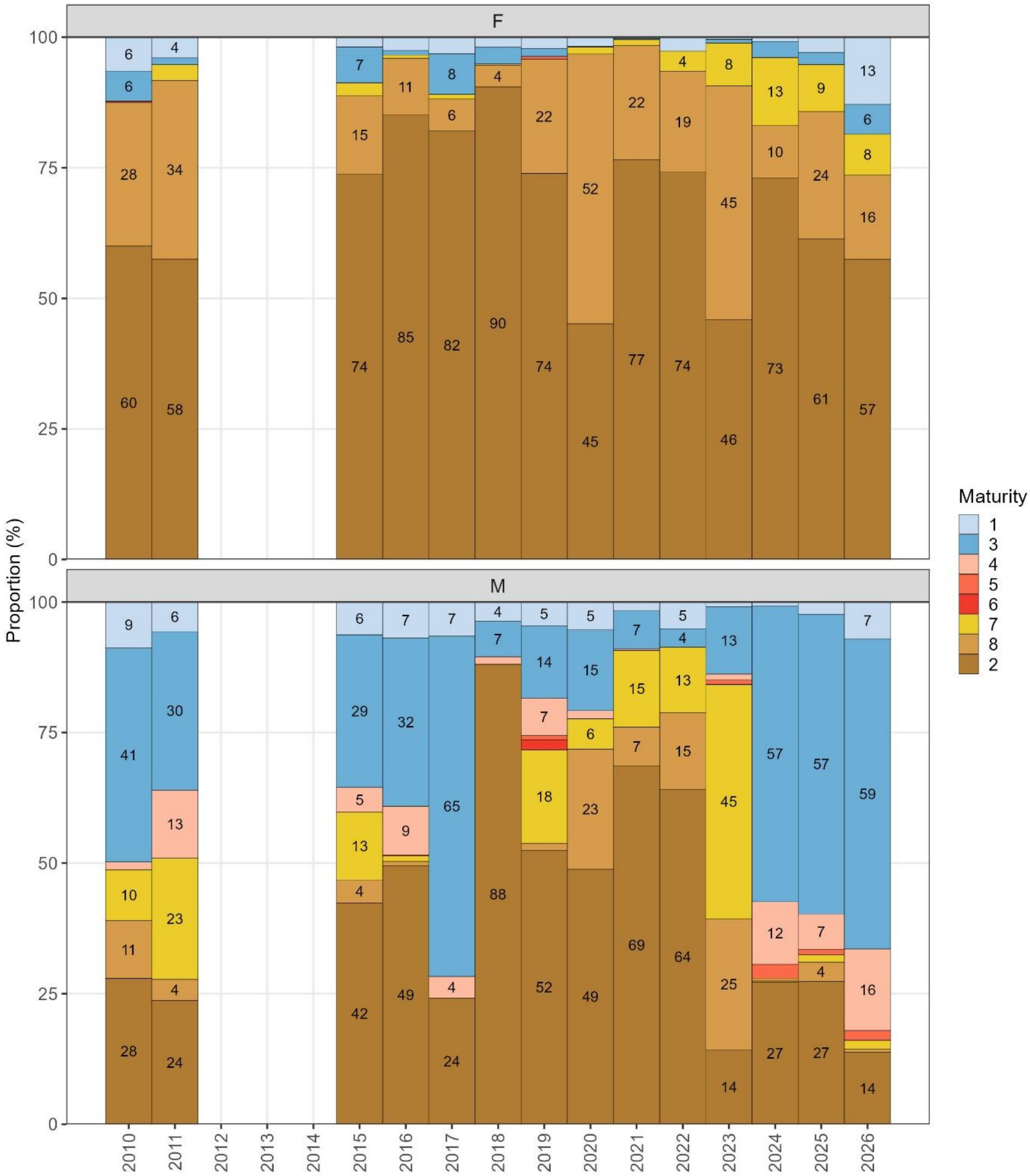


Fig. 66. Proportion by sexual maturity (1, immature; 3, early developing; 4, late developing; 5, ripe; 6, running; 7, spent; 8, recovering spent; 2, resting) of red cod (*Salilota australis*) during February groundfish and calamari pre-season surveys conducted in Falkland Islands waters in 2010–2011 and 2015–2026. Maturity stages ordered by developmental sequence. Labels for proportions < 3% are omitted.

### 4.3.9. Rock cod (*Patagonotothen ramsayi*)

4.3.9.1. Temporal patterns of abundance

On average, 32% of the total rock cod catches in the time series were obtained from groundfish surveys and 68% from calamari pre-season surveys. The highest catch occurred in 2011 (249.38 t). The catch in 2026 (75.50 t) corresponded to 45.9% of the 2010 catch (164.59 t). However, it increased 58.5% relative to the 2025 catch (47.65 t), and corresponded to 89.5% of the 2023–2025 mean catch (84.34 t; Fig. 67a; Appendix II).

The highest densities were recorded in 2011 (10,522.50 ± 5,651.39 kg/km²; mean ± SE; although note the wide confidence intervals). Densities in 2026 (1,702.82 ± 398.52 kg/km²) corresponded to 39.5% of the 2010 densities (4,310.50 ± 660.66 kg/km²). However, densities in 2026 represented nearly a two-fold increase relative to the 2025 densities (926.03 ± 299.04 kg/km²) and relative to the 2023–2025 mean densities (838.89 ± 121.32 kg/km²; Fig. 67b).

Rock cod biomass in 2026 (284,049.54 t) corresponded to 34% of 2010 levels (834,775 t), a significant decrease relative to 2010 ($p < 0.001$). However, it represented a significant 2.3-fold increase relative to 2025 (122,121.43 t; $p = 0.003$), and a significant 2.7-fold increase relative to the 2023–2025 mean (104,411.98 t; $p < 0.001$; Fig. 67c; Table IV–V; Appendix III–IV ). Analysis of the full time series revealed a significant non-linear declining trend in biomass (GAM: edf = 4.47, F = 31.45, $p < 0.001$), with the model explaining 94.7% of the deviance ($R^2$ adj. = 0.981), indicating a strong and consistent decrease in biomass over the time series (Fig. 67c; Appendix V).

4.3.9.2. Spatial patterns of abundance

In 2026, the highest density of rock cod (35,111 kg/km²) occurred to the north-west limit of the FICZ, at approximately 50°S and 62.5°W. A secondary patch of high density was observed at approximately 50.5°S and 61.5°W. The highest densities were also observed to the north-west in the FICZ during 2010, and from 2023 to 2025 (Fig. 68). However, rock cod had a patchy distribution around the Falkland Islands throughout the full time series, and the highest density was calculated for 2011 to the north-east of East Falkland (602,180 kg/km²).

Analysis of the spatial change in density revealed an overall decrease in densities through the survey area. Comparison of densities in 2026 relative to 2010 showed minor increases in density in the south and centre of the 'Loligo Box'. Comparisons of 2026 with 2025, and with the 2023–2025 mean showed minor increases in density through the survey area (Fig. 69).

4.3.9.3. Length composition

Across all survey years combined, total length of rock cod was in the range of 4 to 42 cm; however, 95% of the estimated biomass was comprised of individuals between 13 and 35 cm, with a median length of 24 ± 1.69 cm (median ± SE) and a mean length of 24 ± 1.27 cm (mean ± SE; Fig. 70a).

The distribution of biomass proportions by size class exhibited a 79% overlap between the groundfish and calamari pre-season surveys. Accordingly, the biomass-weighted mean length was not significantly different ($p > 0.05$) between the groundfish (24 ± 1.25 cm; mean ± SE) and the calamari pre-season (22 ± 1.34 cm) surveys, indicating similar size structure between surveys. In the groundfish survey, 95% of the biomass of rock cod was comprised of individuals between 14 and 35 cm, with a median length of 25 ± 1.60 cm (median ± SE). In the calamari pre-season survey, 95% of the biomass of rock cod was comprised of individuals between 13 and 35 cm, with a median length of 22 ± 1.90 cm (Fig. 70b).

The distribution of biomass proportions by size class exhibited a 97% overlap between females and males. Accordingly, the biomass-weighted mean length was not significantly different ($p > 0.05$) between females (24 ± 1.27 cm) and males (24 ± 1.28 cm), indicating similar size structure between females and males. For females, 95% of the biomass was comprised of individuals between 14 and 35 cm, with a median length of 24 ± 1.66 cm. For males, 95% of the biomass was comprised of individuals between 13 and 35 cm, with a median length of 24 ± 1.74 cm (Fig. 70c).

Through the time series, the size structure of rock cod was broad and multimodal, with at least two length-groups that were not clearly distinguished because of size overlap. A small length-group was observed at about 15 cm, another length-group at 20–21 cm, and a larger length-group at 25–28 cm. Different length-groups were dominant in the time series (Fig. 71). In 2026, the size structure remained broad and multimodal. Lengths were in the range of 5 to 38 cm; however, 95% of the biomass was comprised of individuals between 14 and 33 cm, with a median length of 24 ± 1.41 cm and a mean length of 23 ± 0.87 cm. For females, 95% of the biomass was comprised of individuals between 14 and 34 cm, with a median length of 24 ± 1.79 cm and a mean length of 23 ± 1.24 cm. For males, 95% of the biomass was comprised of individuals between 14 and 33 cm, with a median length of 24 ± 1.96 cm and a mean length of 23 ± 1.25 cm (Fig. 71).

Analysis of the full time series revealed significant declines in both mean (GAM: edf = 2.97, F = 21.29, $p < 0.001$, $R^2$ adj. = 0.855, DE = 88.8%) and median (GAM: edf = 2.02, F = 7.26, $p = 0.008$, $R^2$ adj. = 0.563, DE = 63.1%) total lengths. Mean length was approximately 27 cm in 2010, declined to approximately 22 cm in 2021, and remained relatively low through to 2026, at approximately 23 cm. Median length also was approximately 27 cm in 2010, and declined gradually to approximately 23 cm in 2026. The divergence between mean and median from 2015 onwards, with mean lengths being lower than median lengths, may reflect the presence of smaller individuals in the population (Fig. 72).

#### 4.3.9.4. Sex and maturity composition

Across all survey years combined, the biomass composition of rock cod was comprised of 52.9 ± 0.4% (mean ± SE) males, 46.9 ± 0.3% females, and 0.1 ± 0.1% juveniles, with no individuals of undetermined sex recorded in any survey year. Interannual variability was minimal, with the female proportion ranging from 45% in 2022 and 2025 to 49% in 2010, and the male proportion ranging from 50% in 2010 to 55% in 2022 and 2025, reflecting a near-constant male-to-female ratio throughout the time series. The 2026 sex composition was consistent with the time series mean, with males comprising 53% and females 47% of the biomass (Fig. 73).

Maturity composition in rock cod was dominated by post-spawning individuals (mostly recovering spent, and resting) in both sexes throughout the time series (Fig. 74). Females were characterised mainly by resting individual (49–90%), with spent and recovering spent individuals contributing a further 5–27%; immature and early developing individuals together contributed < 25% in every year. Males were mainly characterised by resting individuals (54–90%), with recovering spent individuals contributing up to 19% in some years. Late developing, ripe and running individuals were not reported throughout the time series.

#### 4.3.9.5. Discussion

The highly significant non-linear declining trend in rock cod biomass from February surveys conducted in Falkland Islands waters is consistent with the declining biomass observed in commercial fisheries data from 2005 to 2019 (Winter 2020) and declining CPUE since 2011 (Ramos & Winter 2023a). However, February biomass, July biomass (Ramos 2025), and commercial CPUE have shown signs of stabilisation in recent years, suggesting the rate of decline may be slowing. An apparent shift in geographic distribution, inferred from increasing out-of-zone catches, may have contributed to the reduced abundance observed between 2016 and 2018 (Winter 2021).

The highly significant decline in both mean and median total length indicates a sustained shift in the size structure of the population towards smaller individuals over the February survey period, although mean total length has increased gradually since 2022. This pattern is consistent with the increase in the proportion of rock cod discarded in Falkland Islands fisheries, which rose from an average of 13% annually during 2010–2015 to 72% during 2016–2024, with up to 94% discards reported in 2021 (Falkland Islands Government, *unpublished data*). The Patagonian squid fishery has accounted for the majority of rock cod catches and discards since 2016 (Ramos & Winter 2023a), where rock cod are typically discarded due to their small size. Given that most discarded individuals have not yet reproduced and that survival rates of discarded fish are low, future reproductive potential is removed from the population and represents a source of unaccounted mortality that may not be fully captured in stock assessments (Guillen et al. 2018). Rock cod currently remains a permitted catch under finfish vessel licences with no conservation measures beyond a TAC in place within Falkland Islands fisheries, including the Patagonian squid fishery (Falkland Islands Government 2026). Given the sustained biomass decline, the shift towards smaller individuals, and the high discard rates, measures to address the incidental capture and discard of rock cod may be necessary to prevent further deterioration and facilitate recovery of the stock.

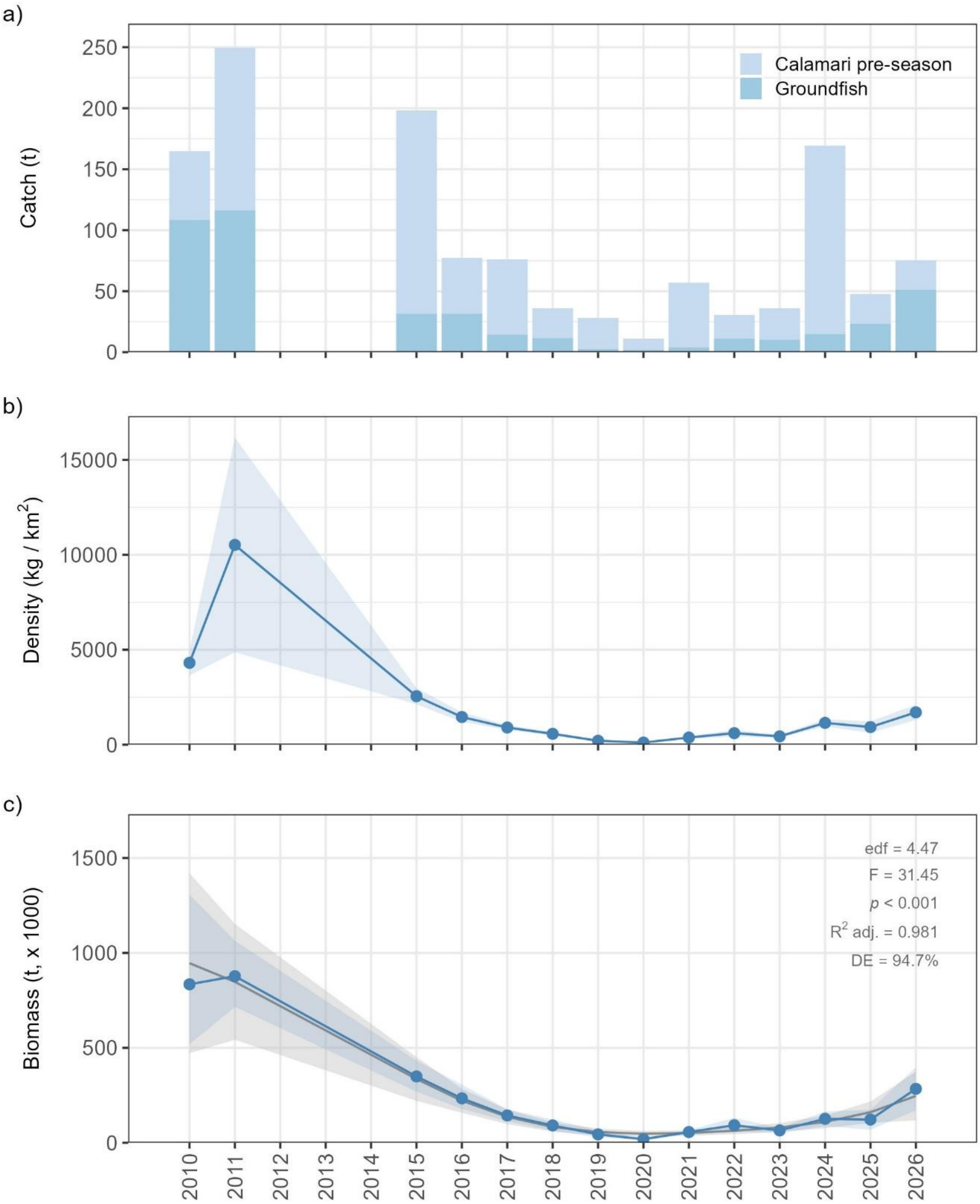


Fig. 67. Abundance of rock cod (*Patagonotothen ramsayi*) during February groundfish and calamari pre-season surveys conducted in Falkland Islands waters in 2010–2011 and 2015–2026. (a) Catch per survey, (b) annual mean density ± SE represented by the blue line and shaded region, respectively, and (c) estimated biomass, where the blue line and shaded region represent the median and 95% pointwise confidence interval derived from 10,000 bootstrap biomass estimates, and the grey line and shaded region represent the fitted Generalised Additive Model (GAM) smooth and its 95% pointwise confidence interval.

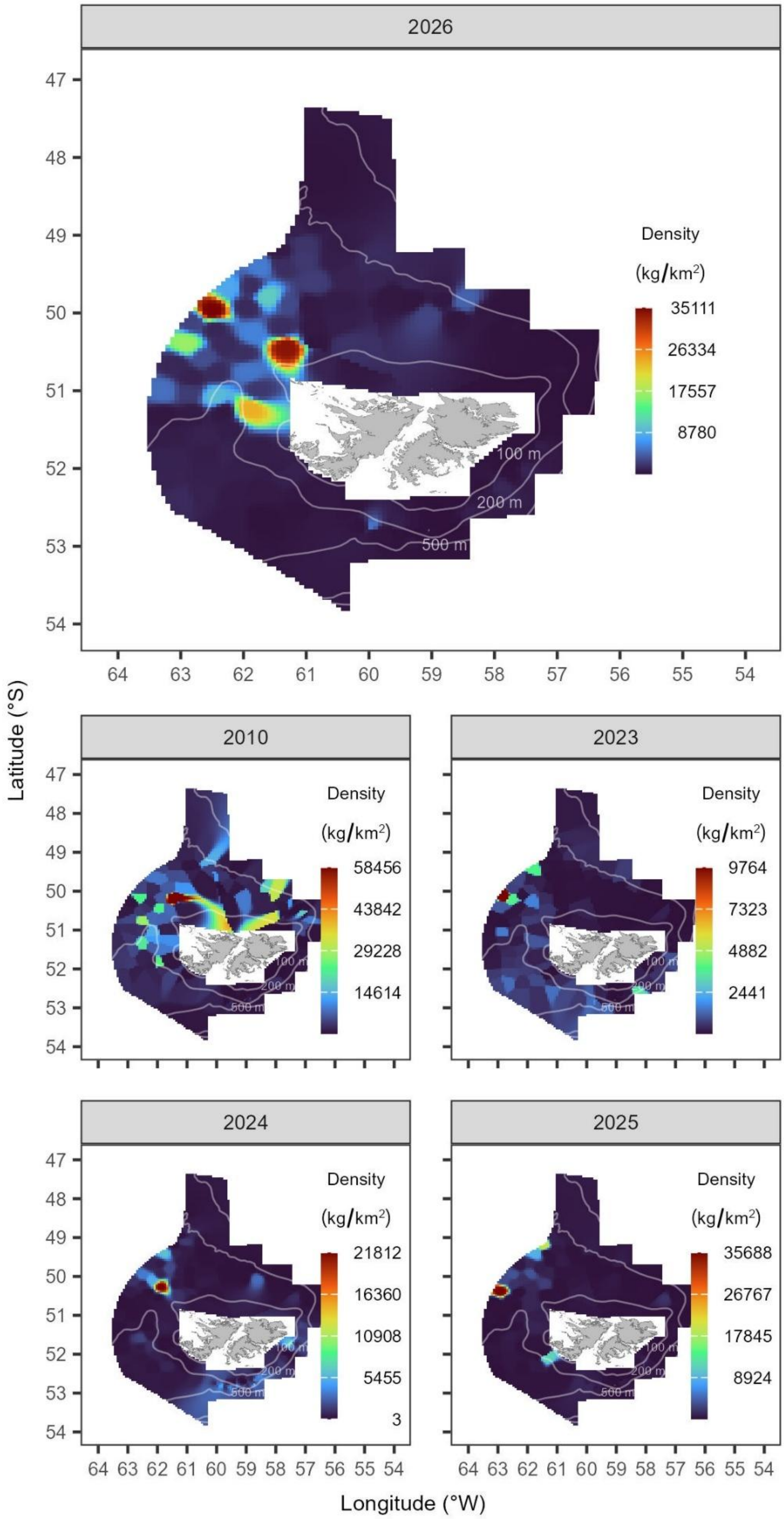


Fig. 68. Distribution and abundance of rock cod (*Patagonotothen ramsayi*) derived from the February 2026 groundfish and calamari pre-season surveys in Falkland Islands waters, compared with the first year of the time series (2010) and the three preceding years (2023–2025). Colour scales are specific to each year. Isobaths at 100 m, 200 m, and 500 m are shown.

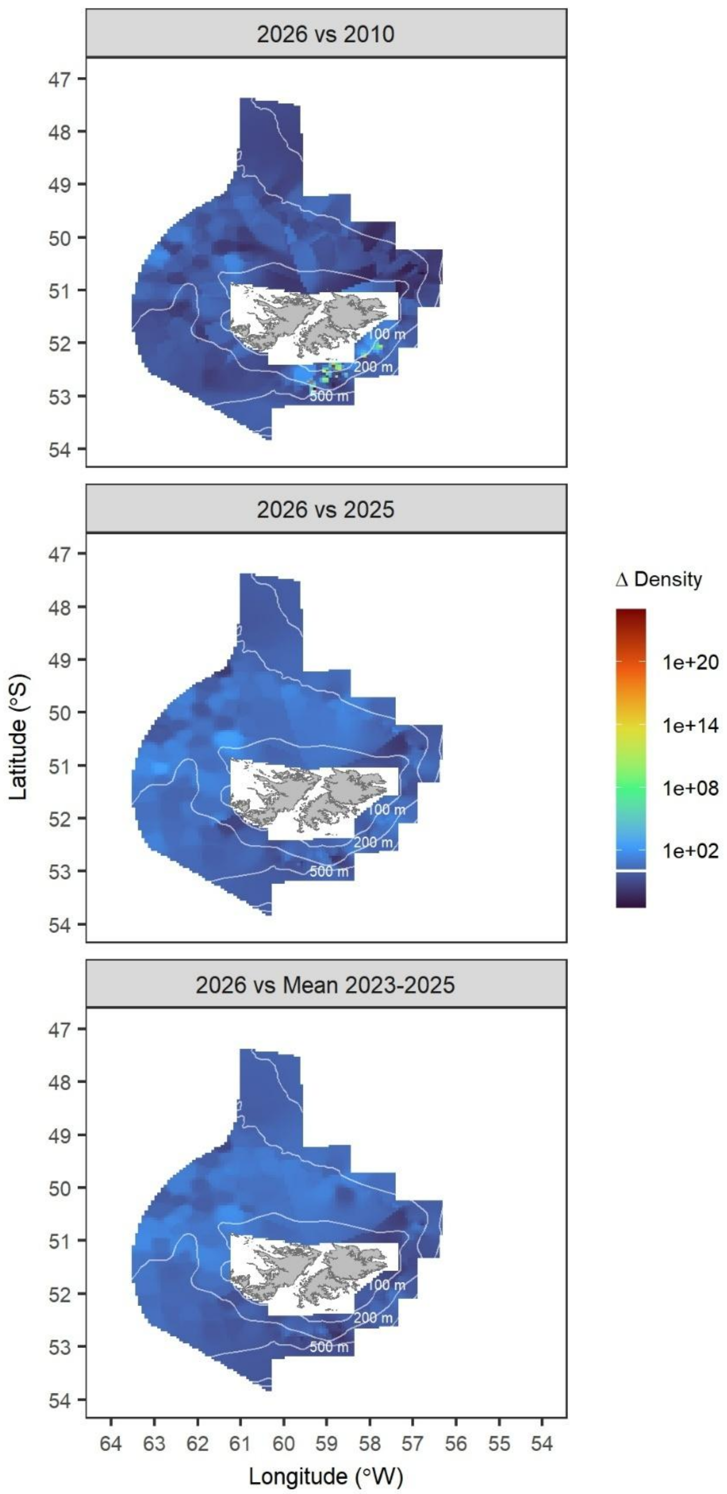


Fig. 69. Spatial change in density of rock cod (*Patagonotothen ramsayi*) derived from the February 2026 groundfish and calamari pre-season surveys in Falkland Islands waters, relative to the first year of the time series (2010), the previous year (2025), and the mean of the three preceding years (2023–2025). The spatial change in density is expressed as the ratio of density (kg/km$^2$) in 2026 relative to the density in the baseline year (2010, 2025, 2023–2025 mean). Isobaths at 100 m, 200 m, and 500 m are shown. The colour scale is $\log_{10}$-transformed to aid visualisation, with increases in density indicated above the horizontal white line towards dark red, and decreases in density indicated below the horizontal white line towards dark blue.

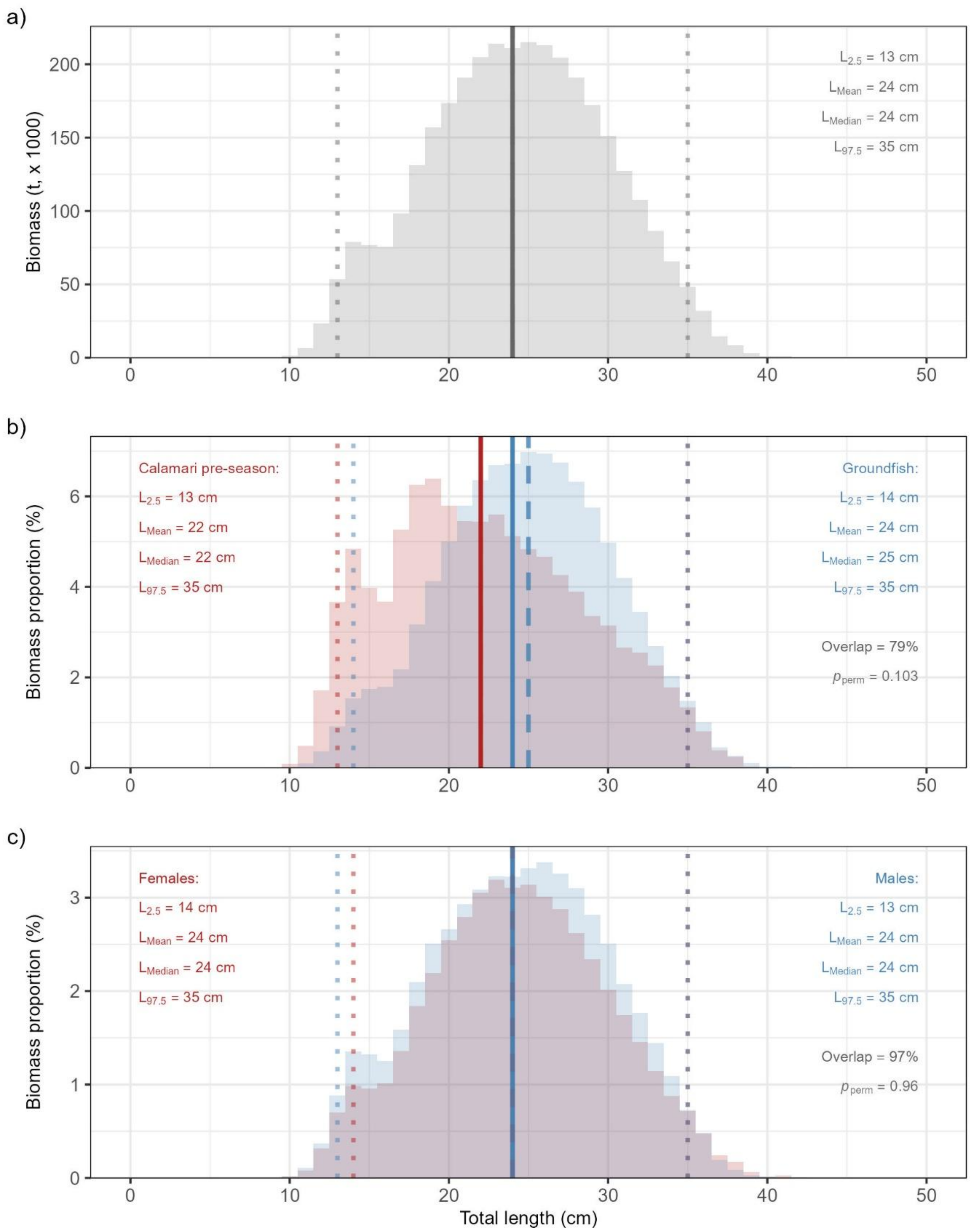


Fig. 70. Biomass-at-length class composition of rock cod (*Patagonotothen ramsayi*) across all years combined, based on February groundfish and calamari pre-season surveys conducted in Falkland Islands waters in 2010–2011 and 2015–2026. a) Overall biomass-at-length frequency distribution. b) Overlap in biomass-at-length distributions between calamari pre-season (red) and groundfish (blue) surveys. c) Overlap in biomass-at-length distributions between females (red) and males (blue). Solid vertical lines indicate the mean length ($L_{Mean}$), dashed lines the median length ($L_{Median}$), and dotted lines the 2.5th and 97.5th length percentiles ($L_{2.5}$ and $L_{97.5}$, respectively). $p_{perm}$ is the significance of the weighted permutation test to assess differences between groups.

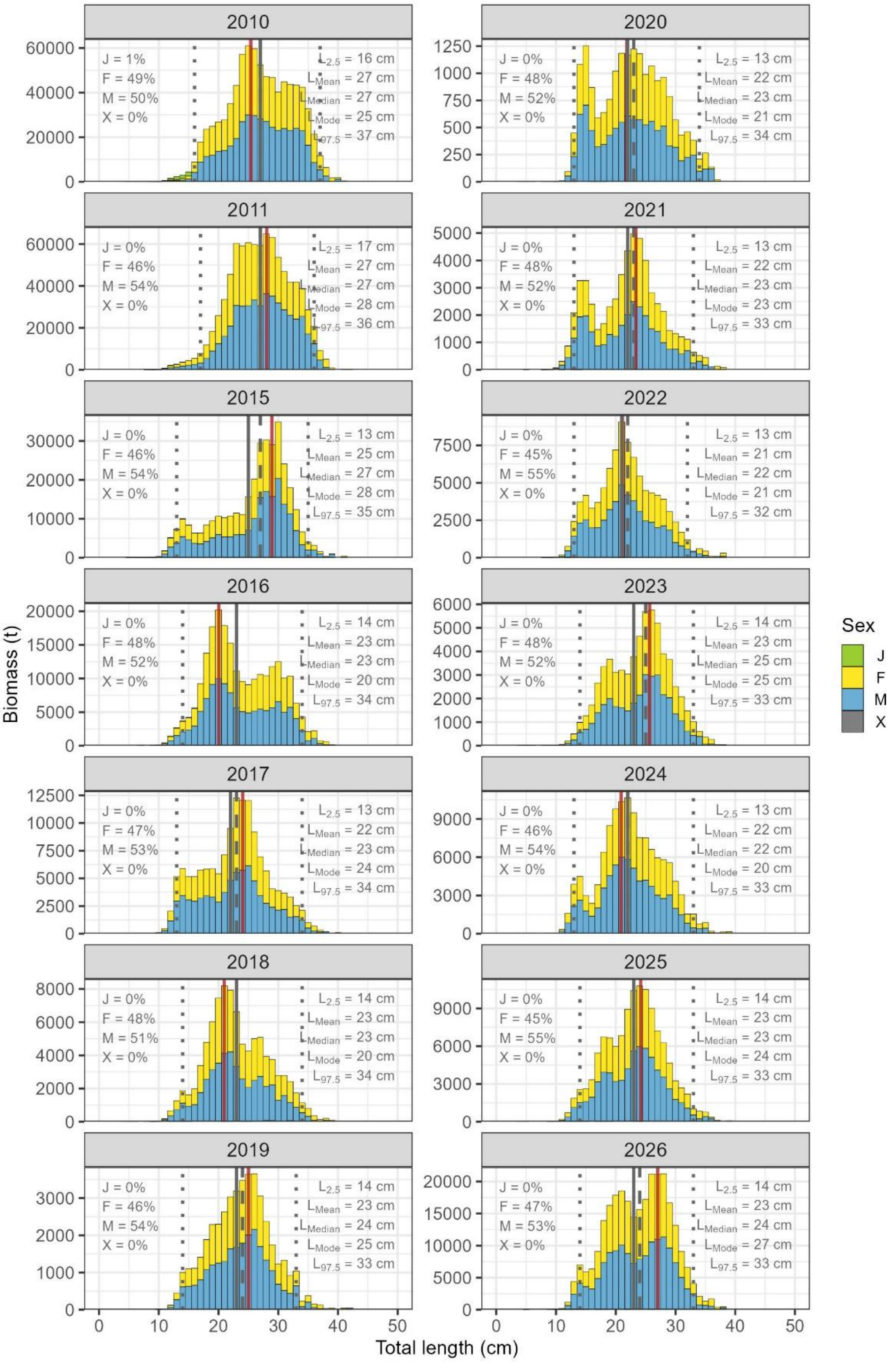


Fig. 71. Annual biomass-at-length class composition of rock cod (*Patagonotothen ramsayi*) during February groundfish and calamari pre-season surveys conducted in Falkland Islands waters in 2010–2011 and 2015–2026. Stacked bars represent biomass (t) per 1.0 cm length class, partitioned by sex (J = juvenile; F = female; M = male; X = undetermined), with the proportion of total annual biomass for each sex indicated in the upper left of each panel. Vertical lines indicate the mean length ($L_{Mean}$, grey solid), median length ($L_{Median}$, grey dashed), modal length ($L_{Mode}$, red solid), and 2.5th and 97.5th percentiles ($L_{2.5}$ and $L_{97.5}$, grey dotted) of the biomass-weighted length distribution. Note the different y-axis scales among years.

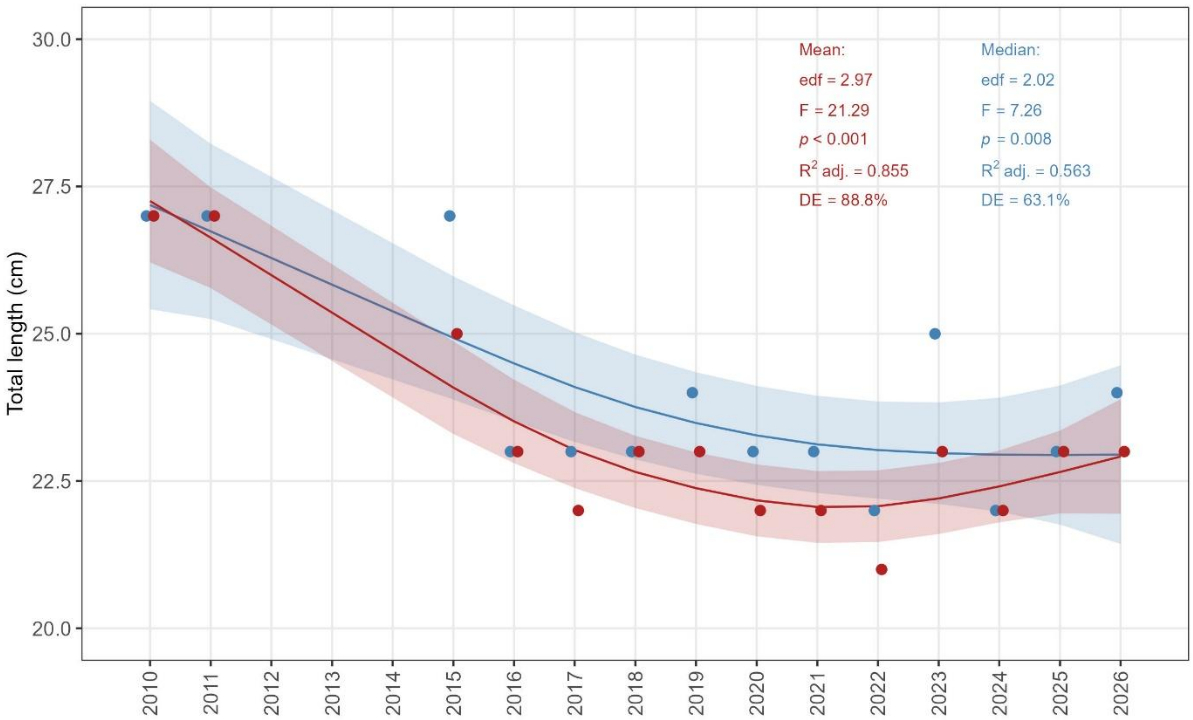


Fig. 72. Median (blue) and mean (red) total length of rock cod (*Patagonotothen ramsayi*) during February groundfish and calamari pre-season surveys conducted in Falkland Islands waters in 2010–2011 and 2015–2026. The line and shaded region represent the fitted Generalised Additive Model (GAM) smooth and its 95% pointwise confidence interval.

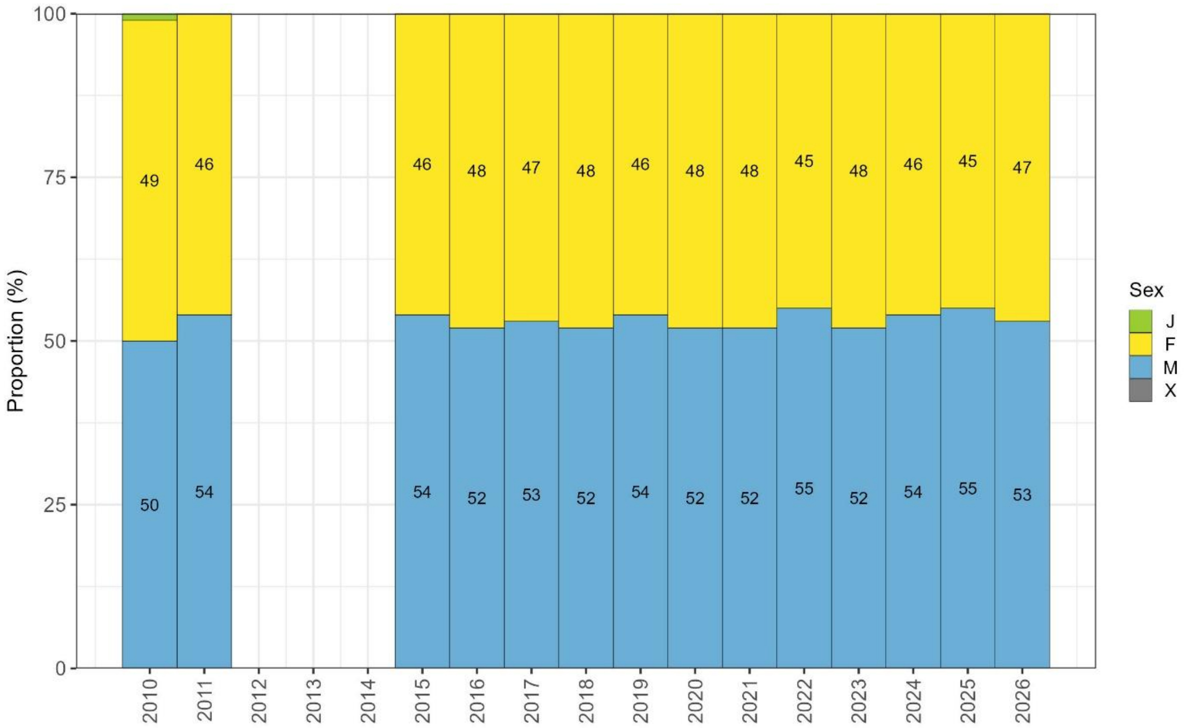


Fig. 73. Proportion by sex (J = juvenile; F = female; M = male; X = undetermined) of rock cod (*Patagonotothen ramsayi*) during February groundfish and calamari pre-season surveys conducted in Falkland Islands waters in 2010–2011 and 2015–2026. Labels for proportions < 3% are omitted.

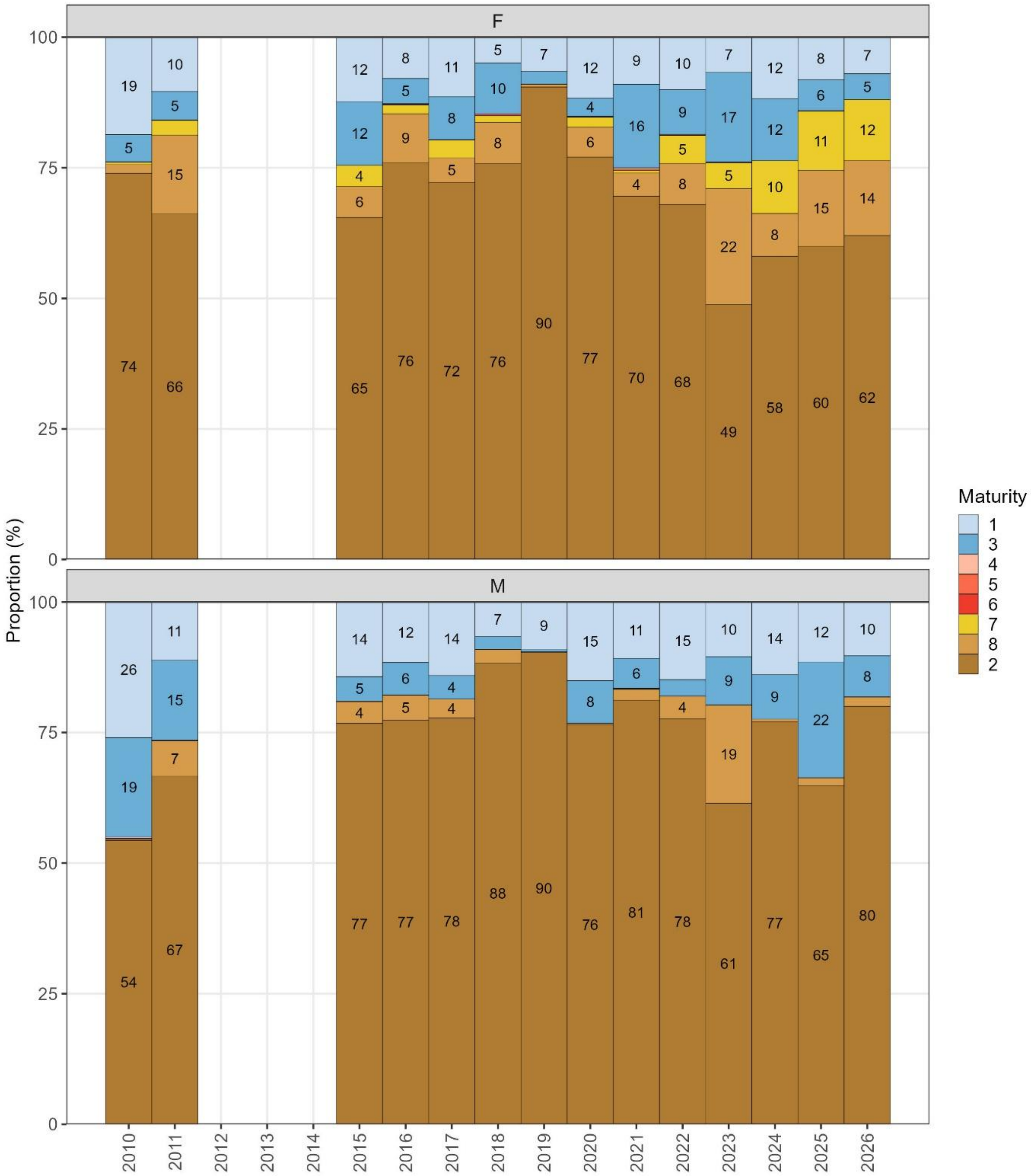


Fig. 74. Proportion by sexual maturity (1, immature; 3, early developing; 4, late developing; 5, ripe; 6, running; 7, spent; 8, recovering spent; 2, resting) of rock cod (*Patagonotothen ramsayi*) during February groundfish and calamari pre-season surveys conducted in Falkland Islands waters in 2010–2011 and 2015–2026. Maturity stages ordered by developmental sequence. Labels for proportions < 3% are omitted.

#### 4.3.10. Southern blue whiting (*Micromesistius australis*)

4.3.10.1. Temporal patterns of abundance

On average, 8% of the total southern blue whiting catches in the time series were obtained from groundfish surveys and 92% from calamari pre-season surveys. The highest catch occurred in 2024 (119.79 t). The catch in 2026 (13.89 t) corresponded to 63.6% of the catch in 2010 (21.87 t), 23.8% of the catch in 2025 (58.51 t), and 19.8% of the 2023–2025 mean catch (70.23 t; Fig. 75a; Appendix II).

The highest densities were recorded in 2016 (1,585.07 ± 1,398.22 kg/km²; mean ± SE; although note the wide confidence intervals). Densities in 2026 (162.22 ± 76.04 kg/km²) corresponded to 45.2% of the 2010 densities (359.03 ± 135.18 kg/km²), 34% of the 2025 densities (476.91 ± 192.51 kg/km²), and 39.3% of the 2023–2025 mean densities (412.98 ± 136.43 kg/km²; Fig. 75b).

Southern blue whiting biomass peaked in 2011 (148,296.01 t), although with wide confidence intervals. Biomass in 2026 (56,940.91 t) corresponded to 94.5% of 2010 levels (60,270.74 t), 84.9% of 2025 levels (67,087.67 t), and represents a 1.6% increase relative to the 2023–2025 mean (56,055.67 t), with none of these differences being statistically significant ($p > 0.05$; Fig. 75c; Table IV–V; Appendix III–IV). Analysis of the full time series revealed no significant temporal trend in biomass (GAM: edf = 2.60, F = 2.22, p = 0.154), with the model explaining 37.3% of the deviance ($R^2$ adj. = 0.246), reflecting moderate interannual variability and no consistent directional change over the time series (Fig. 75c; Appendix V). It should be noted that the k-index (0.747) is below 1, suggesting that the basis dimension may be insufficient to fully capture the complexity of the trend; however, $k$ was set to 10, near the upper limit permissible for the time series length, following the recommendation that $k$ should not exceed $n - 1$, where $n$ is the number of years ($n = 14$; Wood 2017). Increasing $k$ beyond this would risk overfitting by allowing the smooth to fit noise rather than a genuine signal, and results should therefore be interpreted with caution.

4.3.10.2. Spatial patterns of abundance

In 2026, southern blue whiting occurred to the south-west and to the north-east in the FICZ, as well as to the east within the 'Loligo Box'. The highest density (9,623 kg/km$^2$) occurred to the south-west of West Falkland at approximately 52.5–53.5°S and 61–62°W. High densities occurred to the north-east within the 'Loligo Box' in 2010, and from 2023 to 2025 (Fig. 76). However, the highest density in the full time series was calculated for 2016 to the south of East Falkland (203,954 kg/km$^2$).

Analysis of the spatial change in density revealed an overall decrease in densities through the survey area. Comparison of densities in 2026 relative to 2010 showed substantial decrease in densities from the south-west to the north-east in the FICZ, and in the north of the 'Loligo Box''. In contrast, densities mainly increased in the south and centre of the 'Loligo Box', and in localised areas to the north-east and to the north-west of the FICZ. Comparisons of 2026 with 2025 showed substantial decreases in patchy areas to the south-west and to the north-west in the FICZ, and in the south of the 'Loligo Box', while densities increased mainly in small areas to the north-west in the FICZ. Comparisons of 2026 with the 2023–2025 mean showed overall decreases through the survey area, with substantial decreases along the west in the FICZ, and in distinct areas of the 'Loligo Box' (Fig. 77).

4.3.10.3. Length composition

Across all survey years combined, total length of southern blue whiting was in the range of 6 to 72 cm; however, 95% of the estimated biomass was comprised of individuals between 23 and 64 cm, with a median length of 51 ± 2.80 cm (median ± SE) and a mean length of 46 ± 2.21 cm (mean ± SE; Fig. 78a).

The distribution of biomass proportions by size class exhibited a 52% overlap between the groundfish and calamari pre-season surveys. However, the biomass-weighted mean length was not significantly different ($p > 0.05$) between the groundfish (46 ± 2.44 cm; mean ± SE) and the calamari pre-season (47 ± 2.24 cm) surveys, indicating similar size structure between surveys. In the groundfish survey, 95% of the biomass of southern blue whiting was comprised of individuals between 23 and 64 cm, with a median length of 51 ± 4.64 cm. In the calamari pre-season survey, 95% of the biomass of southern blue whiting was comprised of individuals between 23 and 58 cm, with a median length of 51 ± 1.52 cm (Fig. 78b).

The distribution of biomass proportions by size class exhibited a 79% overlap between females and males. Accordingly, the biomass-weighted mean length was not significantly different ($p > 0.05$) between females (48 ± 2.60 cm) and males (46 ± 2.19 cm), indicating similar size structure between females and males. For females, 95% of the biomass was comprised of individuals between 23 and 65 cm, with a median length of 54 ± 4.11 cm. For males, 95% of the biomass was comprised of individuals between 23 and 61 cm, with a median length of 50 ± 2.46 cm (Fig. 78c).

Through the time series, the size structure of southern blue whiting was broad and multimodal, with some length-groups not clearly distinguished because of size overlap. Recruitment of individuals <25 cm seemed poor in 2025 and 2026 (Fig. 79). In 2026, the size structure remained broad and multimodal. Lengths were in the range of 7 to 61 cm; however, 95% of the biomass was comprised of individuals between 35 and 58 cm, with a median length of 52 ± 1.00 cm and a mean length of 49 ± 1.67 cm. For females, 95% of the biomass was comprised of individuals between 35 and 59 cm, with a median length of 54 ± 2.19 cm and a mean length of 50 ± 2.28 cm. For males, 95% of the biomass was comprised of individuals between 35 and 57 cm, with a median length of 52 ± 1.34 cm and a mean length of 49 ± 2.05 cm (Fig. 79).

Analysis of the full time series revealed no statistically significant temporal trend in either mean (GAM: edf = 1.57, $F = 0.99$, $p = 0.466$, $R^2$ adj. = 0.062, DE = 16.9%) or median (GAM: edf = 2.54, $F = 3.17$, $p = 0.073$, $R^2$ adj. = 0.408, DE = 52.3%) total lengths. The two metrics showed different model fits, both being heavily influenced by high interannual variability and potentially anomalous years (i.e., 2022–2023), substantially reducing statistical power and limiting capacity to explain length patterns through time (Fig. 80).

4.3.10.4. Sex and maturity composition

Across all survey years combined, the biomass composition of southern blue whiting was dominated by males with 63.9 ± 2.4% (mean ± SE), followed by females with 35.3 ± 2.1%, juveniles with 0.6 ± 0.5%, and no individuals of undetermined sex. Interannual variability in sex composition was high, with the male proportion ranging from 50% in 2010 and 2011 to 75% in 2019 and 2025, and the female proportion ranging from 25% in 2019 and 2025 to 50% in 2011. The proportion of males increased from 2015 (52%) to a peak of 75% in 2019, remaining at high levels over the following years. Juveniles were recorded only in 2010 (7% of biomass) and 2015 (approximately 1%). The 2026 sex composition was consistent with the time series mean, with males comprising 73% and females 27% of the biomass (Fig. 81).

Maturity composition was dominated by post-spawning individuals (mainly recovering spent and resting) in both sexes throughout the time series (Fig. 82). Females were characterised by resting and recovering spent individuals (47–96%) in every year; immature individuals generally contributed < 30% every year, except for 2022 and 2023 with 50% each. Males were predominantly represented by recovering spent and resting individuals (34–92%) throughout the whole time series, although the presence of immature individuals was higher in 2022 (65%) and in 2023 (47%). Spent individuals were generally scarce but reached 62% of male biomass in 2019. Late developing, ripe and running individuals were mostly absent in both sexes throughout.

#### 4.3.10.5. Discussion

The absence of a significant temporal trend in southern blue whiting biomass from February surveys conducted in Falkland Islands waters is consistent with the low abundance of this stock after heavy exploitation in the Southwest Atlantic beginning in the early 1990s and a stock collapse in 2009 (Navarro et al. 2014; Falkland Islands Government 2026). A no-fishing area established south-west of the Falkland Islands from 1 July to 15 October in 2007 for S-licensed vessels that targeted southern blue whiting and hoki (Falkland Islands Government 2026), and the absence of S-licence fishing since 2017 may have provided some protection. However, given that the Falkland Islands contributed only approximately 4% of the catch shared with Argentina and 2.5% of the total catch shared among Argentina, Chile, and the Falkland Islands from 2017 to 2024 (Ramos & Winter 2023b; Falkland Islands Government 2026; Government of Argentina, www.magyp.gob.ar), the persistently low biomass observed in Falkland Islands waters probably reflects the cumulative effect of high fishing pressure on this stock across multiple EEZs rather than conditions within the Falkland Islands fishing zone alone. The absence of significant temporal trends in both mean and median total length, combined with high interannual variability and anomalously low values in 2022–2023 (Fig. 80), limits the interpretation of size composition trends for this species. Continued protection of the spawning ground located to the south of the Falkland Islands (Shubnikov et al. 1969; Pájaro & Macchi 2001; Macchi et al. 2005) remains essential, particularly given the influence of the intensity of the Falkland Current on its size and location (Arkhipkin et al. 2009, 2012). Any resumption of directed fishing on this stock should be considered cautiously as it may negatively affect the recovery of the stock.

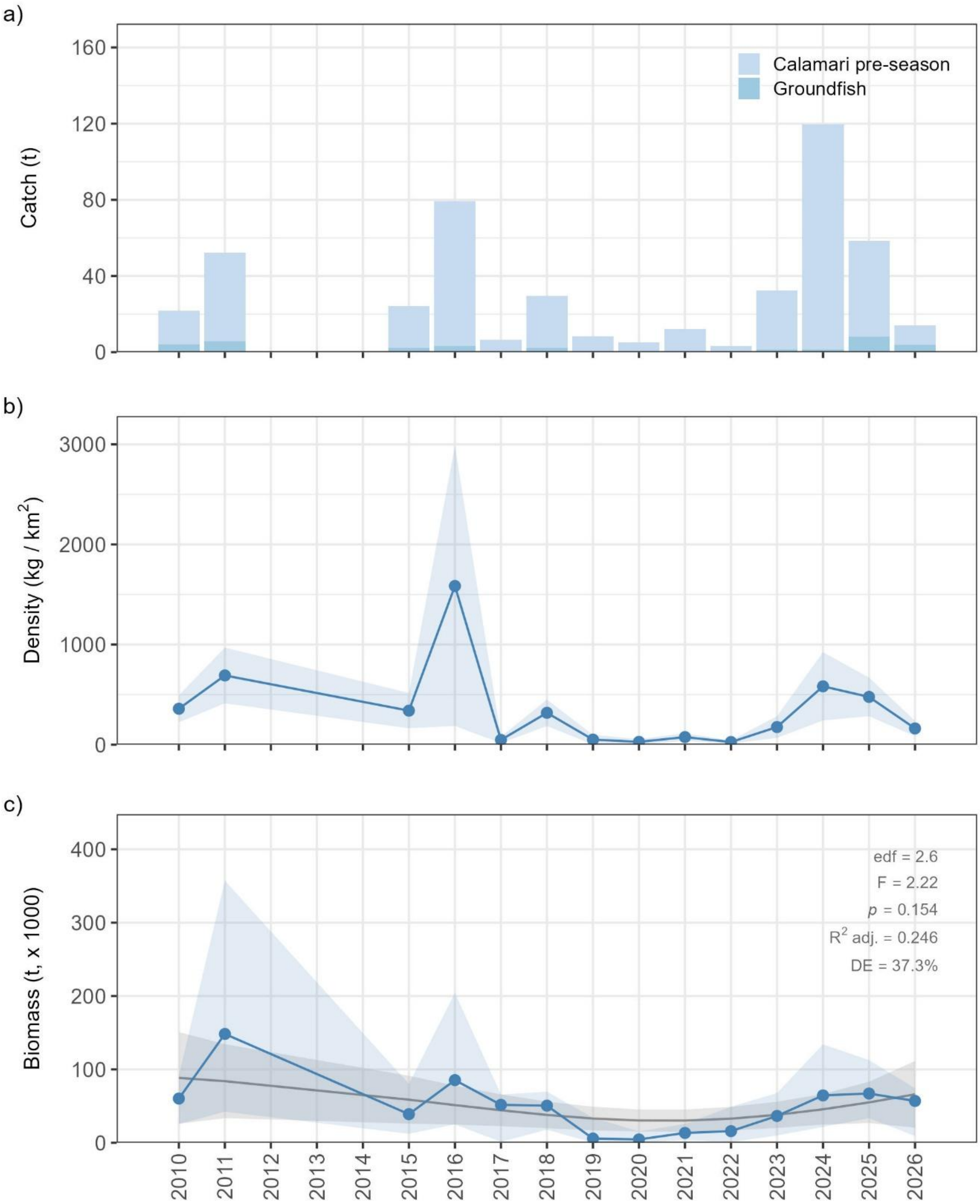


Fig. 75. Abundance of southern blue whiting (*Micromesistius australis*) during February groundfish and calamari pre-season surveys conducted in Falkland Islands waters in 2010–2011 and 2015–2026. (a) Catch per survey, (b) annual mean density ± SE represented by the blue line and shaded region, respectively, and (c) estimated biomass, where the blue line and shaded region represent the median and 95% pointwise confidence interval derived from 10,000 bootstrap biomass estimates, and the grey line and shaded region represent the fitted Generalised Additive Model (GAM) smooth and its 95% pointwise confidence interval.

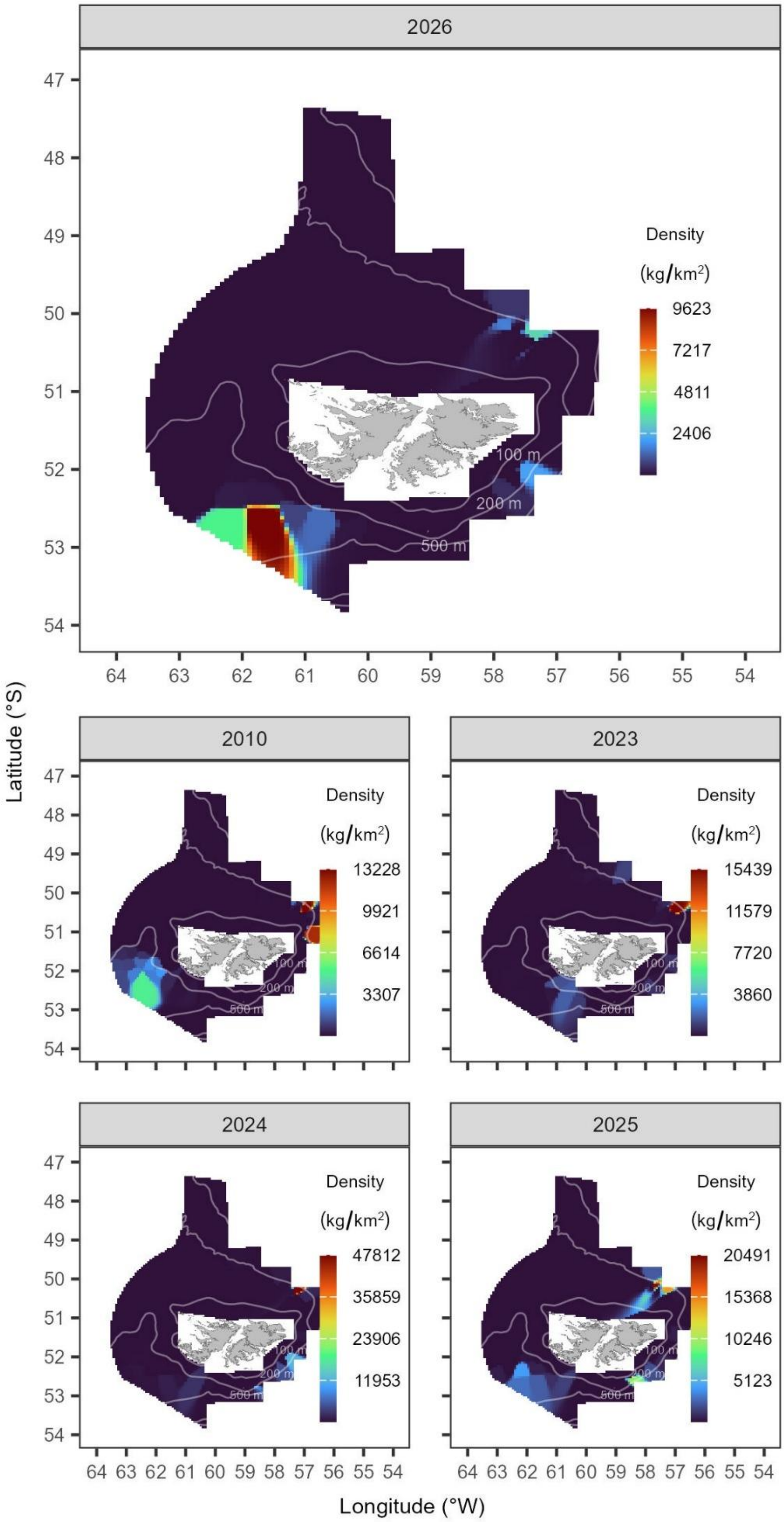


Fig. 76. Distribution and abundance of southern blue whiting (*Micromesistius australis*) derived from the February 2026 groundfish and calamari pre-season surveys in Falkland Islands waters, compared with the first year of the time series (2010) and the three preceding years (2023–2025). Colour scales are specific to each year. Isobaths at 100 m, 200 m, and 500 m are shown.

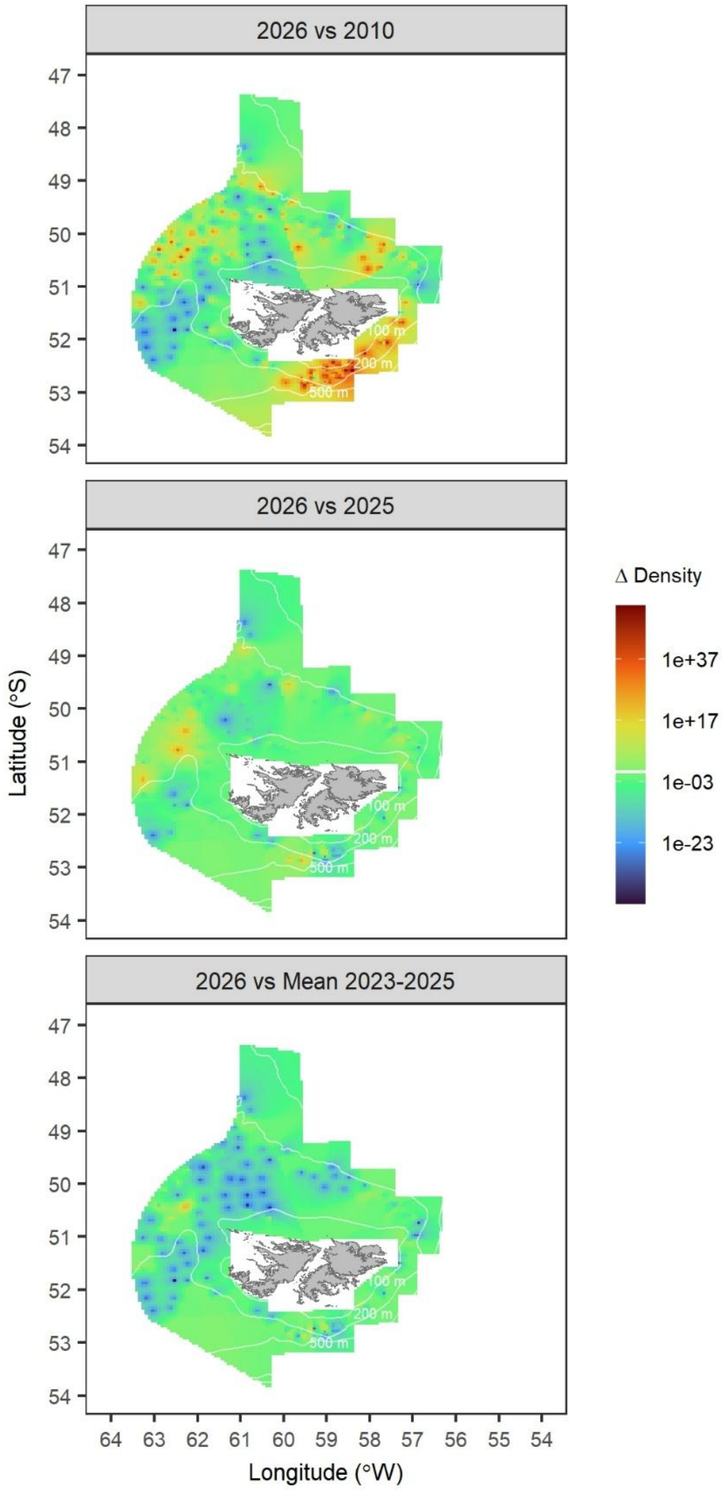


Fig. 77. Spatial change in density of southern blue whiting (*Micromesistius australis*) derived from the February 2026 groundfish and calamari pre-season surveys in Falkland Islands waters, relative to the first year of the time series (2010), the previous year (2025), and the mean of the three preceding years (2023–2025). The spatial change in density is expressed as the ratio of density (kg/km$^2$) in 2026 relative to the density in the baseline year (2010, 2025, 2023–2025 mean). Isobaths at 100 m, 200 m, and 500 m are shown. The colour scale is $\log_{10}$-transformed to aid visualisation, with increases in density indicated above the horizontal white line towards dark red, and decreases in density indicated below the horizontal white line towards dark blue.

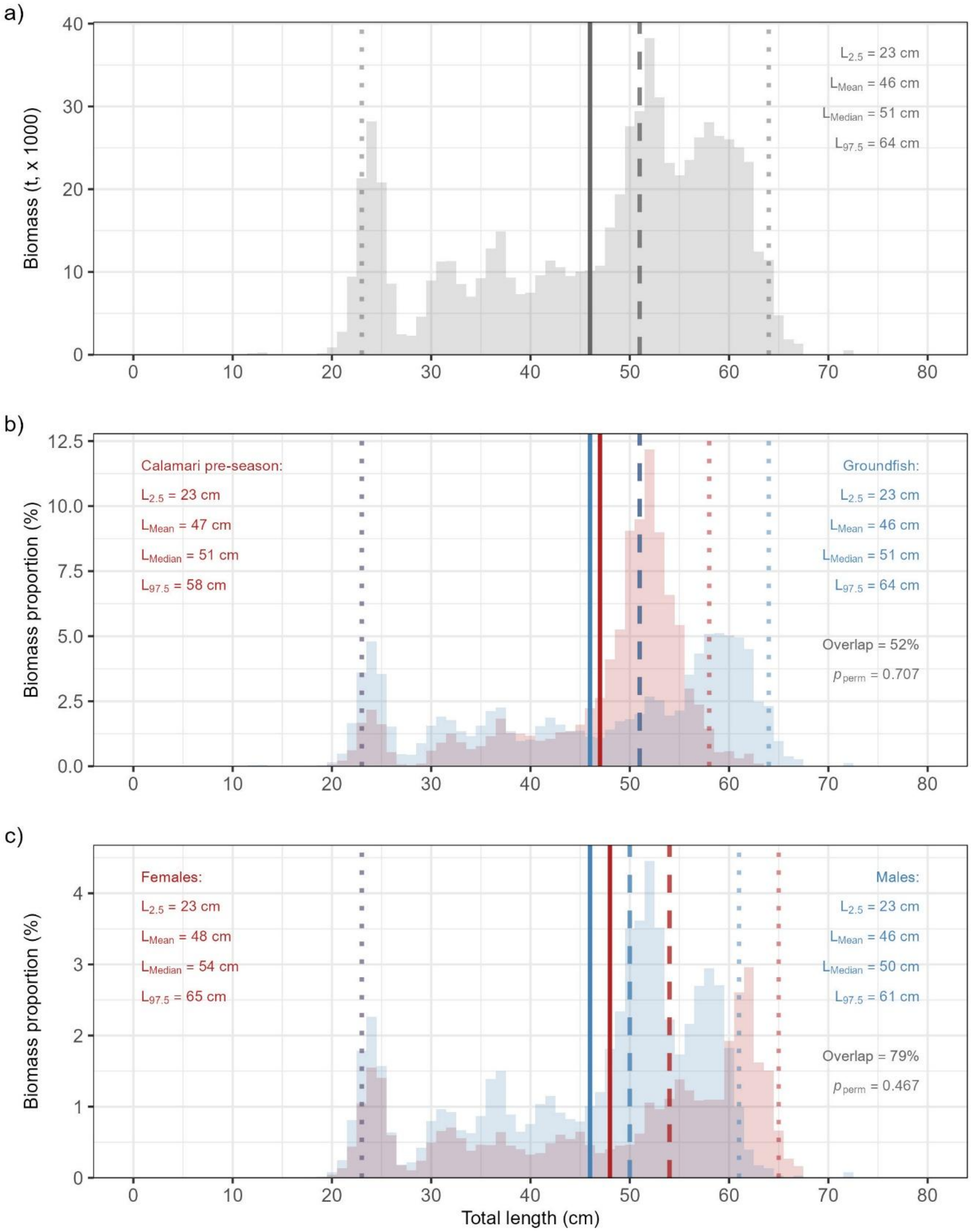


Fig. 78. Biomass-at-length class composition of southern blue whiting (*Micromesistius australis*) across all years combined, based on February groundfish and calamari pre-season surveys conducted in Falkland Islands waters in 2010–2011 and 2015–2026. a) Overall biomass-at-length frequency distribution. b) Overlap in biomass-at-length distributions between calamari pre-season (red) and groundfish (blue) surveys. c) Overlap in biomass-at-length distributions between females (red) and males (blue). Solid vertical lines indicate the mean length ($L_{Mean}$), dashed lines the median length ($L_{Median}$), and dotted lines the 2.5th and 97.5th length percentiles ($L_{2.5}$ and $L_{97.5}$, respectively). $p_{perm}$ is the significance of the weighted permutation test to assess differences between groups.

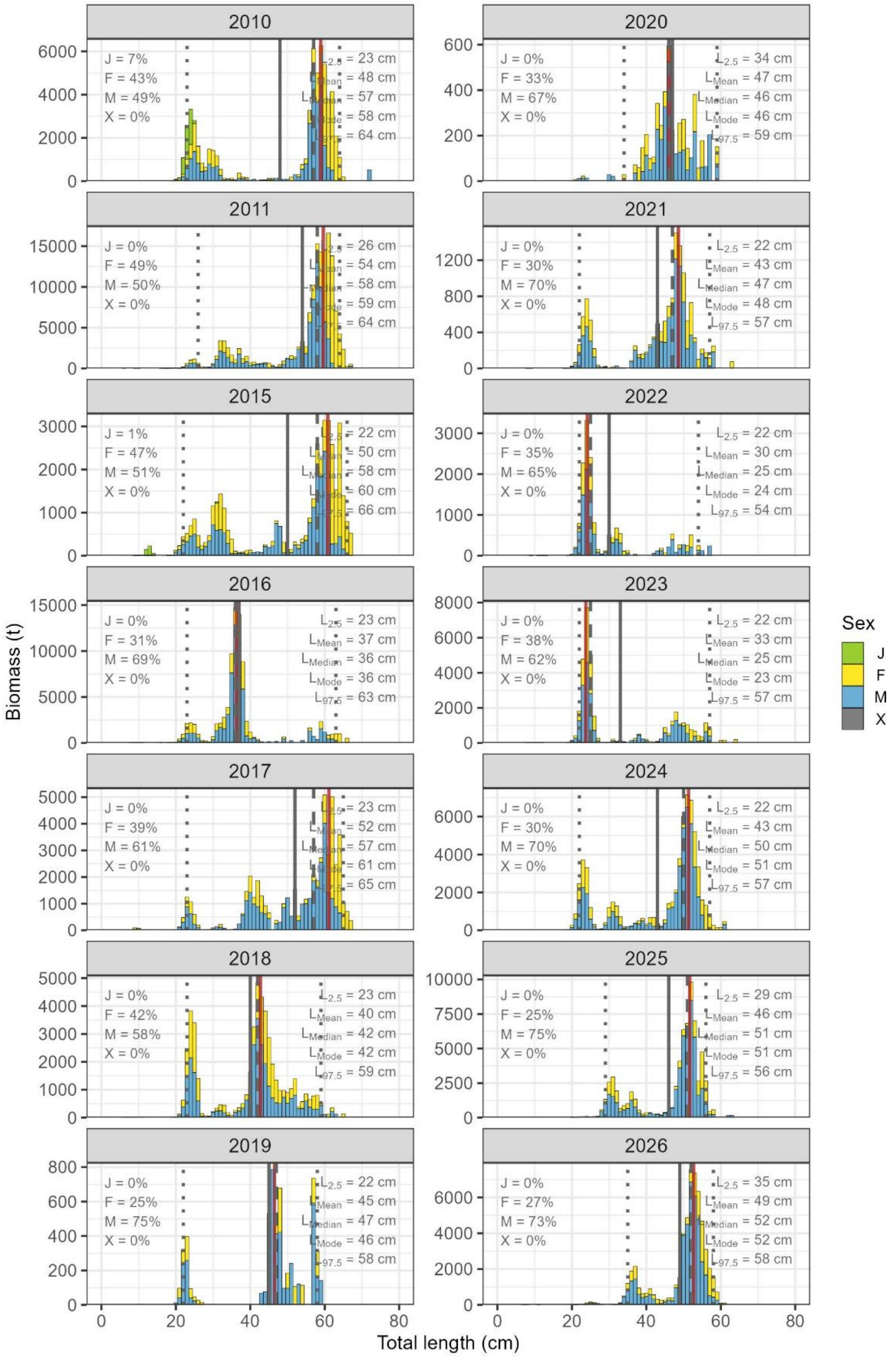


Fig. 79. Annual biomass-at-length class composition of southern blue whiting (*Micromesistius australis*) during February groundfish and calamari pre-season surveys conducted in Falkland Islands waters in 2010–2011 and 2015–2026. Stacked bars represent biomass (t) per 1.0 cm length class, partitioned by sex (J = juvenile; F = female; M = male; X = undetermined), with the proportion of total annual biomass for each sex indicated in the upper left of each panel. Vertical lines indicate the mean length ($L_{Mean}$, grey solid), median length ($L_{Median}$, grey dashed), modal length ($L_{Mode}$, red solid), and 2.5th and 97.5th percentiles ($L_{2.5}$ and $L_{97.5}$, grey dotted) of the biomass-weighted length distribution. Note the different y-axis scales among years.

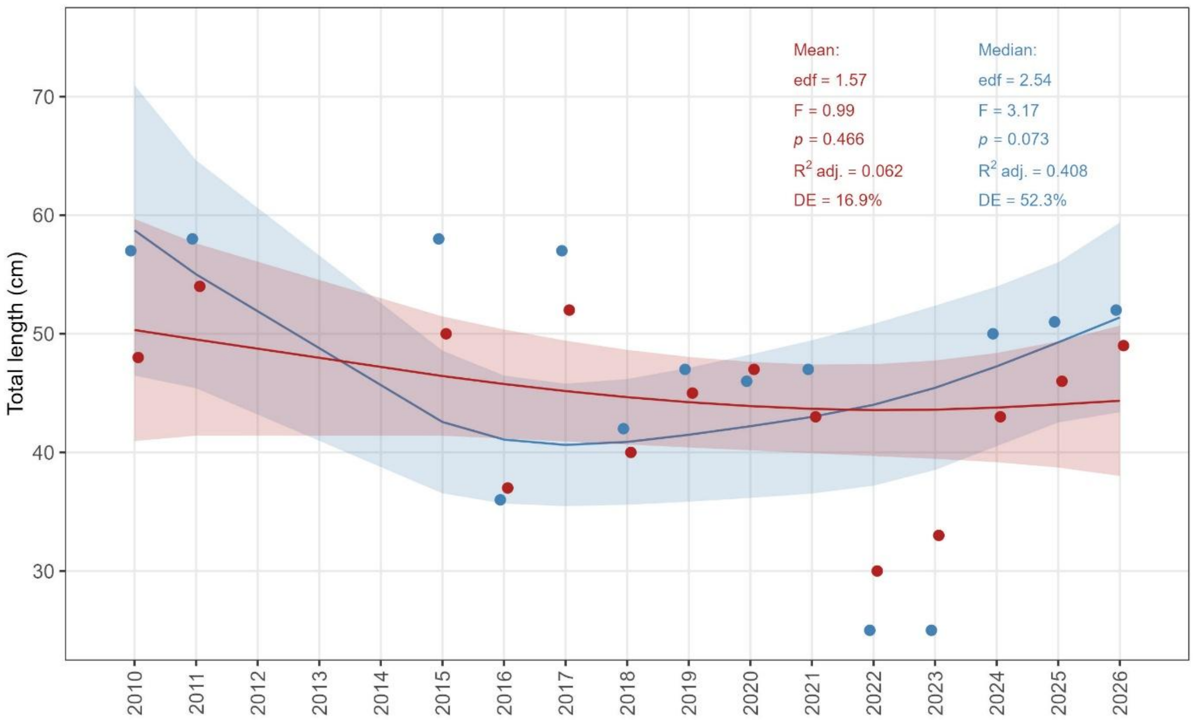


Fig. 80. Median (blue) and mean (red) total length of southern blue whiting (*Micromesistius australis*) during February groundfish and calamari pre-season surveys conducted in Falkland Islands waters in 2010–2011 and 2015–2026. The line and shaded region represent the fitted Generalised Additive Model (GAM) smooth and its 95% pointwise confidence interval.

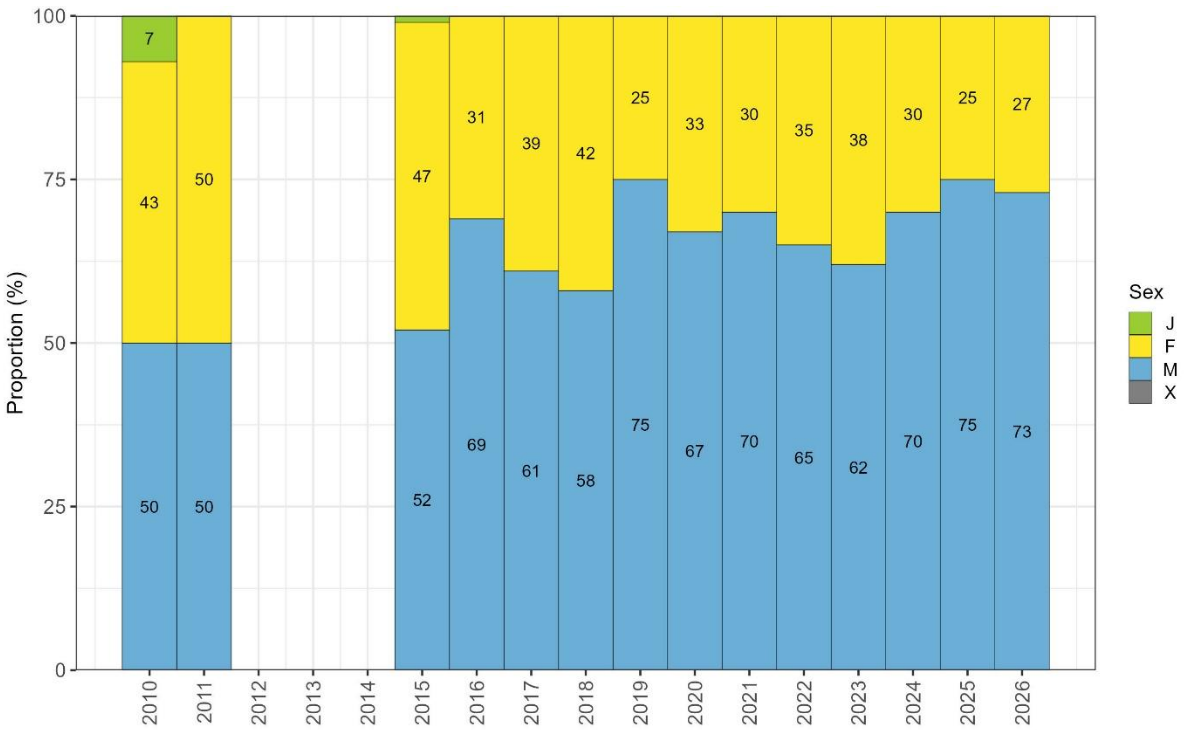


Fig. 81. Proportion by sex (J = juvenile; F = female; M = male; X = undetermined) of southern blue whiting (*Micromesistius australis*) during February groundfish and calamari pre-season surveys conducted in Falkland Islands waters in 2010–2011 and 2015–2026. Labels for proportions < 3% are omitted.

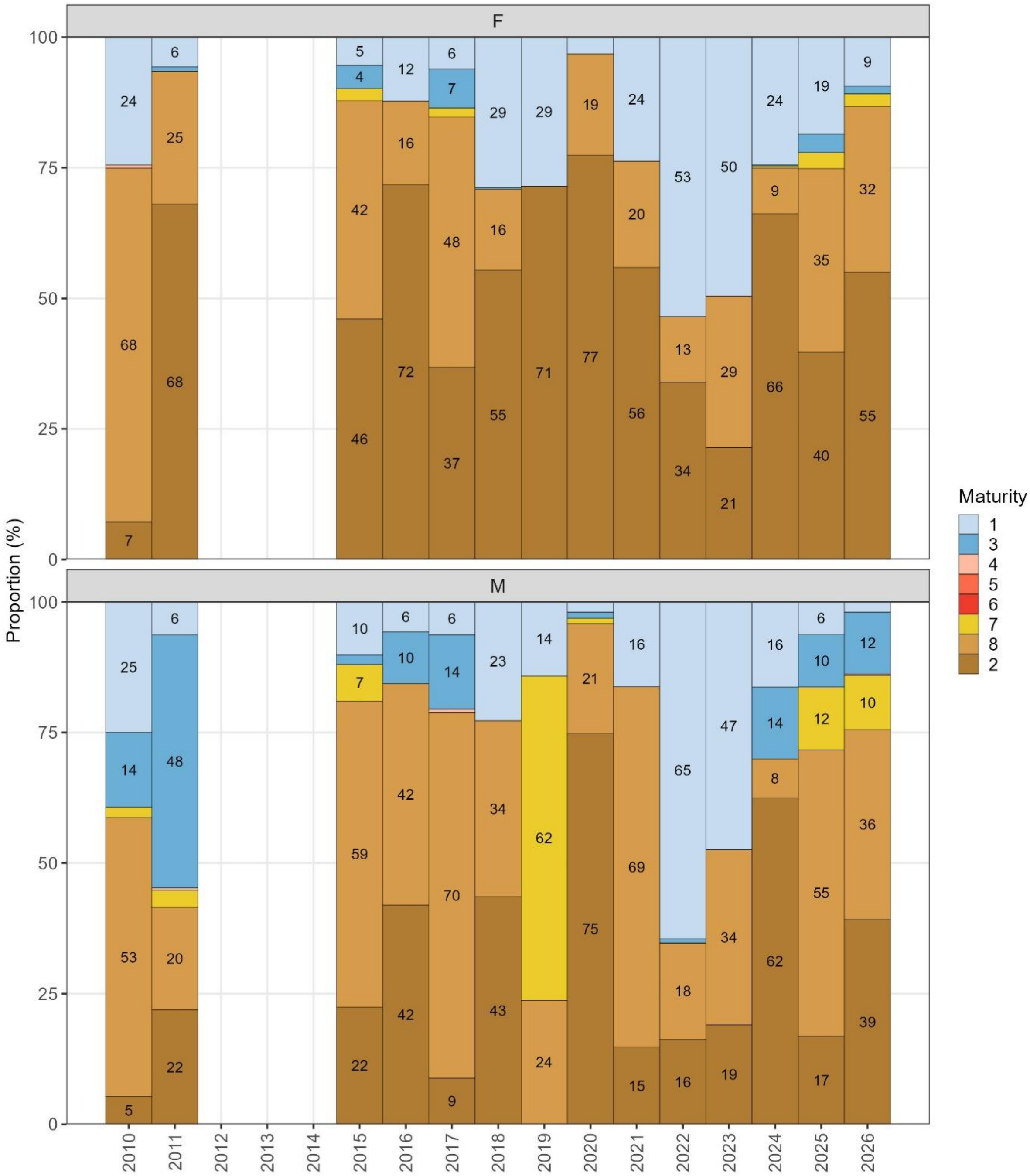


Fig. 82. Proportion by sexual maturity (1, immature; 3, early developing; 4, late developing; 5, ripe; 6, running; 7, spent; 8, recovering spent; 2, resting) of southern blue whiting (*Micromesistius australis*) during February groundfish and calamari pre-season surveys conducted in Falkland Islands waters in 2010–2011 and 2015–2026. Maturity stages ordered by developmental sequence. Labels for proportions < 3% are omitted.

### 4.3.11. Southern hake (*Merluccius australis*)

4.3.11.1. Temporal patterns of abundance

Southern hake are caught in low numbers in Falkland Islands waters. On average, 91% of the total southern hake catches in the time series were obtained from groundfish surveys and 9% from calamari pre-season surveys. The highest total catch occurred in 2026 (1.07 t), representing a 29.8% increase relative to the catch in 2010 (0.82 t), an approximately three-fold increase relative to the catch in 2025 (0.34 t), and an approximately three-fold increase relative to the 2023–2025 mean catch (0.31 t; Fig. 83a; Appendix II). This species is often misidentified as large common hake (*M. hubbsi*). The extent of the effect of misidentification on catch recording, and on density and biomass calculations is unknown. Ongoing research is focused on enhancing the ability to distinguish southern hake from common hake with greater confidence, based on morphological characteristics (Soeth 2024).

The highest densities were recorded in 2026 (28.33 ± 10.11 kg/km²; mean ± SE), corresponding to 91.6% of the 2010 densities (30.92 ± 8.04 kg/km²), but representing an approximately three-fold increase relative to the 2025 densities (10.42 ± 3.45 kg/km²) and relative to the 2023–2025 mean densities (8.78 ± 1.75 kg/km²; Fig. 83b).

Southern hake biomass was highest in 2026 (8,228.23 t), although with wide confidence intervals. Biomass in 2026 represented a non-significant 57.6% increase relative to 2010 levels (5,220.65 t; $p > 0.05$). However, it represented a significant 3.8-fold increase relative to 2025 (2,156.42 t; $p = 0.004$) and a significant 4.2-fold increase relative to the 2023–2025 mean (1,978.29 t; $p = 0.004$; Fig. 83c; Table IV–V; Appendix III–IV). Analysis of the full time series revealed a significant non-linear trend in biomass (GAM: edf = 3.40, F = 8.53, $p = 0.003$), with the model explaining 79% of the deviance ($R^2$ adj. = 0.768), indicating a strong and consistent pattern of increase over the time series (Fig. 83c; Appendix V).

4.3.11.2. Spatial patterns of abundance

In 2026, the highest densities of southern hake in the time series (1,075 kg/km²) were recorded at approximately 52.5–53.5°S and 61–62°W. However, relatively high densities extended towards the west to 52.5°S and 63°W, comprising a wide area located to the south-west near the limit of the FICZ (Fig. 84). The spatial distribution of southern hake remained consistent throughout the time series.

Analysis of the spatial change in density revealed that, relative to 2010, densities in 2026 predominantly increased in the 'Loligo Box', and to the north-west, while densities decreased in the rest of the survey area with substantial decreases to the west and towards the north-east in the FICZ. Comparisons of 2026 with 2025, and with the 2023–2025 mean showed increases in distinct areas in the 'Loligo Box', and in the north and west in the FICZ, while densities decreased through the survey area but mostly to the north-west in the FICZ (Fig. 85).

4.3.11.3. Length composition

Southern hake (*M. australis*) is caught in small quantities in Falkland Islands waters and presents identification challenges within bulk catches of the comparatively more abundant common hake (*M. hubbsi*). Consequently, the number of southern hake individuals sampled per survey was insufficient for a robust analysis of size structure, and the results presented here should be interpreted with caution.

Across all survey years combined, total lengths of southern hake were in the range of 29 to 106 cm; however, 95% of the estimated biomass was comprised of individuals between 56 and 98 cm, with a median length of 72 ± 2.17 cm (median ± SE) and a mean length of 73 ± 1.83 cm (mean ± SE; Fig. 86a).

The distribution of biomass proportions by size class exhibited a 68% overlap between the groundfish and calamari pre-season surveys. Accordingly, the biomass-weighted mean length was not significantly different ($p > 0.05$) between the groundfish survey (73 ± 1.83 cm; mean ± SE) and the calamari pre-season (75 ± 2.23 cm) surveys, indicating similar size structure between surveys. In the groundfish survey, 95% of the biomass of southern hake was comprised of individuals between 56 and 98 cm, with a median length of 72 ± 2.16 cm. In the calamari pre-season survey, 95% of the biomass of southern hake was comprised of individuals between 52 and 96 cm, with a median length of 74 ± 3.63 cm (Fig. 86b).

The distribution of biomass proportions by size class exhibited a 59% overlap between females and males. In contrast, the biomass-weighted mean length was not significantly different ($p > 0.05$) between females (74 ± 1.83 cm) and males (69 ± 1.91 cm), indicating similar structure between females and males. For females, 95% of the biomass was comprised of individuals between 56 and 98 cm, with a median length of 73 ± 2.15 cm. For males, 95% of the individuals were between 53 and 98 cm, with a median length of 69 ± 2.02 cm (Fig. 86c).

Through the time series, the size structure of southern hake was broad and multimodal, with several length-groups not clearly distinguished because of size overlap. More than one length-group was dominant in the time series (Fig. 87). In 2026, the size structure remained broad and multimodal. Lengths were in the range of 45 to 98 cm; however, 95% of the biomass was comprised of individuals between 56 and 95 cm, with a median length of 69 ± 1.92 cm and a mean length of 71 ± 1.76 cm. For females, 95% of the biomass was comprised of individuals between 56 and 95 cm, with a median length of 69 ± 2.15 cm and a mean length of 71 ± 1.92 cm. For males, 95% of the biomass was comprised of individuals between 55 and 83 cm, with a median length of 67 ± 1.99 cm and a mean length of 66 ± 1.75 cm (Fig. 87).

Analysis of the full time series revealed no significant temporal trend in either mean (GAM: edf = 1, F = 0.30, $p = 0.592$, $R^2$ adj. = −0.056, DE = 2.5%) or median (GAM: edf = 1, F = 0.28, $p = 0.605$, $R^2$ adj. = −0.054, DE = 2.3%) total length. Both models converged to a linear smoother and provided no meaningful explanatory power. Both fitted smooths for mean and median lengths remained at approximately 72–74 cm, with no directional change throughout the time series. Observed values revealed moderate interannual variability, likely an artifact caused in part by our limited capacity to detect southern hake individuals amongst the catch (Fig. 88).

#### 4.3.11.4. Sex and maturity composition

Across all survey years combined, the biomass composition of southern hake was dominated by females, comprising 91.0 ± 1.4% (mean ± SE) of the total biomass, followed by males with 8.9 ± 1.4%; individuals of undetermined sex accounted for 0.1 ± 0.1% and no juveniles were recorded in any survey year. Interannual variability was moderate, with female proportion ranging from 80% in 2020 to 99% in 2019, and males ranging from 1% in 2019 to 20% in 2020. The 2026 sex composition was consistent with the time series mean, and it was comprised of 93% females, 6% males, and 1% individuals of undetermined sex (Fig. 89).

Maturity composition comprised a mixture of post-spawning and developing individuals in both sexes throughout the time series (Fig. 90). Females were mostly represented by recovering spent and resting stages (up to 72%), except in 2022 when spent females accounted for 54% of the female biomass, and in 2018 and 2026 when early and late developing females had substantial presence (78% and 55%, respectively). For males, spent, recovering spent, and resting individuals were predominant (33–100%). Developing males contributed up to 41%, whereas ripe and running males were present in most years in small proportions (< 17%), except for 2018 (67%), 2021 (28%) and 2024 (35%).

#### 4.3.11.5. Discussion

The significant non-linear biomass trend of southern hake in Falkland Islands waters reflects a complex pattern characterised by relatively high biomass in 2010–2011, low abundance between 2015 and 2025, and a considerable increase to the maximum level in 2026. Identification challenges associated with distinguishing southern hake from common hake in bulk catches introduce additional uncertainty into these estimates, and results should be interpreted with caution. The Falkland Islands fisheries contribute a minor proportion of the total southern hake catch in the Southwest Atlantic (≤ 12%), with most of the exploitation occurring in Argentine waters (Ramos & Winter 2022e). This suggests that the biomass trends observed in Falkland Islands surveys may primarily reflect broader regional population dynamics and availability of this species to the survey area rather than the direct effects of local fishing pressure. The limited data available from Falkland Islands fisheries further constrains the ability to assess the status of this stock independently.

The absence of temporal trends in both mean and median total length, combined with moderate interannual variability in annual length estimates, suggests that the size composition of southern hake accessible to the surveys has remained relatively stable despite the fluctuating biomass. The presence of late developing and ripe individuals throughout the time series indicates that a proportion of the population is in reproductive condition within the survey area at this time of year.

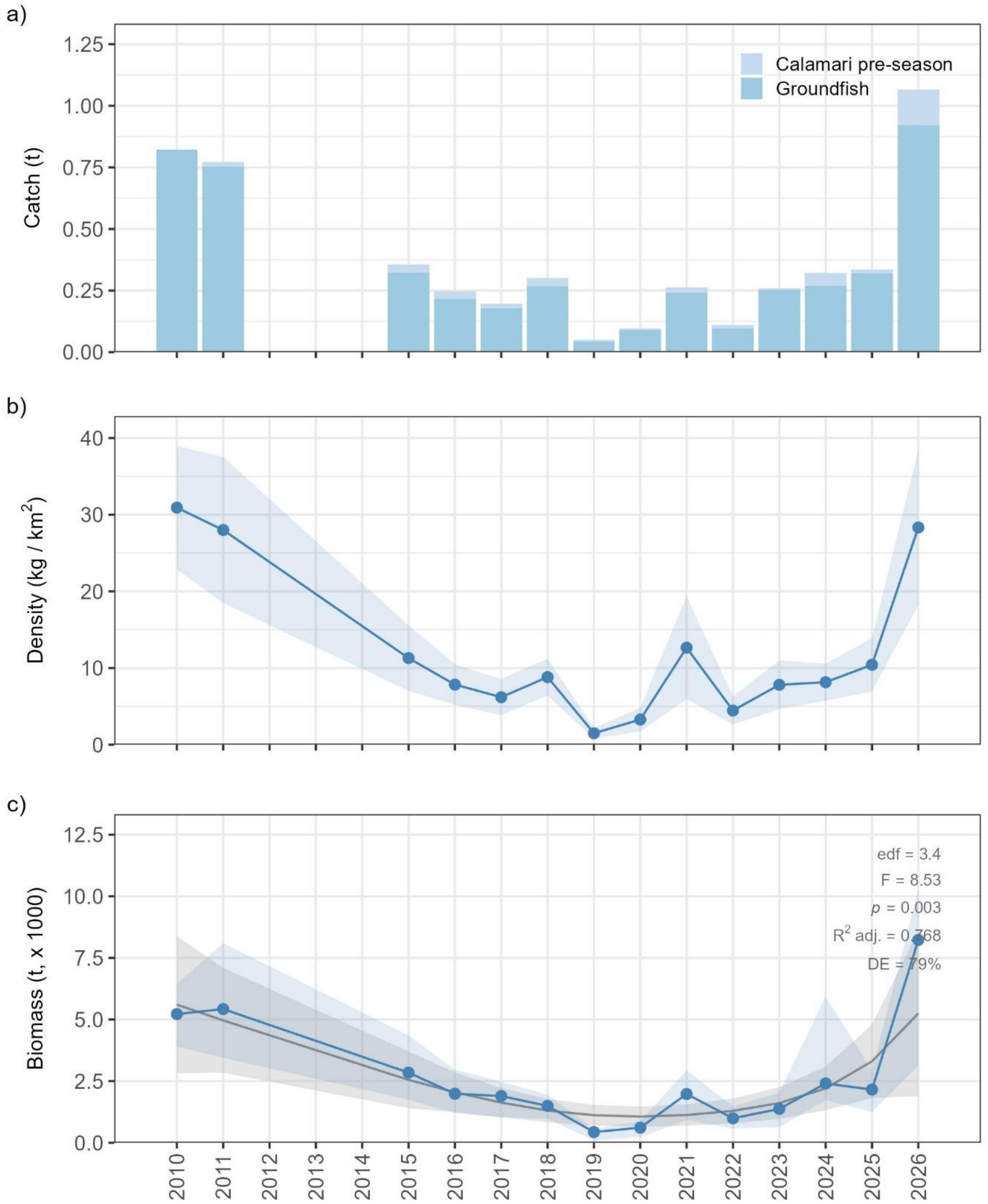


Fig. 83. Abundance of southern hake (*Merluccius australis*) during February groundfish and calamari pre-season surveys conducted in Falkland Islands waters in 2010–2011 and 2015–2026. (a) Catch per survey, (b) annual mean density ± SE represented by the blue line and shaded region, respectively, and (c) estimated biomass, where the blue line and shaded region represent the median and 95% pointwise confidence interval derived from 10,000 bootstrap biomass estimates, and the grey line and shaded region represent the fitted Generalised Additive Model (GAM) smooth and its 95% pointwise confidence interval.

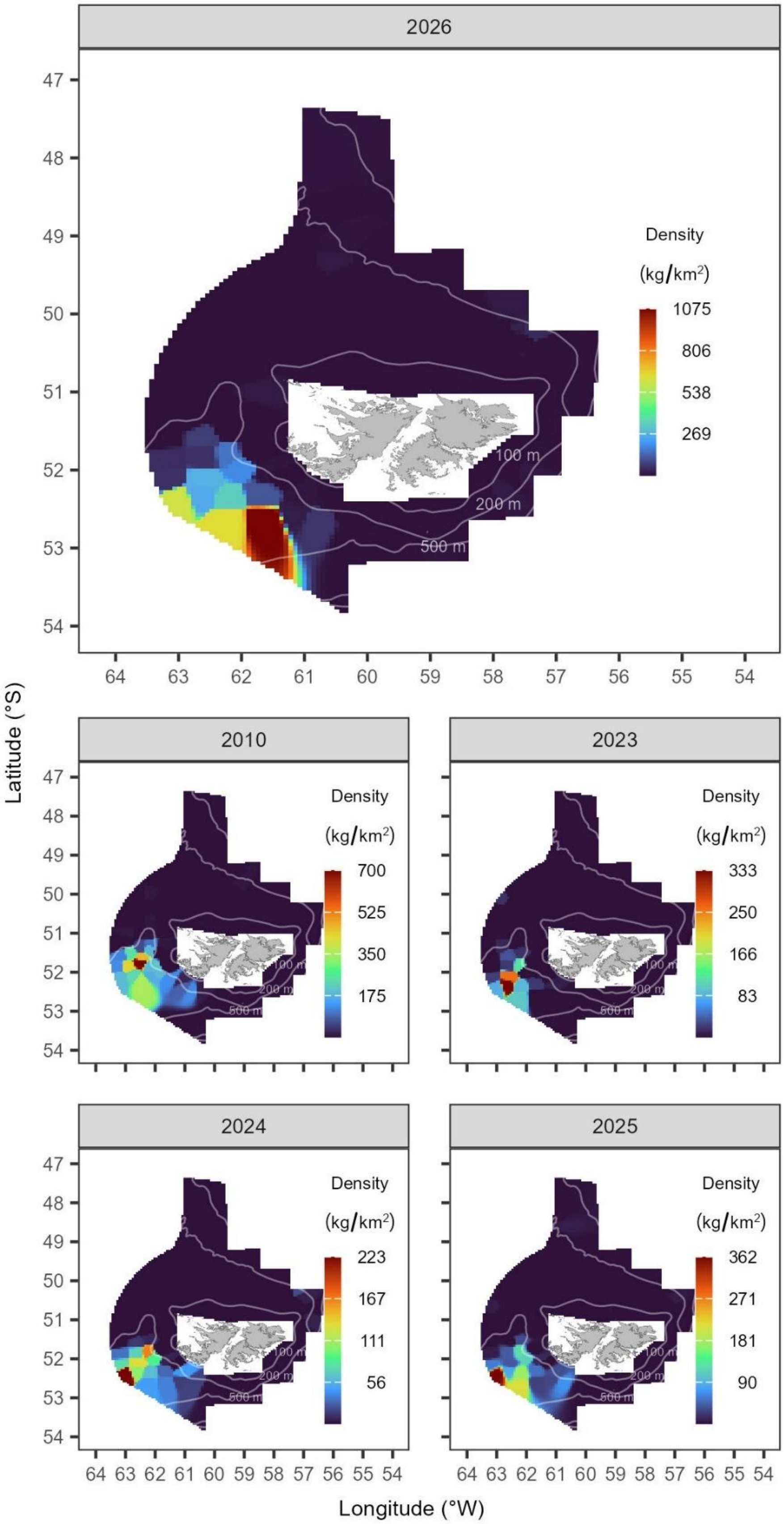


Fig. 84. Distribution and abundance of southern hake (*Merluccius australis*) derived from the February 2026 groundfish and calamari pre-season surveys in Falkland Islands waters, compared with the first year of the time series (2010) and the three preceding years (2023–2025). Colour scales are specific to each year. Isobaths at 100 m, 200 m, and 500 m are shown.

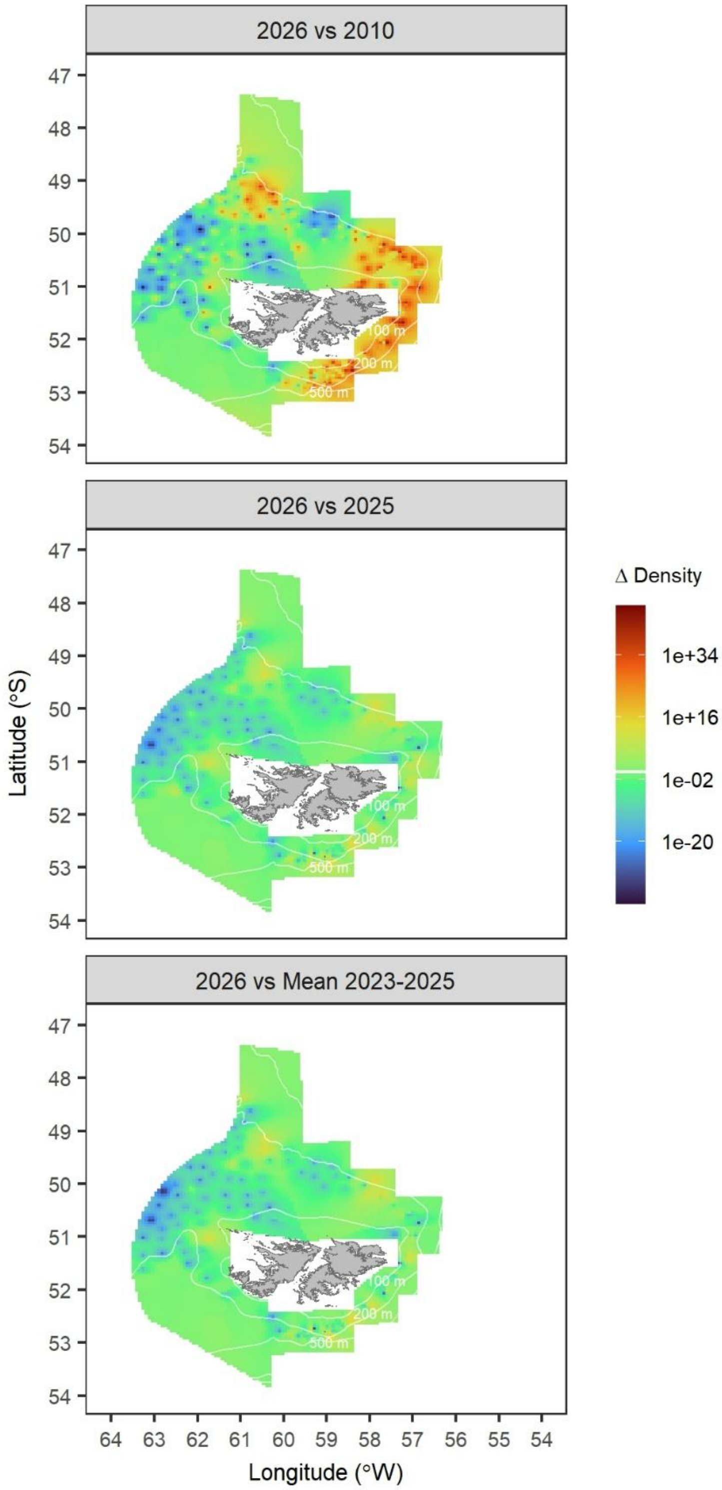


Fig. 85. Spatial change in density of southern hake (*Merluccius australis*) derived from the February 2026 groundfish and calamari pre-season surveys in Falkland Islands waters, relative to the first year of the time series (2010), the previous year (2025), and the mean of the three preceding years (2023–2025). The spatial change in density is expressed as the ratio of density (kg/km$^2$) in 2026 relative to the density in the baseline year (2010, 2025, 2023–2025 mean). Isobaths at 100 m, 200 m, and 500 m are shown. The colour scale is $\log_{10}$-transformed to aid visualisation, with increases in density indicated above the horizontal white line towards dark red, and decreases in density indicated below the horizontal white line towards dark blue.

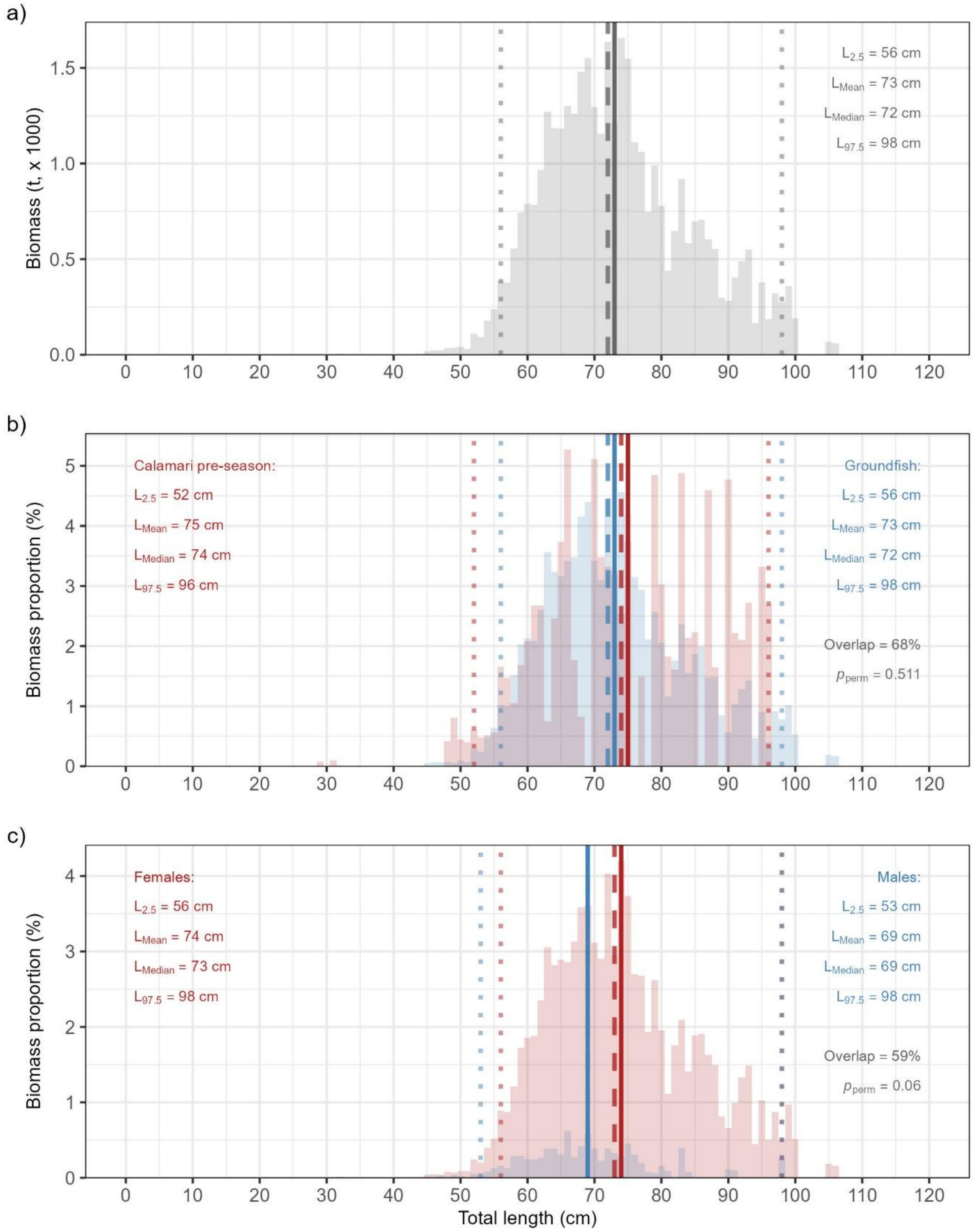


Fig. 86. Biomass-at-length class composition of southern hake (*Merluccius australis*) across all years combined, based on February groundfish and calamari pre-season surveys conducted in Falkland Islands waters in 2010–2011 and 2015–2026. a) Overall biomass-at-length frequency distribution. b) Overlap in biomass-at-length distributions between calamari pre-season (red) and groundfish (blue) surveys. c) Overlap in biomass-at-length distributions between females (red) and males (blue). Solid vertical lines indicate the mean length ($L_{Mean}$), dashed lines the median length ($L_{Median}$), and dotted lines the 2.5th and 97.5th length percentiles ($L_{2.5}$ and $L_{97.5}$, respectively). $p_{perm}$ is the significance of the weighted permutation test to assess differences between groups.

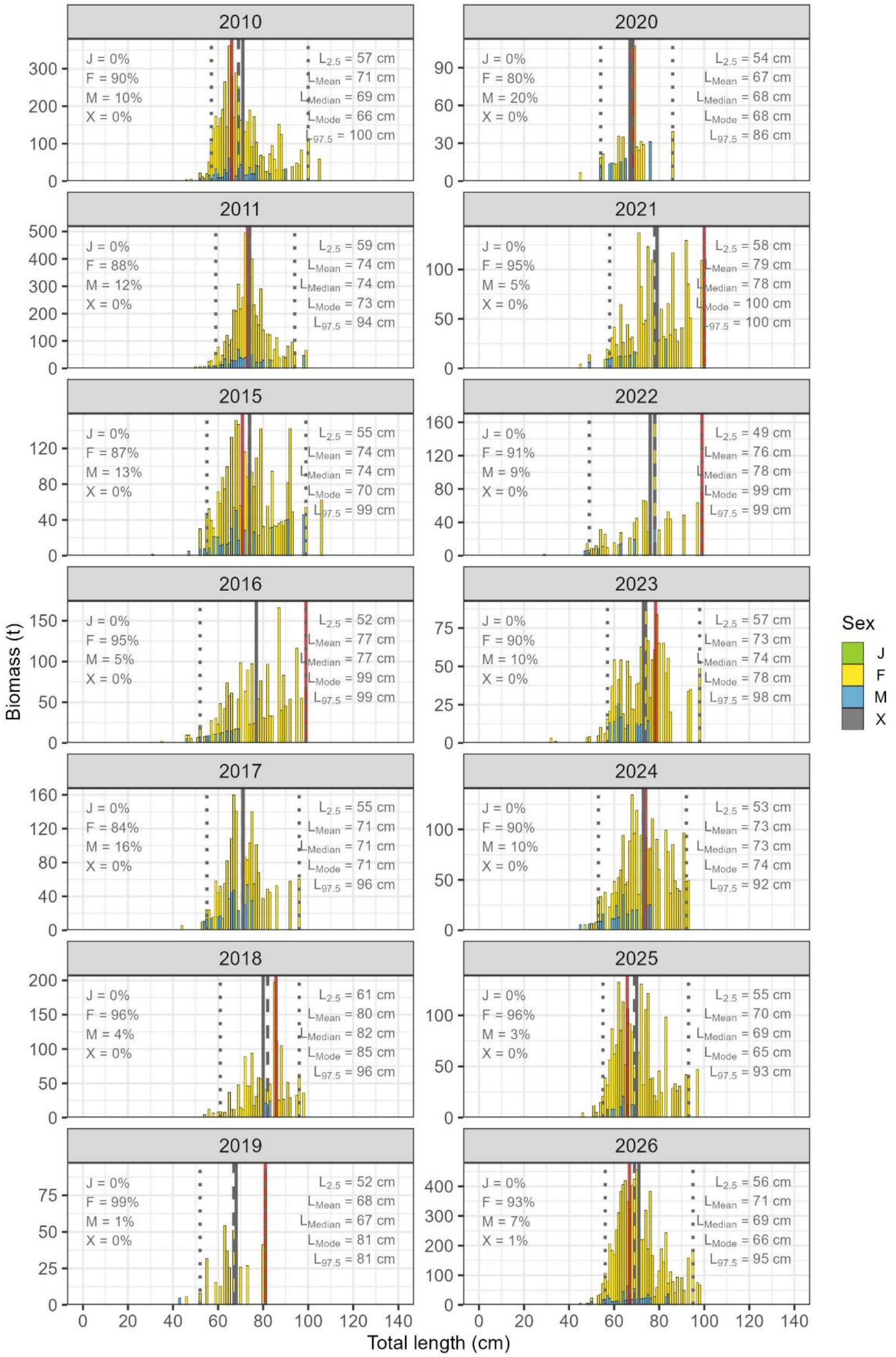


Fig. 87. Annual biomass-at-length class composition of southern hake (*Merluccius australis*) during February groundfish and calamari pre-season surveys conducted in Falkland Islands waters in 2010–2011 and 2015–2026. Stacked bars represent biomass (t) per 1.0 cm length class, partitioned by sex (J = juvenile; F = female; M = male; X = undetermined), with the proportion of total annual biomass for each sex indicated in the upper left of each panel. Vertical lines indicate the mean length ($L_{Mean}$, grey solid), median length ($L_{Median}$, grey dashed), modal length ($L_{Mode}$, red solid), and 2.5th and 97.5th percentiles ($L_{2.5}$ and $L_{97.5}$, grey dotted) of the biomass-weighted length distribution. Note the different y-axis scales among years.

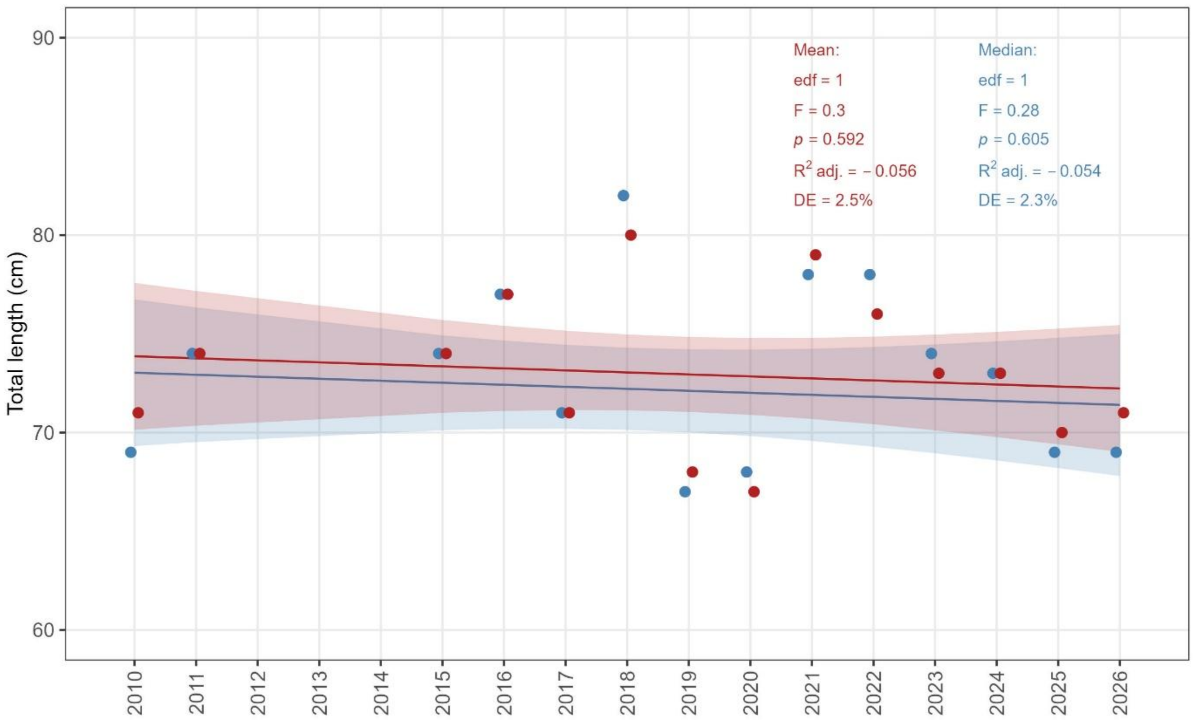


Fig. 88. Median (blue) and mean (red) total length of southern hake (*Merluccius australis*) during February groundfish and calamari pre-season surveys conducted in Falkland Islands waters in 2010–2011 and 2015–2026. The line and shaded region represent the fitted Generalised Additive Model (GAM) smooth and its 95% pointwise confidence interval.

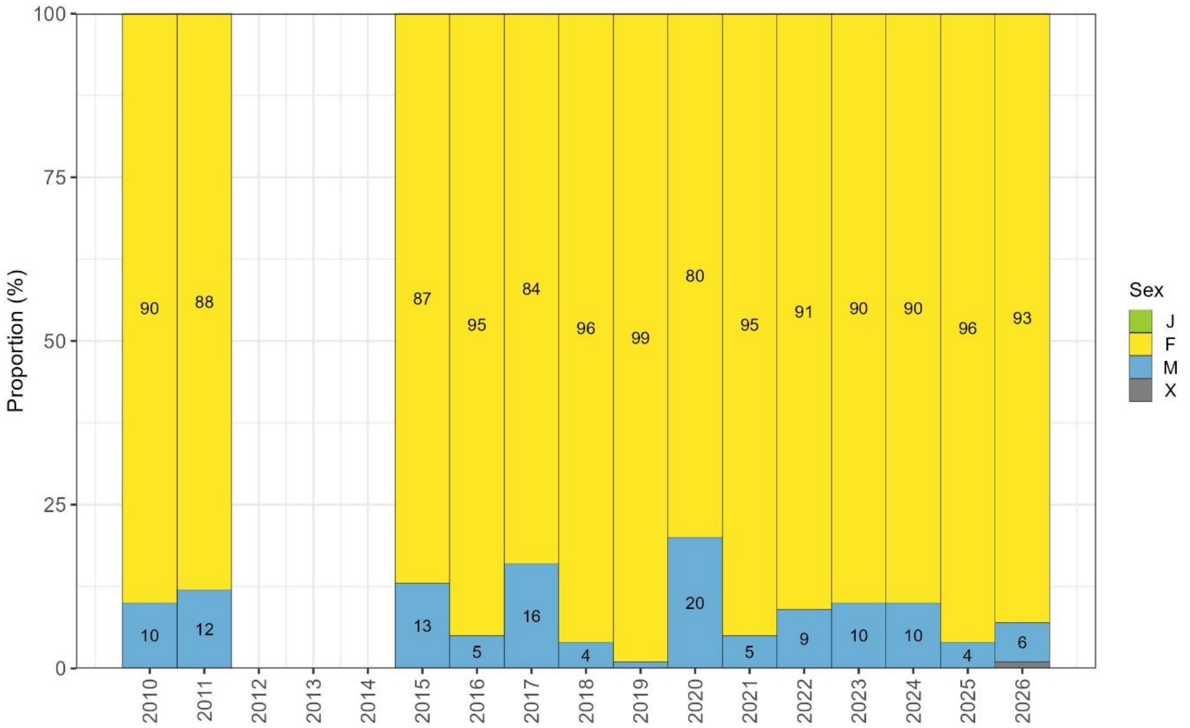


Fig. 89. Proportion by sex (J = juvenile; F = female; M = male; X = undetermined) of southern hake (*Merluccius australis*) during February groundfish and calamari pre-season surveys conducted in Falkland Islands waters in 2010–2011 and 2015–2026. Labels for proportions < 3% are omitted.

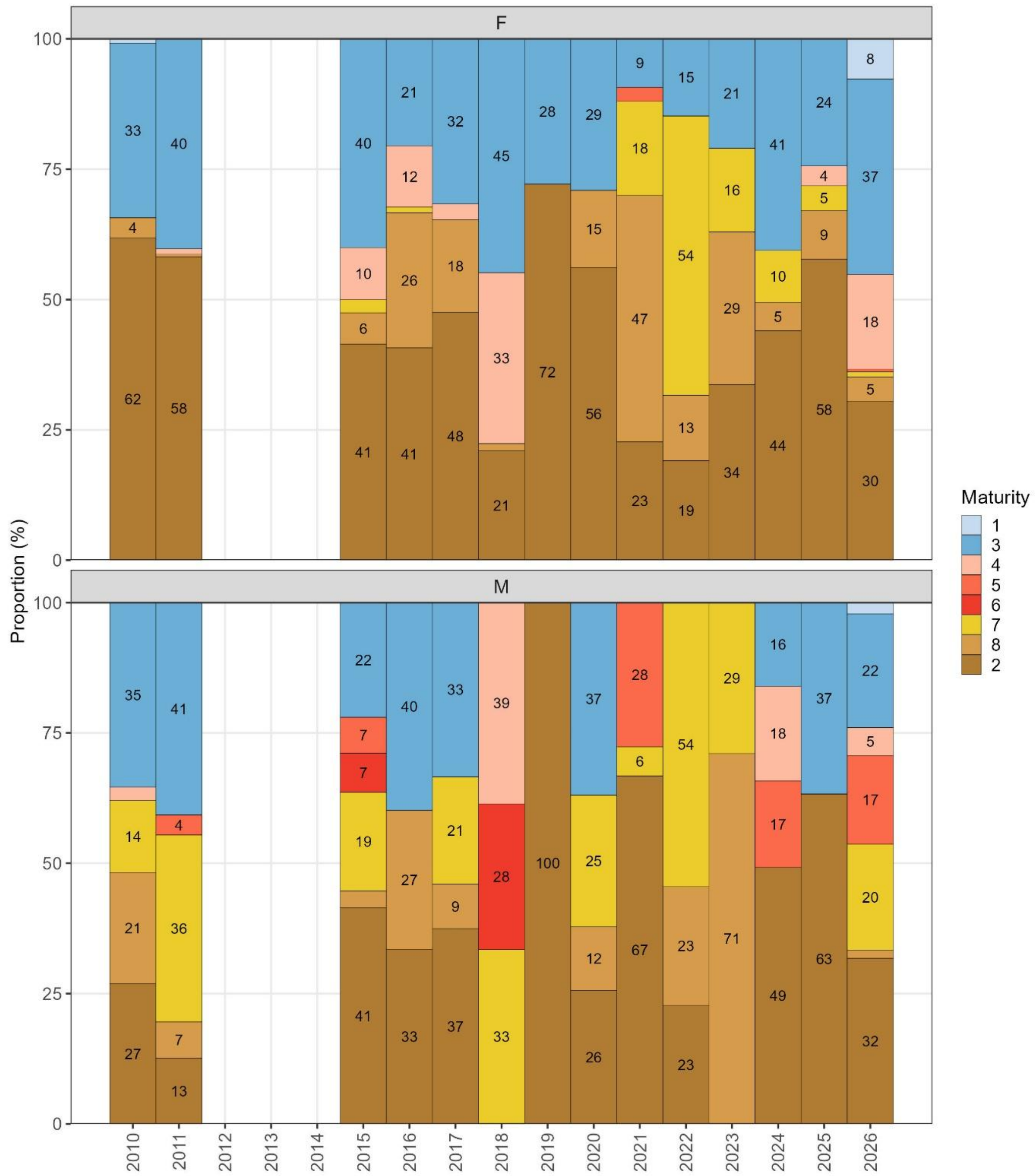


Fig. 90. Proportion by sexual maturity (1, immature; 3, early developing; 4, late developing; 5, ripe; 6, running; 7, spent; 8, recovering spent; 2, resting) of southern hake (*Merluccius australis*) during February groundfish and calamari pre-season surveys conducted in Falkland Islands waters in 2010–2011 and 2015–2026. Maturity stages ordered by developmental sequence. Labels for proportions < 3% are omitted.

## 5. Conclusions

1. Argentine shortfin squid had no significant change in biomass nor in length throughout the time series, with females comprising approximately 65% of the biomass across

survey years. Females were predominantly immature, whereas males were predominantly mature.

2. Banded whiptail grenadier had no significant change in biomass nor in length throughout the time series, with females comprising approximately 84% of the biomass across survey years. Maturity composition was dominated by post-spawning individuals in both sexes. Information on this species from Falkland Islands waters is limited.
3. Common hake had a significant increasing trend in biomass, and mainly from 2021 onwards. Densities increased predominantly along the south-west in the FICZ and in the 'Loligo Box'. Females contributed over 90% of the biomass across survey years, and maturity composition was dominated by post-spawning individuals. Length had a significant decline throughout the time series.
4. Hoki had a marginally non-significant declining trend in biomass, with densities mainly decreasing through the survey area, except for discrete patches including the south and centre of the 'Loligo Box'. Females contributed approximately 64% of the biomass across survey years. Maturity composition was dominated by post-spawning individuals in both sexes. Length had a significant increase since 2021, after a decrease from 2010 to 2020.
5. Kingclip had a significant non-linear biomass trend, with biomass remaining at low levels in recent years. Overall, densities decreased through the survey area, except for discrete patches including the south and centre of the 'Loligo Box'. Females contributed around 67% of the biomass across survey years. Maturity composition was dominated by post-spawning individuals in both sexes. Length had a significant increase since 2021; the presence of large individuals suggests potential for recovery if size-selective management measures are implemented in the commercial bottom trawl fishery.
6. Patagonian squid had no significant temporal trend in biomass; approximately 56% of the biomass was comprised of females across survey years. Maturity composition was dominated by young and immature individuals. Length had no significant change throughout the time series.
7. Patagonian toothfish biomass peaked in 2026, representing a significant biomass increase, with densities increasing in discrete patches through the survey area, including the 'Loligo Box'. Approximately 63% of the biomass was comprised of immature females across survey years. Increase in body size of 2022–2023 recruits likely contributed to the recent increase of biomass. It must be noted that bottom trawl demersal surveys are not representative of the adult component of the stock, which is caught by longlines.
8. Red cod had a significant decline in biomass, with densities decreasing through the survey area, except for discrete patches along the 'Loligo Box'. Approximately 70% of the biomass was comprised of females across survey years, and mostly by post-spawning individuals. No significant change in length was detected. Persistent low biomass and historical declines beyond the FICZ may indicate region-wide vulnerability.
9. Rock cod had a significant decline in biomass, although with signs of stabilisation at low levels in recent years, and with minor increases in density in discrete patches through the survey area, including the 'Loligo Box'. Approximately 53% of the biomass was comprised of males across survey years. Maturity composition was dominated by post-

spawning individuals in both sexes. Length had a significant declining trend. Currently, this species is of little commercial interest due to its small size, as evidenced by extremely high discard rates in commercial bottom trawl fisheries since 2016. The incidental capture of rock cod, predominantly comprising small, immature individuals with low post-release survival, represents a source of fishing mortality that is poorly quantified due to inaccurate discard reporting. This unaccounted mortality, combined with the removal of individuals that have not yet reproduced, limits the capacity of stock assessments to accurately reflect the true state of the stock and may consequently compromise the sustainability of the resource.

10. Southern blue whiting had no temporal biomass trend, and biomass remains at low levels. Approximately 64% of the biomass was comprised of males across survey years. Maturity composition was dominated by post-spawning individuals in both sexes. Length had no temporal trend.

11. Southern hake had a significant increase in biomass in 2026. Densities mainly increased in discrete patches of the survey area, including the 'Loligo Box'. Approximately 91% of the biomass was comprised of females across survey years. Maturity composition comprised a mixture of post-spawning and developing individuals in both sexes. There was no temporal trend in length. These results should be interpreted with caution as estimates carry additional uncertainty arising from the difficulty of distinguishing this species from common hake (*M. hubbsi*) in bulk catches. It is further noted that Falkland Islands fisheries account for ≤ 12% of total catch across the Southwest Atlantic, and the limited availability of local data constrains the ability to assess the status of this stock comprehensively.

## 6. Recommendations

1. Long-term continuity of the February parallel demersal surveys should be maintained to ensure inter-annual comparability. Surveys have been conducted annually from 2010 to 2026, except for 2012–2014, and station totals have ranged from 102 stations in 2022 to 156 stations in 2018. A consistent station array across years is essential for robust trend detection.

2. The quality of station, catch, and biological data should be maintained to the highest standard. Net geometry parameters, particularly net horizontal opening, directly influence density and biomass estimates and should be recorded using net sensors to maximise accuracy. Net sensors have been used in groundfish surveys since 2016 (Gras et al. 2016), and will be tested in the July 2026 calamari pre-season survey; an additional set may be purchased to ensure consistent sensor-based records across both survey programmes. Station and catch data should be verified record by record to improve the accuracy of abundance and distribution calculations, and the same standard should be applied to biological data to ensure the reliability of length trends and biomass composition estimates.

3. The spatial coverage of the groundfish survey should be reassessed. Biomass estimates for deep-water species exhibited wide confidence intervals, likely reflecting the limited number of stations in areas where these species occur. As noted by Soeth et al. (2025), deep-shelf species associated with depths of 250–350 m are likely under-represented

in the current survey area, and expanding spatial coverage into these depths may improve the reliability of biomass estimates for these species.

4. The population structure, dynamics, and trophic ecology of common hake require further research. Given the current high abundance of this species, improved understanding of these aspects would inform management measures and support sustainable fishing practices. Regional collaboration would strengthen stock assessments and facilitate the development of targeted management strategies.

5. A precautionary approach should be maintained for Patagonian squid throughout both fishing seasons. The first fishing season, when the autumn-spawning cohort is primarily exploited, has remained relatively stable. It is suspected that a portion of the spring-spawning cohort is taken towards the end of the first fishing season; however, this is currently not well understood and is under investigation. Adaptive decision-making throughout the first fishing season may help sustain a higher abundance of the spring-spawning cohort during the second fishing season, when this cohort is primarily exploited. The recent decline in biomass and body size during July demersal parallel surveys (Ramos 2025), along with the distributional shift observed in 2024 and the low catches during the 2025 second fishing season, highlights the need for continuous in-season monitoring. Close collaboration with the fishing industry, and the flexibility to close the fishing season when biomass thresholds are not met, are essential for the long-term sustainability of this stock. Enhancing the understanding of environmental drivers would also improve predictions of recruitment variability.

6. Implement conservation measures for finfish stocks in poor state. The poor state of several finfish stocks (i.e., hoki, kingclip, red cod, rock cod, and southern blue whiting) in Falkland Islands waters calls for immediate conservation action. The following options should be considered to reduce fishing pressure on these stocks:

   6.1. Inclusion into the daily by-catch limit for finfish licences (A, G, and W licences), which triggers a move-on rule and no fishing during 10 days in the grid square where the by-catch limit was reached. The 10% proportion of the by-catch limit and the 10-day duration of the move-on rule could be re-assessed.

   6.2. Temporary closure of high-catch grid squares.

   6.3. Protection of spawning grounds. For instance, continue the protection of spawning grounds for southern blue whiting and red cod to the south-west of the Falkland Islands, and protect the spawning grounds for hoki and rock cod.

7. Reduce catch rates of juveniles. High juvenile catch rates pose significant risk to future biomass and recruitment. Measures to reduce juvenile catch rates could include:

   7.1. Increase observer coverage and improve catch reporting, essential to support more reliable stock assessments.

   7.2. Implement spatial or temporal closure of areas with high juvenile abundance to help protect vulnerable life stages and reduce discard mortality, and

   7.3. Implement modifications to the fishing gear to reduce the by-catch of juveniles.

8. Include biomass calculations in stock assessments where commercial fisheries catch, fishing effort, and biological data are available and appropriate. The lack of biomass calculations from commercial data for several species since 2019 limits comparability

with fisheries independent biomass trends and our understanding of their current stock status and trends.

9. Evaluate the biomass estimation approach. The inverse distance weighting approach currently used for biomass estimation was originally implemented at FIFD to assess rock cod (Winter 2019), a species with a wide spatial distribution in the FICZ. This approach appears adequate for species distributed widely across the survey area. However, it has limitations for species with restricted habitat preferences, as it may attribute biomass to areas where the species does not occur. This is evidenced by the differences between the Patagonian squid biomass estimated here and that reported from the calamari pre-season survey alone, which applies a smaller area and accounts for habitat preference (Chemshirova et al. 2026). Models tailored to each species, integrating the effects of depth and environmental variables, would provide more accurate estimates and improve understanding of the drivers behind inter-annual fluctuations in biomass. Where a species is assessed by different groups for different purposes, ideally the same estimation approach and assumptions should be applied, to allow comparability between the assessments conducted at FIFD.

## 7. References

Agnew DJ (2002) Critical aspects of the Falkland Islands pelagic ecosystem: distribution, spawning and migration of pelagic animals in relation to oil exploration. Aquatic Conservation 12: 39–50.

Akaike H (1974) A new look at the statistical model identification. IEEE Transactions on Automatic Control 19: 716–723. https://doi.org/10.1109/TAC.1974.1100705

Alglave, B, Rivot E, Etienne MP, Woillez M, Thorson JT, Vermard Y (2022) Combining scientific survey and commercial catch data to map fish distribution. ICES Journal of Marine Science 79: 1133–1149. https://doi.org/10.1093/icesjms/fsac032

Arkhipkin AI, Schuchert PC, Danyushevsky L (2009) Otolith chemistry reveals fine population structure and close affinity to the Pacific and Atlantic oceanic spawning grounds in the migratory southern blue whiting (*Micromesistius australis australis*). Fisheries Research 96: 188–194. doi: 10.1016/j.fishres.2008.11.002

Arkhipkin AI, Laptikhovsky VV (2010) Convergence in life-history traits in migratory deep-water squid and fish. ICES Journal of Marine Science 67: 1444–1451.

Arkhipkin A, Winter A, May T (2010) *Loligo gahi* Stock Assessment Survey, First Season 2010. Fisheries Department, Directorate of Natural Resources, Falkland Islands Government, Stanley, Falkland Islands. 13 p.

Arkhipkin A, Bakanev S, Laptikhovsky V (2011) Rock cod Biomass Survey – 2011. Report number ZDLT1-02-2011. Fisheries Department, Directorate of Natural Resources, Falkland Islands Government, Stanley, Falkland Islands. 37 p.

Arkhipkin A, Brickle P, Laptikhovsky V, Winter A (2012) Dining hall at sea: feeding migrations of nektonic predators to the eastern Patagonian Shelf. Journal of Fish Biology 81: 882–902. https://doi.org/10.1111/j.1095-8649.2012.03359.x

Arkhipkin AI, Laptikhovsky VV, Barton AJ (2015) Biology and fishery of common hake (*Merluccius hubbsi*) and southern hake (*Merluccius australis*) around the Falkland/Malvinas Islands on the Patagonian shelf of the Southwest Atlantic Ocean. In H. Arancibia (Ed.), Hakes, Biology and Exploitation (pp. 154–184). Oxford: Wiley.

Arkhipkin A, Lee B, Goyot L, Ramos JE, Chemshirova I, Roberts G, Costa M, Blake A (2019) Demersal biomass survey. Report number ZDLM3-02-2019. Fisheries Department, Directorate of Natural Resources, Falkland Islands Government, Stanley, Falkland Islands. 44 p.

Arkhipkin AI, Winter AG, Nigmatullin CM (2022a) Heavy fishery exploitation does not affect sizes at recruitment and maturity of squid *Illex argentinus* and *Doryteuthis gahi*, in the Southwest Atlantic. ICES Journal of Marine Science 79: 182–192. https://doi.org/10.1093/icesjms/fsab253

Arkhipkin A, Evans D, Raczynski M, Winter A (2022b) Southern blue whiting and red cod spawning survey. Cruise Report ZDLV-09-2022. Fisheries Department, Directorate of Natural Resources, Falkland Islands Government, Stanley, Falkland Islands. 28 p.

Bianchi A, Massonneau M, Olevera RM (1982) Análisis estadístico de las características T–S del sector austral de la Plataforma Continental Argentina. Acta Oceanológica Argentina 3: 93–118. *In:* Arkhipkin A, Brickle P, Laptikhovsky V, Winter A (2012) Dining hall at sea: feeding migrations of nektonic predators to the eastern Patagonian Shelf. Journal of Fish Biology 81: 882–902. https://doi.org/10.1111/j.1095-8649.2012.03359.x

Boltovskoy D (Ed.) (1999) South Atlantic Zooplankton. *In:* Arkhipkin A, Brickle P, Laptikhovsky V, Winter A (2012) Dining hall at sea: feeding migrations of nektonic predators to the eastern Patagonian Shelf. Journal of Fish Biology 81: 882–902. https://doi.org/10.1111/j.1095-8649.2012.03359.x

Brickle P, Laptikhovsky V, Arkhipkin A (2005) Reproductive strategy of a primitive temperate notothenioid *Eleginops maclovinus*. Journal of Fish Biology 66: 1044–1059. https://doi.org/10.1111/j.1095-8649.2005.00663.x

Brickle P, Laptikhovsky V, Arkhipkin A, Portela J (2006) Reproductive biology of *Patagonotothen ramsayi* (Regan, 1913) (Pisces: Nototheniidae) around the Falkland Islands. Polar Biology 29: 570–580. https://doi.org/10.1007/s00300-005-0090-5

Brickle P, Laptikhovsky V (2010) Rock cod Biomass Survey. Report number ZDLT1-02-2010. Fisheries Department, Directorate of Natural Resources, Falkland Islands Government, Stanley, Falkland Islands. 31 p.

Chemshirova I, Raczynski M, Ongoro F, Winter A (2024) 2024 1st Pre-season Assessment Survey Falkland calamari (*Doryteuthis gahi*). ZDLF2-S1-2024. Fisheries Department, Directorate of Natural Resources, Falkland Islands Government, Stanley, Falkland Islands. 18 p.

Chemshirova I, Amukwaya A, Garcia D (2025) 2025 1st Pre-season Assessment Survey Falkland calamari (*Doryteuthis gahi*). ZDLC1-S1-2025. Fisheries Department, Directorate of Natural Resources, Falkland Islands Government, Stanley, Falkland Islands. 22 p.

Chemshirova I, Shcherbich Z, Amukwaya A, Elebrashi O (2026) 2026 1st Pre-season Assessment Survey Falkland calamari (*Doryteuthis gahi*). ZDLM3-S1-2026. Fisheries

Department, Directorate of Natural Resources, Falkland Islands Government, Stanley, Falkland Islands. 26 p.

Di Marco E (2022) Evaluación del efectivo de abadejo (*Genypterus blacodes*) en el Atlántico Sudoccidental (período 1980–2021). Captura biológicamente aceptable para el año 2022 y provisoria para el año 2023. Inf. Tec. Oficial INIDEP Nº 035/22. 39 p.

Efron B, Tibshirani RJ (1993) *An Introduction to the Bootstrap*. Chapman & Hall, New York.

Falkland Islands Government (1989) Fisheries Report, FIG Stanley, Fisheries Department. 45 p.

Falkland Islands Government (2025) Fisheries Department Fisheries Statistics, Vol. 29, FIG Stanley, Fisheries Department. 84 p.

Falkland Islands Government (2026) Fisheries Department Fisheries Statistics, Vol. 30, FIG Stanley, Fisheries Department. 85 p.

Froese R (2006) Cube law, condition factor and weight–length relationships: history, meta-analysis and recommendations. Journal of Applied Ichthyology 22, 241–253. https://doi.org/10.1111/j.1439-0426.2006.00805.x

Gallo ND, Bowlin NM, Thompson AR, Satterthwaite EV, Brady B, Semmens BX (2022) Fisheries surveys are essential ocean observing programs in a time of global change: A synthesis of oceanographic and ecological data from U.S. west coast fisheries surveys. Frontiers in Marine Science 9: 1–18. https://doi.org/10.3389/fmars.2022.757124

García D (2024) Stock assessment of kingclip (*Genypterus blacodes*) in the Falkland Islands using JABBA. SA–2024–KIN. Fisheries Department, Directorate of Natural Resources, Falkland Islands Government. Stanley, Falkland Islands. 69 p.

García D (2025) Stock Assessment of kingclip (*Genypterus blacodes*) in the Falkland Islands using length-based methods and yield per recruit approach. SA–2025–KIN. Fisheries Department, Directorate of Natural Resources, Falkland Islands Government. Stanley, Falkland Islands. 45 p.

Guillen J, Holmes SJ, Carvalho N, Casey J, Dorner H, Gibin M, Mannini A, Vasilakopoulos P, Zanzi A (2018) A Review of the European Union Landing Obligation Focusing on Its Implications for Fisheries and the Environment. Sustainability 10: 900. https://doi.org/10.3390/su10040900

Gras M, Blake A, Pompert J, Jürgens L, Visauta E, Busbridge T, Rushton H, Zawadowski T (2015) Rock cod Biomass Survey. Report number ZDLT1-02-2015. Fisheries Department, Directorate of Natural Resources, Falkland Islands Government, Stanley, Falkland Islands. 45 p.

Gras M, Pompert J, Blake A, Boag T, Grimmer A, Iriarte V, Sánchez B (2016) Finfish and Rock cod Biomass Survey. Report number ZDLT1-02-2016. Fisheries Department, Directorate of Natural Resources, Falkland Islands Government, Stanley, Falkland Islands. 72 p.

Gras M, Pompert J, Blake A, Busbridge T, Derbyshire C, Keningale B, Thomas O (2017) Groundfish survey. Report number ZDLT1-02-2017. Fisheries Department, Directorate of Natural Resources, Falkland Islands Government, Stanley, Falkland Islands. 83 p.

Gras M, Randhawa H, Blake A, Busbridge T, Chemshirova I, Guest A (2018) Groundfish survey. Report number ZDLM3-02-2018. Fisheries Department, Directorate of Natural Resources, Falkland Islands Government, Stanley, Falkland Islands. 81 p.

Harrell FE (2024) *Hmisc: Harrell Miscellaneous*. R package version 5.2.4.

Hilborn R, Walters CJ (1992) Quantitative fisheries stock assessment: Choice, dynamics and uncertainty. New York, USA: Chapman & Hall.

Holm S (1979) A simple sequentially rejective multiple test procedure. Scandinavian Journal of Statistics 6: 65–70.

Kish L (1965) *Survey Sampling*. John Wiley & Sons, New York.

Komsta L & Novomestky F (2022) moments: Moments, Cumulants, Skewness, Kurtosis and Related Tests. R package version 0.14.1. https://CRAN.R-project.org/package=moments

Laptikhovsky VV, Arkhipkin AI, Brickle P (2008) Life history, fishery and stock conservation of the Patagonian toothfish around the Falkland Islands. American Fisheries Society Symposium 49: 1357–1363. *In:* Arkhipkin A, Brickle P, Laptikhovsky V, Winter A (2012) Dining hall at sea: feeding migrations of nektonic predators to the eastern Patagonian Shelf. Journal of Fish Biology 81: 882–902. https://doi.org/10.1111/j.1095-8649.2012.03359.x

Laptikhovsky V, Arkhipkin A, Brickle P (2013) From small bycatch to main commercial species: Explosion of stocks of rock cod *Patagonotothen ramsayi* (Regan) in the Southwest Atlantic. Fisheries Research 147: 399–403. http://dx.doi.org/10.1016/j.fishres.2013.05.006

Le Cren ED (1951) The length-weight relationship and seasonal cycle in gonad weight and condition in the perch (*Perca fluviatilis*). Journal of Animal Ecology 20: 201–219.

Lipinski M (1979) Universal maturity scale for the commercially-important squids (Cephalopoda: teuthoidea). The results of maturity classification of the *Illex illecebrosus* (LeSueur. 1821) populations for the years 1973–1977. ICNAF Fish. Res. Doc. 79/. II/38.

Macchi GJ, Pájaro M, Wöhler OC, Acevedo MJ, Centurión RL, Urteaga DG (2005) Batch fecundity and spawning frequency of southern blue whiting (*Micromesistius australis*) in the southwest Atlantic Ocean. New Zealand Journal of Marine and Freshwater Research 39: 993–1000. https://doi.org/10.1080/00288330.2005.9517370

Macchi GJ, Domínguez-Petit R, Militelli MI (2021) Dinámica reproductiva en el dominio demersal. Ecología Reproductiva y Pesquerías en el Contexto Iberoamericano. Red Iberoamericana de Investigación para el Uso Sostenible de los Recursos Pesqueros (RED INVIPESCA). 31 Diciembre de 2021. 61–94.

Macchi GJ, Alvarez-Colombo G, Belleggia M, Betti P, Brown D, Cepeda G, Derisio C, Diaz MV, Ehrlich M, Leonarduzzi E, Machinandiarena L, Martos P, Santos B, Schiariti A, Sobrero L, Temperoni B (2023) Recruitment of the Argentine hake, *Merluccius hubbsi*, from Patagonian stock: a review of main features affecting the reproductive potential and survival during early life stages. Marine and Fishery Sciences 36: 323–358. https://doi.org/10.47193/mafis.3632023010901

Manly BFJ (2007) *Randomization, Bootstrap and Monte Carlo Methods in Biology* (3rd ed.). Chapman & Hall/CRC.

MEP (2020) Annex 3: Review of Finfish Stock Assessments. Report for Falkland Islands Government. MacAlister Elliot & Partners Ltd. 47 p.

Navarro G, Rozycki V, Monsalvo M (2014) Estadísticas de la pesca marina en la Argentina. Evolución de los desembarques 2008-2013. Ministerio de Agricultura, Ganadería y Pesca de la Nación. Buenos Aires, 144 p.

Nikolsky GV (1963) The Ecology of Fishes. New York: Academic Press.

Pájaro M, Macchi GJ (2001) Spawning pattern, length at maturity, and fecundity of the southern blue whiting (*Micromesistius australis*) in the south-west Atlantic Ocean. New Zealand Journal of Marine and Freshwater Research 35: 375–385. https://doi.org/10.1080/00288330.2001.9517008

Padgham M, Sumner M (2025) geodist: Fast, Dependency-Free Geodesic Distance Calculations. https://doi.org/10.32614/CRAN.package.geodist

Payá I, Brickle P, Laptikhovsky V, Winter A (2010) Vessel Units, Allowable Effort, and Allowable Catch 2011. Fisheries Department, Directorate of Natural Resources, Falkland Islands Government, Stanley, Falkland Islands. 53 p.

Pedersen TL (2024) patchwork: The Composer of Plots. R package version 1.3.0. https://CRAN.R-project.org/package=patchwork

Peterson RG, Whitworth III T (1989) The Subantarctic and Polar fronts in relation to deep water masses through the Southwestern Atlantic. Journal of Geophysical Research 94: 10817–10838. *In:* Arkhipkin A, Brickle P, Laptikhovsky V, Winter A (2012) Dining hall at sea: feeding migrations of nektonic predators to the eastern Patagonian Shelf. Journal of Fish Biology 81: 882–902. https://doi.org/10.1111/j.1095-8649.2012.03359.x

R Core Team (2025). R: A Language and Environment for Statistical Computing. R Foundation for Statistical Computing, Vienna, Austria. https://www.R-project.org/.

Ramos JE, Winter A (2019) Stock assessment of hoki (*Macruronus magellanicus*) in the Falkland Islands. SA–2019–WHI. Fisheries Department, Directorate of Natural Resources, Falkland Islands Government. Stanley, Falkland Islands. 47 p.

Ramos JE, Winter A (2022a) Stock assessment of common hake (*Merluccius hubbsi*) in the Falkland Islands. SA–2022–HAK. Fisheries Department, Directorate of Natural Resources, Falkland Islands Government, Stanley, Falkland Islands. 36 p.

Ramos JE, Winter A (2022b) February bottom trawl survey biomasses of fishery species in Falkland Islands waters, 2010–2022. SA–2022–05. Fisheries Department, Directorate of Natural Resources, Falkland Islands Government, Stanley, Falkland Islands. 86 p.

Ramos JE, Winter A (2022c) Stock assessment of hoki (*Macruronus magellanicus*) in the Falkland Islands. SA–2022–WHI. Fisheries Department, Directorate of Natural Resources, Falkland Islands Government, Stanley, Falkland Islands. 39 p.

Ramos JE, Winter A (2022d) Stock assessment of red cod (*Salilota australis*) in the Falkland Islands. SA–2022–BAC. Fisheries Department, Directorate of Natural Resources, Falkland Islands Government, Stanley, Falkland Islands. 39 p.

Ramos JE, Winter A (2022e) Stock assessment of Southern hake (*Merluccius australis*) in the Falkland Islands. SA–2022–PAT. Fisheries Department, Directorate of Natural Resources, Falkland Islands Government, Stanley, Falkland Islands. 37 p.

Ramos JE, Winter A (2023a) Stock assessment of rock cod (*Patagonotothen ramsayi*) in the Falkland Islands. SA–2023–PAR. Fisheries Department, Directorate of Natural Resources, Falkland Islands Government, Stanley, Falkland Islands. 49 p.

Ramos JE, Winter A (2023b) Stock assessment of southern blue whiting (*Micromesistius australis*) in the Falkland Islands. SA–2022–BLU. Fisheries Department, Directorate of Natural Resources, Falkland Islands Government, Stanley, Falkland Islands. 36 p.

Ramos JE, Soeth M, Hoyer P, Amukwaya A, Peruzzo M, Villarroel M, Vukasin V, Blake A (2024a) Cruise Report 2024-02-ZDLT1. Groundfish survey. Fisheries Department, Directorate of Natural Resources, Falkland Islands Government. Stanley, Falkland Islands. 45 p.

Ramos JE, Soeth M, García D (2024b) Analysis of net geometry across February groundfish surveys, 2010–2024. 2024-12-GSNG. Fisheries Department, Directorate of Natural Resources, Falkland Islands Government, Stanley, Falkland Islands. 25 p.

Ramos JE (2025) July bottom trawl survey biomasses of fishery species in Falkland Islands waters, 2017–2025. SA-2025-12. Fisheries Department, Directorate of Natural Resources, Falkland Islands Government, Stanley, Falkland Islands. 98 p.

Ramos JE, Soeth M, Desmet L, Minichino R, Orlandi N, Peruzzo M, Villarroel M, Blake A (2025) Cruise Report 2025-02-ZDLU1. Groundfish survey. Fisheries Department, Directorate of Natural Resources, Falkland Islands Government. Stanley, Falkland Islands. 50 p.

Randhawa HS, Goyot L, Blake A, Ramos JE, Roberts G, Brewin J, Evans D (2020) Cruise Report ZDLT1-02-2020: 2020 Demersal Biomass Survey. Fisheries Department, Directorate of Natural Resources, Falkland Islands Government, Stanley, Falkland Islands. 97 p.

Santos BA, Villarino MF, Pedernera MF, Suby A (2024) Evaluación del estado de explotación del efectivo sur de 41°S de merluza (*Merluccius hubbsi*) y estimación de la captura biológicamente acceptable para 2025. Inf. Tec. Oficial INIDEP Nº 032/24. 34 p.

Seafish (2010) Bridle angle and wing end spread calculations. Research and development catching sector fact sheet. Available at: www.seafish.org

Shubnikov DA, Permitin YE, Voznyak SP (1969) Biology of the pelagic gadoid fish *Micromesistius australis* Norman. Trudy VNIRO 66: 299–306. *In:* Arkhipkin AI, Schuchert PC, Danyushevsky L (2009) Otolith chemistry reveals fine population structure and close affinity to the Pacific and Atlantic oceanic spawning grounds in the migratory southern blue whiting (*Micromesistius australis australis*). Fisheries Research 96: 188–194. https://doi.org/10.1016/j.fishres.2008.11.002

Skeljo F, Winter A (2025) Stock assessment of Falkland calamari (*Doryteuthis gahi*) in the 2nd season 2025. Technical Document, Falkland Islands Fisheries Department. 35 p.

Soeth M (2024) *Merluccius hubbsi* and *Merluccius australis* species identification: notes from February 2024 groundfish survey. Fisheries Department, Directorate of Natural Resources, Falkland Islands Government. Stanley, Falkland Islands. 6 p.

Soeth M, Ramos JE, Minichino R, Amukwaya A, Ongoro F, Elebrash O, Pedrero R, Blake A, Trevizan T (2025) Cruise Report 2025-07-ZDLU1. Groundfish survey. Fisheries Department, Directorate of Natural Resources, Falkland Islands Government. Stanley, Falkland Islands. 134 p.

Soeth M, Desmet L, Villarroel M, Orlandi N, Jarvis S, Burke C, Gorostola MWG, Pedrero R, Blake A, Trevizan T (2026) Cruise Report 2026-02-ZDLU1. Groundfish survey. Fisheries Department, Directorate of Natural Resources, Falkland Islands Government. Stanley, Falkland Islands. 181 p.

Swanson GA, Krapu GL, Bartonek JC, Serie JR, Johnson DH (1974) Advantages in mathematically weighting waterfowl food habits data. *Journal of Wildlife Management* 38, 302–307.

Trevizan T, Ramos JE, Blake A, Brewin J, Büring T, Claes J, Evans D (2021) Cruise Report ZDLT1-2021-02. Demersal survey. Fisheries Department, Directorate of Natural Resources, Falkland Islands Government. Stanley, Falkland Islands. 50 p.

Trevizan T, Evans D, Büring T, Ramos JE, Santana-Hernandez N, Sadd D, Copping EA, Piontek R, Blake A (2022) Cruise Report ZDLT1-2022-02. Demersal survey. Fisheries Department, Directorate of Natural Resources, Falkland Islands Government. Stanley, Falkland Islands. 34 p.

Trevizan T, Shcherbich Z, Büring T, Ramos JE, Nicholls R, Hoyer P, Amukwaya A, Fournier-Carnoy L, Piontek R (2023) Cruise Report ZDLT1-2023-02. Demersal survey. Fisheries Department, Directorate of Natural Resources, Falkland Islands Government. Stanley, Falkland Islands. 39 p.

Troccoli GH, Di Marco EJ, Cortés F (2024) Estimación de la biomasa del bacalao austral en el Atlántico Sudoccidental durante el periodo 1980–2023: una comparación entre el Modelo de Ensamble y el Modelo Bayesiano JABBA. Inf. Invest. INIDEP N° 071/24. 23 p.

Ver Hoef JM, Boveng PL (2007) Quasi-Poisson vs. negative binomial regression: How should we model overdispersed count data? Ecology 88: 2766–2772. https://doi.org/10.1890/07-0043.1

Wickham H (2016) ggplot2: Elegant Graphics for Data Analysis. Springer-Verlag, New York. https://ggplot2.tidyverse.org

Winter A, Laptikhovsky V, Brickle P, Arkhipkin A (2010) Rock cod (*Patagonotothen ramsayi* (Regan, 1913)) stock assessment in the Falkland Islands. Fisheries Department, Directorate of Natural Resources, Falkland Islands Government, Stanley, Falkland Islands. 12 p.

Winter A, Davidson D, Watson M (2011) *Loligo gahi* Stock Assessment Survey, 1st Season 2011. Fisheries Department, Directorate of Natural Resources, Falkland Islands Government, Stanley, Falkland Islands. 18 p.

Winter A (2015) Loligo Stock Assessment, First Season 2015. Fisheries Department, Directorate of Natural Resources, Falkland Islands Government, Stanley, Falkland Islands. 28 p.

Winter A, Jones J, Shcherbich Z (2015) *Loligo* Stock Assessment Survey, 1st Season 2015. Fisheries Department, Directorate of Natural Resources, Falkland Islands Government, Stanley, Falkland Islands. 16 p.

Winter A, Zawadowski T, Shcherbich Z, Bradley K, Kuepfer A (2016) Falkland calamari Stock Assessment Survey, 1st Season 2016. Fisheries Department, Directorate of Natural Resources, Falkland Islands Government, Stanley, Falkland Islands. 19 p.

Winter A, Jones J, Shcherbich Z, Iriarte V (2017) Falkland calamari Stock Assessment Survey, 1st Season 2017. Fisheries Department, Directorate of Natural Resources, Falkland Islands Government, Stanley, Falkland Islands. 17 p.

Winter A, Iriarte V, Zawadowski T (2018) *Doryteuthis gahi* Stock Assessment Survey, 1st Season 2018. Fisheries Department, Directorate of Natural Resources, Falkland Islands Government, Stanley, Falkland Islands. 20 p.

Winter A, Lee B (2018) Stock assessment of grenadier (*Macrourus carinatus* and *Coelorinchus fasciatus*). Fisheries Department, Directorate of Natural Resources, Falkland Islands Government, Stanley, Falkland Islands. 13 p.

Winter A (2019) Rock cod stock assessment (*Patagonotothen ramsayi*). Fisheries Department, Directorate of Natural Resources, Falkland Islands Government, Stanley, Falkland Islands. 23 p.

Winter A, Zawadowski T, Tutjavi V (2019) *Doryteuthis gahi* Stock Assessment Survey, 1st Season 2019. Fisheries Department, Directorate of Natural Resources, Falkland Islands Government, Stanley, Falkland Islands. 18 p.

Winter A (2020) Rock cod stock assessment (*Patagonotothen ramsayi*). Fisheries Department, Directorate of Natural Resources, Falkland Islands Government, Stanley, Falkland Islands. 33 p.

Winter A, Lee B, Arkhipkin A, Tutjavi V, Büring T (2020) 2020 1st Season Assessment Survey Falkland calamari (*Doryteuthis gahi*). ZDLY-S1-2020. Fisheries Department, Directorate of Natural Resources, Falkland Islands Government, Stanley, Falkland Islands. 16 p.

Winter A (2021) Rock cod (*Patagonotothen ramsayi*) stock assessment. SA–2021–PAR. Fisheries Department, Directorate of Natural Resources, Falkland Islands Government, Stanley, Falkland Islands. 29 p.

Winter A, Shcherbich Z, Matošević N (2021) 2021 1st Season Assessment Survey Falkland calamari (*Doryteuthis gahi*). ZDLY-S1-2021. Fisheries Department, Directorate of Natural Resources, Falkland Islands Government, Stanley, Falkland Islands. 18 p.

Winter A, Lee B, Shcherbich Z, Nicholls R (2022) 2022 1st Pre-season Assessment Survey Falkland calamari (*Doryteuthis gahi*). ZDLS3-S1-2022. Fisheries Department, Directorate of Natural Resources, Falkland Islands Government, Stanley, Falkland Islands. 15 p.

Winter A, Raczynski M, Peruzzo M (2023) 2023 1st Pre-season Assessment Survey Falkland calamari (*Doryteuthis gahi*). ZDLE1-S1-2023. Fisheries Department, Directorate of Natural Resources, Falkland Islands Government, Stanley, Falkland Islands. 17 p.

Wood SN (2003) Thin-plate regression splines. *Journal of the Royal Statistical Society: Series B* 65: 95–114. https://doi.org/10.1111/1467-9868.00374

Wood SN (2011) Fast stable restricted maximum likelihood and marginal likelihood estimation of semiparametric generalised linear models. *Journal of the Royal Statistical Society: Series B* 73: 3–36. https://doi.org/10.1111/j.1467-9986.2010.01122.x

Wood SN (2017) *Generalized Additive Models: An Introduction with R* (2nd ed.). Chapman and Hall/CRC. https://doi.org/10.1201/9781315370279

Zavatteri A, Giussi A (2022) Evaluación de la abundancia de merluza de cola (*Macruronus magellanicus*) del Atlántico Sudoccidental. Periodo 1985–2021. Inf. Tec. Oficial INIDEP Nº 057/22. 28 p.

**Appendix I**. Length-weight relationship

Length-weight relationship for females and males of main commercial species in Falkland Islands waters. Dorsal mantle length was measured for Argentine shortfin squid and Patagonian squid. Total length was measured for common hake, kingclip, red cod, rock cod, southern blue whiting, southern hake, and Patagonian toothfish. Pre-anal length was measured for banded whiptail grenadier and hoki.

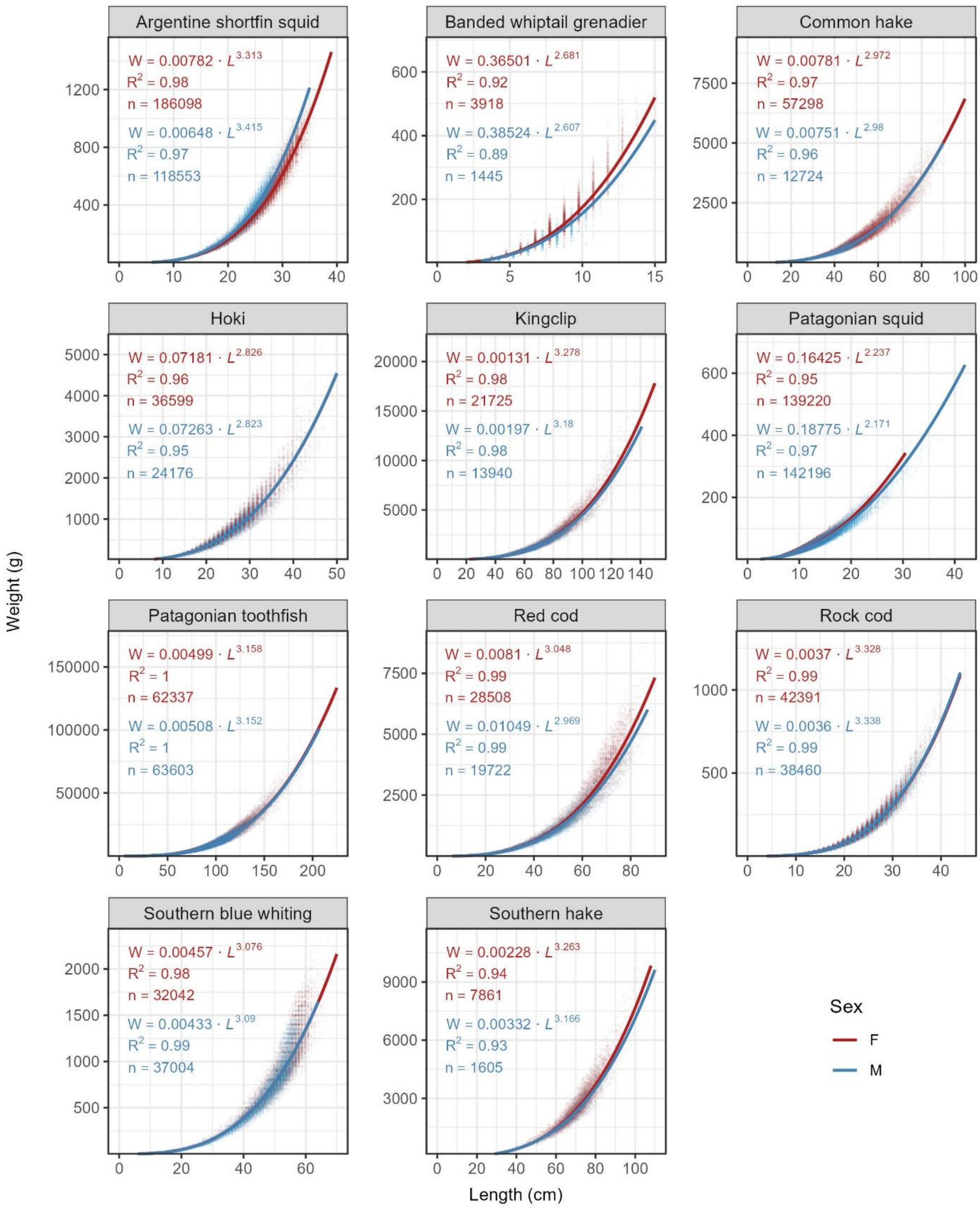

**Appendix II**. February surveys catches

Catch (t) of main commercial species during the February 2010–2011 and 2015–2026 groundfish and calamari pre-season surveys in Falkland Islands waters.

| Year | Argentine shortfin squid | Banded whiptail grenadier | Common hake | Hoki | Kingclip | Patagonian squid | Patagonian toothfish |
|---|---|---|---|---|---|---|---|
| 2010 | 0.882 | 8.047 | 1.308 | 79.780 | 3.238 | 356.763 | 1.391 |
| 2011 | 1.947 | 6.200 | 1.672 | 56.000 | 8.589 | 50.511 | 2.421 |
| 2015 | 31.867 | 6.580 | 3.166 | 26.364 | 14.732 | 186.136 | 0.770 |
| 2016 | 0.099 | 3.277 | 0.693 | 38.915 | 5.448 | 66.895 | 1.752 |
| 2017 | 2.485 | 3.973 | 2.940 | 3.695 | 4.260 | 185.231 | 2.500 |
| 2018 | 10.704 | 7.537 | 1.732 | 30.017 | 3.586 | 115.843 | 1.930 |
| 2019 | 9.412 | 2.505 | 2.754 | 7.554 | 4.418 | 386.017 | 0.829 |
| 2020 | 17.915 | 2.624 | 0.725 | 14.382 | 3.625 | 272.080 | 0.488 |
| 2021 | 10.309 | 6.532 | 8.150 | 30.832 | 4.787 | 285.543 | 0.731 |
| 2022 | 0.776 | 4.504 | 5.651 | 9.712 | 2.790 | 422.739 | 0.331 |
| 2023 | 3.216 | 5.106 | 8.589 | 14.407 | 10.758 | 554.942 | 1.314 |
| 2024 | 16.505 | 3.927 | 6.111 | 20.839 | 5.025 | 683.307 | 1.609 |
| 2025 | 13.005 | 4.657 | 16.993 | 1.085 | 2.424 | 346.146 | 2.139 |
| 2026 | 0.293 | 8.957 | 14.750 | 21.142 | 3.956 | 549.845 | 4.949 |
| Mean | 8.530 | 5.316 | 5.374 | 25.337 | 5.545 | 318.714 | 1.654 |

**Appendix II**. *continued*

| Year | Red cod | Rock cod | Southern blue whiting | Southern hake |
|---|---|---|---|---|
| 2010 | 13.539 | 164.591 | 21.868 | 0.822 |
| 2011 | 23.540 | 249.384 | 52.293 | 0.773 |
| 2015 | 21.809 | 198.272 | 24.120 | 0.357 |
| 2016 | 19.947 | 77.308 | 79.360 | 0.246 |
| 2017 | 13.822 | 76.133 | 6.407 | 0.196 |
| 2018 | 13.301 | 35.922 | 29.512 | 0.301 |
| 2019 | 13.682 | 27.932 | 8.375 | 0.051 |
| 2020 | 3.707 | 10.978 | 5.100 | 0.095 |
| 2021 | 6.040 | 57.157 | 12.169 | 0.264 |
| 2022 | 10.413 | 30.816 | 3.272 | 0.110 |
| 2023 | 11.071 | 36.213 | 32.386 | 0.259 |
| 2024 | 6.409 | 169.167 | 119.795 | 0.321 |
| 2025 | 3.347 | 47.646 | 58.508 | 0.336 |
| 2026 | 7.483 | 75.504 | 13.898 | 1.067 |
| Mean | 12.008 | 89.787 | 33.362 | 0.371 |

**Appendix III.** Year-to-baseline biomass differences

L95) Lower 95% confidence interval; U95) Upper 95% confidence interval; p positive) p value of biomass increase at 95% significance; p negative) p value of biomass decrease at 95% significance. Argentine shortfin squid (ILL); Banded whiptail grenadier (GRF); Common hake (HAK); Hoki (WHI); Kingclip (KIN); Patagonian squid (LOL); Patagonian toothfish (TOO); Red cod (BAC); Rock cod (PAR); Southern blue whiting (BLU); Southern hake (PAT). Bold font indicates significant changes (p adjusted threshold = 0.017).

| Species | Comparison | Mean difference | L95 | U95 | p positive | p negative | Change |
|---|---|---|---|---|---|---|---|
| ILL | 2010 vs 2026 | -7497.19 | -12675.48 | -2771.64 | 1.000 | 0.000 | Decrease |
| ILL | 2025 vs 2026 | -52897.75 | -74003.05 | -31872.36 | 1.000 | 0.000 | Decrease |
| ILL | Mean vs 2026 | -43051.38 | -51981.51 | -34586.03 | 1.000 | 0.000 | Decrease |
| GRF | 2010 vs 2026 | -16431.08 | -48261.80 | 17502.02 | 0.845 | 0.155 | None |
| GRF | 2025 vs 2026 | 25872.47 | 7023.32 | 45608.23 | 0.055 | 1.000 | Increase |
| GRF | Mean vs 2026 | 20989.64 | 2638.96 | 40508.31 | 0.013 | 0.987 | Increase |
| HAK | 2010 vs 2026 | 58686.31 | 45115.89 | 76415.63 | 0.000 | 1.000 | Increase |
| HAK | 2025 vs 2026 | -18690.16 | -43576.05 | 9319.18 | 1.000 | 0.731 | None |
| HAK | Mean vs 2026 | 19169.22 | 1180.48 | 38316.87 | 0.020 | 0.980 | Increase |
| WHI | 2010 vs 2026 | -149998.11 | -386706.95 | 53896.75 | 0.897 | 0.103 | None |
| WHI | 2025 vs 2026 | 151126.59 | 8977.83 | 296580.42 | 0.016 | 1.000 | Increase |
| WHI | Mean vs 2026 | 98868.34 | -56828.28 | 248965.01 | 0.335 | 0.665 | None |
| KIN | 2010 vs 2026 | -8684.34 | -19224.40 | 2399.12 | 0.937 | 0.063 | None |
| KIN | 2025 vs 2026 | 958.22 | -11439.38 | 12397.11 | 1.000 | 1.000 | None |
| KIN | Mean vs 2026 | -10056.53 | -20928.75 | 864.99 | 0.964 | 0.036 | None |
| LOL | 2010 vs 2026 | -36411.25 | -94011.46 | 23010.26 | 0.893 | 0.107 | None |
| LOL | 2025 vs 2026 | 45079.50 | -498.54 | 96099.29 | 0.293 | 1.000 | None |
| LOL | Mean vs 2026 | -22813.49 | -70828.91 | 29041.46 | 0.817 | 0.183 | None |
| TOO | 2010 vs 2026 | 6484.69 | 3054.71 | 9919.72 | 0.000 | 1.000 | Increase |
| TOO | 2025 vs 2026 | 9588.04 | 6637.19 | 12499.60 | 0.000 | 1.000 | Increase |
| TOO | Mean vs 2026 | 11319.98 | 8647.33 | 13946.28 | 0.000 | 1.000 | Increase |
| BAC | 2010 vs 2026 | -55421.88 | -129384.16 | 16931.54 | 0.852 | 0.148 | None |
| BAC | 2025 vs 2026 | 14873.39 | -3652.63 | 33429.37 | 0.683 | 1.000 | None |
| BAC | Mean vs 2026 | -1769.33 | -18934.68 | 17240.92 | 0.589 | 0.411 | None |
| PAR | 2010 vs 2026 | -579732.14 | -1042742.21 | -206259.82 | 1.000 | 0.000 | Decrease |
| PAR | 2025 vs 2026 | 164000.25 | 38006.48 | 290113.65 | 0.040 | 1.000 | Increase |
| PAR | Mean vs 2026 | 180503.60 | 64741.51 | 296136.86 | 0.000 | 1.000 | Increase |
| BLU | 2010 vs 2026 | -12347.63 | -66192.07 | 33999.59 | 0.649 | 0.352 | None |
| BLU | 2025 vs 2026 | -20801.90 | -82771.06 | 28047.24 | 1.000 | 1.000 | None |
| BLU | Mean vs 2026 | -9420.61 | -59792.70 | 28654.01 | 0.585 | 0.415 | None |
| PAT | 2010 vs 2026 | 2200.98 | -2314.23 | 5512.71 | 0.198 | 0.802 | None |
| PAT | 2025 vs 2026 | 5244.85 | 813.28 | 8266.58 | 0.050 | 1.000 | Increase |
| PAT | Mean vs 2026 | 5305.60 | 931.70 | 8288.34 | 0.004 | 0.996 | Increase |

**Appendix IV.** Year-to-baseline biomass differences histograms

Biomass differences calculated from the year-to-baseline paired 10,000 bootstrap iterations. Zero represents equality and is indicated by the dashed red line.

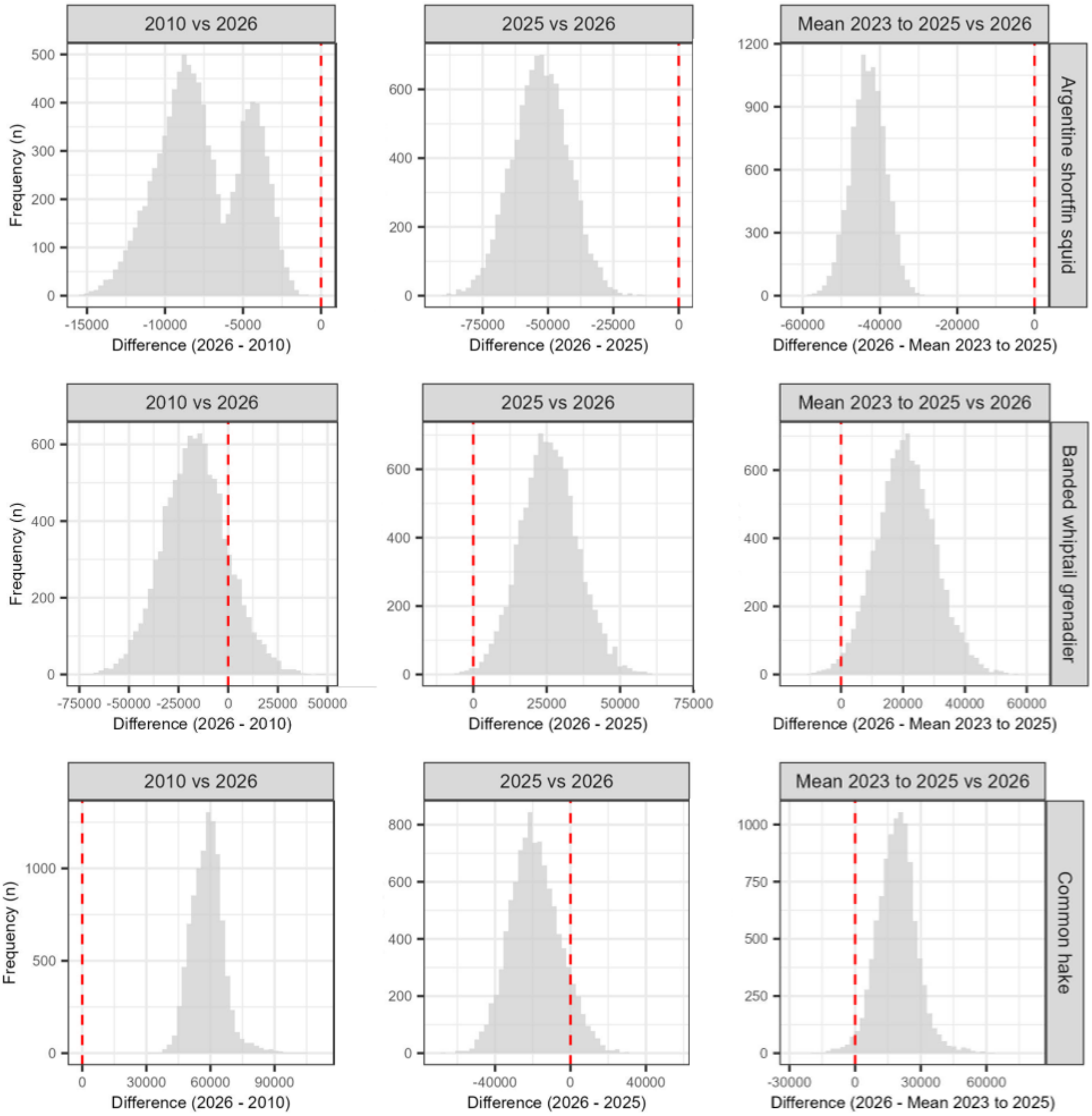

**Appendix IV.** *continued*

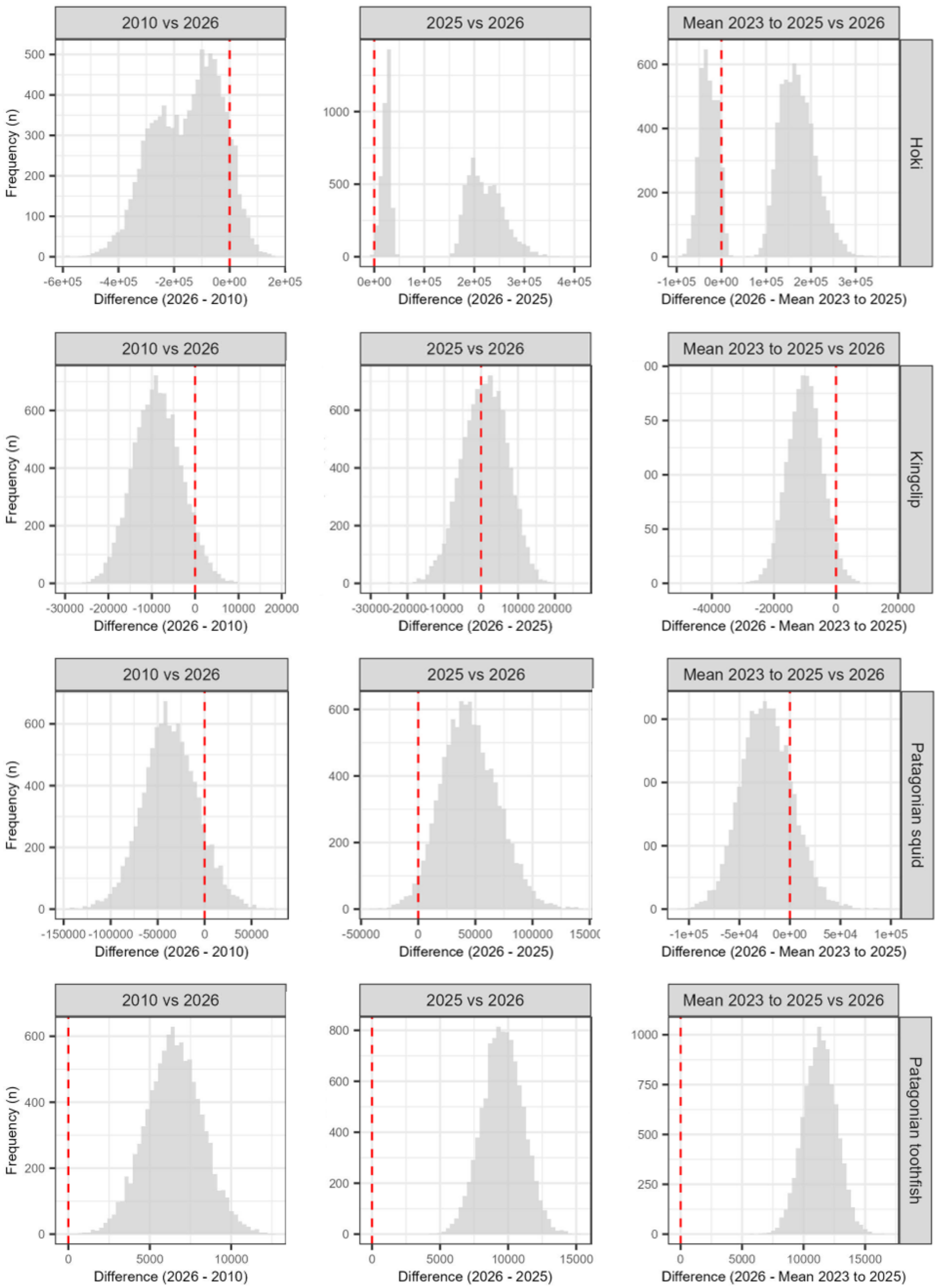

**Appendix IV.** *continued*

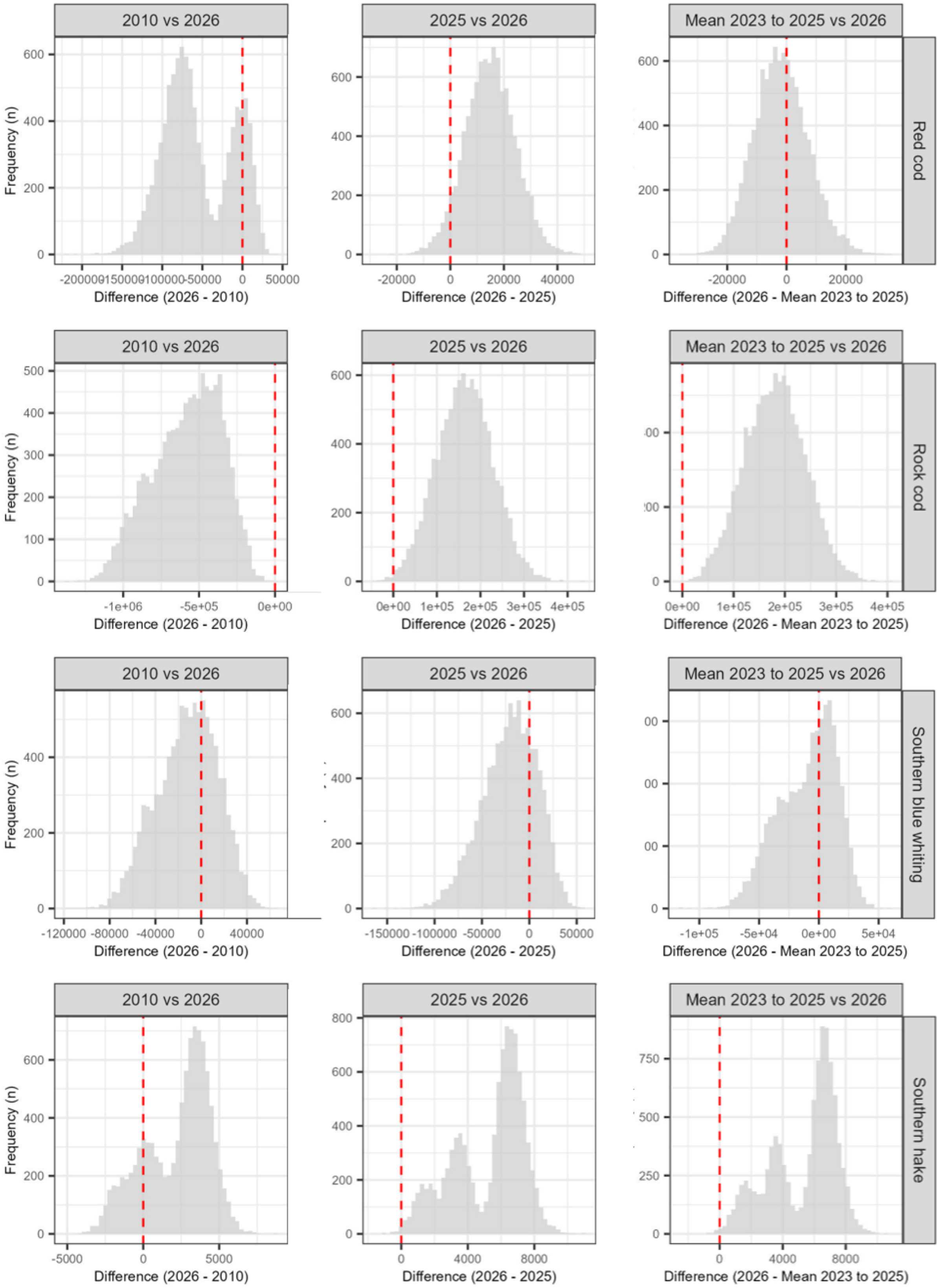

**Appendix V.** Generalised Additive Models for biomass trends

Inv. CV: normalised inverse coefficient of variation; Sqrt. Inv. Var.: square-root normalised inverse variance; edf: estimated degrees of freedom; Ref. df: reference degrees of freedom; F: F-statistic for the year smooth term; p value: Significance for the year smooth term; $R^2$ adj.: adjusted $R^2$; Dev. exp.: percentage deviance explained; AIC: Akaike Information Criterion; ΔAIC: difference in AIC relative to the best-fitting model for each species; ***k***-index: basis dimension adequacy index; ***k*** p value: Significance for the ***k***-index diagnostic.

| Common name | Scientific name | Model | edf | Ref. df | F | p value | R2 adj. | Dev. Exp. | AIC | *k* index | *k* p value | ΔAIC |
|---|---|---|---|---|---|---|---|---|---|---|---|---|
| **Argentine shortfin squid** | ***Illex argentinus*** | **M2: Gamma, Inv. CV** | **1.34** | **1.60** | **0.36** | **0.758** | **-0.053** | **4.5** | **81.1** | **1.098** | **0.703** | **0.0** |
| | | M1: Gamma, unweighted | 1.46 | 1.77 | 0.32 | 0.710 | -0.042 | 6.5 | 139.8 | 1.021 | 0.645 | 58.7 |
| | | M4: Gaussian, Sqrt. Inv. var. | 1.00 | 1.00 | 0.06 | 0.810 | -0.100 | 0.5 | 142.5 | 0.536 | 0.527 | 61.4 |
| | | M3: Gaussian, unweighted | 1.22 | 1.40 | 0.05 | 0.894 | -0.058 | 4.1 | 160.3 | 1.270 | 0.733 | 79.2 |
| **Banded whiptail grenadier** | ***Coelorinchus fasciatus*** | **M2: Gamma, Inv. CV** | **1.52** | **1.86** | **1.32** | **0.388** | **0.139** | **20.7** | **67.5** | **1.021** | **0.432** | **0.0** |
| | | M4: Gaussian, Sqrt. Inv. var. | 1.73 | 2.12 | 1.46 | 0.274 | 0.134 | 25.5 | 117.6 | 1.105 | 0.540 | 50.1 |
| | | M1: Gamma, unweighted | 1.42 | 1.72 | 0.95 | 0.510 | 0.069 | 14.8 | 119.4 | 0.997 | 0.392 | 51.9 |
| | | M3: Gaussian, unweighted | 1.49 | 1.82 | 1.29 | 0.402 | 0.071 | 17.8 | 120.5 | 1.064 | 0.488 | 53.0 |
| **Common hake** | ***Merluccius hubbsi*** | **M2: Gamma, Inv. CV** | **2.13** | **2.63** | **9.18** | **0.003** | **0.746** | **64.3** | **77.8** | **1.324** | **0.870** | **0.0** |
| | | M1: Gamma, unweighted | 2.10 | 2.57 | 10.73 | 0.002 | 0.696 | 66.7 | 111.7 | 1.298 | 0.825 | 33.9 |
| | | M4: Gaussian, Sqrt. Inv. var. | 3.18 | 3.83 | 5.37 | 0.015 | 0.547 | 69.9 | 113.3 | 1.396 | 0.960 | 35.5 |
| | | M3: Gaussian, unweighted | 2.42 | 2.96 | 10.03 | 0.002 | 0.686 | 74.5 | 120.0 | 1.428 | 0.897 | 42.2 |
| **Hoki** | ***Macruronus magellanicus*** | **M2: Gamma, Inv. CV** | **1.00** | **1.00** | **4.42** | **0.057** | **0.390** | **20.2** | **76.5** | **1.118** | **0.590** | **0.0** |
| | | M3: Gaussian, unweighted | 1.85 | 2.28 | 2.52 | 0.109 | 0.286 | 38.7 | 165.4 | 1.134 | 0.535 | 88.9 |
| | | M4: Gaussian, Sqrt. Inv. var. | 1.93 | 2.33 | 4.86 | 0.025 | 0.437 | 53.4 | 166.4 | 1.123 | 0.880 | 89.9 |
| | | M1: Gamma, unweighted | 1.00 | 1.00 | 1.82 | 0.202 | 0.197 | 10.4 | 167.8 | 1.075 | 0.565 | 91.3 |

**Appendix V.** *continued*

| Common name | Scientific name | Model | edf | Ref. df | F | p value | R2 adj. | Dev. Exp. | AIC | *k* index | *k* p value | ΔAIC |
|---|---|---|---|---|---|---|---|---|---|---|---|---|
| **Kingclip** | ***Genypterus blacodes*** | **M2: Gamma, Inv. CV** | **6.71** | **7.76** | **7.51** | **0.012** | **0.753** | **92.3** | **68.1** | **1.428** | **0.915** | **0.0** |
| | | M1: Gamma, unweighted | 7.11 | 8.11 | 10.81 | 0.005 | 0.809 | 94.5 | 94.7 | 1.524 | 0.930 | 26.6 |
| | | M4: Gaussian, Sqrt. Inv. var. | 1.00 | 1.00 | 2.12 | 0.171 | 0.085 | 15.0 | 111.1 | 0.642 | 0.078 | 43.0 |
| | | M3: Gaussian, unweighted | 5.23 | 6.29 | 3.56 | 0.051 | 0.627 | 77.7 | 114.7 | 1.368 | 0.870 | 46.6 |
| **Patagonian squid** | ***Doryteuthis gahi*** | **M2: Gamma, Inv. CV** | **1.00** | **1.00** | **0.74** | **0.407** | **-0.004** | **5.2** | **110.3** | **1.430** | **0.943** | **0.0** |
| | | M3: Gaussian, unweighted | 1.00 | 1.00 | 1.36 | 0.267 | 0.027 | 10.2 | 158.9 | 1.456 | 0.890 | 48.6 |
| | | M1: Gamma, unweighted | 1.00 | 1.00 | 1.1 | 0.316 | 0.032 | 7.6 | 160.4 | 1.477 | 0.948 | 50.1 |
| | | M4: Gaussian, Sqrt. Inv. var. | 1.00 | 1.00 | 3.08 | 0.105 | 0.118 | 20.4 | 160.7 | 1.404 | 0.925 | 50.4 |
| **Patagonian toothfish** | ***Dissostichus eleginoides*** | **M2: Gamma, Inv. CV** | **4.93** | **5.95** | **9.47** | **0.003** | **0.855** | **86.6** | **40.8** | **1.335** | **0.833** | **0.0** |
| | | M3: Gaussian, unweighted | 5.81 | 6.91 | 7.77 | 0.007 | 0.805 | 89.2 | 62.0 | 1.477 | 0.948 | 21.2 |
| | | M4: Gaussian, Sqrt. Inv. var. | 5.34 | 6.40 | 6.09 | 0.010 | 0.747 | 85.3 | 64.2 | 1.365 | 0.838 | 23.4 |
| | | M1: Gamma, unweighted | 4.78 | 5.77 | 6.21 | 0.011 | 0.761 | 81.1 | 64.9 | 1.381 | 0.877 | 24.1 |
| **Red cod** | ***Salilota australis*** | **M2: Gamma, Inv. CV** | **1.00** | **1.00** | **19.82** | **< 0.001** | **0.637** | **60.2** | **89.7** | **1.281** | **0.825** | **0.0** |
| | | M1: Gamma, unweighted | 1.00 | 1.00 | 21.85 | < 0.001 | 0.627 | 61.5 | 131.1 | 1.287 | 0.777 | 41.4 |
| | | M3: Gaussian, unweighted | 1.00 | 1.00 | 24.96 | < 0.001 | 0.648 | 67.5 | 132.3 | 1.213 | 0.740 | 42.6 |
| | | M4: Gaussian, Sqrt. Inv. var. | 1.67 | 2.07 | 7.73 | 0.008 | 0.502 | 59.7 | 132.8 | 1.180 | 0.662 | 43.1 |

**Appendix V.** *continued*

| Common name | Scientific name | Model | edf | Ref. df | F | p value | R2 adj. | Dev. Exp. | AIC | *k* index | *k* p value | ΔAIC |
|---|---|---|---|---|---|---|---|---|---|---|---|---|
| **Rock cod** | ***Patagonotothen ramsayi*** | **M2: Gamma, Inv. CV** | **4.47** | **5.41** | **31.45** | **< 0.001** | **0.981** | **94.7** | **102.5** | **1.181** | **0.672** | **0.0** |
| | | M4: Gaussian, Sqrt. Inv. var. | 5.32 | 6.36 | 51.89 | < 0.001 | 0.955 | 97.8 | 143 | 1.490 | 0.932 | 40.5 |
| | | M3: Gaussian, unweighted | 5.62 | 6.71 | 116.88 | < 0.001 | 0.984 | 99.1 | 148.2 | 1.595 | 0.978 | 45.7 |
| | | M1: Gamma, unweighted | 4.56 | 5.53 | 26.51 | < 0.001 | 0.98 | 93.8 | 156.6 | 1.22 | 0.715 | 54.1 |
| **Southern blue whiting** | ***Micromesistius australis*** | **M2: Gamma, Inv. CV** | **2.60** | **3.16** | **2.22** | **0.154** | **0.246** | **37.3** | **85.9** | **0.747** | **0.150** | **0.0** |
| | | M4: Gaussian, Sqrt. Inv. var. | 3.36 | 4.09 | 4.96 | 0.018 | 0.578 | 70.4 | 131.9 | 1.266 | 0.812 | 46.0 |
| | | M1: Gamma, unweighted | 3.91 | 4.75 | 5.01 | 0.017 | 0.444 | 66.4 | 134.3 | 1.071 | 0.552 | 48.4 |
| | | M3: Gaussian, unweighted | 2.60 | 3.18 | 3.57 | 0.056 | 0.442 | 55.4 | 139.3 | 1.385 | 0.877 | 53.4 |
| **Southern hake** | ***Merluccius australis*** | **M2: Gamma, Inv. CV** | **3.40** | **4.14** | **8.53** | **0.003** | **0.768** | **79.0** | **30.1** | **1.252** | **0.750** | **0.0** |
| | | M4: Gaussian, Sqrt. Inv. var. | 3.31 | 4.04 | 8.93 | 0.002 | 0.714 | 79.9 | 41.9 | 1.108 | 0.603 | 11.8 |
| | | M1: Gamma, unweighted | 3.42 | 4.16 | 7.55 | 0.004 | 0.774 | 77.9 | 43.3 | 1.249 | 0.757 | 13.2 |
| | | M3: Gaussian, unweighted | 4.08 | 4.96 | 9.10 | 0.002 | 0.776 | 84.6 | 48.3 | 1.319 | 0.887 | 18.2 |